This Project has received funding from European Comission by means of Horizon 2020, The EU Framework Programme for Research and Innovation, under Grant Agreement no. 700174

WWW.RESCCUE.EU

#resccueEU

RESCCUE

RESILIENCE TO COPE WITH CLIMATE CHANGE IN URBAN AREAS.

Deliverable D1.2

Final climate scenarios report

R. Monjo[1], J. Pórtoles[1], E. Gaitán[1], D. Redolat[1], C. Paradinas[1], C. Prado[1], L. Torres[1], J. Ribalaygua[1], B. Russo[2], M. Velasco[2]

[1]Climate Research Foundation (FIC);
[2]AQUATEC

30 October 2017

DELIVERABLE NUMBER:	D1.2
DELIVERABLE NAME:	Final climate scenarios report
WP:	WP1
DELIVERY DUE DATE:	31/10/2017
ACTUAL DATE OF SUBMISSION:	31/10/2017
DISSEMINATION LEVEL:	Public
LEAD BENEFICIARY:	FIC
RESPONSIBLE SCIENTIST/ADMINISTRATOR:	Robert Monjo (FIC)
CONTRIBUTOR(S):	R. Monjo, J. Pórtoles, E. Gaitán, D. Redolat, C. Paradinas, C. Prado, L. Torres, J. Ribalaygua, B. Russo, M. Velasco
INTERNAL REVIEWER:	Jaime Ribalaygua (FIC)
EXTERNAL REVIEWER:	Paul Fleming (Seattle Public Utilities)

Table of contents

Tables Summary

Figures Summary

Report Summary

Abstract

The collected climatic data and the climatic hazards identified in the previous report (D1.1) have served as requirement basis for the climate scenarios generation. Future local climate projections and decadal predictions have been obtained for Barcelona, Lisbon and Bristol under the main Representative Concentration Pathways. For this purpose, several statistical downscaling methods (analogous stratification and transfer functions among others) have been combined to project the local climate according to the identified climate drivers: temperature, precipitation, wind, relative humidity, sea level pressure, potential evapotranspiration, snowfall, wave height and sea level. A verification of the downscaling methods has been performed using the ERA-Interim re-analysis as a reference for reproducing the past climate. In a similar way, a validation process has been applied to evaluate the suitability of combining the chosen downscaling methods and the available CMIP5 climate models. Both verification and validation processes showed an adequate performance of the downscaling methods for all simulated climate variables, with negligible systematic errors and typical random errors which are lesser than reference simulation based on climatic averages. Finally, most of climate simulations project coherent changes for the studied climate variables. Main outputs are available in https://www.ficlima.org/intercambio/indexed/RESCCUE/

Main results

The most important changes in the future climate of Barcelona, Lisbon and Bristol are given by the temperature rise. By the end of century, annual mean temperature could rise more than 2°C in the three cities. The worst scenarios (RCP8.5) project a maximum warming up to 6°C in Barcelona and 5.5°C in Lisbon and Bristol (Table 1).

Annual rainfall could experience a significant increase between 5% and 40% in Bristol by 2100 under the RCP8.5 scenario. Lisbon would experience a possible decrease in annual rainfall down to -15% for the 2016-2035 period. Projections for Barcelona show no significant changes in average rainfall, but with a large uncertainty range. However, an increment of the potential evapotranspiration would cause a greater water stress in Barcelona (up to +0.6 mm/day) and Bristol (up to +0.4 mm/day).

Moreover, the snowfalls could decrease between 50% and 100% by the end of century in Barcelona and Bristol. This would cause an important reduction of the water reserves.

Finally, the mean sea level could rise up to +50 cm in Barcelona (medium value of +30 cm), and up to +60 cm in Lisbon and Bristol (medium about +40 cm) by 2100 under the RCP8.5, but with larger uncertainty for Barcelona.

Table 1. Summary of mean changes projected to 2035 and 2100 according to the RESCCUE decadal and climate models. The 10th-90th percentile values of each projected change are shown.

Climate variable	Spatial coverage	2035												2100					
		Decadal predictions vs 1986-2015						Climate change vs 1976-2005						Climate change vs 1976-2005					
		Teleconnections (2016-2035)			Drift-corrections (2016-2035)			RCP4.5 (2006-2035)			RCP8.5 (2006-2035)			RCP4.5 (2071-2100)			RCP8.5 (2071-2100)		
		Barcelona	Lisbon (urban)	Bristol	Barcelona	Lisbon (urban)	Bristol	Barcelona	Lisbon (urban)	Bristol	Barcelona	Lisbon (urban)	Bristol	Barcelona	Lisbon (urban)	Bristol	Barcelona	Lisbon (urban)	Bristol
Temperature (°C)	Regional	+0.1+1.5	+0.0+1.0	+0.4+2.0	+0.6+1.0	+0.0+0.3	+0.0+1.0	+0.4+1.6	+0.3+1.0	+0.4+1.4	+0.4+1.5	+0.3+1.2	+0.4+1.5	+1.0+3.5	+1.0+3.0	+0.7+3.1	**+2.3+6.5**	**+2.0+5.4**	**+1.7+5.8**
	Urban	+0.2+1.5		+0.4-1.9	+0.2+1.0		+0.5+0.8	+0.5+1.5		+0.5+1.3	+0.5+1.5		+0.3+1.4	+1.0+3.0		+1.0+3.0	**+2.2+5.8**		**+2.3+5.6**
Precipitation (%)	Regional	-10+10	-15-5	+0+30	-5+5	-15-0	-1+2	-10+10	-10+15	-2+15	-15+10	-15+15	-5+15	-15+15	-10+15	+5+20	-20+25	-15+15	+10+40
	Urban	-10+10		-5+10	-5+5		-1+2	-15+10		-2+15	-20+10		-5+15	-15+10		+5+20	-30+30		+10+40
Wind (m/s)	Regional				-0.6+0.0	-0.1-0.0	-0.2+0.2	-0.5+0.5	-0.6+0.2	-0.4+0.4	-0.5+0.5	-0.4+0.4	-0.4+0.4	-0.5+0.5	-0.4+0.2	-0.4+0.4	-0.5+0.5	-0.4+0.2	-0.4+0.4
	Urban				-0.6+0.0		-0.1+0.1	-0.2+0.2		-0.4+0.4	-0.2+0.2		-0.4+0.4	-0.2+0.2		-0.4+0.4	-0.2+0.2		-0.4+0.4
Snowfall (mm/year)	Regional	-80-0		-70-0	-80-0		-60-0	-60-8		-55-0	-70-6		-50+10	**-90-50**		-90+15	**-100-85**		**-100-40**
	Urban	-80-0		-70-0	-70-0		-60-0	**-100-20**		-60-15	-100+10		-50-15	**-100-80**		**-80-50**	**-100-95**		**-100-60**
ETP (%)	Regional	+0+5	+0+8	+0+5	+1+5	+0+7	-1+1	+1+6	+0+9	+1+6	+0+6	+0+10	+1+6	+0+14	+0+12	+0+11	+0+27	+0+22	+0+22
RH (%)	Urban							-0.5+0.5	-0.5+0.5	-0.5+0.5	-0.5+0.5	-0.5+0.5	-0.5+0.5	-2.0+1.0	-1.5+0.5	-2.0+0.5	-3.0+1.0	-2.0+0.0	-2.0+0.5
Sea level (cm)	Urban							-1+10	+5+15	+5+14	-1+10	+5+15	+5+15	+10+40	+20+50	+20+50	+10+50	+25+60	+30+60
Wave height (cm)	Urban							+0+4		-1+1	+0+4		-1+1	-5-0		-1+2	-10-0		-1+2
Surge (%)	Urban									-2+1			-2+3			-1+3			-2+2
Pressure (hPa)	Regional						-1.0+0.5			-1.0+1.5			-1.0+1.5			-1.0+2.0			-0.5+2.0

Legend:

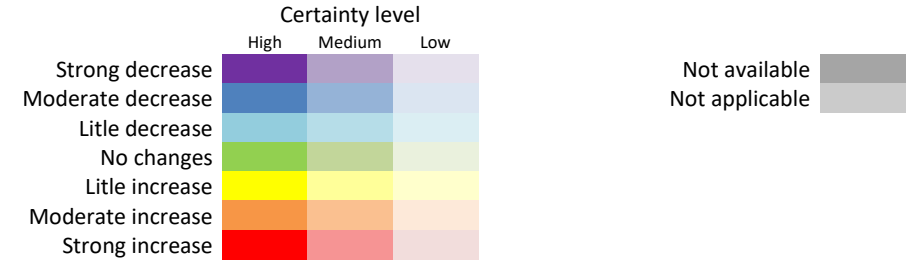

1. Introduction

1.1. Motivation and objectives

1.1.1. Deliverable

The goal of the second deliverable (D1.2) of the RESCCUE WP1 is to provide the final report on climate scenarios. This corresponds to the Task 1.3, "*Generation of climate simulations for the pilot cases"*, scheduled between months 6 and 12, reporting in month 18 and lead by the Climate Research Foundation (FIC).

To contextualize this task, we remember that WP1 consists of the following four tasks:

Task 1.1: Climate change drivers
Task 1.2: Data collection & quality control
Task 1.3: Generation of climate simulation for the pilot cases
Task 1.4: Projection/prediction of extreme events

According to the WP1 Implementation plan and the RESCCUE Grant Agreement, climate downscaled simulations were expected to be generated for the historical period (as a control period) and for future scenarios corresponding to the last Intergovernmental Panel on Climate Change (IPCC) Assessment Report (AR5). For this purpose, as is shown in the Deliverable D1.1, instrumental data were collected from several meteorological institutions and climate model outputs were extracted from the Coupled Model Intercomparison Project Phase 5 (CMIP5).

The report D1.2 corresponds to three different simulations (Appendix I): *Climate model downscaling*, *Decadal model downscaling* and *Subdaily precipitation scaling*. Climate downscaling was applied for a *historical* period (1951-2005) and for a *future* period (2006-2100) considered by the CMIP5 models, which are running under the main Representative Concentration Pathways (RCP) scenarios (RCP4.5 and RCP8.5). A statistical downscaling method is applied to the climate models in order to obtain simulations at local scale for Barcelona, Lisbon and Bristol. Near-term (or decadal) climate prediction is performed by using two approaches, a multi-year teleconnection-based method and a bias-correction of the CMIP5 decadal model outputs, which are running under the RCP4.5. Finally, the sub-daily precipitation scaling is performed for all climate models and for all time periods.

The simulated climate variables were chosen according to the climatic hazards previously identified in the Task 1.1 (Deliverable D1.1). The main climatic variables are usually maximum and minimum temperature, sub-daily precipitation and sea level rise. As some observed data were missing for the D1.1, this report incorporates an appendix for showing the quality control of these data (Appendix II).

1.1.2. Report objectives

In addition to the above goal, some report aims can be identified. Firstly, it is required a summary of the methods used for downscaling the climate simulations at local scale. The second and third objectives are the verification and validation processes, which consist on analysing the performance of the downscaling methods. Particularly, all methods are verified with observations and the joint performance of their application to the CMIP5 climate models was validated. Finally, future climate scenarios are shown for all climate variables and they are statistically analysed.

All information and data files described in this report have been generated according to the data requirements of Aquatec, Cetaqua, LNEC and Uni Exeter. Climate scenarios provided in the WP1 will be used in the rest of RESCCUE project, especially for feeding multisectorial assessment models and focusing on climate change impacts on the urban services.

1.2. Structure of the report

Following the objectives, the report is divided into two main sections, Methodology and Results & Discussion. In turn, these sections are structured in several subsections corresponding to the report objectives:

- Used methodology
  - Description of all used methods
  - Description of the statistics for the verification and validation
- Results and discussion
  - Verification of the methods comparing with observations
  - Validation of the methods to be applied to climate models
  - Climate projections for the 21st century and the next decades

In addition to this, an appendix has been incorporated at the end of the report to show the quality control of the missing observed data that was not included in D1.1.

1.3. Summary of the used data

The present report is based on the collected data reported in the first deliverable D1.1, entitled "Data collection and quality control; summary of studies on climate variables at the research cities". In this deliverable, exhaustive climate hazard identification was performed for Barcelona, Lisbon and Bristol in order to properly drive the research about possible climate change impacts on their urban areas. In particular, past climatic trends and future projections were examined according to previous studies. Climate change drivers and their related climate variables were evaluated according to the importance in the RESCCUE project.

Once identified all climate variables, data collection was performed for the three cities. Observed data were considered for both atmospheric and oceanic variables. For the observed variables, the largest database achieved consists of temperature, precipitation, relative humidity, wind, pressure, wave height and sea level (Table 2). A set of tests were applied over all time series: general consistency, outliers and inhomogeneities. The results of the tests showed an acceptable quality for most of the datasets.

The studied climate variables were also collected from the ERA-Interim reanalysis and CMIP5 climate/decadal models (Table 3 and Table 4). Unlike the direct output of the models, the reanalysis tries to reproduce the meteorological variability day-to-day. However, both kinds of simulations show important errors in their probability distributions due to several factors. The physical limitations from the low spatial resolution and from the used equations or parameterizations cause unrealistic simulations of extreme values. Therefore, it is required to apply some type of downscaling or correction method to adequately simulate climate variability at local scale.

Remark: In order to apply the chosen statistical downscaling, it is enough to use at least 5 years of observed data (Ribalaygua *et al.* 2013). Thus, data collection described in

the previous Deliverable D1.1 focused on all the stations that satisfied these criterion (Table 2). This is independent of the historical period chosen to verificate and validate the method, or to referenciate projected climate changes (see Sec. 2).

Table 2. Data requirements for climate variables related with the identified potential hazards in each city.

Variables (sub-variables included)	**City**			**Spatial coverage**	**Spatial resolution** (km^2/station)	**Time series length** (years)	**Temporal resolution**	**Potential hazards**
	Barcelona	**Lisbon**	**Bristol**					
Temperature (mean, maximum, and minimum)	X		X	Watershed	10-1000	> 5	Daily	Drought
	X	X	X	Urban	1-10	> 5	5-10 min	Heat / Cold events and heat burst
Precipitation (sum of liquid and solid)	X		X	Watershed	10-1000	> 5	Daily	Drought and flooding
	X	X	X	Urban	1-10	> 5	5-10 min	Flash flood and hail
Snow (observed and estimated)	X		X	Watershed	10-1000	> 5	Daily	Snowstorm
	X		X	Urban	1-10	> 5	5-10 min	Thundersnow
Wind (mean and gust)		X	X	Ocean areas	10-1000	> 20	Daily	Windstorm
	X	X	X	Urban	10	> 20	Daily	local severe wind
Potential Evapotranspiration	X		X	Watershed	10-1000	> 5	Daily	Drought and flooding
Relative Humidity (maximum, and minimum)	X	X	X	Urban	1-10	> 5	Daily	Heat events
Atmospheric pressure		X	X	Coastal waters	10-1000	> 20	Daily	Storm surge and windstorm
Sea level	X	X	X	Urban	10-100	> 20	Daily	Sea level rise and storm surge
Wave height (mean and extremes)		X	X	Urban	10-100	> 20	Hourly /daily	Storm surge and sea storm
River flow	X		X	Watershed	100-1000	> 20	Hourly /daily	River-basin flooding
Flood coverage		X	X	Urban	10 meters / pixel	> 20	Daily	Drought and flooding

Table 3. Available CMIP5 climate models. The table shows the model name, the responsible institution, the model references, their spatial resolution for the AGCM, the run code used in this study, the available RCPs and the projection period.

Model	Institution	Reference	AGCM resolution (Lon×Lat)	Run	RCP				Projection period
					2.6	4.5	6.0	8.5	
ACCESS1-0	CSIRO, BOM	Bi *et al.* (2013)	1.87°×1.25°	r1i1p1		X		X	2005-2100
BCC-CSM1-1	BCC	Xiao-Ge *et al.* (2013)	2.8°×2.8°	r1i1p1	X	X	X	X	2005-2100
CanESM2	CC-CMA	Chylek *et al.* (2011)	2.8°×2.8°	r2i1p1	X	X		X	2005-2100
CNRM-CM5	CNRM-CERFACS	Voldoire *et al.* (2013)	1.4°×1.4°	r1i1p1	X	X		X	2005-2100
GFDL-ESM2M	GFDL	Dunne *et al.* (2012)	2°×2.5°	r1i1p1	X	X	X	X	2005-2100
HADGEM2-CC	MOHC	Collins *et al.* (2008)	1.87°×1.25°	r1i1p1		X		X	2005-2099
MIROC-ESM-CHEM	JAMSTEC, AORI, NIES	Watanabe *et al.* (2011)	2.8°×2.8°	r1i1p1	X	X	X	X	2005-2100
MPI-ESM-MR	MPI-M	Marsland *et al.* (2003)	1.8°×1.8°	r1i1p1	X	X		X	2005-2100
MRI-CGCM3	MRI	Yukimoto *et al.* (2011)	1.2°×1.2°	r1i1p1	X	X	X	X	2005-2100
NorESM1-M	NCC	Bentsen *et al.* (2012), Iversen *et al.* (2012)	2.5°×1.9°	r1i1p1	X	X	X	X	2005-2100

Acronyms:

AORI: Atmosphere and Ocean Research Institute (Japan)
BCC: Beijing Climate Center, China Meteorological Administration (China)
BOM Bureau of Meteorology (Australia)
CC-CMA: Canadian Centre for Climate Modelling and Analysis (Canada)
CERFACS: Centre Europeen de Rechercheet Formation Avancees en CalculScientifique (France)
COLA: Center for Ocean-Land-Atmosphere Studies (US)
CMCC: Centro Euro-Mediterraneo sui Cambiamenti Climatici (Italy)
CNRM: Centre National de RecherchesMeteorologiques (France)
CSIRO Commonwealth Scientific and Industrial Research Organisation (Australia)
IPSL: Institut Pierre-Simon Laplace (France)
JAMSTEC: Japan Agency for Marine-Earth Science and Technology (Japan)
GFDL: Geophysical Fluid Dynamics Laboratory (USA)
MOHC: Met Office Hadley Centre (UK)
NIES: National Institute for Environmental Studies (Japan)
MPI-M: Max Planck Institute for Meteorology (Germany)
MRI: Meteorological Research Institute (Japan)
NCC: Norwegian Climate Centre (Norway)
NCEP: National Centers for Environmental Prediction (USA)

Table 4. Daily and monthly fields extracted from decadal model outputs (RCP4.5 scenario). Table shows the available projection period (10: ten years; 30: thirty years; X: both) for each combination variable/model.

	Variable	Decadal model (runs)								
		BCC-CSM1-1 (4)	CanCM4 (4)	CMCC-CM (1)	CNRM-CM5 (4)	HadCM3 (4)	IPSL-CM5A-LR (4)	MIROC5 (4)	MPI-ESM-LR (3)	MRI-CGCM3 (3)
Daily	Sea Level Pressure	30	X	30	30	30	30	30	X	X
	Precipitation	30	X	30	30	30	30	30	X	X
	Convective Precipitation		10	30			30	30		
	Solid Precipitation		10	30			30	30		
	Daily Maximum Near-Surface Air Temperature	30	X	30	30	30	30	30	X	X
	Daily Minimum Near-Surface Air Temperature	30	X	30	30	30	30	30	X	X
	Near-Surface Air Temperature	30	X	30	30	30	30	30	X	X
	Air Temperature			30		30	30	30		
	Sea Surface Temperature		30						X	X
	Daily Maximum Near-Surface Wind Speed		10	30		30	30	30		
	Daily-Mean Near-Surface Wind Speed		X			30	30	30	X	X
	Eastward Wind			30		30	30	30		
	Northward Wind			30		30	30	30		
	Eastward Near-Surface Wind		10	30			30	30		
	Northward Near-Surface Wind		10	30			30	30		
Monthly	Sea Surface Height Above Geoid	30	X	30	30		30	X	10	X
	Global Average Thermosteric Sea Level Change	30	X	30	30		30	X	10	X
	Global Average Sea Level Change	30	X	30	30		30	X	10	X

2. Methodology

2.1. General view

The generation of climate scenarios (Task 1.3) uses a set of statistical methods that depend on the simulated climate variable. However, a general scheme of the generation process is common for all them. To summarise the whole process scheme, we can divide the work in three parts (Fig. 1): (1) Method design/adaptation, (2) Methodology application (downscaled outputs) and (3) Cascade of uncertainties.

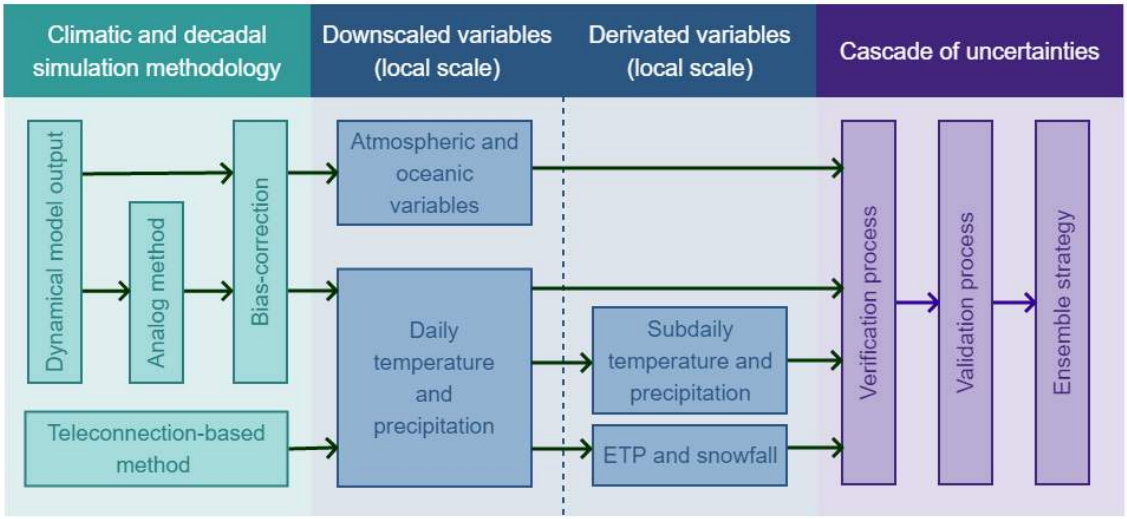

Figure 1. General scheme of the used methodology.

The methodology description has been separated into several sections according to the temporal scale considered. The purely climate simulations (until 2100) are based on analogous stratification (Sec. 2.2.1) and transfer functions or bias correction (Sec. 2.2.2) of CMIP5 climate models. Near-term climate or *decadal* predictions (10 to 30 years) were performed using two methods, the drift correction (Sec. 2.2.3) of dynamical model outputs and the combination of several teleconnection indices (Sec. 2.2.4). Drift correction is a special case of bias-correction method, and therefore it requires to be explained in a separated section.

The sub-daily scale (Sec. 2.2.5) is performed using the method of the *n*-index (Monjo, 2016), and the derivated variables was obtained according to Hargreaves (1994) and Redolat (2014).

With all this, future local climate projections and decadal predictions have been obtained for Barcelona, Lisbon and Bristol (Sec. 4) by using several statistical downscaling methods applied to a set of CMIP5 climate models (Table 3 and Table 4).

The downscaling methods were verified using the ERA-Interim re-analysis as a reference for reproducing the past climate (Fig. 2). In a similar way, the application of these methods to the available climate models was also validated according to several statistical measures (Sec. 2.3).

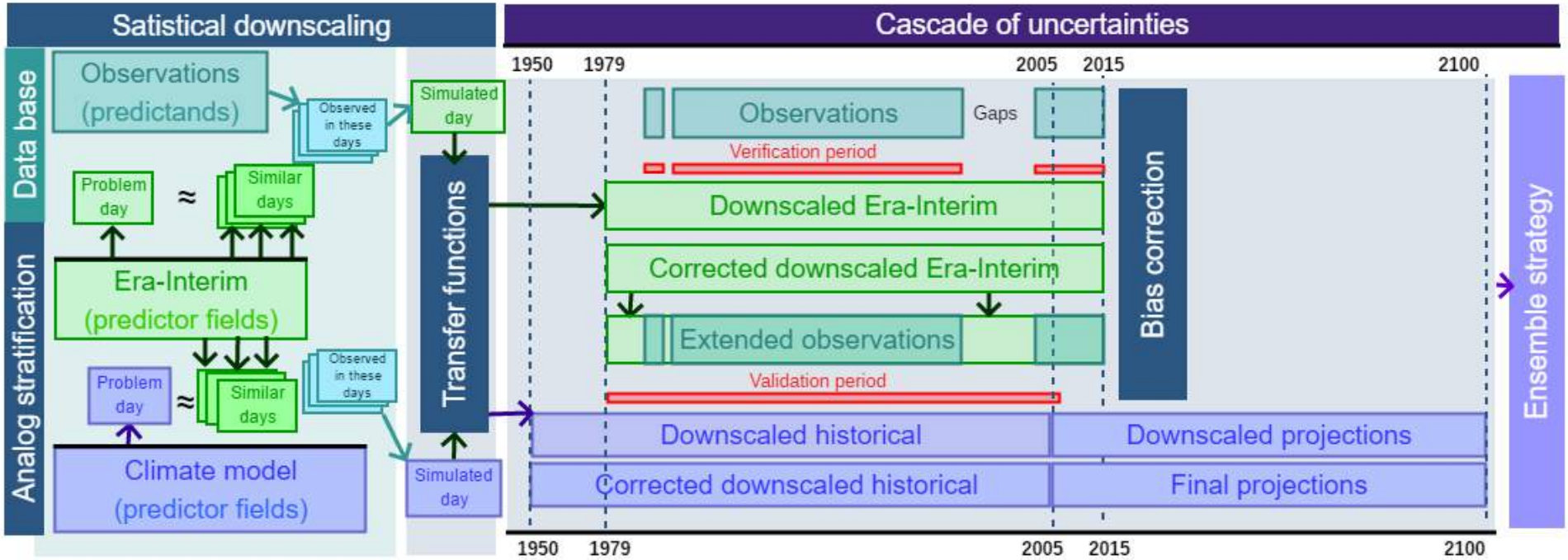

Figure 2. Detailed scheme of the statistical downscaling method used in this study and the corresponding cascade of uncertainties.

2.2. Statistical downscaling methods

2.2.1. Analogy-based approach

This work uses the two-step statistical downscaling method developed by Ribalaygua *et al.* (2013). A brief summary of the two-step method is presented in this section.

The first step is common for all simulated climate variables and it is based on an analogue stratification (Zorita *et al.* 1993): the *n* most similar days to the day to be downscaled are selected. The similarity between two days was measured using a weighted Euclidean distance according to three nested synoptic windows and four large-scale fields used as predictors: (1) speed and (2) direction of the geostrophic wind at 1000 hPa and (3) speed and (4) direction of the geostrophic wind at 500 hPa. For each predictor, the distance was calculated and standardised by substituting it by the closest centile of a reference population of distances for that predictor. The four predictors were finally equally weighted, while the synoptic windows had different weights.

Temperature

In the second step, a transfer function is applied to the *n* analogous days previously selected in the first step. This function depends on the downscaled variable. For temperature, it is a linear function obtained by stepwise regression for *n* = 150 analogous.

Although predictor/predictand relationships determined in this second step are linear, an important part of the non-linearity of the links between free atmosphere variables and surface temperatures is reduced with the first step (analogue) stratification, which selects the most similar days with respect to precipitation and cloudiness (two of the variables which introduce most non-linearity in the relationships). Linear regression performs quite well for the estimation of surface maximum and minimum temperatures due to the near-normal statistical distribution of these variables. It is important to remember that when using linear regression the predictand quantity is bound to have essentially the same statistical distribution as the predictor(s) variable(s) (Bürguer 1996). In this regard, potential predictors should possess close-to-normal distributions.

The multiple linear regression is performed independently for each surface point, and uses forward and backward stepwise selection of predictors. There are four potential predictors:

1. 1000/500 hPa thickness above the surface station.
2. 1000/850 hPa thickness above the surface station.
3. A sinusoid function of the day of the year.
4. A weighted average of the station mean daily temperatures of the ten previous days.

Both thicknesses are used to include the strong relationship between lower troposphere and surface temperatures (a meteorological factor). The sinusoid function of the day of the year is used to consider the number of sunlight hours and its effect on the warming/cooling of the surface air (a seasonal factor). And the ten days

temperature weighted average is used to account for the soil thermal inertia influence (a soil memory factor). The non-linear influence of other important meteorological factors, such as cloudiness, precipitation and low troposphere wind speed, is considered through the first-step of analogue stratification. The regression is performed for a population of *n* days which present very similar precipitation, and subsequently very similar cloudiness conditions. For each station (and each problem day) the regression is performed twice using as predictands maximum and minimum temperatures. Thus two diagnostic equations are calculated (using the predictand and predictor values of the n analogous days population) and applied to estimate both daily temperatures for each station and problem day.

Precipitation

For precipitation, we downscale together a group of *m* problem days (we use the whole days of a month). For each problem day we obtain a "preliminary precipitation amount" averaging the rain amount of its *n* most analogous days, so we can sort the *m* problem days from the highest to the lowest "preliminary precipitation amount". And for assigning the final precipitation amount, all amounts of the *m*×*n* analogous days are sorted and clustered in *m* groups. Every quantity is finally assigned, orderly, to the *m* days previously sorted by the "preliminary precipitation amount". An example of this is shown in Table 2.

The first and second steps of the downscaling method are linked: particularly, the choice of *m* depends on the value of *n*. It is assumed that the climatic characteristics of rainfall vary little within a month. For this reason, the *n*×*m* analogous days of a month can be mixed in order to obtain a better probability distribution (or Empirical Cumulative Distribution, ECDF), i.e. with less smoothed tails. Therefore, the number of problem days is chosen as *m* = 30, and the number of analogous days (*n*) was selected based on this assumption.

Several tests were previously performed to find the best *n* for this work. The analogue stratification obtained similar Ranking Probability Score (RPS about 8%) for values of *n* between 20 and 40 analogues per day. Therefore, the second step was crucial to determine the best *n*: If the population of analogues (*n*) exceeds the number of problem days (*m*), the final precipitation is too smooth (underestimates heavy rain and dry days) due to the average per problem day. The probability distribution of the simulated precipitation is more similar to that observed when *n* is smaller because its average is least smooth. In theory, it is expected that *n* = 1 obtains the highest similarity in the ECDF. However, the RPS is better for *n* higher than 20 and therefore we chosen *n* = *m* = 30. This case is an optimum value even compared with the ECDF simulated with *n* = 1, at least according to the Anderson Darling test (Ribalaygua *et al.* 2013).

Other climate variables

For wind, humidity, wave height, pressure and meteorological tide (including storm surge), the second step is a transfer function between the observed probability distribution and the simulated one using the averaged values from the *n* = 30 analogous days. Particularly, a parametric bias correction (see Sec. 2.2.2) was

performed to the time-series obtained from the analogue stratification (first step). In order to estimate the improvement of this procedure, the bias correction was also applied to the direct model outputs. With this, a comparison was performed between the combination of both steps and the application of the only second step.

For the direct model outputs, the four closest grid points for each of the stations were considered, depending on their latitude and longitude. An averaged time-series was built from the bilinear interpolation of the four grid points. As an example, the series for Barcelona are displayed in Figure 3, for the three working variables.

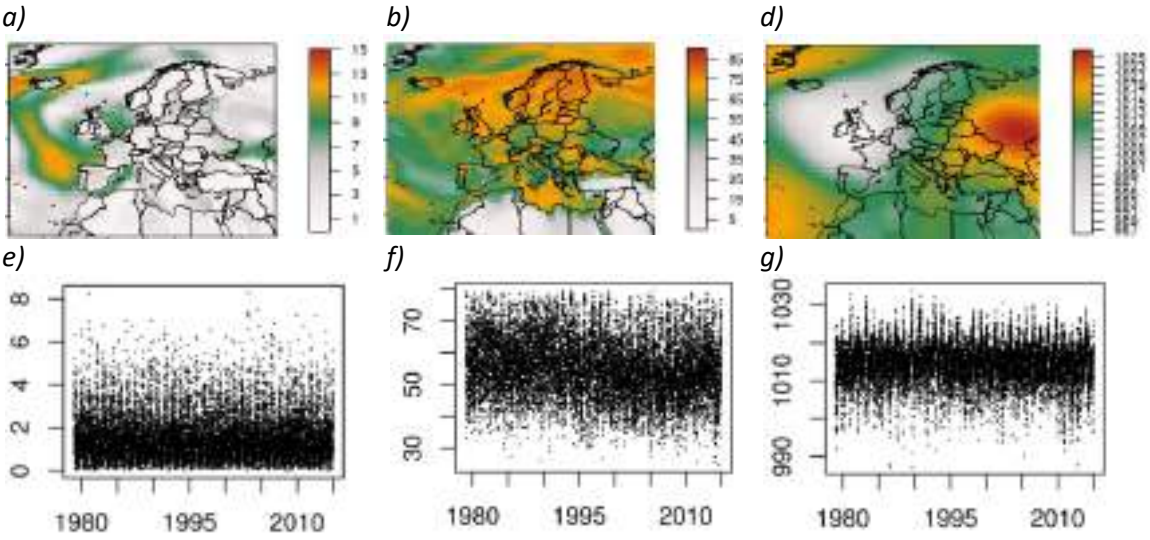

Figure 3. Examples of direct model output: three atmospheric fields for a problem day over Europe according to the ERA-Interim (a, b, c) and 1979-2015 time-series built from the four closest grid points to the city of Barcelona (e, f, g). The variables are: wind (m/s) at 1000hPa (a, e), relative humidity (%) at 1000hPa (b, f) and mean sea level pressure (hPa) for the same grid point (d, g).

2.2.2. Parametric bias-correction

Cumulative Probability Functions

Systematic error or bias is corrected for all climate variables using parametric functions chosen from several theoretical probability distributions. Let *p* a specific value for a daily climate variable, the cumulative probability distribution (π) describes the *quantile* or probability of registering a value equal or minor than *p*, i.e., the sum of frequency of days with a value equal or minor than *p*. We can distinguish between empirical and theoretical distributions: If the curve is estimated from a time series of precipitation (observed or simulated), we will refer to an *empirical cumulative distribution function* (ECDF). However, if the curve is obtained by a theoretical mathematical function, we refer to it as *theoretical cumulative distribution function* (TCDF).

For each variable, transference between observed and simulated CDF is performed throughout fitting TCDFs for each ECDF. For some climate variables, the fitted TCDFs differ in little and therefore the transference can be performed using a linear or logarithmic quantile mapping. For example, temperature is almost a *normal* or Gaussian variable and then linear correction is sufficient (using the mean and standard deviation), but precipitation requires to test a great set of theoretical distributions.

For precipitation, all theoretical functions that have been considered require a *standard precipitation*, λ, defined as:

$$\lambda(p;P_o,P_1) \equiv \frac{p-P_o}{P_1} \qquad \text{Eq. 1}$$

where the parameter P_o is the most probable value and P_1 is the scale factor. Both parameters depend on the probability distribution used. Theoretical distributions able to fit the entire set of empirical values have been chosen, including the zeros. Thus, the possible overfitting of the end of the probability curve is greatly reduced. In particular, several probability distributions have been used, based on four-parametric versions $\pi(p; P_o, P_1, w, h)$ of five distributions (Eq. 2 to 6): Gamma, Weibull, Classical Gumbel, Reverse Gumbel and Modified Log-logistic (Monjo *et al.* 2014, 2016).

$$\pi_1 = \frac{\gamma\left(h,\lambda^w\right)}{\Gamma(h)} \qquad \text{Eq. 2}$$

$$\pi_2 = 1-\exp\left(-\lambda^w-h\right) \qquad \text{Eq. 3}$$

$$\pi_3 = \exp\left[-\exp\left(-\lambda^w-h\right)\right] \qquad \text{Eq. 4}$$

$$\pi_4 = 1-\exp\left[-\exp\left(\lambda^w+h\right)\right] \qquad \text{Eq. 5}$$

$$\pi_5 = 1-\frac{1}{1+\lambda^{w+\lambda\cdot h}} \qquad \text{Eq. 6}$$

where P_o, P_1, w and h are the four parameters of the probability distributions. Each theoretical distribution is fitted to the empirical cumulative probability using a Newton-type algorithm (Dennis and Schnabel 1983). In order to obtain a better correspondence between precipitation and return period, the mean square error was minimized not only for the low cumulative probability but also for the high

(symmetrical weighting for the lowest and highest values), thus the measure to minimize is a Dual mean Normalized Square Error (DNSE):

$$DNSE = \frac{1}{N}\sum_{i=1}^{N}\frac{\left(\pi_{k,i}-\pi_{emp,i}\right)^2}{\pi_{emp,i}^{\ 2}}\cdot\frac{\left[\left(\pi_{k,i}-1\right)-\left(\pi_{emp,i}-1\right)\right]^2}{\left(\pi_{emp,i}-1\right)^2} \qquad \text{Eq. 7}$$

where the first and second factors of the product are respectively for low and high cumulative probability. All the fits were carried out using a parametric initialization obtained by maximum likelihood inference (Coles 2001, Raue *et al.* 2009). Inference with Profile Log-Likelihood approach was applied to the CDF.

Systematic error correction

The systematic error is obtained by comparing the simulated precipitation (from climate models *historical experiment*) with the observed precipitation (from reference time-series). In order to correct this systematic error, it is necessary to have long time-series of reference, because the large natural variability of precipitation has a significant uncertainty associated. For that reason, we have extended the observed time series downscaling ERA40 reanalysis (1958-2000) before validation. Due to systematic error that downscaling method introduces into the extreme rainfall, we chose to correct the ECDF of each ERA40 simulation (p_{era}), with reference to observations (p_{obs}) in the common period (marked as *). This correction is based on quantile-quantile parametric transferences (Benestad 2010, Monjo *et al.* 2014). Therefore, the extended time-series (p_{obs}') of each rain gauge is:

$$p_{obs}' = p_{obs} \cup \pi_{obs*}^{-1}\left(\pi_{era*}(p_{era})\right) \qquad \text{Eq. 8}$$

where π_{obs*} and π_{era*} are the ECDFs of the observed rainfall and of the downscaled ERA40 simulation, estimated in the common period. The symbol $\cup$ joins two time-series: the term on the right is the result of the correction of downscaled ERA40 rainfall, while the term on the left is the original observed time-series (p_{obs}).

After obtaining the extended time-series (p_{obs}'), the same probabilistic correction was applied for the direct outputs and the downscaled projections simulated by the climate models (CMs), according to:

$$p_{CM}' = \pi_{obs'*}^{-1}\left(\pi_{CM*}(p_{CM})\right) \qquad \text{Eq. 9}$$

where π_{CM*} is the ECDF of the downscaled CM simulation, estimated in the common period with the extended time-series, and $\pi_{obs'*}$ is the ECDF of this extended observed time-series (p_{obs}').

Quantile-quantile mapping

For wind, humidity and pressure, the fitted TCDFs differ in little and therefore the transference was performed using a linear or logarithmic quantile mapping. For each model regression, an expansion in Taylor series was considered until the quadratic order.

In all, three different theoretical functions were used: linear model, simple logarithm and logarithm with offset. The best function was chosen according to the highest Pearson correlation R^2 between empirical and theoretical quantile-quantile.

Thus, each original and downscaled ERA time-series was corrected with the corresponding fitted parameters.

Together with this, the Kolmogorov-Smirnov test was applied before and after corrections to analyse whether each simulated time-series is indistinguishable of the observed one (passing test according to the threshold *p*-value > 0.05). An example of the result of corecting one station can be seen in Figure 4. It is obtained, in this way, a specific ERA time-series for every station of each region, time-series that could be used afterwards as a historical input to run climate projections.

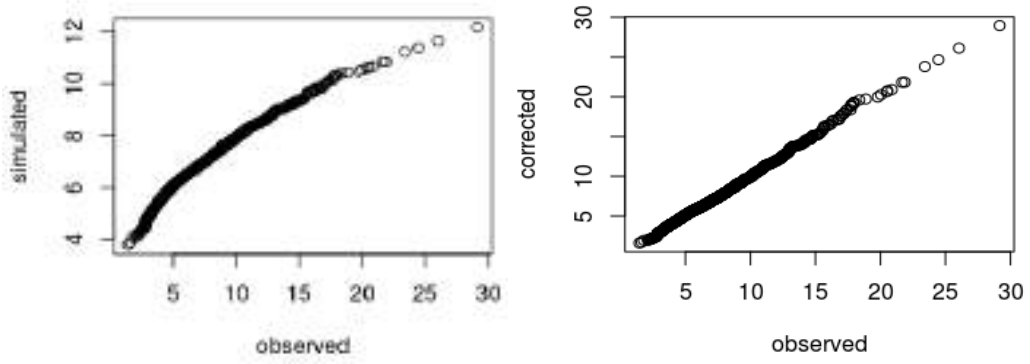

Figure 4. Example of quantile-mapping between simulated (ERA direct output) and observed time-series, for the wind (m/s) recorded in the station 03520 of Lisbon, before correction (left) and after correction (right).

2.2.3. Decadal: dynamical output correction

Drift correction

The data assimilation carried out for the initialization of both climate and decadal models causes a *drift* in the bias of the simulated variables until they are stabilized (Kim *et al.* 2012, Doblas-Reyes *et al.* 2013). That is, the drift is produced until the model simulates enough transitory time since the beginning of the run (around 10-year horizon). Since near-term climate models predict for 10 to 30 years (decadal models), the drift must be taken into consideration because it could extend for a half of the forecast term.

A greater number of projections were collected for reducing the uncertainty of the decadal prediction (Table 4). Particularly, data from nine decadal models with four different initialization *runs* have been used (except for CMCC-CC that only has *run*1, and MPI-ESM-LR and MRI-CGCM3 that do not have *run*4).

For each initialization *run*, a total of ten *historical* experiments (the maximum for some decadal models) have been considered to estimate the bias drift. Daily output obtained for each city has been aggregated to the corresponding annual time-series. As the bias drift depends on the temporal horizon (ten years), drift was separately computed for each horizon *h* of the ten experiments. For example, if h_{ij} is the *i*-year horizon for the *j*-experiment, we jointly compute all the h_{1j} for the first year horizon (where j = 1,…,10), and so on for each horizon.

Drift correction used in this section is a type of parametric bias-correction. In particular, we have chosen the *normal* or Gaussian distribution approach according to two reasons. Firstly, a few *historical* experiments are available for the correction process, which hinders the use of multi-parametric theoretical distributions. Secondly, it is required to use annual values to estimate the bias drift (against the noisy variability at daily scale), and climate variable averaged at annual or multi-annual scale tends to resemble to the normal distribution.

In order to keep the natural signal of the variable along the decade and to preserve the temporal resolution available, *time horizon* was redefined as a temporal unit of prediction. In other words, the value at the *k*-horizon (H_{kj}) is calculated as the mean of the *k* previous years (Eq. 10), being therefore a value representative of the whole period and the trend of the variable within it.

$$H_{kj} = \frac{1}{k}\sum_{i=1}^{k} h_{kj} \qquad \text{Eq. 10}$$

From the ten experiments (j = 1,…,10), the groups of horizons H_{kj} were then arranged to obtain ten 1-horizons (H_{1j}), ten 2-horizons (H_{2j}), etc. To correct the drift, these *k*-horizons series are standardised by using their equivalent Z-value (standard score), and then the mean (M_k) and standard deviation (S_k) are obtained as fitting parameters for each *k*. Rearranging these *k*-horizons of Z-values, we obtain ten drift-corrected time-series (of 10 horizons each one), which replace the original ten *historical* runs (Fig. 5).

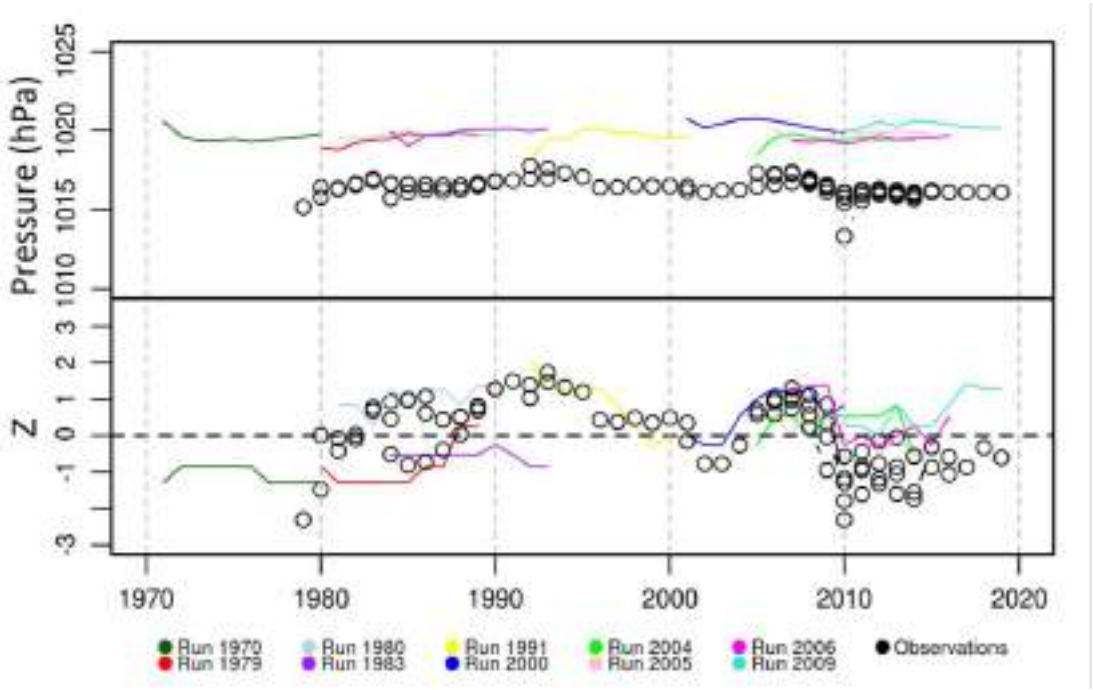

Figure 5. Example of drif-correction by standardisation. *Top*: raw decadal runs of CanCM4 model regarding Sea Level Pressure variable downscaled for the 0200E station (Barcelona). *Bottom*: the same but for normalised (Z) time-series.

For the decadal projections, four different runs from the 2005 experiment were taken, which correspond to the 2006-2035 period. Data from every model output have been linearly interpolated to each city coordinates. The decadal projections were drift-corrected using the parameters M_k and S_k obtained from the ten *historical* experiments. Particularly, the temporal evolution of these parameters was analysed for horizons lower than 10 years and then they were extrapolated for horizons greater than 10 years.

The climate variables predicted using decadal simulations are: precipitation, maximum and minimum temperatures, wind and mean sea level pressure. The probability distribution considered for precipitation and wind is *log-normal* instead of *normal*. That is, if x is the original daily value of precipitation or wind, the used value for the whole drift-correction process is $x' = \log(1+x)$.

The verification process of the historical experiments was separately performed for each horizon H_k comparing with the corresponding observed value.

Multi-decadal composition

The set of runs/experiments presents gaps and overlaps depending on the considered horizon year and model. In order to obtain one complete time-series for each decadal model, a merging process was performed to collapse all of the standardised runs into just one, by using the median of the values of each year. Since the merge process can affect the normal distribution, the resulting time-series is again standardised taking the mean and standard deviation of its 1986-2015 period as climatic reference. Therefore a multi-decadal time-series is obtained for each decadal model (Fig. 6).

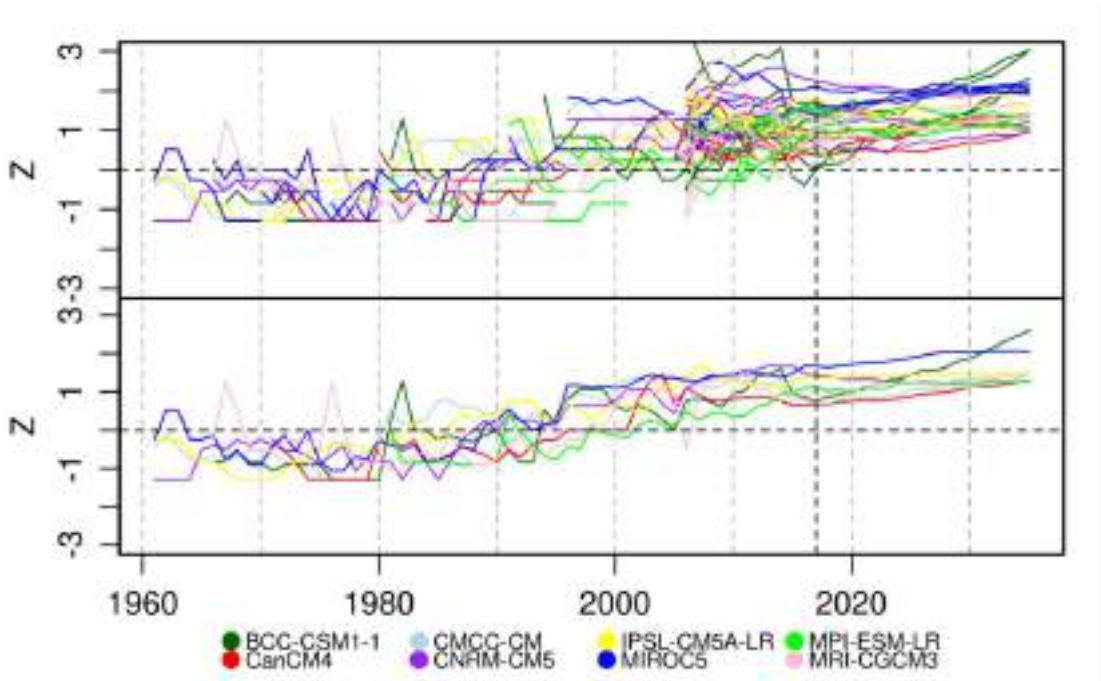

Figure 6. Example of drift-corrected output. *Top*: Z-values for minimum temperature variable in Barcelona, according all runs/experiments available for each decadal model. *Bottom*: Z-values for the same variable according to the complete time-series obtained after the merge process for each decadal model. Vertical dashed line marks the end of the past period (2017).

The standardised multi-decadal time-series are useful to obtain downscaled projections, specific for each observatory. Particularly, a transfer function is required to be applied to all standardised decadal models, using the statistical features (mean and standard deviation) of each observed time-series.

In average terms, the multi-decadal time-series represents approximately a 5-year moving average (from merging 1 to 10 horizons years). Therefore, we considered to use a 5-year moving average for the observed time-series. From this, mean and standard deviation were estimated and applied to each multi-decadal time-series.

The whole process of drift-correction applied to the annual mean values was repeated for the standard deviation at daily scale (computed with 30-day moving window), whose bias drift was also treated using annual averages.

In order to obtain daily time-series for the historical experiments and future decadal projections, the empirical distribution function of the original daily outputs was corrected according to the mean and standard deviation (at daily scale) obtained for each drift-corrected year-horizon.

2.2.4. Decadal: teleconnection indices

Motivation and selection of the method

Near-term climate models based on dynamical simulation require an assimilation of the initial conditions of the climate system (Doblas-Reyes *et al.* 2013). The global oceans are the main component of the climate system for the near-term climate predictions (10-30 years), because they transfer large-scale energy fluctuations to the atmosphere.

Nevertheless, the initial conditions of the ocean currents are little known, especially in the deep ocean (due to lack of observations). This causes that dynamical models are not able to adequately simulate some important climate variability modes. In fact, decadal models present low skill for simulate quasi-oscillations as PDO or SAHEL (Kim *et al.* 2012, Gaetani and Mohino 2013).

For this reason, a purely statistical approach was used in order to complete the decadal predictions obtained from the drift-corrected dynamical outputs. The statistical approach should simulate the main modes of natural variability by using the predictability of some quasi-oscillations. In particular, we have chosen an approach based on ten teleconnection indices commonly used for the Western Europe (Table 5).

Table 5. Indices and their variables considered. SST is sea surface temperature, SLP represents sea level pressure, R is rainfall, and Z500 is geopotential height at 500 hPa.

Index	Start	End	Used variable	Used region	Reference
ENSOi	1870	2015	SST	El Niño 3.4 (170ºW to 120° W-EQ)	NOAA (2017)
NAOi	1950	2015	SLP	Ponta Delgada–Reykjavik	NOAA (2017)
AOi	1950	2015	SLP	Atlantic 20°N to North Pole	NOAA (2017)
AMOi	1870	2015	SST	Atlantic 0º–60ºN and 7.5ºW–7.5ºE	NOAA (2017)
MOi	1948	2015	SLP	Algiers–Cairo	CRU (2017)
WeMOi	1821	2013	SLP	Padua–San Fernando	UB (2017)
ULMOi-C4	1951	2015	Z500	Mediterranean: 36.5 to 42.5°N, –2.20 to 4.4°E, and 29 to 32.5°N, 14 to 25.5°E	Redolat *et al.* (2017)
PDOi	1854	2016	SST	Pacific 20ºN	JISAO (2017)
SAHEL-Pi	1901	2016	R	Africa 8° to 20°N – 20°W to 10ºE	JISAO (2017)
GSNWi	1966	2010	SST	Atlantic 55º to 75ºW - 35ºN	Taylor (2011)

Acronyms:

NOAA: National Oceanic and Atmospheric Administration (USA).
JISAO: Joint Institute for the Study of the Atmosphere and Ocean (USA).
CRU: Climate Research Unite (UK)
UB: University of Barcelona (Spain)
ENSOi: El Niño South Oscillation index

NAOi: North Atlantic Oscillation index
AOi: Artic Oscillation index
AMOi: Atlantic Multidecadal Oscillation index
MOi: Mediterranean Oscillation index
WeMOi: Western Mediterranean Oscillation index
ULMOi: Upper Level Mediterranean Oscillation index
PDOi: Pacific Decadal Oscillation
SAHEL-Pi: Sahelian Precipitation index
GSNW: Gulf Stream North Wall index

Statistical approach description

The teleconnection-based method was applied to predict temperature and precipitation anomalies following three steps:

Firstly, the best predictors are chosen for each station according to the Akaike Information Criterion (AIC) resulting from a backward stepwise regression (Venables and Ripley 2002). The second step is a fitting process of a *n*-harmonic model (η) for each index, which parameters (frequencies, phases and amplitudes) are separately obtained: A filtered Faster Fourier Transformation (FFT) is used for the frequency spectrum (ω_i), a Newton-type non-linear algorithm is applied to find the sinusoidal phases (φ_i), and finally a backward stepwise regression was applied to obtain the final *n* sinusoidal amplitudes (A_i) and to reject the no significant ones:

$$\eta = \sum_{i=1}^{n} A_i \sin(\omega_i t + \varphi_i) \qquad \text{Eq. 11}$$

where *t* is the time in years. The third and simplest step is to extrapolate this model for the future horizons.

A *hindcast* cross-validation was performed using the *n*-harmonic model in order to evaluate its performance in the past (verification). Therefore, a confidence level was obtained for each forecast horizon according to the verification process (especially with SAE).

The entire statistical process was applied and verified using detrended anomalies of temperature and precipitation. Thus, the final predictions were performed combining the *n*-harmonic model and the (30-year moving averaged) climate projections under the RCP4.5 and RCP8.5 scenarios, obtained from the statistical downscaling (Sec. 2.2).

2.2.5. Time-scaling simulation

Sub-daily temperature

Temperature is a quasi-Gaussian variable and therefore it facilitates the use of analogous techniques based on averages (e.g. the mean of *n* analogous days). As in daily temperature, the simulation of sub-daily temperature was performed using a two-step statistical downscaling method. The first step consists of the selection (like in daily simulation, Sec. 2.2.1) of *n* most analogous days for each problem day and then averaging the sub-daily temperature recorded in those analogous days. With this, a soft curve is obtained for the daily cycle of temperature, but extremes (maximum and minimum temperatures) are underestimated. For this reason, an additional post-process is required.

The second step consists in a correction of the sub-daily thermal amplitude (ΔT) taking into account the maximum (T_x) and minimum temperature (T_n) simulated from the daily downscaling (previous sections). Particularly, this is the following linear correction:

$$T' = T_n + \left(T - \min(T)\right)\frac{T_x - T_n}{\Delta T} \qquad \text{Eq. 12}$$

where T and T' are respectively the before and after-correction sub-daily temperature (at 5-min time resolution) and $\Delta T \equiv \max(T) - \min(T)$ is the sub-daily thermal amplitude. In order to guarantee the temporal coherence (without daily jumps at 00Z) for the corrected sub-daily time-series, all parameters (T_x, T_n, ΔT and $\min(T)$) are interpolated at the same sub-daily resolution (5-min) keeping the extreme moments (i.e., staying invariant the extreme values for the corresponding hours for the maximum and minimum temperature).

Sub-daily precipitation

As precipitation is a very irregular climate variable (highly frequent extremes), it is not possible to use averages of analogous days (which greatly softens the probability distribution). Therefore it is required to use stochastic methods as weather generators, Marcov chains or fractal simulation.

For this work we have used a fractal method based on the rainfall time-structure n-index (Monjo 2016). This method is a two-step process that combines transfer functions and stochastic generation of synthetic hyetographs for individual rainfall events, alternating with realistic dry episodes.

Firstly, probability distributions are computed for five main features extracted from the daily and sub-daily wet/dry spells, i.e. statistics for each rainfall event or dry event at 1-day and 5-min time resolution. These five features are: Precipitation amount (p), reference intensity (I_o), n-index of wet spells (n), duration of wet spells (t_w) and duration of dry spells (t_d).

In this first step, theoretical transfer functions are fitted for the quantile mapping ($Q_{d\to s}$) between daily ($\pi_d(v_{id})$) and sub-daily ($\pi_s(v_{is})$) probability values of each feature $v_i \in (p, I_o, n, t_w, t_d)$.

$$v_{is}' = Q_{d\to s}(v_{id}) \equiv \pi_s^{-1}\left(\pi_d(v_{id})\right) \qquad \text{Eq. 13}$$

where v_{is}' is the simulated sub-daily feature v_i from the daily value v_{id}'.

The selected theoretical functions $Q_{d\to s}$ are mainly logarithmic (log-normal distribution) and log-logarithmic (Gumbel distribution), especially for p, I_o, t_w and t_d. For n-

index, trigonometric functions have been chosen due to its natural range (between 0 and 1).

Regarding the second step, it corresponds to a stochastic generation of sub-daily time-series alternating synthetic hyetographs of individual rainfall events and fractal succession of dry episodes. For this purpose, the simulated sub-daily features (v_{is}') are used for the simulation of each sub-daily time-series.

2.2.6. Derived variables

Snowfall estimation

One of the most complicated hydrometeors to measure is the snowfall. The classification of precipitation according to its phase state requires remote sensors (radars), very expensive instruments (disdrometers) or observers of meteorology. In addition, the measures of snow depth (e.g. with snow gauge & pillow) present a great uncertainty due to the blizzards and the rapid fusion in some events.

Therefore there is a great shortage of data available on snowfall, which makes climate studies difficult. In order to estimate the impacts of climate change on snow, the frequency and amount of snowfalls have been estimated by using the derived method of Redolat (2014). This method is an effective way to simulate days of snow taking into account daily thresholds of only three surface variables: precipitation, maximum and minimum temperature.

The thresholds considered for this study have been 0.1 mm for precipitation, 0°C for minimum temperature and 9°C for maximum temperature. Those days whose daily maximum and minimum temperatures are below the thresholds and, in addition, precipitation have been registered are considered as days of snowfall. In the same way, the total amount of precipitation registered those days is considered as *snow water equivalent*. It is important to highlight that this simulation gives the amount of snow falling, not lying on the ground.

It has been obtained a snowfall simulation for each observatory considered. Furthermore, two historical simulations have been obtained. One of them was calculated by using temperature and precipitation data from the downscaled re-analysis ERA-Interim and the second one by using the same data but having previously applied a bias-correction (Sec. 2.2.2) in order to obtain more accurate values for the variables studied.

Potential evapotranspiration

Potential evapotranspiration simulations have been calculated by using a version of the Hargreaves approach. It computes the monthly reference evapotranspiration (ET_0) of a grass crop based on the original Hargreaves equation (Hargreaves, 1994).

This original equation considers maximum temperature (T_x), minimum temperature (T_n) and extraterrestrial radiation (RA) as parameters. If radiation data are not available it can be estimated from the latitude and the month of the year. The equation used for this study is a modified form due to Droogers and Allen (2002) that also includes total precipitation (P) as parameter:

$$ET_0 = 0.0013 \cdot 0.408\, RA \cdot \left(\left(\frac{T_x+T_n}{2}\right) + 17\right) \cdot \left((T_x - T_n) - 0.0123 \cdot P\right)^{0.76} \quad \text{Eq. 14}$$

The potential evapotranspiration has been calculated in a daily basis and aggregated monthly afterwards.

2.3. Uncertainty analysis

2.3.1. Verification of the methodology

The performance of all used methods were analysed comparing the observed and the simulated-by-reanalysis time-series for a past reference period (verification process). Particularly, the common time period between observations and ERA-Interim reanalysis is 1979-2015.

The mean absolute or relative error (MAE and MRE) were estimated for most of climate variables as main measure of the method performance for reproducing the day-to-day weather variability. This analysis is important because the physical forcings of each climate variable should be adequately captured for the used method in order to detect possible changes in their intensity of frequency of occurrence.

Ranking Probability Score (RPS) was calculated for precipitation simulation to compare the method ability respect to two reference predictions: *persistence* and *climatology*. The *persistence* is a prediction based on the observations from the previous day, while the *climatology* is the prediction based on the climatic average for each day of the year.

In a similar way, the Standardised mean Absolute Error (SAE) is estimated for decadal simulations comparing their MAE with the obtained one from the *climatology* forecast.

Finally, the Kolmogorov-Smirnov (KS) test was applied to analyse the statistical significance of the similarity of the simulated probability distributions respect to the observed ones (Marsaglia *et al.* 2003). This test is useful for measuring the method ability to reproduce not only the mean distribution but also the extreme values. The KS test was also applied to measure the good performance of the bias correction (Sec. 2.2.2).

2.3.2. Validation for the CMIP5 models

Validation process consists of evaluating the performance of applying the selected method to each climate and decadal model. Unlike the reanalysis, a *historical experiment* of a climate model does not try to reproduce the real day-to-day weather evolution in the reference period, rather it tries to simulate the climate variability at daily scale. Therefore, the errors obtained from day-to-day comparison between time-series (as MAE, MRA and RPS) do not make sense. Alternatively, other statistics are commonly used to measure the good reproducing of the climate averages and variability.

One of the main statistics for a model is the *bias* of the mean and the standard deviation. For each climate variable, it is calculated as the average of the total error for each station. The *bias* is important because a model should adequately reproduce the spatial distribution of the climate average. That is, bias with high dispersion for a set of observatories could suppose a distortion of this regional variability and then an unrealistic reproduction of the main climatic features.

Nevertheless, the climatic averages are not sufficient to evaluate a climate model, but climate variability should be also evaluated throughout other statistics. In this

sense, the non-parametric KS test is useful for measuring the distance between two probability distributions taking into account the entire distribution. Therefore, the KS *p*-value indicates if two distributions are indistinguishable (particularly, we use *p*-value > 0.05).

Because observed time-series present gaps, and in order to perform the comparison between instrumental data and the historical experiment (1950-2005) of each model, observations were extended/filled using the corrected downscaled Era-Interim re-analysis (1979-2015) (see Sec. 2.2.2). As a result of this procedure, *extended observations* were obtained for the validation process and, therefore, the common period was 1979-2005.

Remark: Regarding the decadal simulations, it is important to indicate the different considerations between the both used approaches: Firstly, drift-corrected outputs are validated according the performance of each downscaled model, but the used method cannot be verified because there is no decadal re-analysis (to which to apply the drift-correction). Secondly, the teleconnection-based approach is verified as a method applied to the past, but it is not considered a validation process because there are no decadal models in the same sense than the previous cases.

2.3.3. Projection uncertainty

The cascade of uncertainties in climate simulation at local scale is given by four main sources: (1) The used statistical downscaling method [verification process], (2) The model/run selection and the method/model performance [validation processes], (3) the RCP scenarios considered, and (4) the climate natural variability.

The last two uncertainty sources have been treated by using the ensemble strategy. That is, once bias-correction is applied to all models, a combination (ensemble) of those models provides an estimation of the uncertainty caused by the (past and future) climate variability. An ensemble is performed for each RCP scenario in order to evaluate the effect of the possible future economies. All climate projections are performed on absolute and relative changes for the yearly averages and the seasonal cycle.

Note that climate projections are not considered forecasts because they are simulated under several RCP scenarios, whose probability is not easy to determine because it depends on the decisions made by politicians and citizens. Nevertheless, decadal simulations are considered forecasts because, although they are performed under the RCP4.5, these simulations reflect the predictable natural variability (which is in the same order of magnitude or higher than the changes projected under the different RCPs).

The ensemble of projections (climate) and predictions (decadal) are represented by using uncertainty areas. Particularly, it is considered as the 10th–90th percentile values and the median value for each year-horizon, calculated from all stations and models validated for each climate variable (Fig. 7).

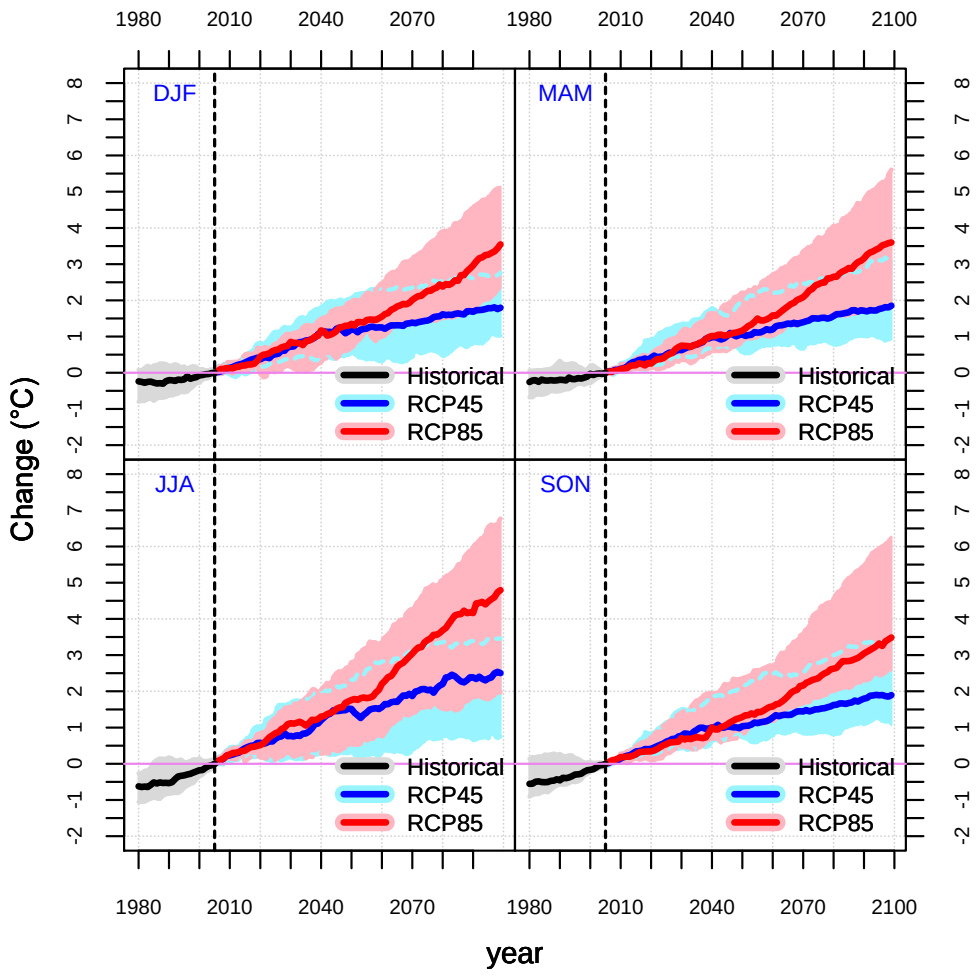

Figure 7. Example of ensemble strategy. Panel shows seasonal climate projections of changes in temperature for a random city. The ensemble median (solid lines) and the 10th–90th percentile values (shaded areas) are displayed. The vertical dashed line marks the end of the Historical data (2005).

3. Results of verification and validation

3.1. Verification of the downscaling methods

3.1.1. About this

Section 3.1 presents the results of the verification carried out for all the statistical downscaling methods described in Sec. 2.2.1 and 2.2.2, and used to generate the long-term climate projections. In general terms, the verification process of a method is based on comparing the simulation obtained for the past climate and real observations of this climate. In this study, as it is described in Sec. 2.3.1, the past climate is simulated by the downscaled ERA-Interim reanalysis.

Results of verification are structured in three subsections according to the studied cities (Barcelona, Lisbon and Bristol) and their surrounding areas. In turn, each subsection enumerates the verification of all climate variables simulated by the downscaled ERA-Interim reanalysis.

Due to the importance of the hydrological issues in RESCCUE, the uncertainty measures for precipitation and temperature are presented more detailed than compared to the other climate variables. Finally, Sec. 3.1.5 summarises the main results of the verification process for all the variables and cities.

3.1.2. Barcelona

3.1.2.1. Temperature

Daily maximum and minimum temperature

Verification process for maximum and minimum temperatures showed an accurate distribution of the climate averages for all stations corresponding to the metropolitan area of Barcelona and the Ter-Llobregat system, with bias lower than 0.2°C (Fig. 8 and Fig. 9). The MAE is generally lower than 1.5°C, which is acceptable given the high daily variability and the instrumental error (around 1°C).

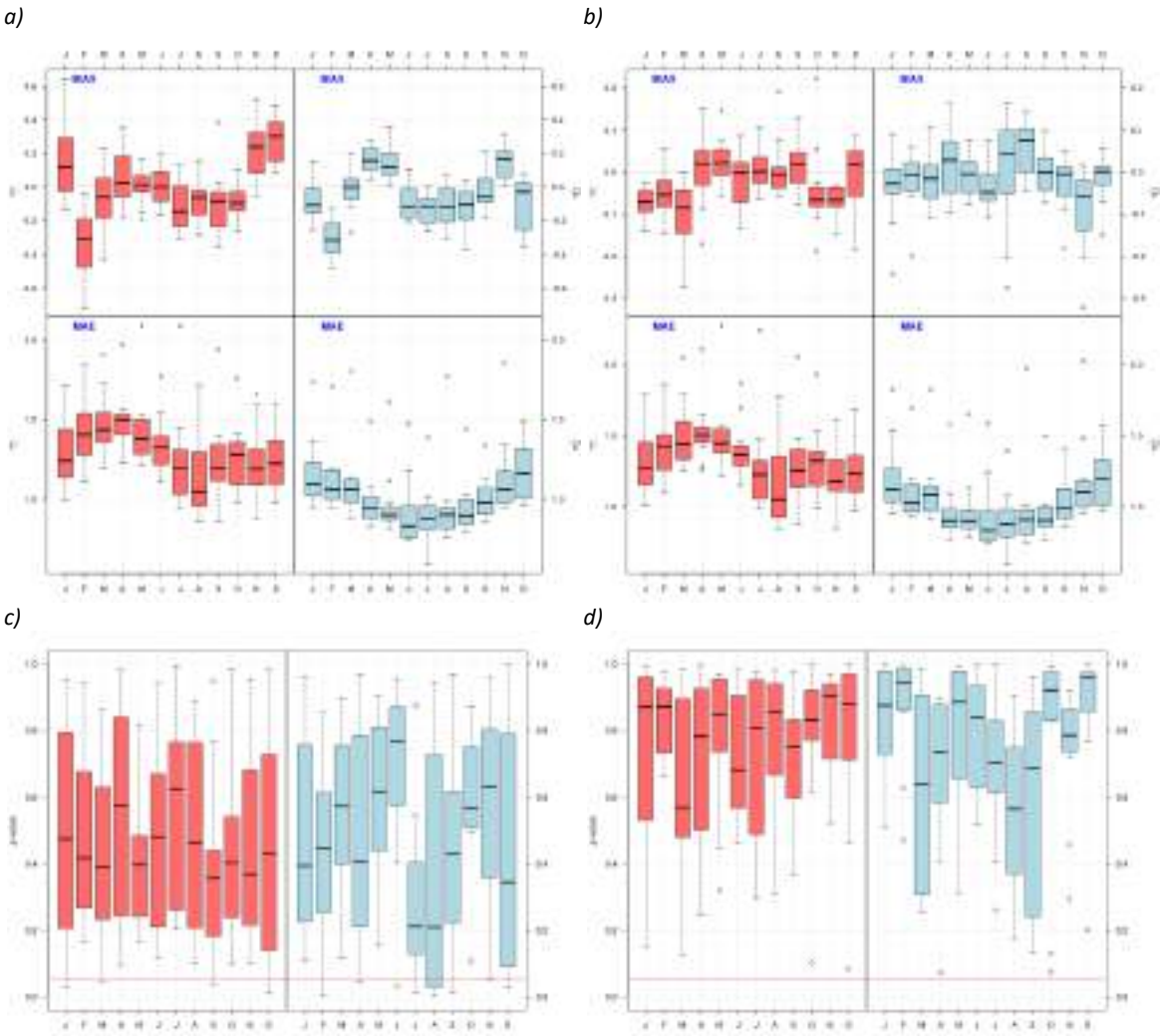

Figure 8. Verification results for temperature in Barcelona: Bias and MAE (*a*, *b*) and KS p-value (c, d) of the daily maximum (red) and minimum (blue) temperature simulated from the downscaled downscaled data of the ERA-Interim reanalysis, before (*a*, *c*) and after (*b*, *d*) the correction. Boxplots corresponds to the monthly means of Bias (*top*) and MAE (*bottom*). Box: 25th and 75th percentiles; whiskers: 5th and 95th percentiles.

a) *b)*

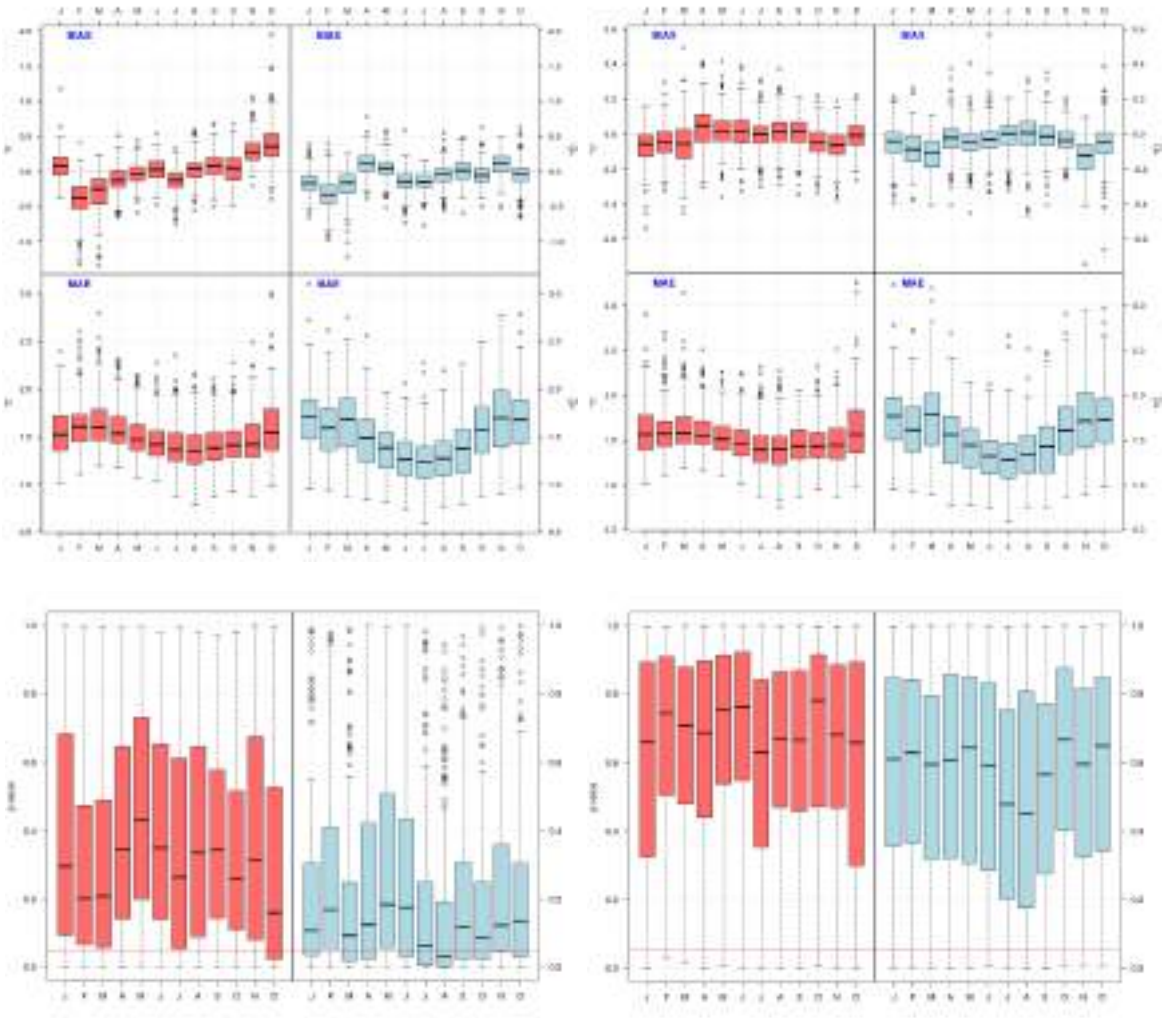

Figure 9. The same as Fig. **8** for Ter-Llobregat system.

Subdaily temperature

Verification process for subdaily temperature obtained good results in MAE (around 1°C in winter and 1.5°C in summer). Simulation passed the Kolmogorov-Smirnov test for the subdaily distribution during all months of the year (Fig. 10).

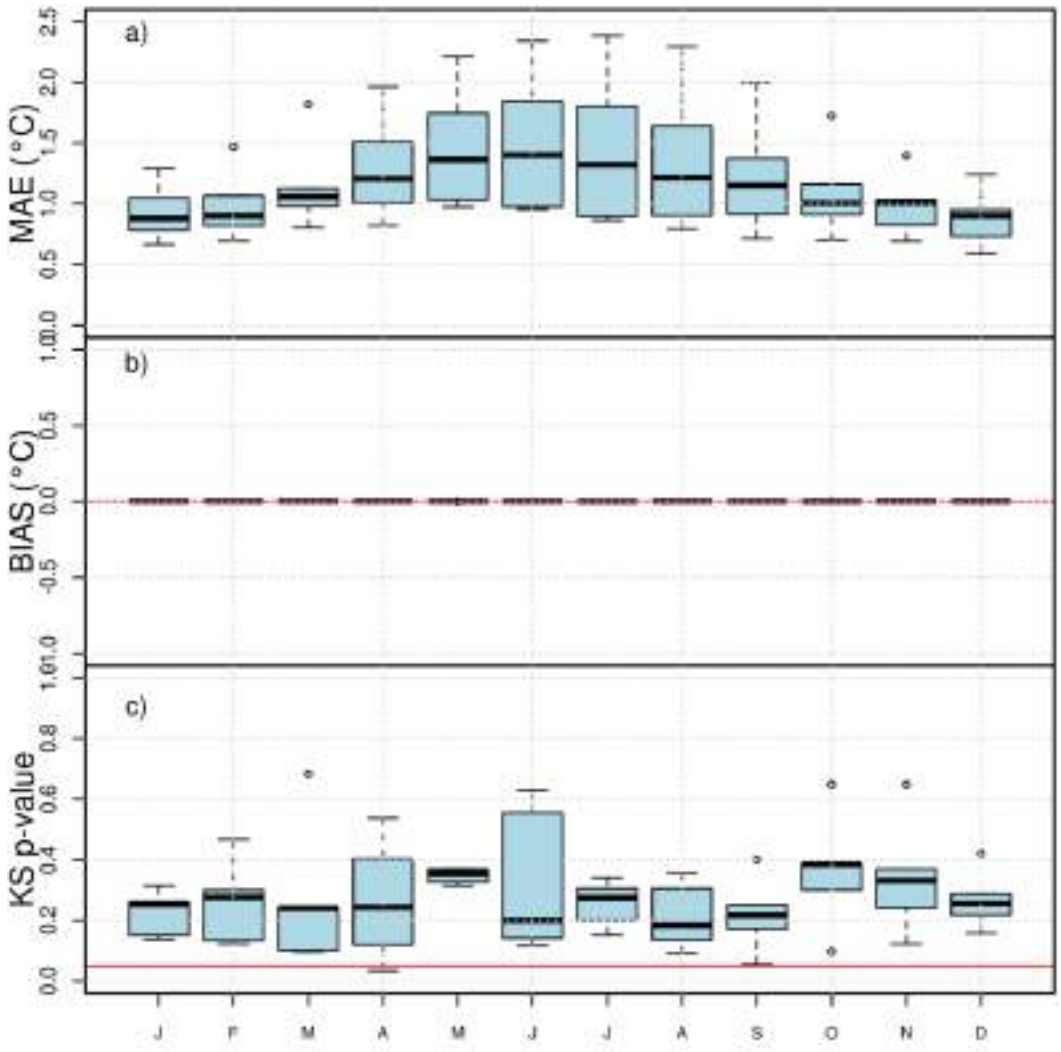

Figure 10. Verification results for sub-daily temperature in Barcelona: MAE (*a*), Bias (*b*) and KS p-value (*c*) for 5-min temperature simulated using the downscaled ERA-Interim reanalysis.

3.1.2.2. Precipitation

Daily precipitation

Verification process for precipitation showed an accurate distribution of the climate averages for all stations corresponding to the metropolitan area of Barcelona and the Ter-Llobregat system, with bias lower than 10% and acceptable KS p-values after correction of the systematic error (Fig. 11 and 12).

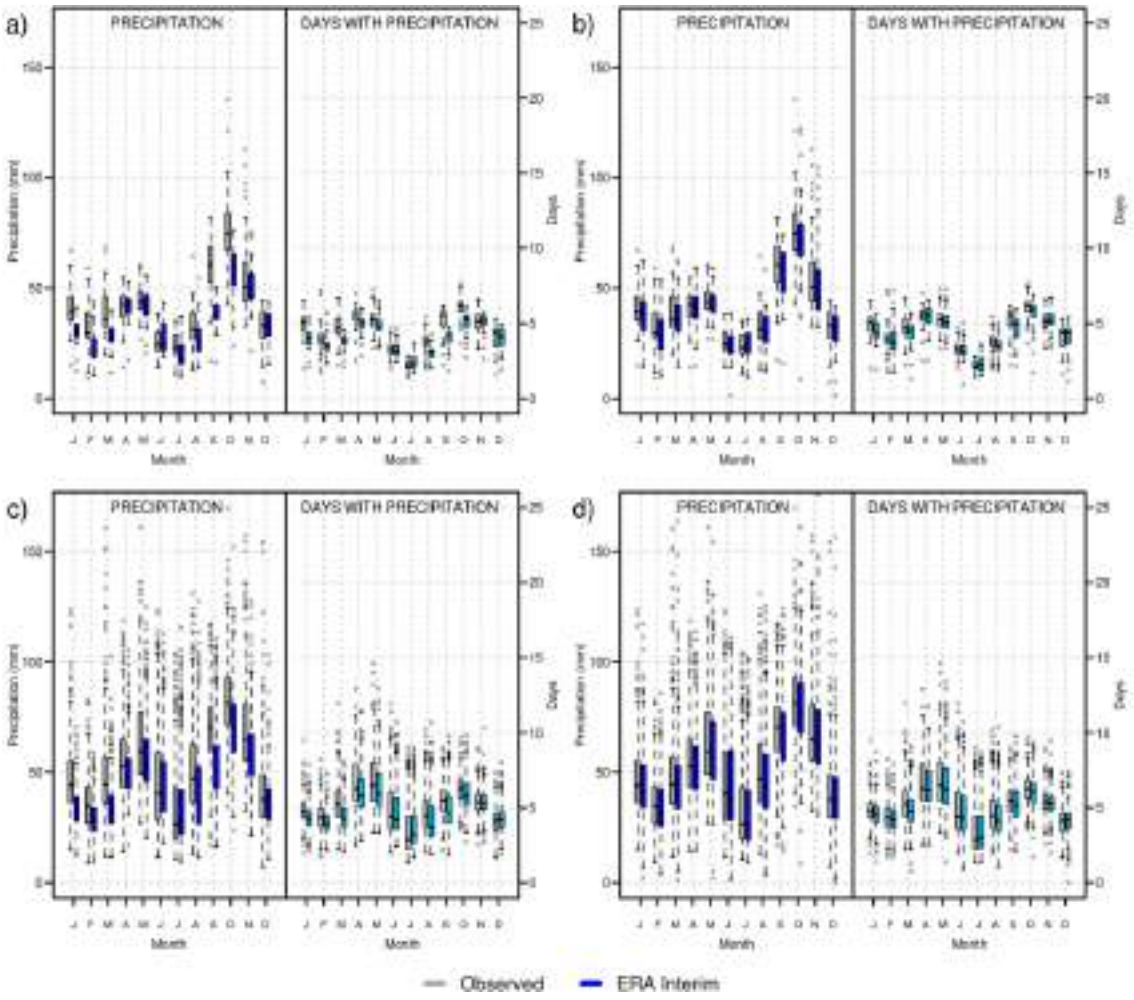

Figure 11. Verification results for daily precipitation in Barcelona: Monthly amounts (*left*) and wet days (*right*), observed (gray) and simulated (blue) using the downscaled ERA-Interim reanalysis for Barcelona (*a*, *b*) and Ter-LLobregat system (*c*, *d*), before (*a*, *c*) and after (*b*, *d*) the correction.

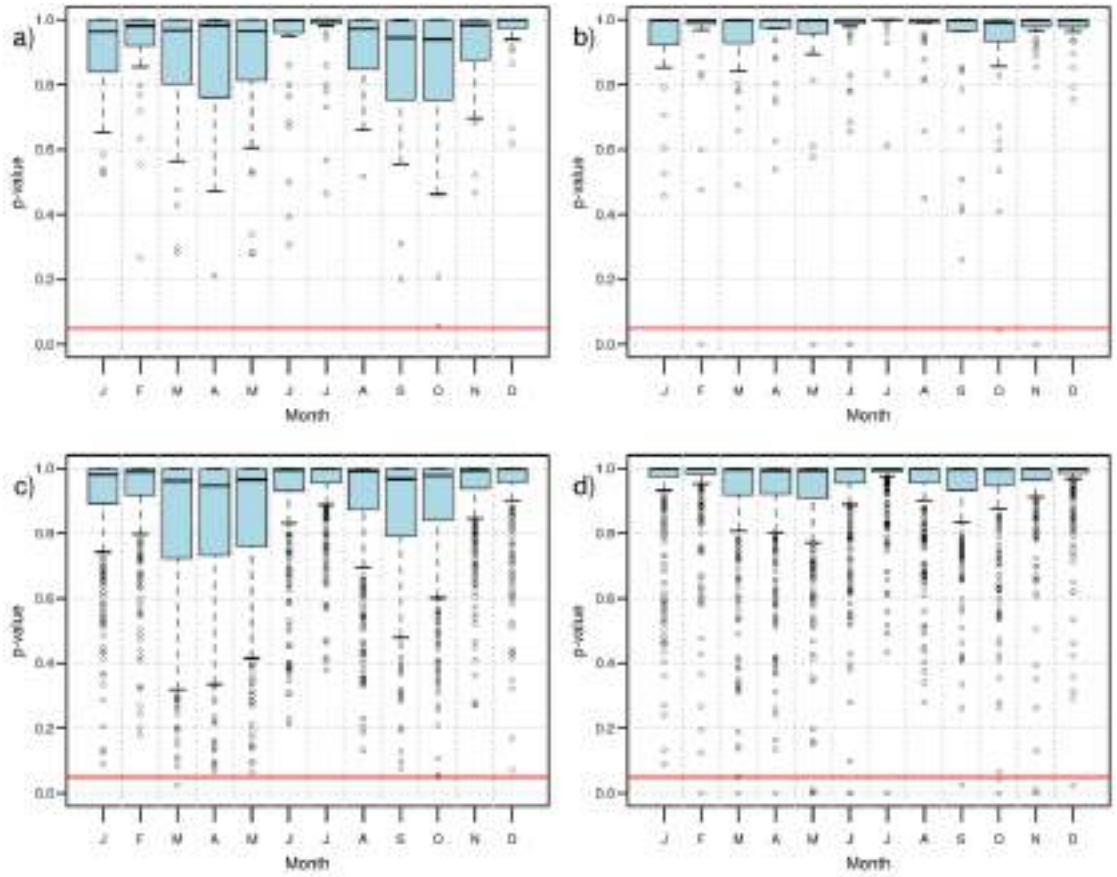

Figure 12. KS p-values for the simulated daily precipitation amount comparing with the observed data for Barcelona (a, b) and Ter-LLobregat system (c, d), before (a, c) and after (b, d) the correction.

Sub-daily precipitation

Results for 5-min precipitation showed an adequate reproduction of the probability distribution of the main six features of the sub-daily precipitation: precipitation amount, rainfall event n-index (n) and its reference intensity (I_0), dry spell length distribution, dry spell n-index and its corresponding reference maximum length. Kolmogorov-Smirnov p-value passed the 0.05 threshold for most of stations (Fig. 13).

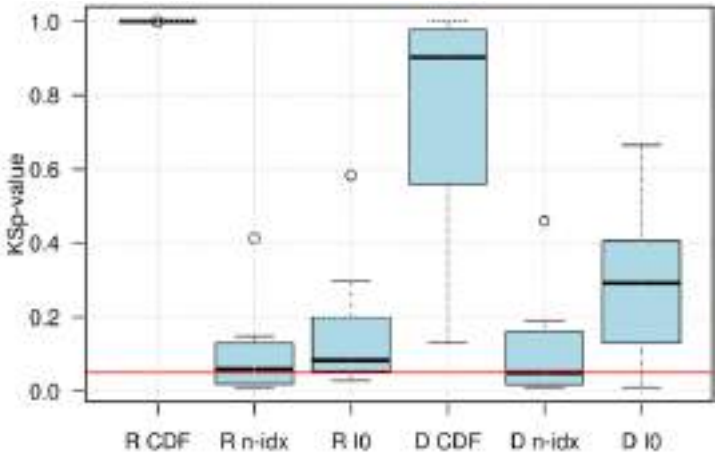

Figure 13. Verification results for sub-daily precipitation in Barcelona: KS p-value for the rainfall probability distribution (R CDF), rainfall event n-index (R n-idx), rainfall event reference-maximum-intensity (R I0), dry spell probability distribution (D CDF), dry spell n-index (D n-idx) and dry spell reference-maximum-length (D I0).

3.1.2.3. Other variables

Wind, relative humidity and pressure

The discussion for Barcelona and its watershed can be summarised here at the same time. The results are alike for both locations despite the greater number of stations considered for the Ter-Llobregat System. The verification statistics of wind, relative humidity and pressure can be seen in Fig. 14-15. It can be highlighted that, for both before and after the bias correction, the analogous output shows better results than the ERA-Interim direct output in all of the cases, with a lower MAE and an almost zero BIAS. Regarding the KS *p*-value, both corrected outputs showed a great upper significance level (p-value > 0.05), with the analogous output generally above ERA-Interim direct values. These results confirm that the analog method is a powerful tool to simulate accurately these variables.

Regarding the wind RPS, the boxplots corresponding to the analogues method gather the lowest RPS, improving notably the values from the climatology. Values from ERA method happen to be way bigger than climatology, which proves the inconveniency of the method. It can be concluded as well that the analogues method is better suidted for treating both Barcelona and its river basin data.

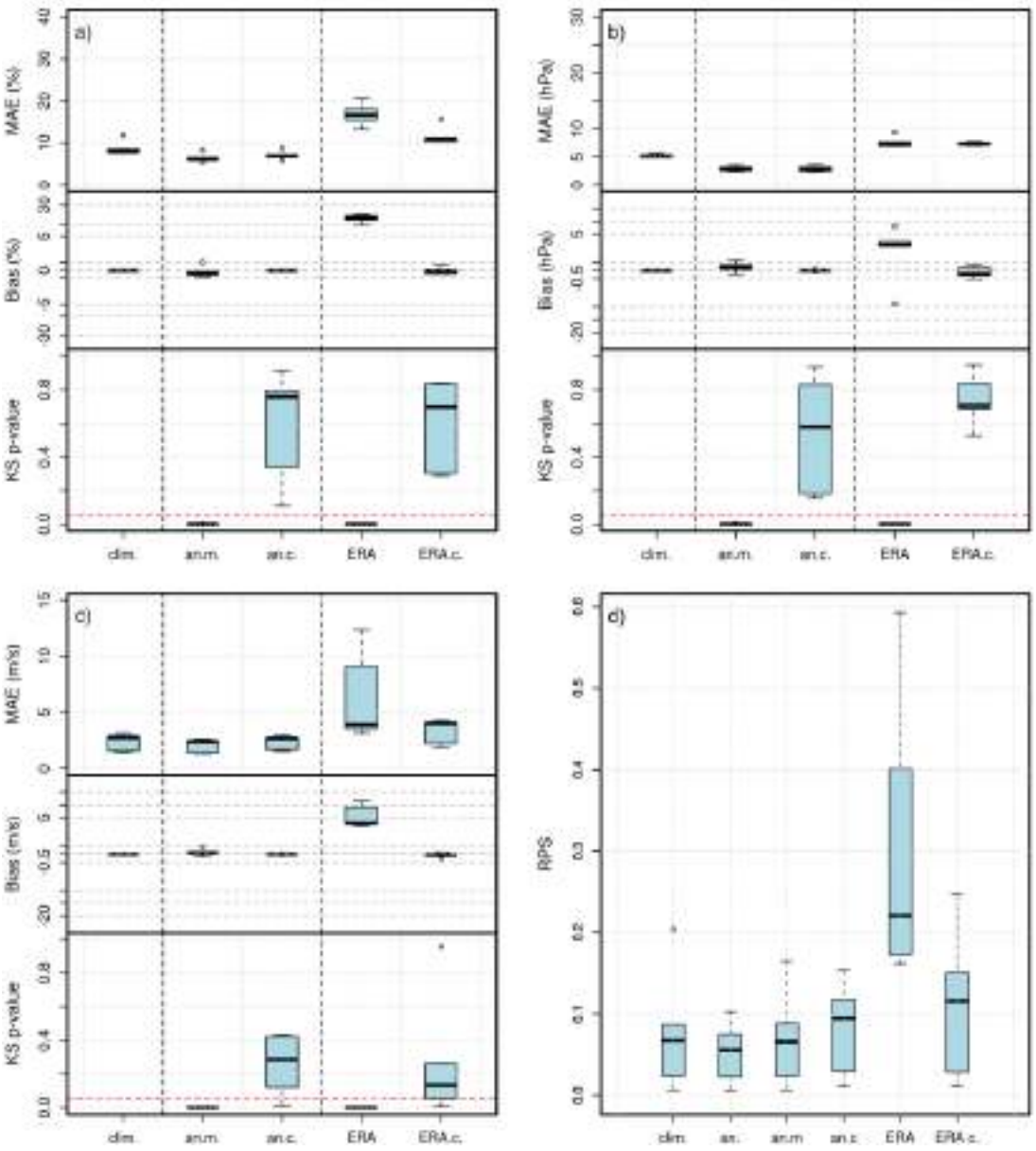

Figure 14. Verification results for other variables in Barcelona: a) MAE, Bias and KS p-value for the relative humidity simulation. b) MAE, Bias and KS p-value for sea level pressure simulation. c) MAE, Bias and KS p-value for wind simulation. d) RPS for wind simulation. Red lines are the 0 for Bias and 0.05 for the KS p-value. X-axis corresponds to: climatology simulation (*Clim*), 30-analogous ensemble (*30an*), 30 analogous mean (*an.mean*), corrected 30-analogous mean (*an.corr*), ERA-Interim direct output (*ERA*) and corrected downscaled ERA-Interim (*ERA.corr*).

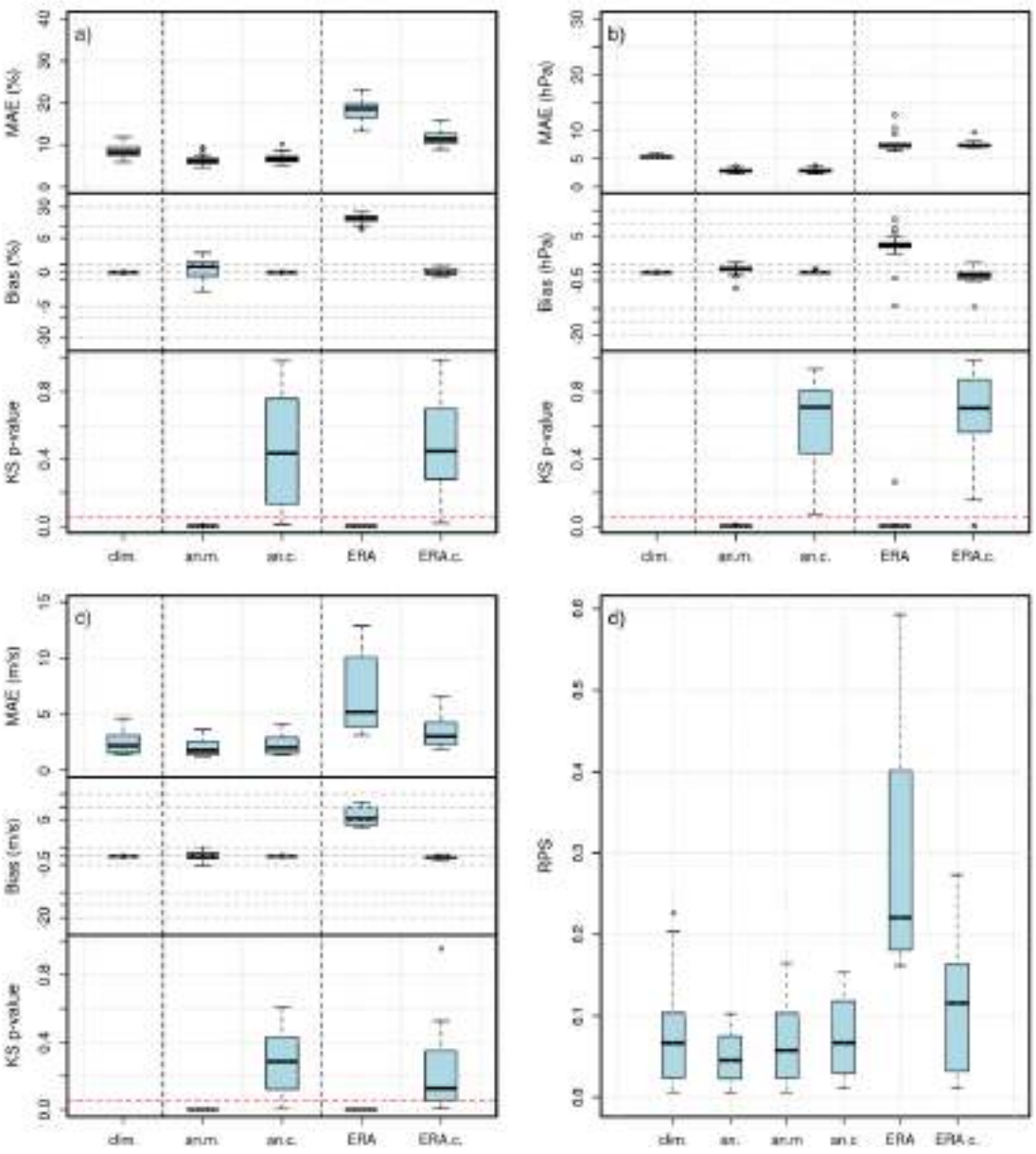

Figure 15. The same of Fig. 14 but for Ter-Llobregat System.

Oceanic variables: Wave height and sea level

The simulation of wave height presents a good result comparing with the simulation of reference *Climatology* (Fig. 16).

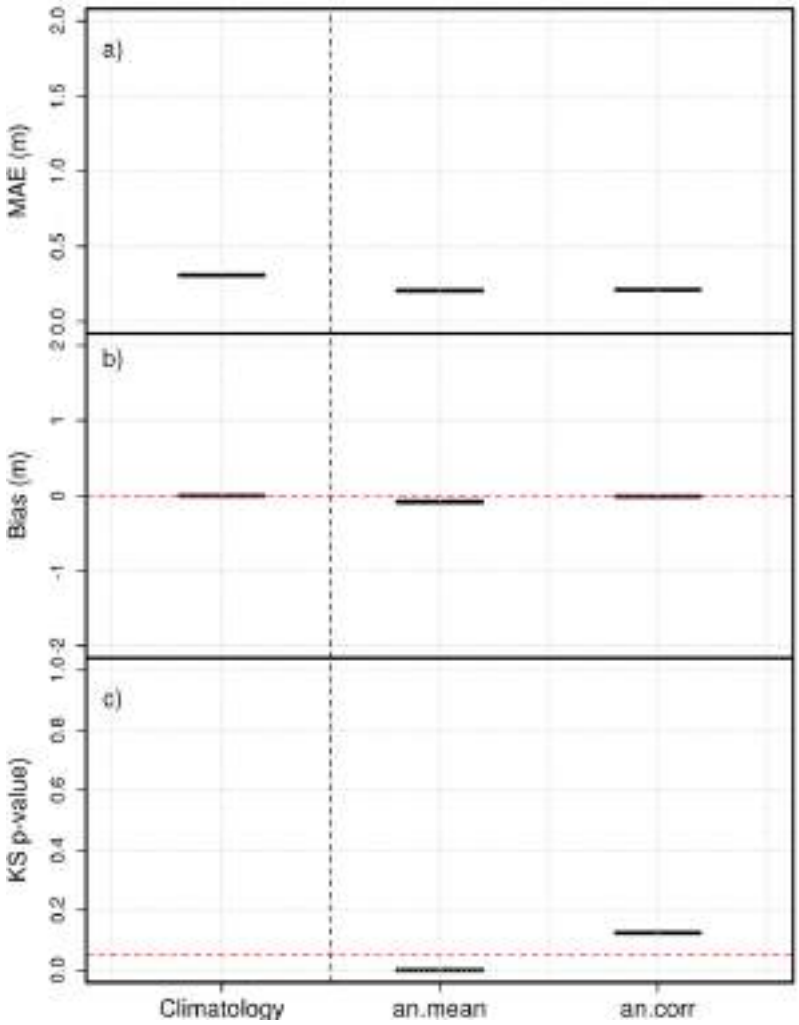

Figure 16. Verification results for the wave height in Barcelona buoy: *a*) MAE, *b*) Bias and *c*) KS p-value. X-axis corresponds to: climatology simulation (*Clim*), 30-analogous ensemble (*30an*), and 30 analogous mean (*an.mean*).

Sea level rise for Barcelona presents a high uncertainty in the past due to that sea level evolution depends on the considered source. Observations obtained from the Barcelona buoy show a light but significant increase of the sea level, while the GODAS re-analysis shows a statistically significant decrease.

The correction method used for the sea level rise obtained suitable results in the verification process. The standard deviation of the annual sea level values improved after correction (Fig. 17). Nevertheless, the observed trend sign cannot be corrected for the GODAS re-analysis nor climate models, because it could suppose a substantial modification of the used simulation.

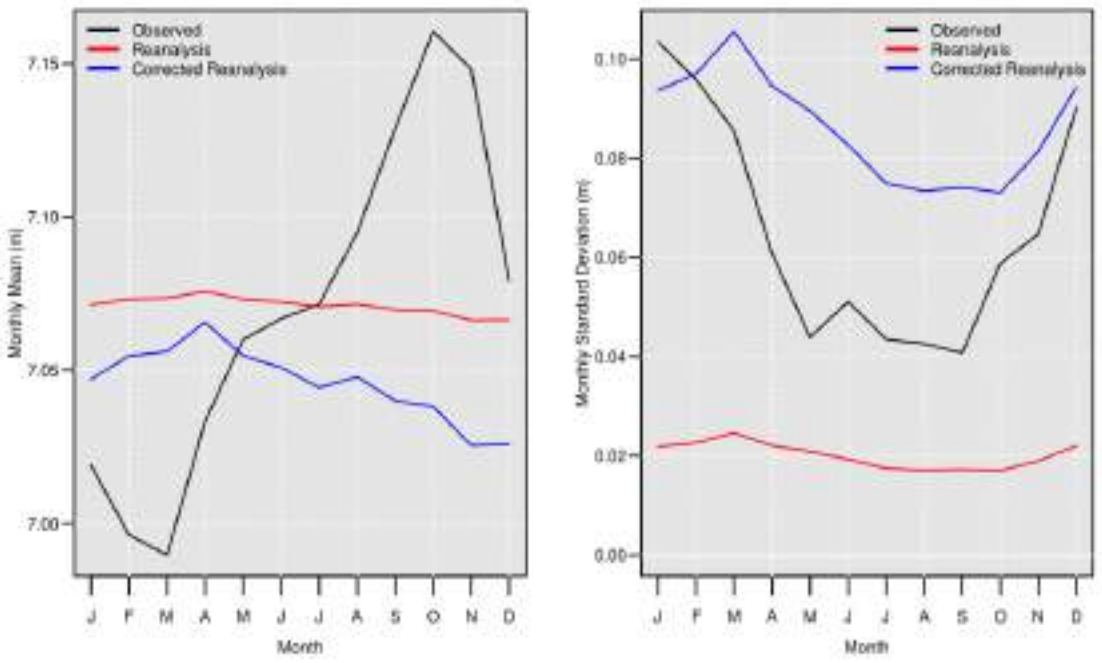

Figure 17. Verification results for the sea level variability in Barcelona buoy.

Derived variables: snowfall and evapotranspiration

The high number of stations considered in the region of Barcelona (Ter-Llobregat system) and their geographical spread have important consequences in the results obtained for snowfall simulations. Many of the stations are located along the coast line and others near the pre-Pyrenees mountains, so the difference in days of snowfall between the stations is remarkable.

Observatories located in the area of Barcelona city present an average of 0.1 days of snow per year in January (one day per decade) while some of the observatories close to the mountains can add up to 25 days of snow per year (Fig. 18).

The Mediterranean features of the region's climate are also reflected in the results: it presents high amounts of snow despite the few days of snowfall. This suggests that episodes of snowfall are rare but intensity of snowfall can be very high.

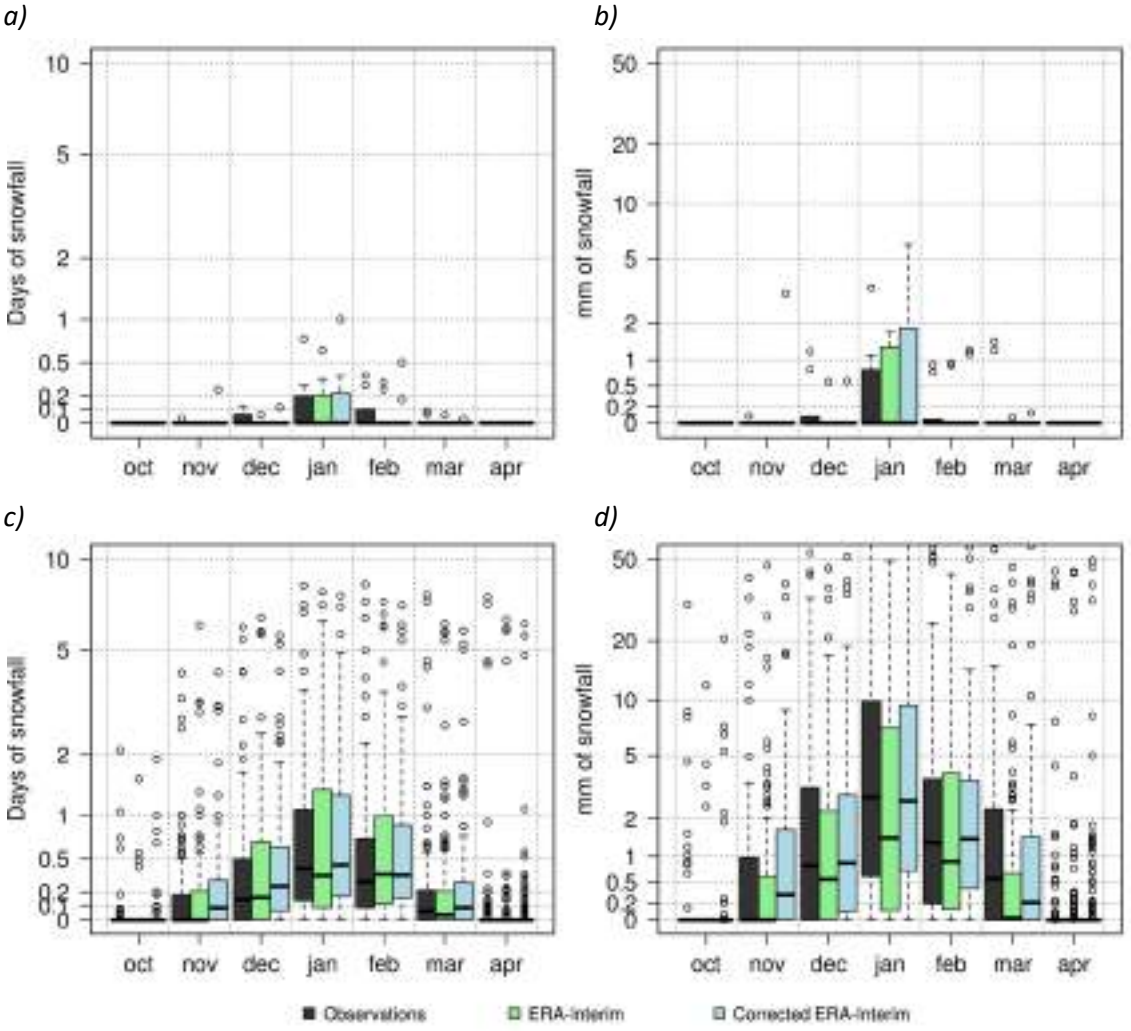

Figure 18. Verification results for snow simulation in Barcelona: Snowfall days (*left*) and snow water equivalent (*right*) per year in Barcelona (*top*) and in Ter-Llobregat System (*bottom*) according to observations and downscaled re-analysis.

Potential evapotranspiration, as expected, is higher in the summer, reaching an average of 130mm/month in July. On the other hand, it decreases in winter months up to 60mm/month in December and January (Fig. 19).

The dispersion observed in the figure is due to the different location of the observatories: those which are located on the coast or close to the mountains present a wetter and cooler climate than those which are on inland plains, so evapotranspiration is much lower in the first locations.

The verification results are remarkably consistent as differences between observations and ERA-Interim simulations are very small.

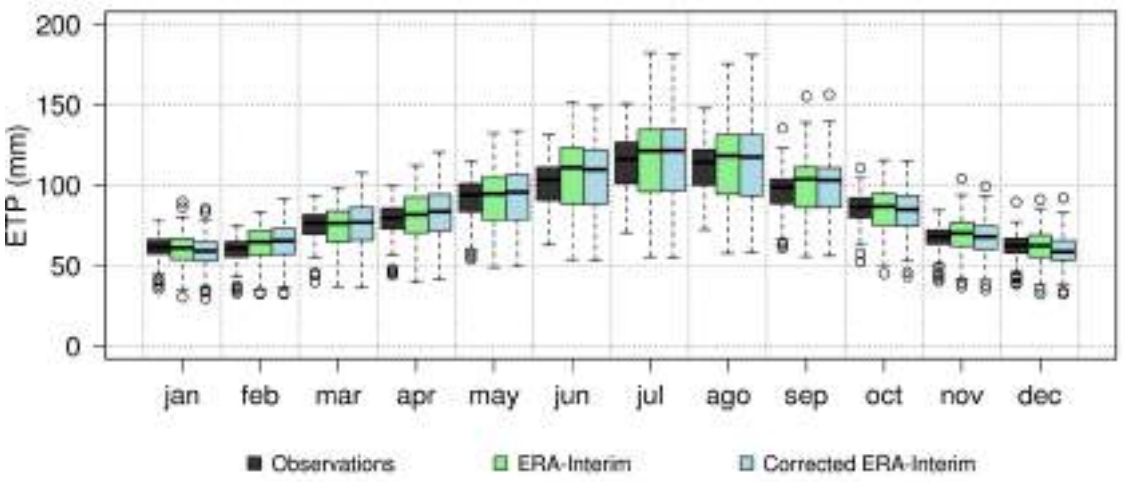

Figure 19. Verification results for potential evapotranspiration (mm per year) in Ter-Llobregat System: comparison between observations and simulations before and after the bias-correction.

3.1.3. Lisbon

3.1.3.1. Temperature

Daily maximum and minimum temperature

Verification process for maximum and minimum temperatures showed an accurate distribution of the climate averages for all stations corresponding to the metropolitan area of Lisbon, with bias lower than 0.2°C except December (Fig. 20).

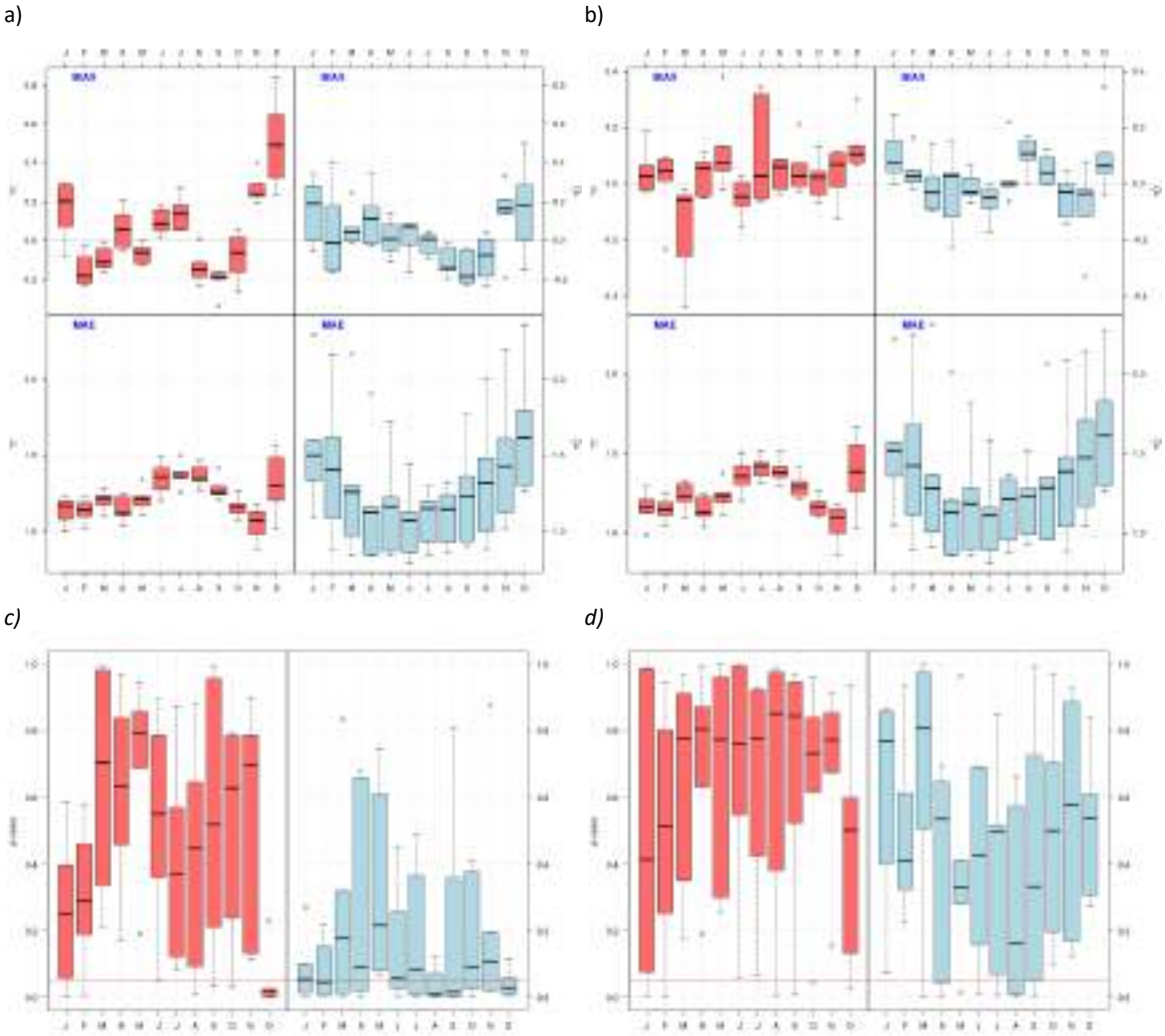

Figure 20. Verification results for temperature in Lisbon: Bias and MAE (*a*, *b*) and KS p-value (c, d) of the daily maximum (red) and minimum (blue) temperature simulated from the downscaled downscaled data of the ERA-Interim reanalysis, before (*a*, *c*) and after (*b*, *d*) the correction. Boxplots corresponds to the monthly means of Bias (*top*) and MAE (*bottom*).

Sub-daily temperature

As in Barcelona, verification process for sub-daily temperature in Lisbon obtained good results in MAE (around 1°C in winter and 1.5°C in summer). Simulation passed the Kolmogorov-Smirnov test for the sub-daily distribution during all months of the year (Fig. 21).

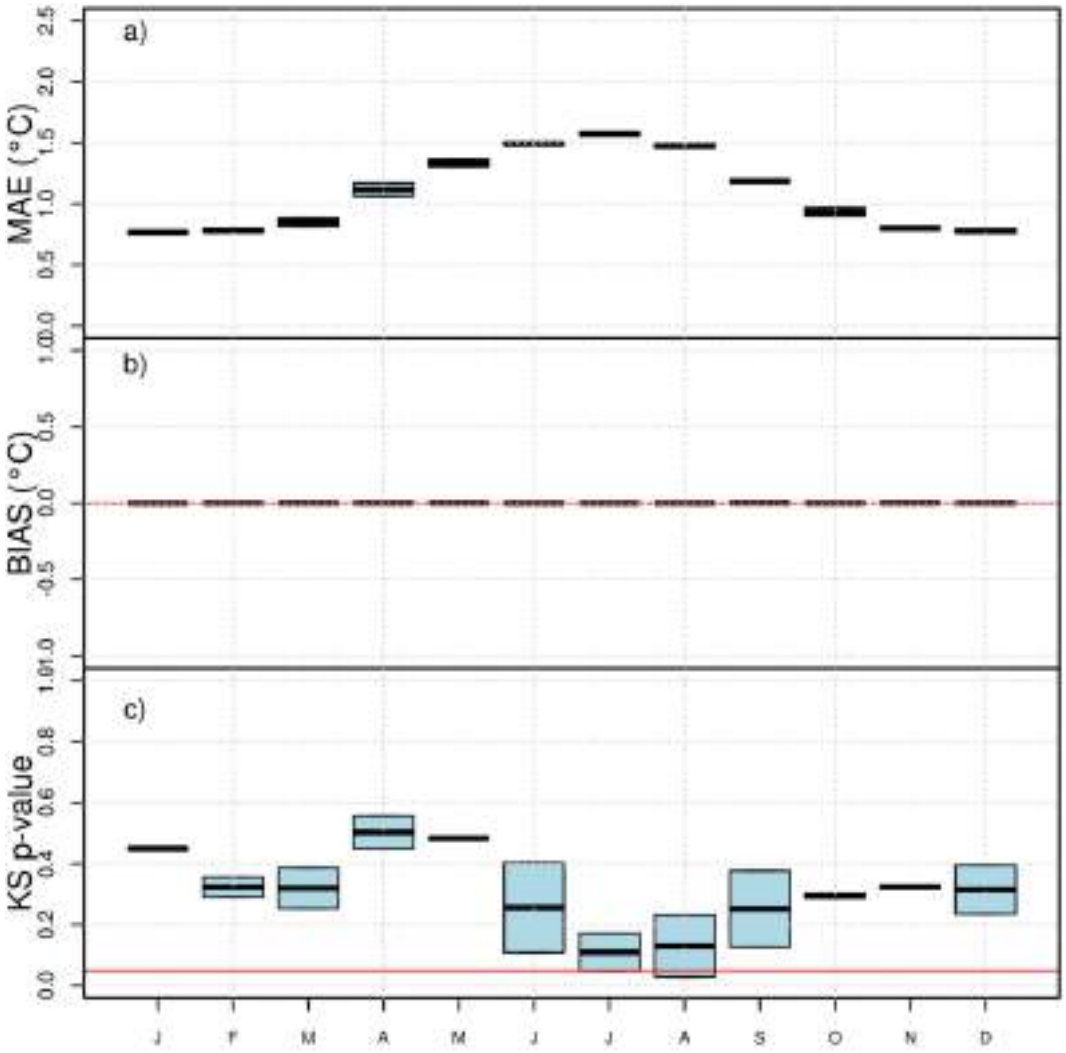

Figure 21. Verification results for sub-daily temperature in Lisbon: MAE (*a*), Bias (*b*) and KS p-value (*c*) for 5-min temperature simulated using the downscaled ERA-Interim reanalysis.

3.1.3.2. Precipitation

Daily precipitation

Verification process for precipitation showed an accurate distribution of the climate averages for all stations corresponding to the metropolitan area of Lisbon, with bias generally lower than 10% and acceptable KS p-values after correction of the systematic error (Fig. 22-23).

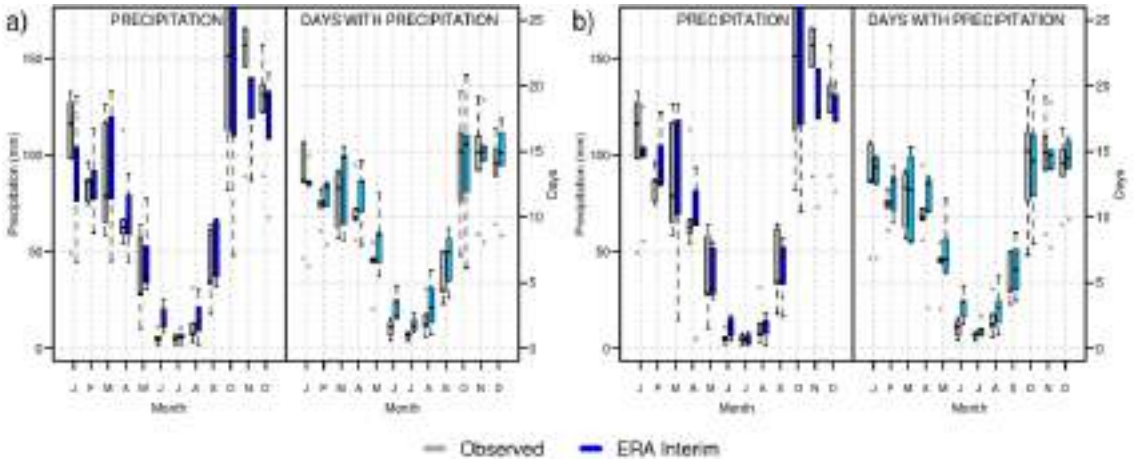

Figure 22. Verification results for daily precipitation in Lisbon: Monthly amounts (*left*) and wet days (*right*), observed (gray) and simulated (blue) using the downscaled ERA-Interim reanalysis, before (*a*) and after (*b*) the correction.

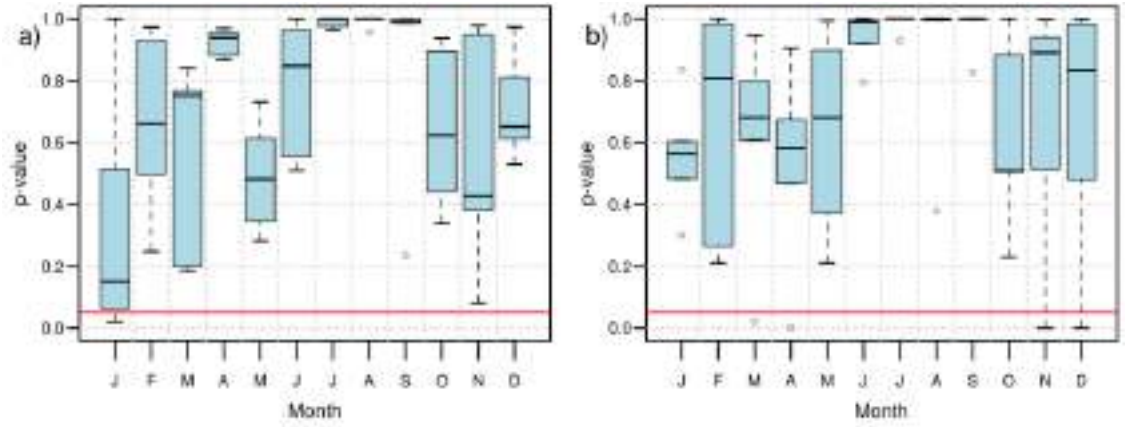

Figure 23. KS p-values for the simulated daily precipitation amount comparing with the observed data for Lisbon, before (*a*) and after (*b*) the correction.

Sub-daily precipitation

Results for 5-min precipitation showed an adequate reproduction of the probability distribution of the main six features of the sub-daily precipitation: precipitation amount, rainfall event *n*-index (*n*) and its reference intensity (I_0), dry spell length distribution, dry spell *n*-index and its corresponding reference maximum length. Kolmogorov-Smirnov *p*-value passed the 0.05 threshold for most of stations (Fig. 24).

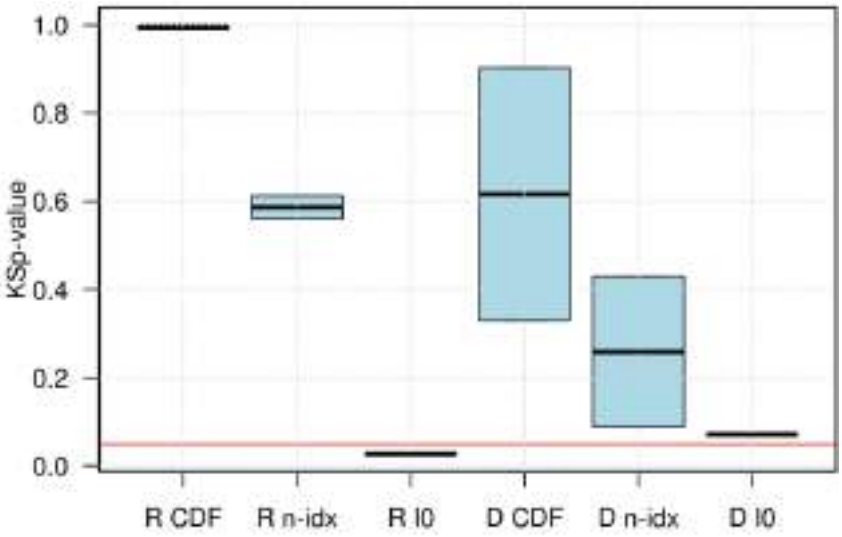

Figure 24. Verification results for sub-daily precipitation in Lisbon: KS p-value for the rainfall probability distribution (R CDF), rainfall event n-index (R n-idx), rainfall event reference-maximum-intensity (R I0), dry spell probability distribution (D CDF), dry spell n-index (D n-idx) and dry spell reference-maximum-length (D I0).

3.1.3.3. Other variables

Wind, relative humidity and pressure

The analog method presented better results than the ERA-Interim output for the wind, relative humidity and pressure, with a lower MAE (both before and after the bias correction) and an almost zero BIAS (Fig. 25). Regarding *p*-value, both methods show most of their values being upper significance level (*p*-value > 0.05), despite being one more dispersed than the other depending on the variable.

The RPS obtained for the wind is in accordance with the rest of statistics (Fig. 25c). The analog method presents the minimum RPS, in both its median and its dispersion. The mean of the analogous days, used as a predictor, also results to be better than the climatology (with the lower median), before and after correction. As the correction process is optimised for the climatic probability distribution, errors for day-to-day weather reproduction (e.g. MAE and RPS) are usually greater after correction. Despite this, considering the *p*-value associated to the Kolmogorov-Smirnov test, it can be concluded as well that the analog method suits the best for treating Lisbon data.

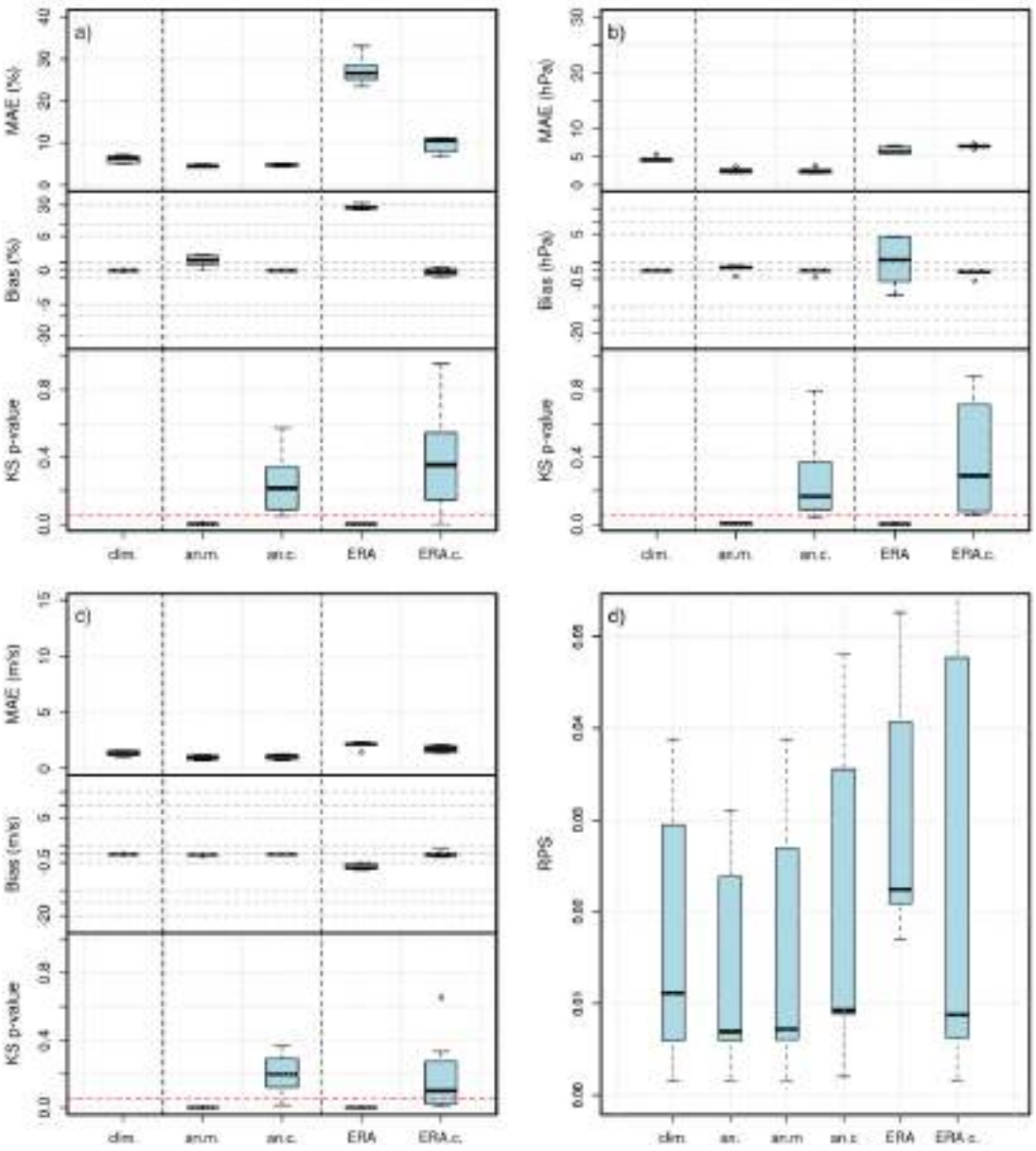

Figure 25. Verification results for other variables in Lisbon: *a*) MAE, Bias and KS p-value for the relative humidity simulation. *b*) MAE, Bias and KS p-value for sea level pressure simulation. *c*) MAE, Bias and KS p-value for wind simulation. *d*) RPS for wind simulation. Red lines are the 0 for Bias and 0.05 for the KS p-value. X-axis corresponds to: climatology simulation (*Clim*), 30-analogous ensemble (*30an*), 30 analogous mean (*an.mean*), corrected 30-analogous mean (*an.corr*), ERA-Interim direct output (*ERA*) and corrected downscaled ERA-Interim (*ERA.corr*).

Oceanic variables: Sea level

Sea level rise simulated using the corrected GODAS re-analysis showed a good performance for most of the statistical measurements. The seasonal mean values of the sea level (SL) were suitable before correction and they are improved after correction (Fig. 26). The standard deviation of SL obtained from the re-analysis was highly underestimated but the correction process produced a general improvement for all months, although winter is still underestimated. The corrected simulation presents a historical trend very similar to the observed one and therefore the confidence level of the simulation is very high. In fact, the confidence for Lisbon is the greatest comparing with Barcelona and Bristol.

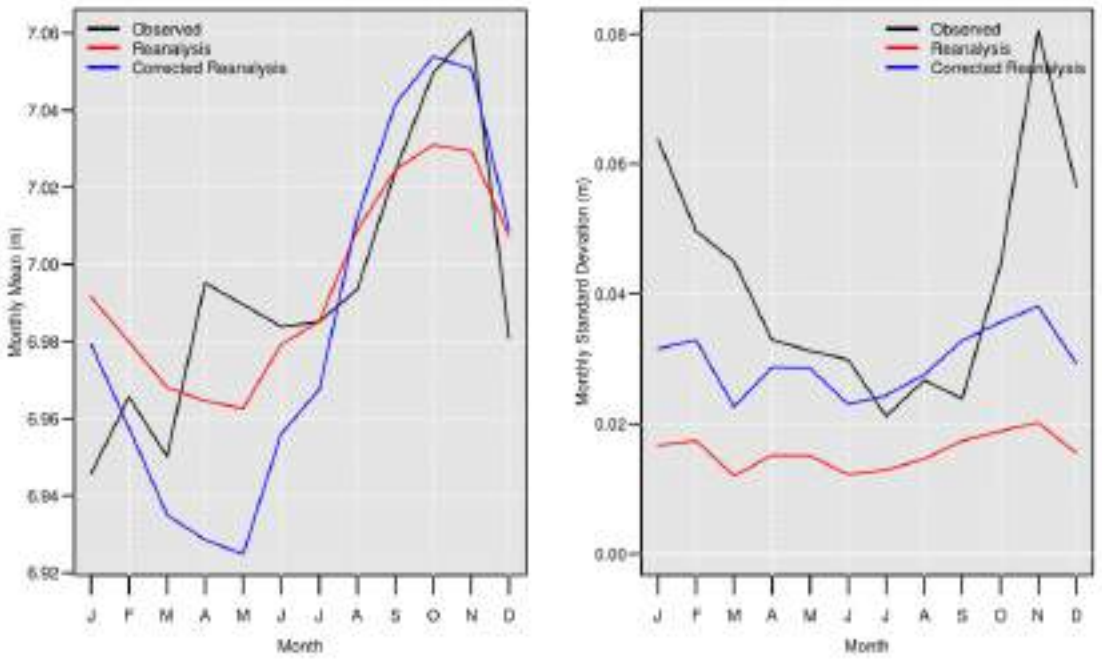

Figure 26. Verification results for the sea level variability in Cascais buoy: Comparison between observed and simulated sea level before and after correction

Derived variables: evapotranspiration

Evapotranspiration in Lisbon (Fig. 27) follows the same pattern as in Barcelona: about 60mm/month in winter and 120mm/month in summer. Values present a very low dispersion as only five observatories have been considered and their location is geographically identical.

The verification shows better results for summer months, presenting a slight deviation from October to May.

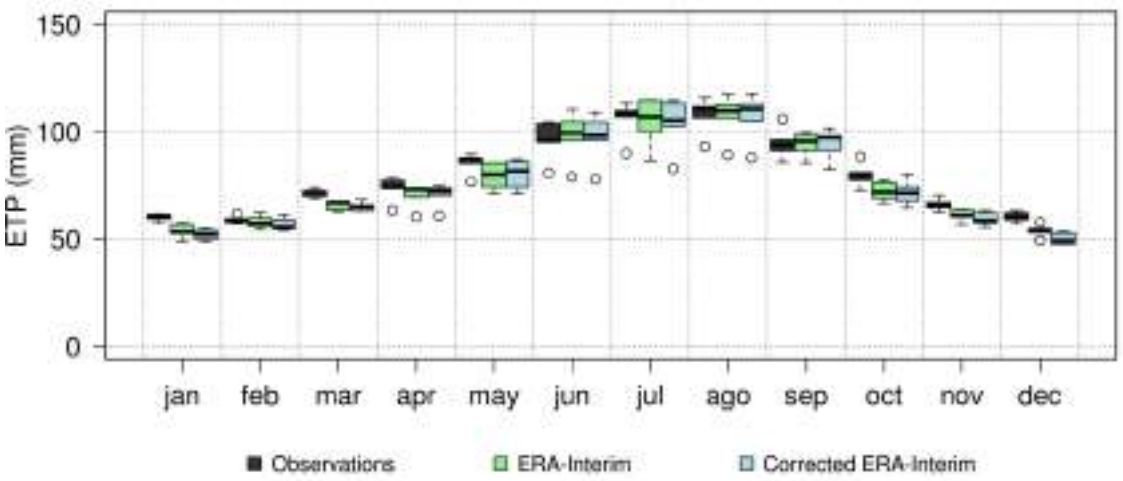

Figure 27. Verification results for potential evapotranspiration (mm per year) in Lisbon: comparison between observations and simulations before and after the bias-correction.

3.1.4. Bristol

3.1.4.1. Temperature

Verification process for maximum and minimum temperatures showed an accurate distribution of the climate averages for all stations corresponding to the metropolitan area of Bristol and the Southwest England – South Wales, with bias lower than 0.2°C (Fig. 28 and 29).

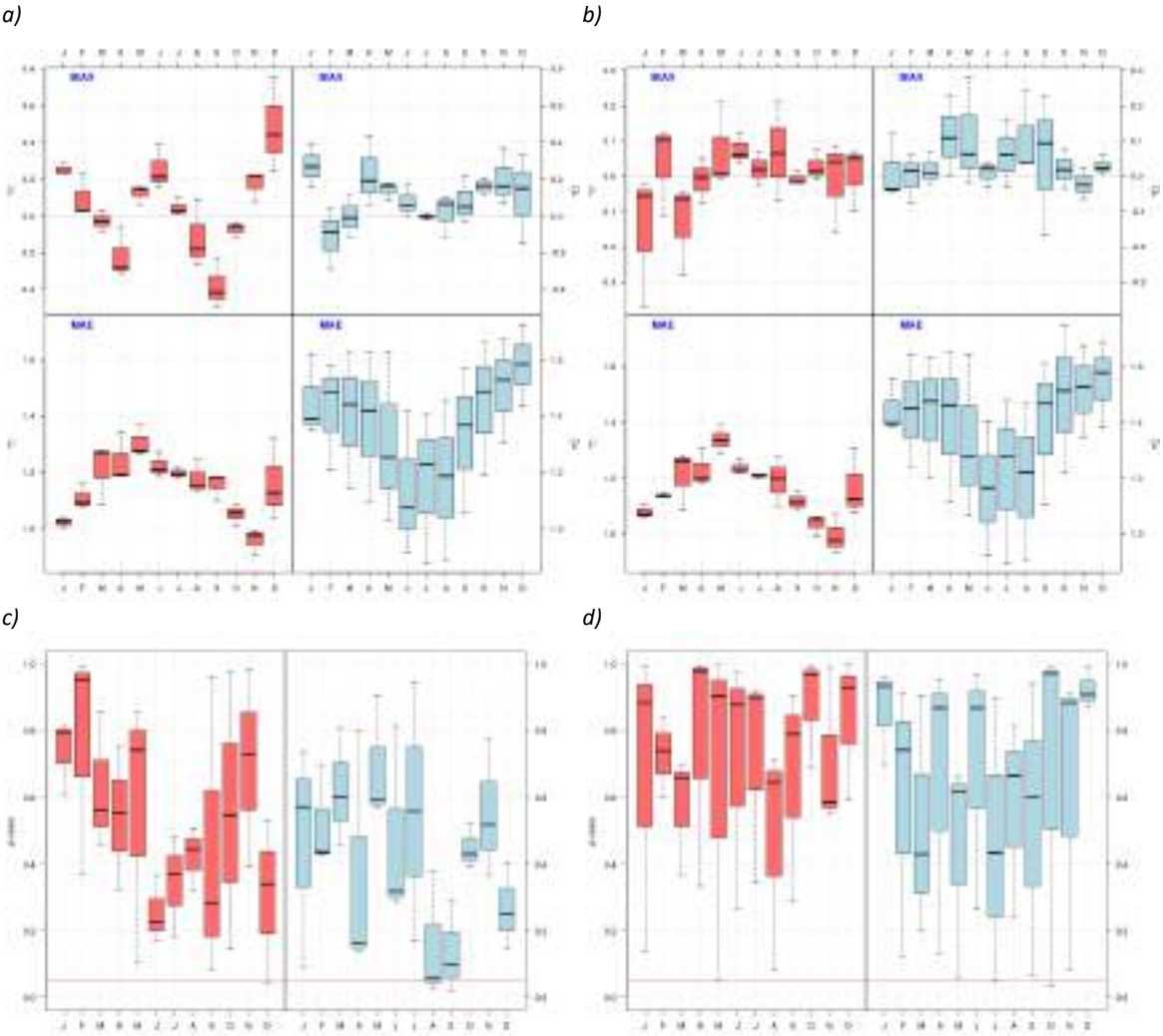

Figure 28. Verification results for daily temperature in Bristol: Bias and MAE (*a*, *b*) and KS p-value (*c*, *d*) for before (*left*) and after (*right*) the correction of the downscaled ERA-Interim reanalysis. Boxplots corresponds to the monthly means of Bias (*top*) and MAE (*bottom*) for the maximum temperature (left, red) and for the minimum temperature (right, blue) between the simulated and the observed data.

a) *b)*

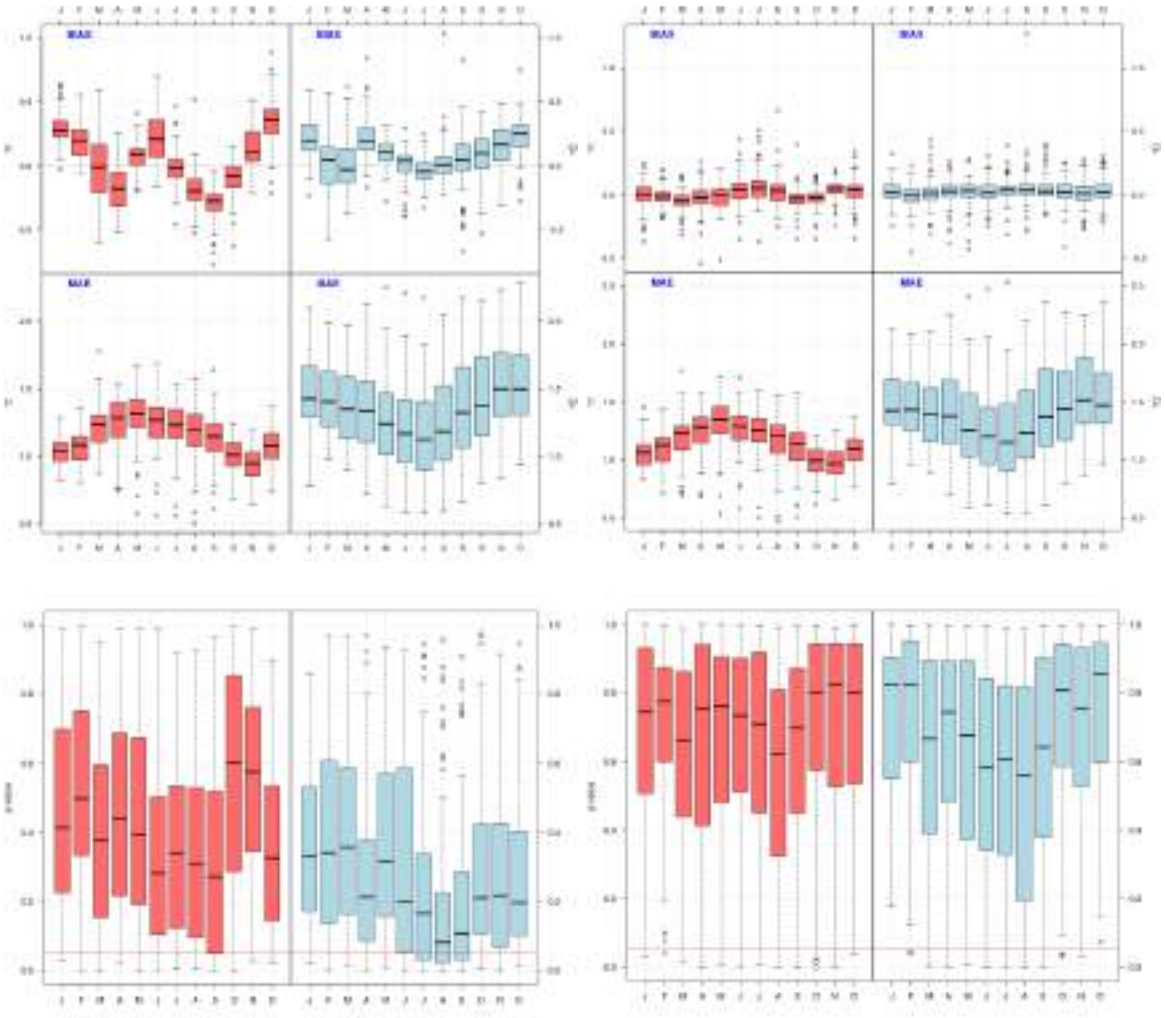

Figure 29. The same as Fig. 28 but for Southwest England – South Wales.

Sub-daily temperature

As in Barcelona and Lisbon, verification process for sub-daily temperature in Bristol obtained good results in MAE (around 1°C in winter and 1.5°C in summer). Simulation passed the Kolmogorov-Smirnov test for the sub-daily distribution during all months of the year (Fig. 30).

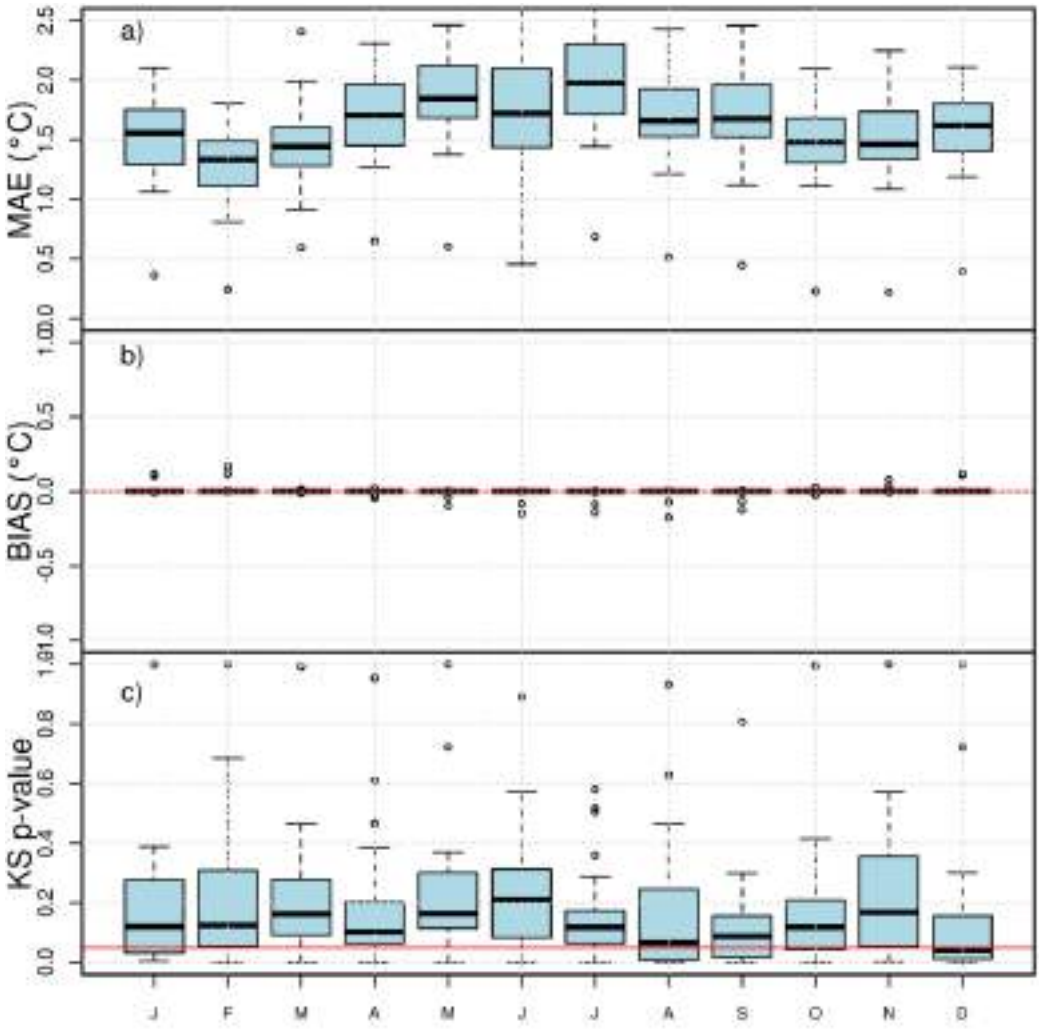

Figure 30. Verification results for sub-daily temperature in Bristol: MAE (a), Bias (b) and KS p-value (c) for 5-min temperature simulated using the downscaled ERA-Interim reanalysis.

3.1.4.2. Precipitation

Daily precipitation

Verification process for precipitation showed an accurate distribution of the climate averages for all stations corresponding to the metropolitan area of Bristol and Southwest England – South Wales, with bias generally lower than 20% and acceptable KS p-values after correction of the systematic error (Fig. 31-Figure 32).

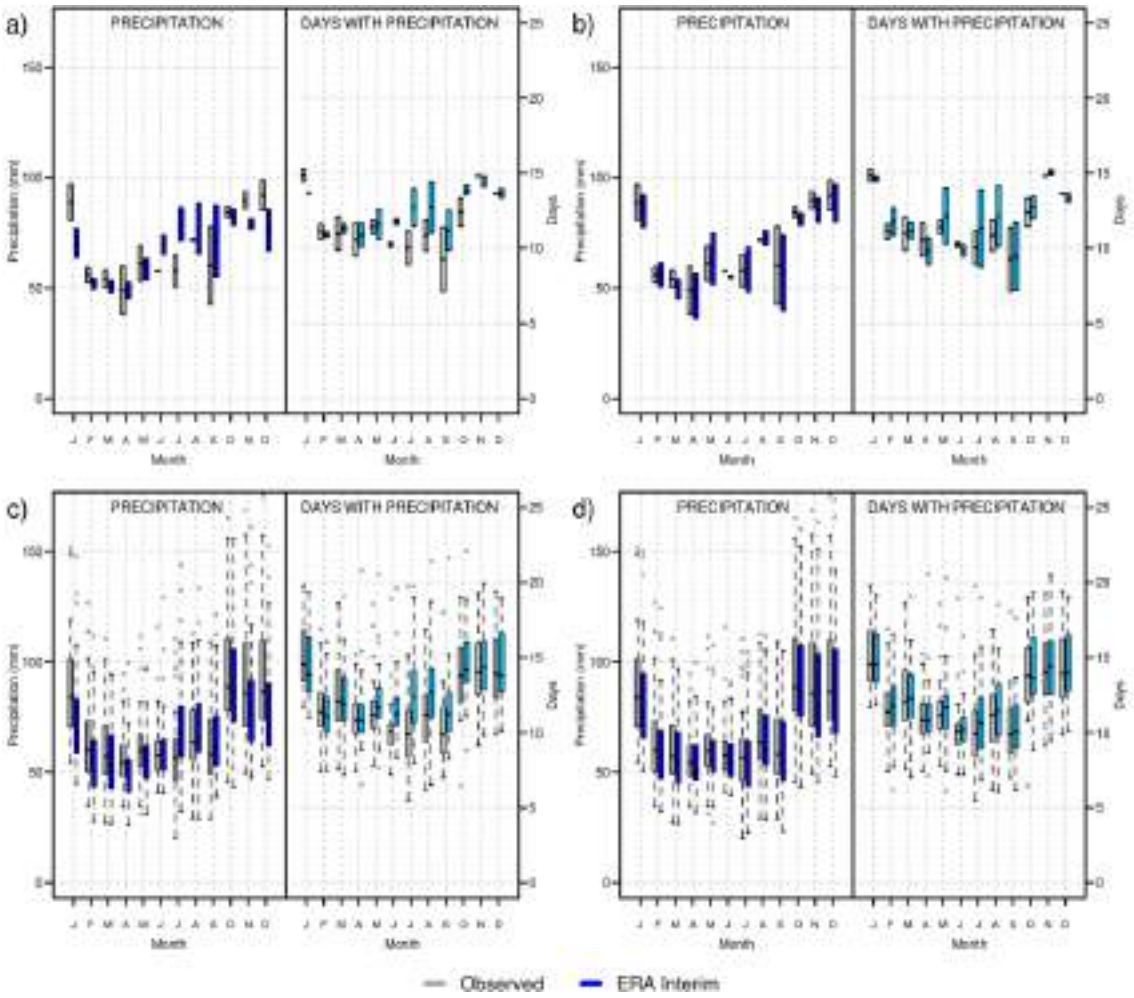

Figure 31. Verification results for daily precipitation in Bristol: Monthly amounts (*left*) and wet days (*right*), observed (gray) and simulated (blue) using the downscaled ERA-Interim reanalysis for Bristol (a, b) and Southwest England – South Wales (*c*, *d*), before (a, c) and after (*b*, *d*) the correction.

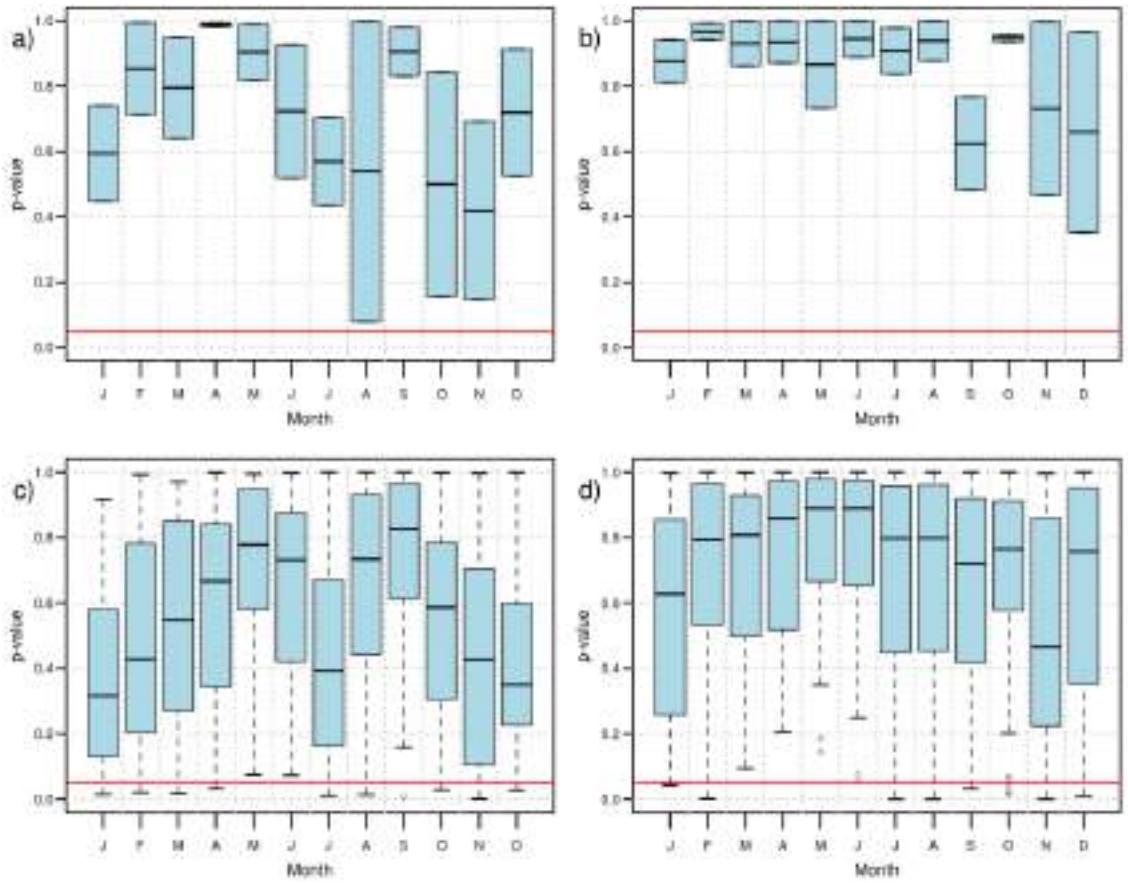

Figure 32. KS p-value of the daily precipitation simulated by using the downscaled ERA-Interim reanalysis: *a*) Bristol area stations before correction for Bristol (*a*, *b*) and Southwest England – South Wales (*c*, *d*), before (*a*, *c*) and after (*b*, *d*) the correction.

Sub-daily precipitation

Results for 5-min precipitation showed an adequate reproduction of the probability distribution of the main six features of the sub-daily precipitation: precipitation amount, rainfall event n-index (n) and its reference intensity (I_0), dry spell length distribution, dry spell n-index and its corresponding reference maximum length. Kolmogorov-Smirnov p-value passed the 0.05 threshold for most of stations (Fig. 33).

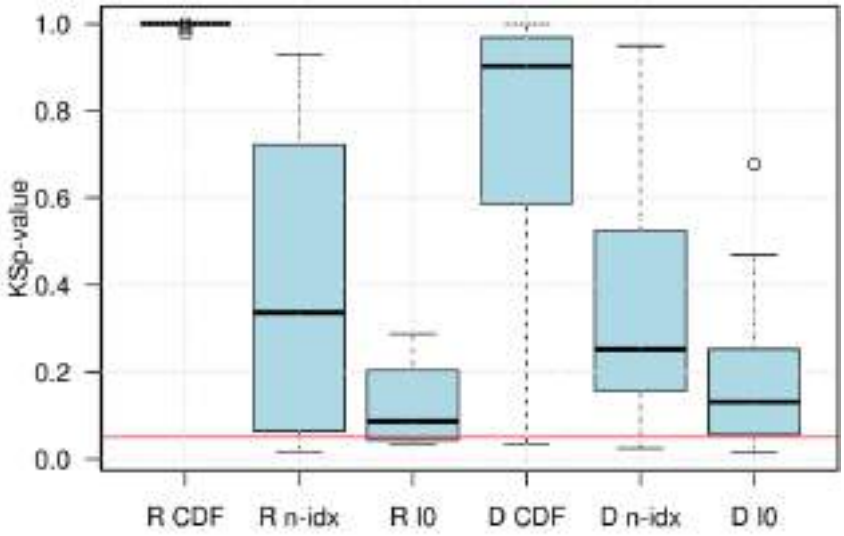

Figure 33. Verification results for sub-daily precipitation in Bristol: KS p-value for the rainfall probability distribution (R CDF), rainfall event n-index (R n-idx), rainfall event reference-maximum-intensity (R I0), dry spell probability distribution (D CDF), dry spell n-index (D n-idx) and dry spell reference-maximum-length (D I0).

3.1.4.3. Other variables

Wind, relative humidity and pressure

Results for Bristol and adjoining regions (Southwest England and South Wales) are similar despite the greater number of stations (close to 150) considered for the region. As it was previously seen, analogous method provides better results than the ERA-Interim output in all of the cases, presenting the smallest MAE and an almost zero BIAS. Regarding the KS p-value, both methods show a great upper acceptance threshold (p-value > 0.05), being direct outputs the ones presenting no acceptable values (Fig. 34 and 35). From the corrected ones, the analogues method presents generally values alike ERA-Interim. However, considering the rest of the indices, the analogous method appears as the best method.

Regarding the RPS for wind, boxplots correponding to the analogous method show the lowest values; although for Bristol city happen to be close to climatology RPS, for the region as a whole the values for the analogues improve for the results. Values from ERA-Interim outputs get worse, paradoxically, when corrected for both locations. However, the best result was obtained using the downscaled ERA-Interim with analogues, and then this method was selected for following steps.

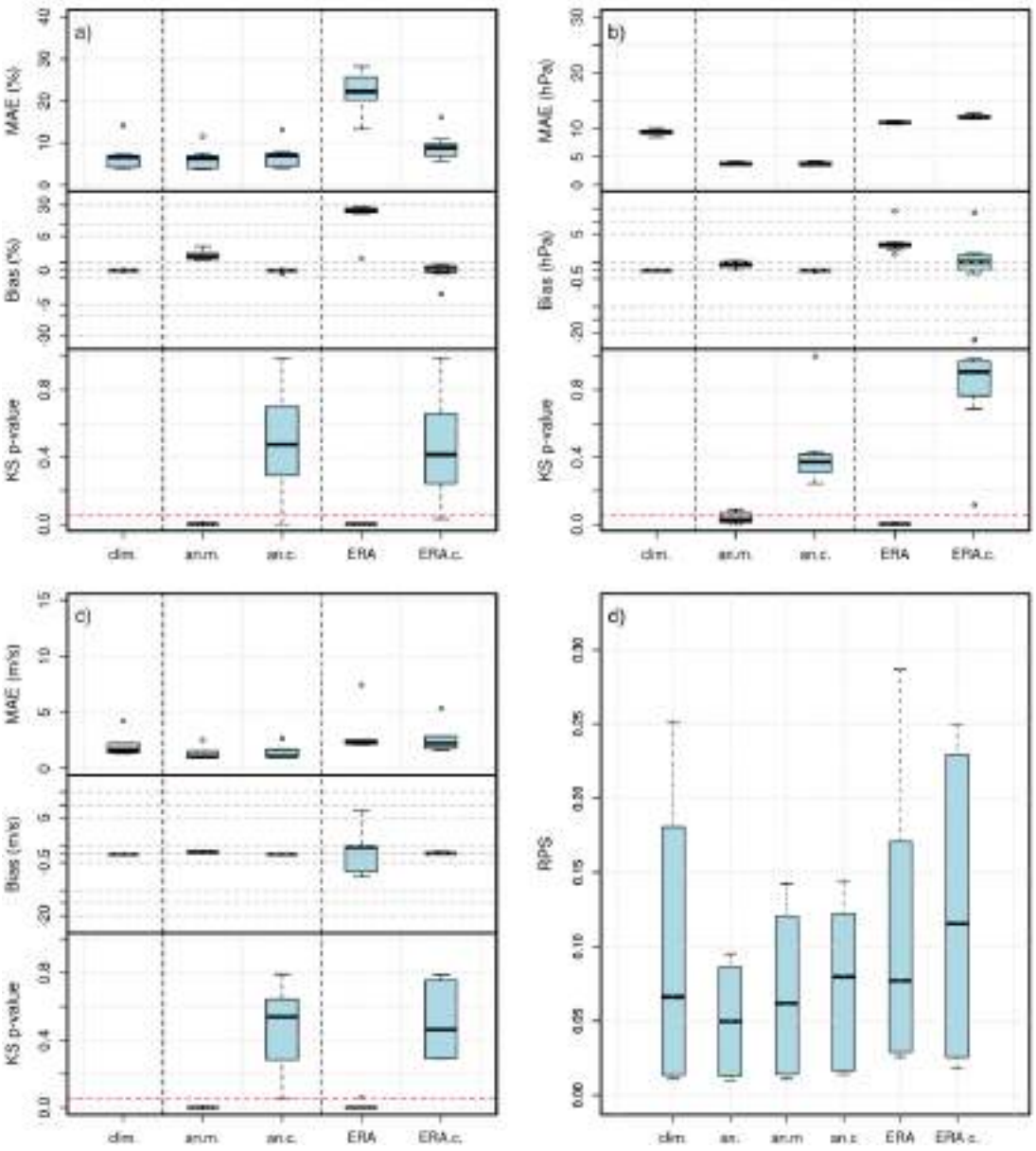

Figure 34. Verification results for other variables in Bristol city: *a*) MAE, Bias and KS p-value for the relative humidity simulation. *b*) MAE, Bias and KS p-value for sea level pressure simulation. *c*) MAE, Bias and KS p-value for wind simulation. *d*) RPS for wind simulation. Red lines are the 0 for Bias and 0.05 for the KS p-value. X-axis corresponds to: climatology simulation (*Clim*), 30-analogous ensemble (*30an*), 30 analogous mean (*an.mean*), corrected 30-analogous mean (*an.corr*), ERA-Interim direct output (*ERA*) and corrected downscaled ERA-Interim (*ERA.corr*).

.

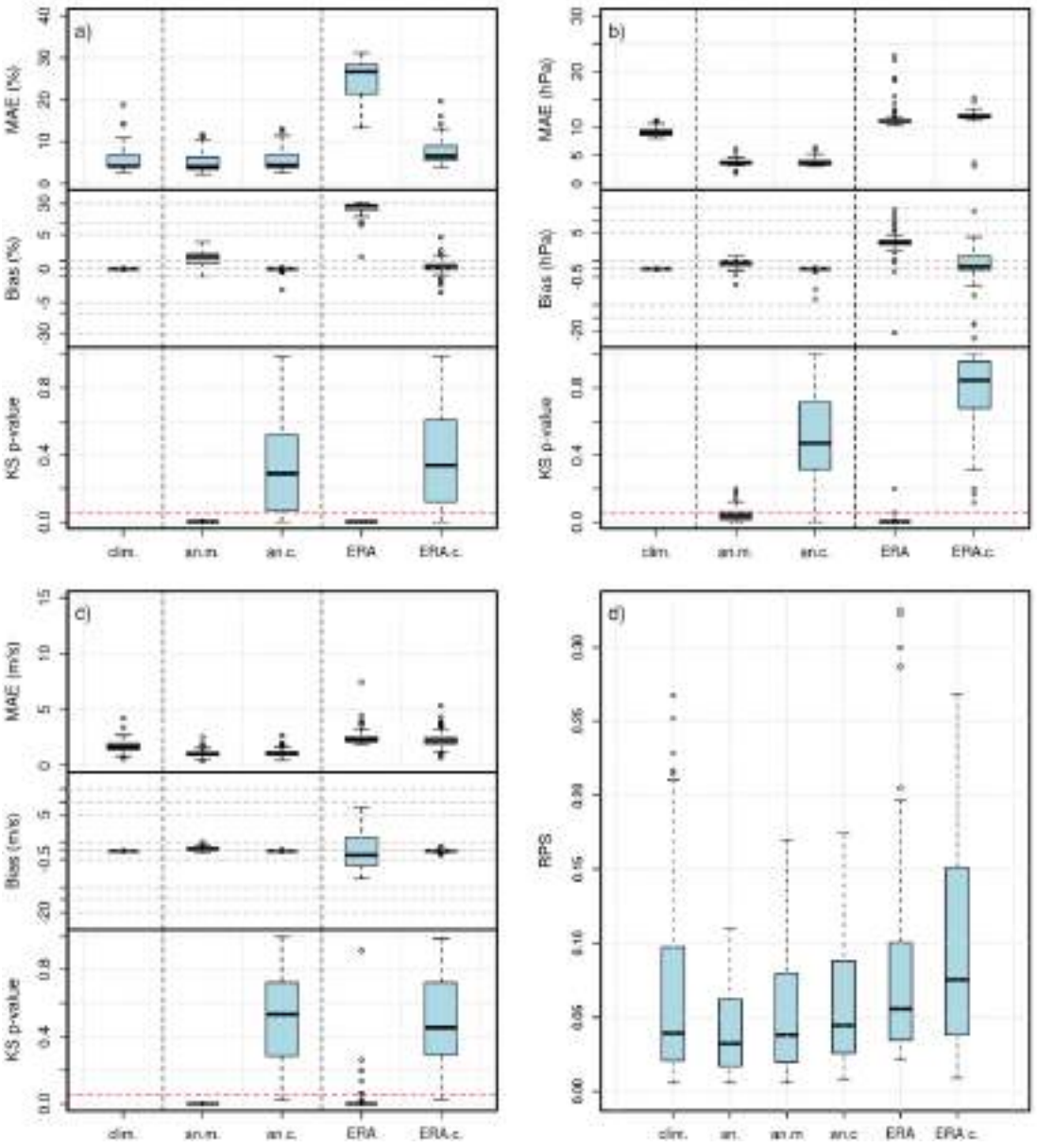

Figure 35. The same as Fig. **34** but for Southwest England and South Wales.

Oceanic variables: Wave height and sea level

The simulation of wave height presents a good result comparing with the simulation of reference *Climatology* (Fig. 36).

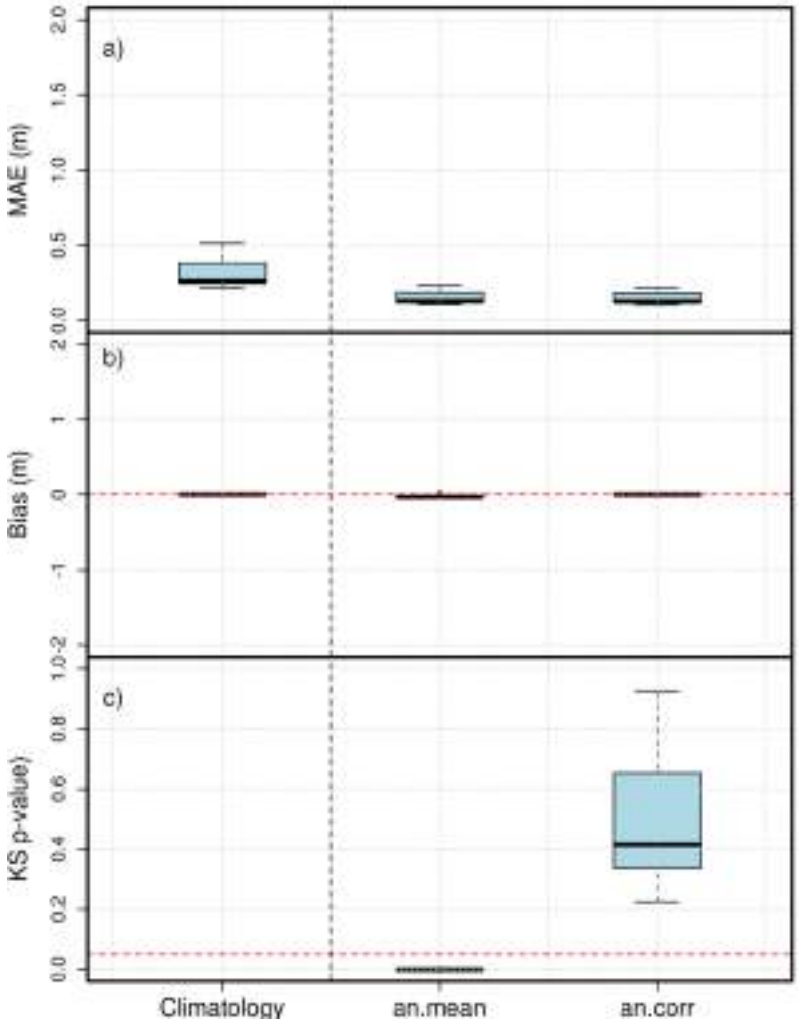

Figure 36. Verification results for the wave height in the Bristol buoys according to: *a*) MAE, *b*) Bias and *c*) KS p-value. X-axis corresponds to: climatology simulation (*Clim*), 30-analogous ensemble (*30an*), and 30 analogous mean (*an.mean*).

Regarding the verification of the sea level, GODAS re-analysis corrected by the FIC method presents a seasonal evolution very similar than the observed one, but a lesser variability (Fig. 37). Annual evolution is generally suitable except for some isolated years, but these affect the simulated trend causing a large uncertainty.

The verification process for the simulation of the meteorological sea level (surge), considered three daily statistics: mean, maximum and minimum value of the residual tide (total minus astronomical tide). All those presented lower mean absolute errors (MAE) than the climatic reference (Fig. 38).

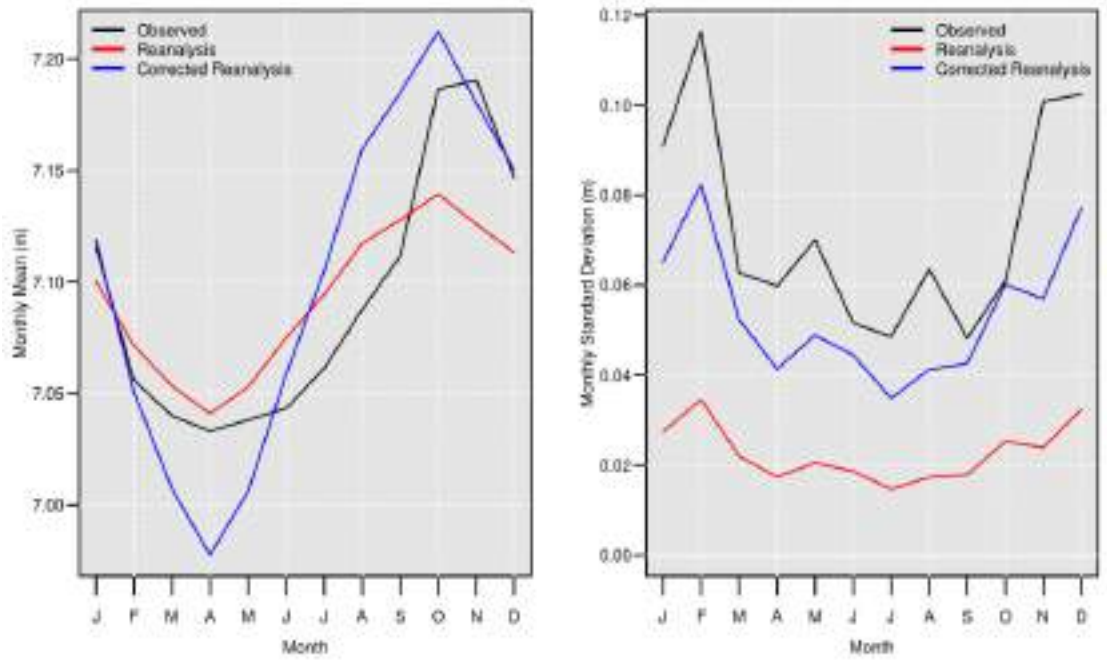

Figure 37. Verification results for the sea level variability in Bristol buoy (Hinkley point): Comparison between observed and simulated sea level before and after correction

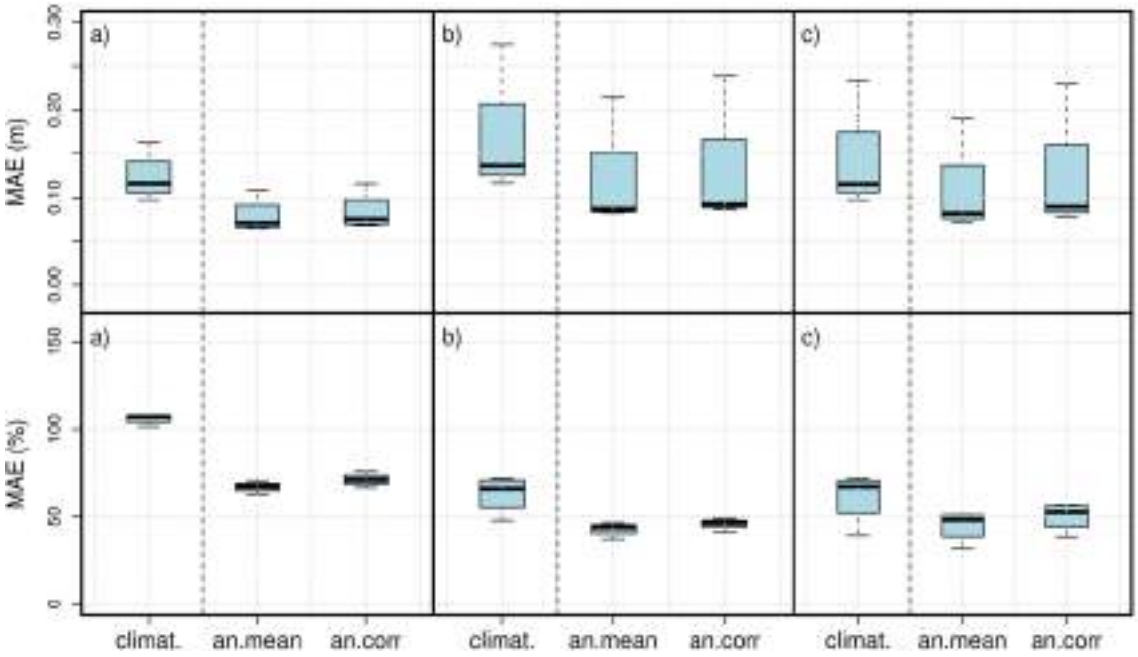

Figure 38. Verification results for the surge simulation in Bristol buoys: Absolute (top) and relative (bottom) mean error of three aggregated daily statistics: *a*) mean, *b*) maximum and *c*) minimum surge. *Clim* is the climatology simulation, *an.mean* is the mean of the 30 analogous days, *an.corr* is the corrected mean of the analogues

Derived variables: snowfall and evapotranspiration

Snow days are adequately simulated for the studied area of Bristol and adjoining regions (Fig. 39). The snowfall frequency is typically between 1 and 2 days from December to March, being below 1 day in October, November and April. The pattern in Bristol observatories is slightly different: January has an average of 2 days of snowfall but the rest of the months it is more unlikely to have snow episodes in Bristol than in the rest of the studied area. Nevertheless, the amount of snow falling in Bristol in January is higher than in other areas.

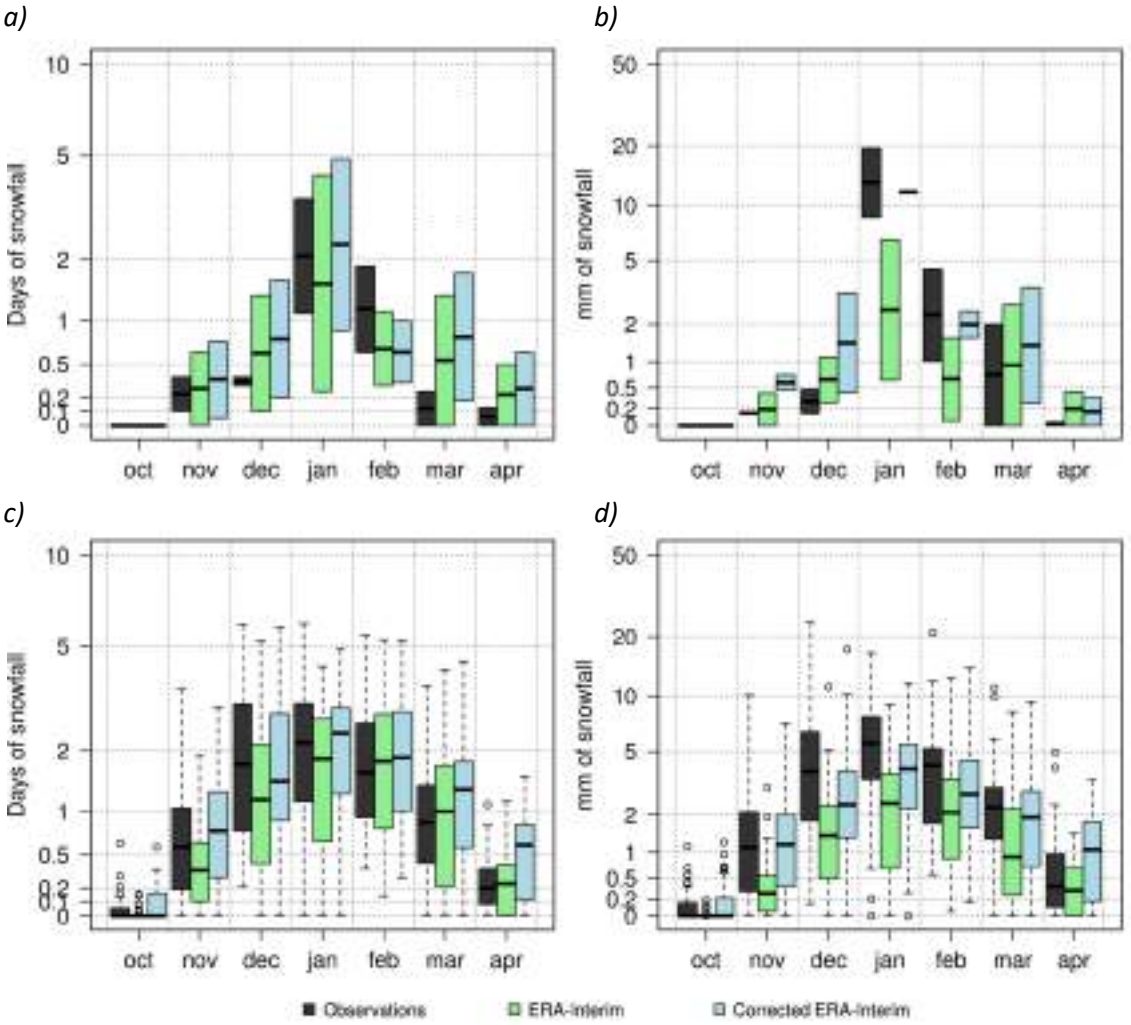

Figure 39. Verification results for snow simulation in Bristol area: Snowfall days (*left*) and snow water equivalent (*right*) per year in Bristol (*top*) and in Southwest England - South Wales (*bottom*) according to observations and downscaled re-analysis.

Potential Evapotranspiration in Southwest England and South Wales is significantly lower than in Barcelona and Lisbon due to its colder weather and higher latitude. Average values are adequately simulated from 30mm/month in winter to 70mm/month in summer, presenting the verification a better performance in summer months again (Fig. 40).

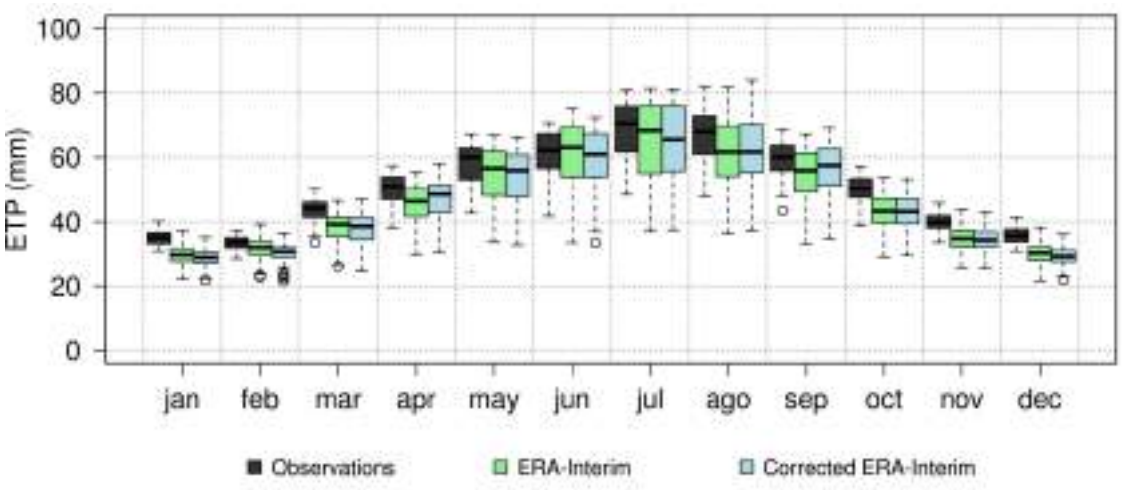

Figure 40. Verification results for potential evapotranspiration (mm per year) in Southwest England and South Wales: comparison between observations and simulations before and after the bias-correction.

3.1.5. Summary of the downscaling verification

All climate variables are adequately simulated by the downscaling methods except the sea level in Barcelona (Table 6). This is due to errors in salinity simulated by the used oceanic re-analysis (GODAS), which cannot be satisfactorily corrected by any statistical method.

Nevertheless, the downscaling method applied to the oceanic models does not require using the GODAS re-analysis and therefore the validation process is not affected by the verification uncertainty.

Table 6. Summary of the verification process for all downscaled simulations.

City	Variable									
	Temperature	Precipitation	Wind	Snowfall	ETP	RH	Sea level	Wave height	Surge	Pressure
Barcelona										
Lisbon										
Bristol										

Legend:

- Valid according to less than 50% of statistics
- Valid according to more than 50% and less than 70% of statistics
- Valid according to more than 70% of statistics
- Not available
- Not applicable

The rest of the variables were adequately simulated. Daily maximum/minimum temperature showed bias and MAE respectively lower than 0.2°C and 2°C, with accurate sub-daily values (MAE around 1°C in winter and 1.5°C in summer). All simulations passed the Kolmogorov-Smirnov test for the daily and sub-daily distribution during all months of the year. In the same way, precipitation (bias lower than 10%) presented acceptable KS p-values after correction of the systematic error, also for the main features of the sub-daily rainfall.

The verification statistics of wind, relative humidity and pressure showed that, the analogous method obtained the lowest MAE and an almost zero BIAS, with a KS test passed satisfactorily (p-value > 0.05). These results confirm that the analogous method is a powerful tool to simulate accurately these variables.

3.2. Verification of the teleconnection-based method

3.2.1. About this

Section 3.2 presents the results about the verification process of the teleconnection-based method described in Sec. 2.2.4 and used to generate the near-term (decadal) climate predictions of temperature and precipitation. In contrast with the drift-correction method (Sec. 2.2.3 and Sec. 3.4), this decadal prediction does not use dynamical models, but historical observations of teleconnection indices. This allows a verification process based on simulating past climate anomalies using only previous values.

Verification results of the decadal hindcast of temperature and precipitation are structured in three subsections according to the studied cities (Barcelona, Lisbon and Bristol) and their surrounding areas. Finally, Sec. 3.2.5 summarises the main results of the verification process for all the cases.

3.2.2. Barcelona

3.2.2.1. Temperature

The verification process of the decadal prediction was focused on the SAE obtained in the detrended hindcast. According to this, temperature in Barcelona was well predicted for practically all horizons (2-30 years), for at least a half of the studied stations (Fig. 41). Therefore, only these stations (156/300) were considered for the teleconnection-based predictions.

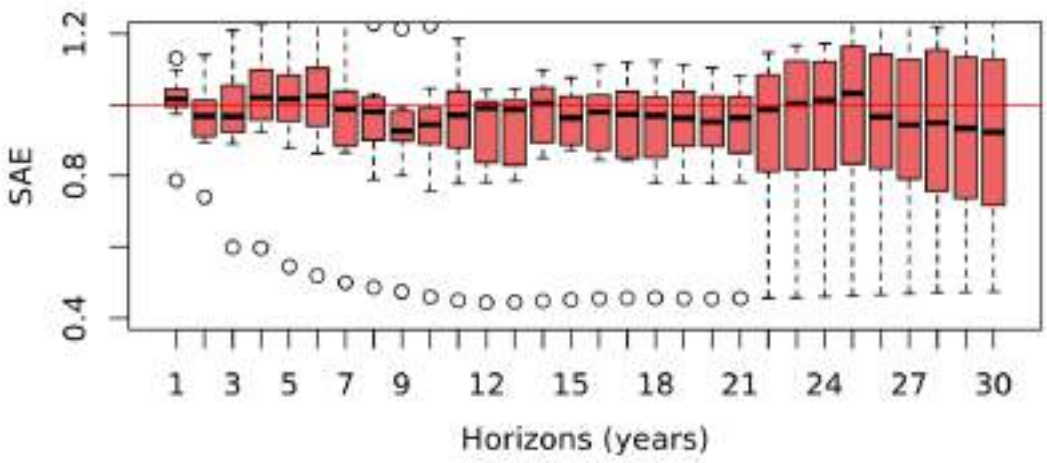

Figure 41. Verification results (SAE) for the decadal hindcast of temperature in Barcelona, according to the teleconnection-based method.

3.2.2.2. Precipitation

Verification process for precipitation, show that two stations of Barcelona are well predicted, obtaining a SAE lower than or close to 0.5 for most of the horizons (Fig. 42). The rest of stations showed a good predictability for horizons greater than 12 years. For this reason, all stations of Barcelona (196) were considered for the predictions.

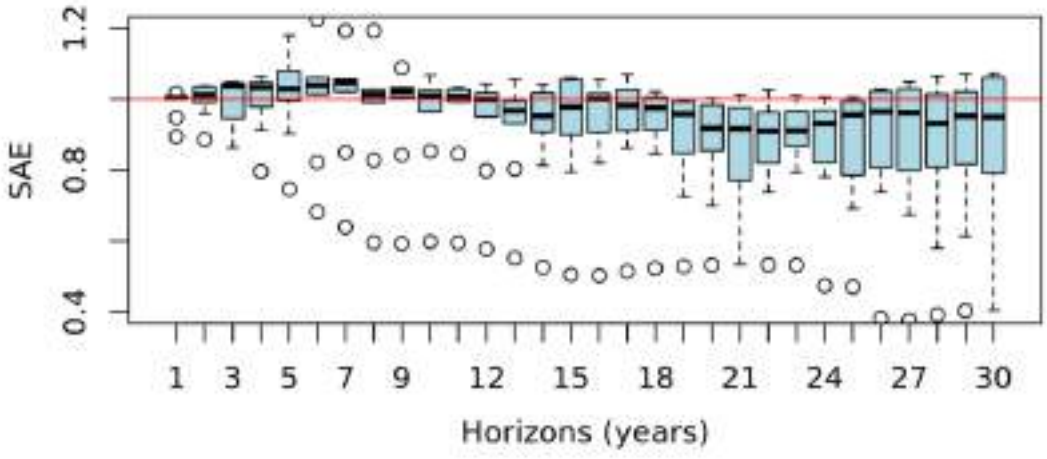

Figure 42. Verification results (SAE) for the decadal hindcast of precipitation in Barcelona, according to the teleconnection-based method.

3.2.3. Lisbon

3.2.3.1. Temperature

Regarding the decadal hindcast of detrended temperature in Lisbon, the verification process showed that no station is predictable for the 1-16 years horizons. However, three of the five stations are predictable for the 20-30 years horizons (Fig. 43). These stations were considered for the decadal predictions, taking into account the limited (optimum) forecast horizons. The limited predictability of temperature in Lisbon is due to the low inter-annual variability of the climate anomalies, being a non-cyclical signal for the near-term prediction (< 20 years).

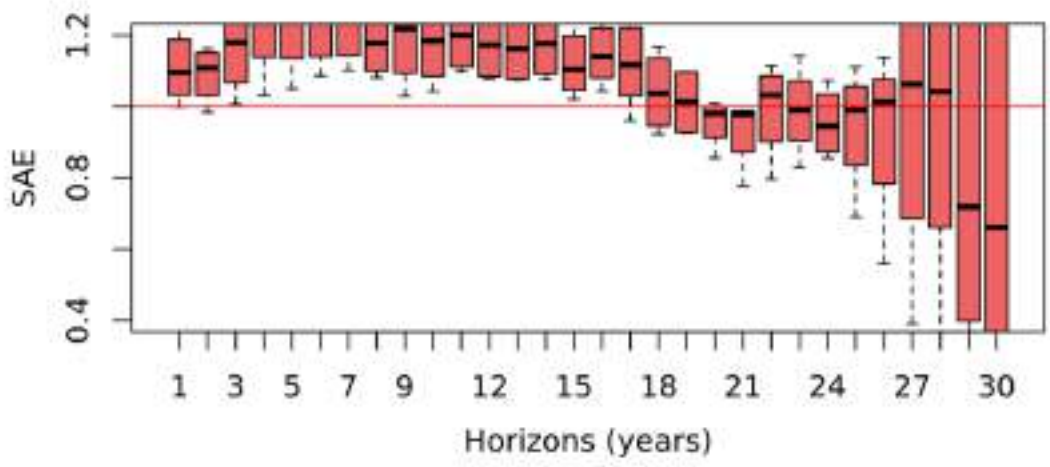

Figure 43. Verification results (SAE) for the decadal hindcast of temperature in Lisbon, according to the teleconnection-based method.

3.2.3.2. Precipitation

Verification process for precipitation in Lisbon showed slightly better results than temperature. Time-series of all stations were predictable for horizons greater than 15 years (Fig. 44). Therefore, all stations were considered for the final decadal predictions of the precipitation in Lisbon.

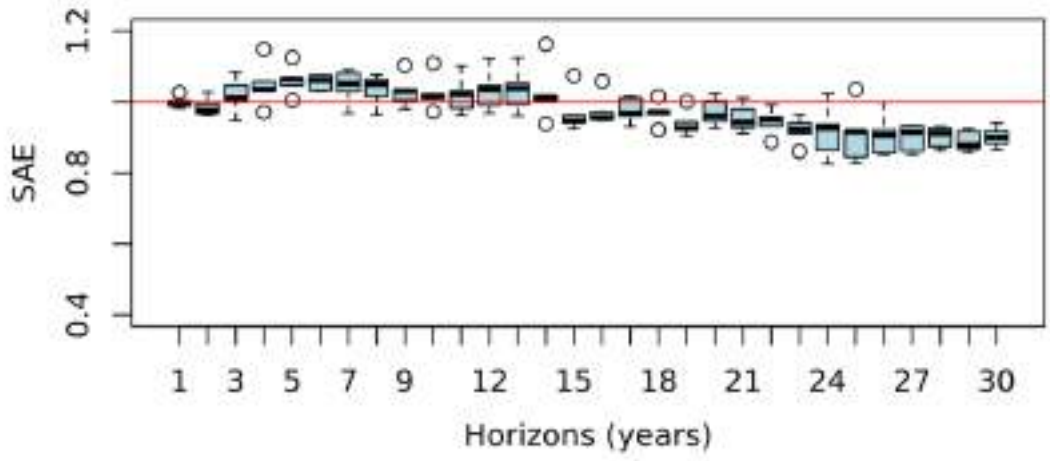

Figure 44. Verification results (SAE) for the decadal hindcast of precipitation in Lisbon, according to the teleconnection-based method.

3.2.4. Bristol

3.2.4.1. Temperature

Detrended temperature predicted by the teleconnection-based method showed a low error in Bristol for horizons less than 21 years (Fig. 45).

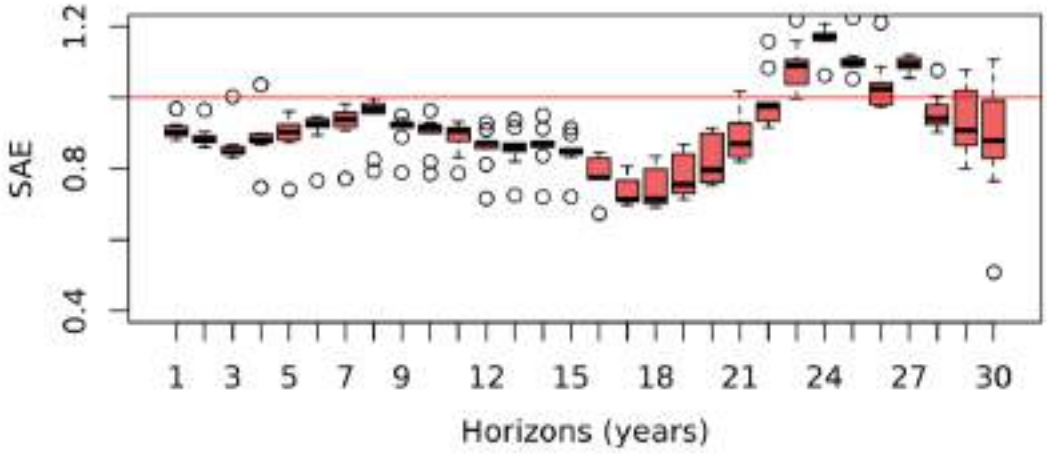

Figure 45. Verification results (SAE) for the decadal hindcast of temperature in Bristol, according to the teleconnection-based method.

3.2.4.2. Precipitation

Verification process for precipitation in Bristol provided good results for some stations since the 14-years horizon (Fig. 46).

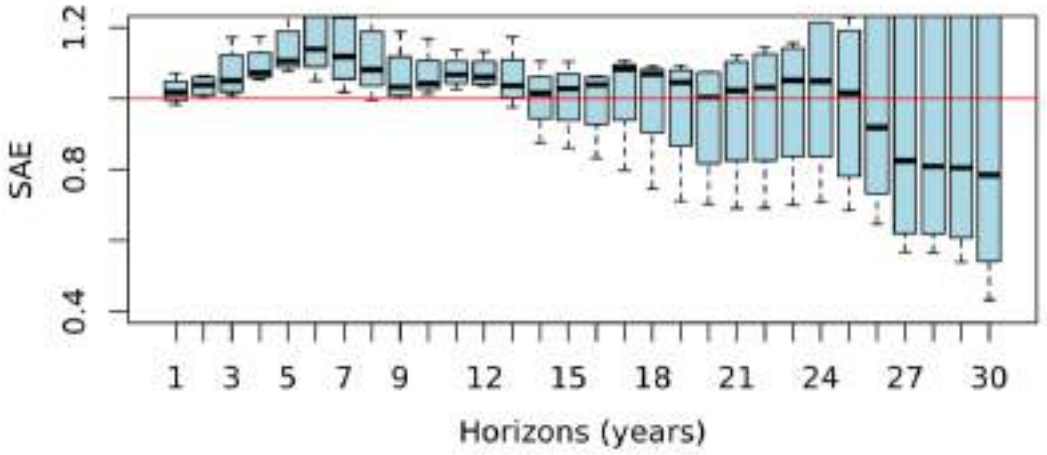

Figure 46. Verification results (SAE) for the decadal hindcast of precipitation in Bristol, according to the teleconnection-based method.

Regionally, results for temperature and precipitation are similar to the city, and therefore are not shown.

3.2.5. Summary of the teleconnection verification

Temperature is well simulated by the teleconnection-based method, even for the 10-years horizon in Barcelona and Bristol (Table 7). However, detrended temperature in Lisbon presented predictability only for the largest horizons. Precipitation is only predictable in the three cities for horizons equal or greater than 20 years.

Therefore, it can be interpreted that, using teleconnections the optimum horizon for the decadal forecast is around 20 years.

Table 7. Indices and their variables considered. SST is sea surface temperature, SLP represents sea level pressure, R is rainfall, and Z500 is geopotential height at 500 hPa. The blue box remarks the optimum forecast horizon.

Variable	City	Horizons (years)																												
		1	2	3	4	5	6	7	8	9	10	11	12	13	14	15	16	17	18	19	20	21	22	23	24	25	26	27	28	29	30
Temperature	Barcelona																													
	Lisbon																													
	Bristol																													
Precipitation	Barcelona																													
	Lisbon																													
	Bristol																													

Legend:

- SAE < 1 for less than 50% of the stations
- SAE < 1 for more than 50% and less than 70% of the stations
- SAE < 1 for more than 70% of the stations

3.3. Validation of the application to the CMIP-5 Models

3.3.1. About this

Section 3.3 presents the results of the validation carried out for all downscaled climate models (Table 3), according to the statistical downscaling method described in Sec. 2.2.1 and 2.2.2. In the climate model downscaling context, the validation process consists on evaluating the applicability of a method using selected predictor fields of each climate model used.

In this study, the validation for all climate models was performed comparing the *downscaled historical experiment* and the *extended observations* as it is described in Sec. 2.3.2. Generally, real observations present gaps and, therefore, they cannot be used for the validation of downscaled climate models.

Results of validation are structured in three subsections according to the studied cities (Barcelona, Lisbon and Bristol) and their surrounding areas. In turn, each subsection enumerates the verification of all climate variables simulated by the downscaled CMIP5 climate models. Finally, Sec. 3.3.5 summarises the main results of the validation process for all variables and cities

.

3.3.2. Barcelona

3.3.2.1. Temperature

Temperature simulation in Barcelona presents adequate validation results for maximum and minimum values once corrected. Before correcting with extended observations, all of the downscaled models represent values oscillating around the observed values, with little dispersion in maximum temperatures and more scattered values in minimum temperatures. There is the exception of GFDL-ESM2M, whose values are far from being considered correct. After correction, all the models presented almost no deviation, representing therefore a good result.

In order to summarise the validation results, the KS p-value are shown for before and after correction (Fig. 47 and 48). Before correction, a few downscaled models passed the KS test for the minimum and none for the maximum temperature. Nevertheless, all downscaled models are usable after correction, since all of them passed the test.

Similar conclusions can be reached according to the improvements in the standard deviation. All corrected climate model outputs presented low errors, including GFDL-ESM2M, which presented very bad results before correction (Fig. 49 and 50).

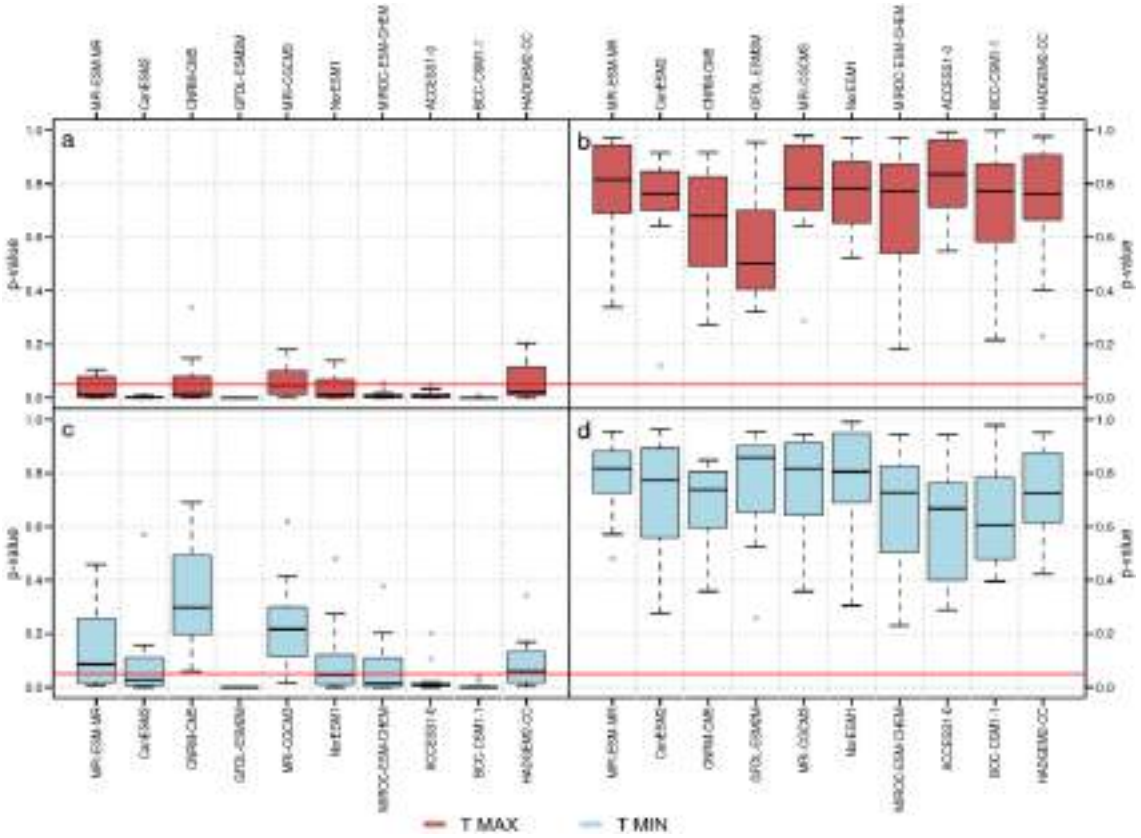

Figure 47. Validation results for temperature in Barcelona: KS p-value of the climate simulations of maximum (*a*, *b*) and minimum (c, d) temperature, obtained by comparison of the downscaled climate models, before (*a*, *c*) and after (b, d) the bias-correction, with the extended observations.

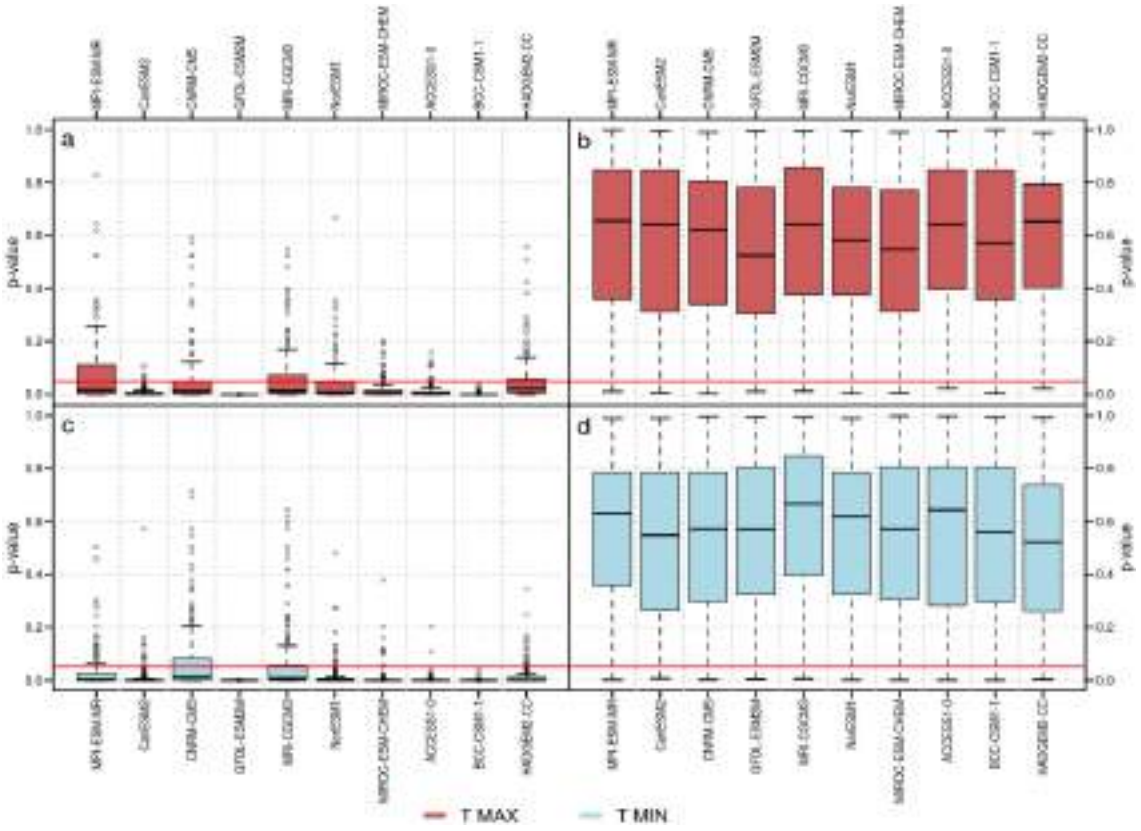

Figure 48. The same as Fig. 47 for Ter-Llobregat system.

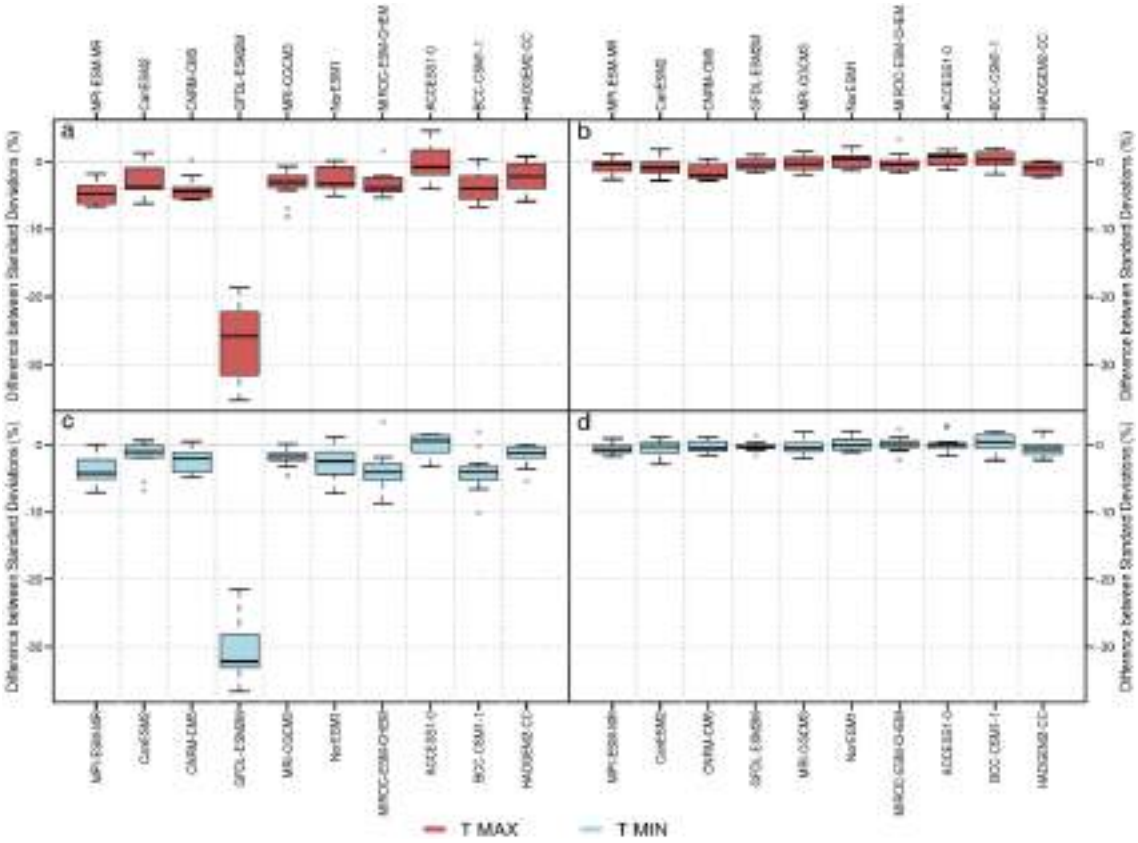

Figure 49. Error of the standard deviation in daily maximum (*a*, *b*) and minimum (*c*, *d*) temperature in Barcelona, obtained by comparison of the downscaled climate models, before (*a*, *c*) and after (*b*, *d*) the bias-correction, with the extended observations.

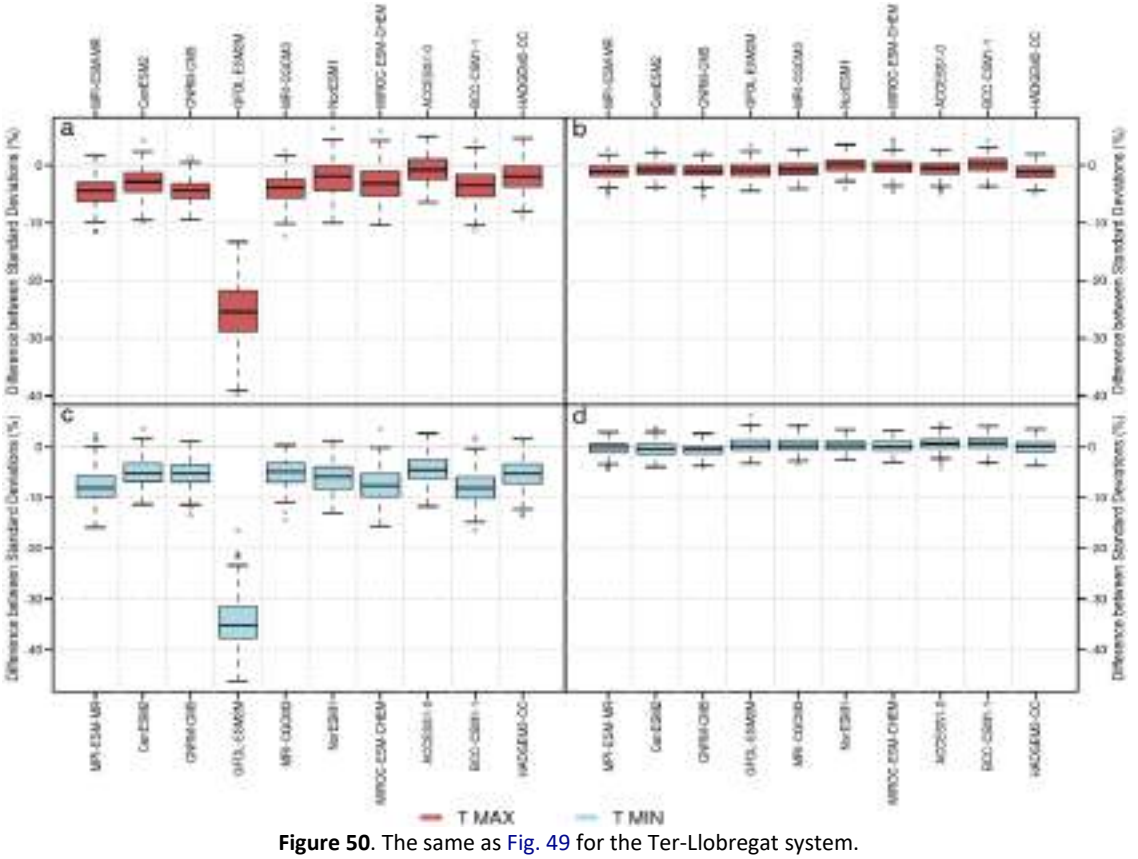

Figure 50. The same as Fig. 49 for the Ter-Llobregat system.

3.3.2.2. Precipitation

The validation for the precipitation in Barcelona presented good results after the bias correction. Initially, some downscaled climate models did not pass the KS test for the positive values of precipitation but, after correction, they passed the test in all cases (Fig. 51).

Regarding Ter-Llobregat system, results are better than those of the city except for the downscaled HADGEM2-CC (Fig. 52). Even after correction, this model output did not passed the KS test for the positive values of precipitation. Relative error in standard deviation leads to similar conclusions (Fig. 53 and 54). HADGEM2-CC cannot be used for the climate projections in Ter-Llobregat system.

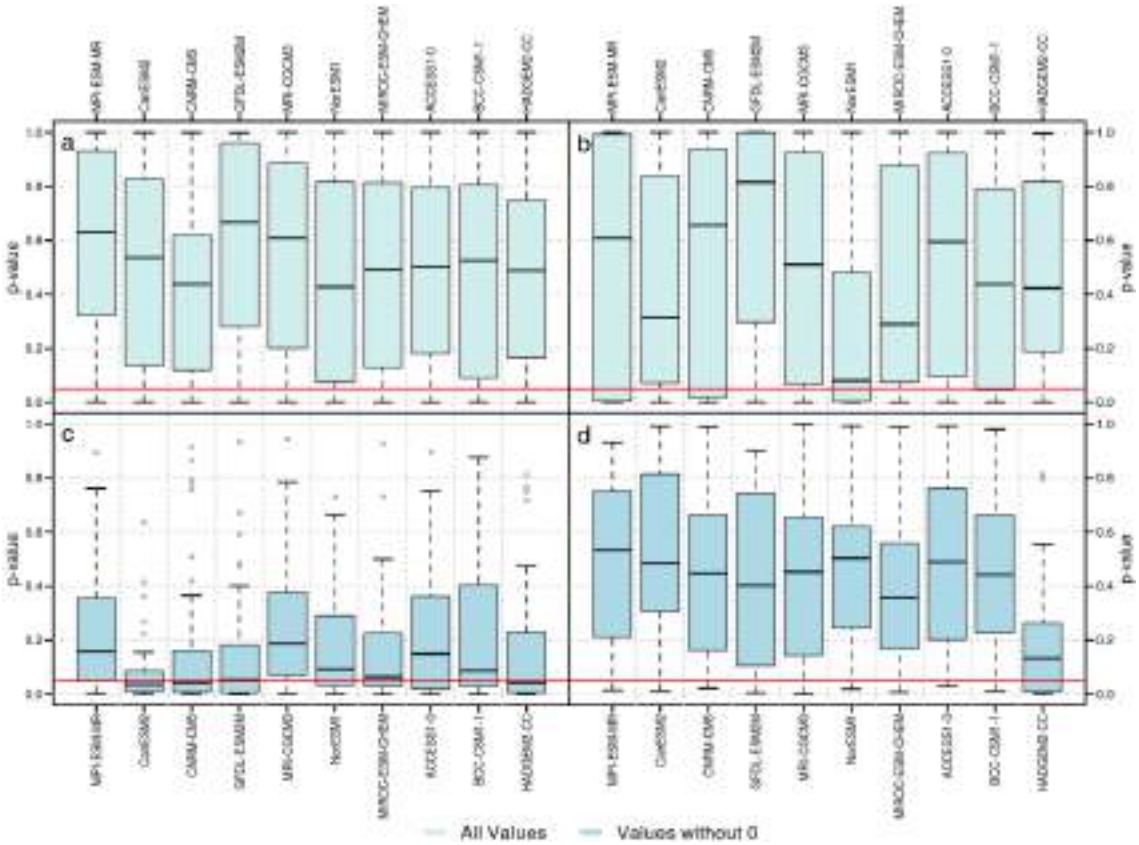

Figure 51. Validation results for precipitation in Barcelona: KS p-value of the climate simulations of dry/wet (*a*, *b*) and only wet (*c*, *d*) values of precipitation, obtained by comparison of the downscaled climate models, before (*a*, *c*) and after (*b*, *d*) the bias-correction, with the extended observations.

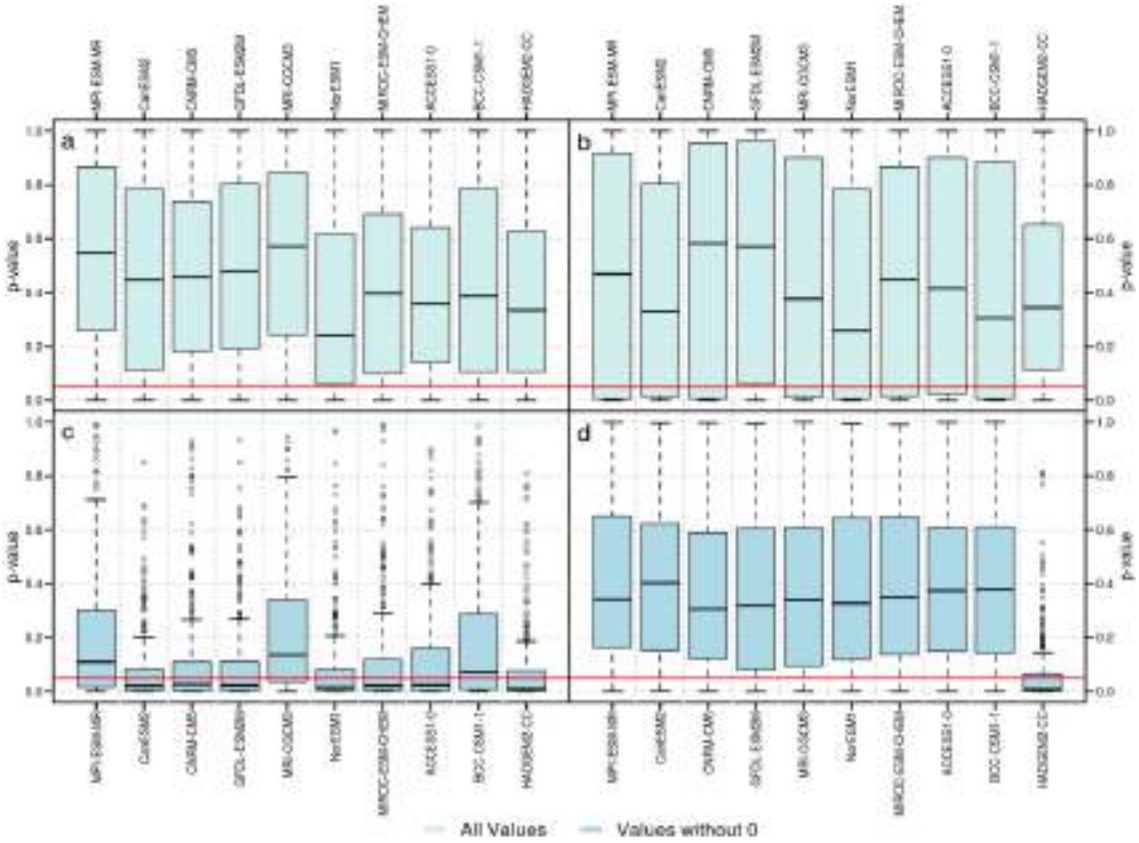

Figure 52. The same as Fig. 51 for the Ter-Llobregat system.

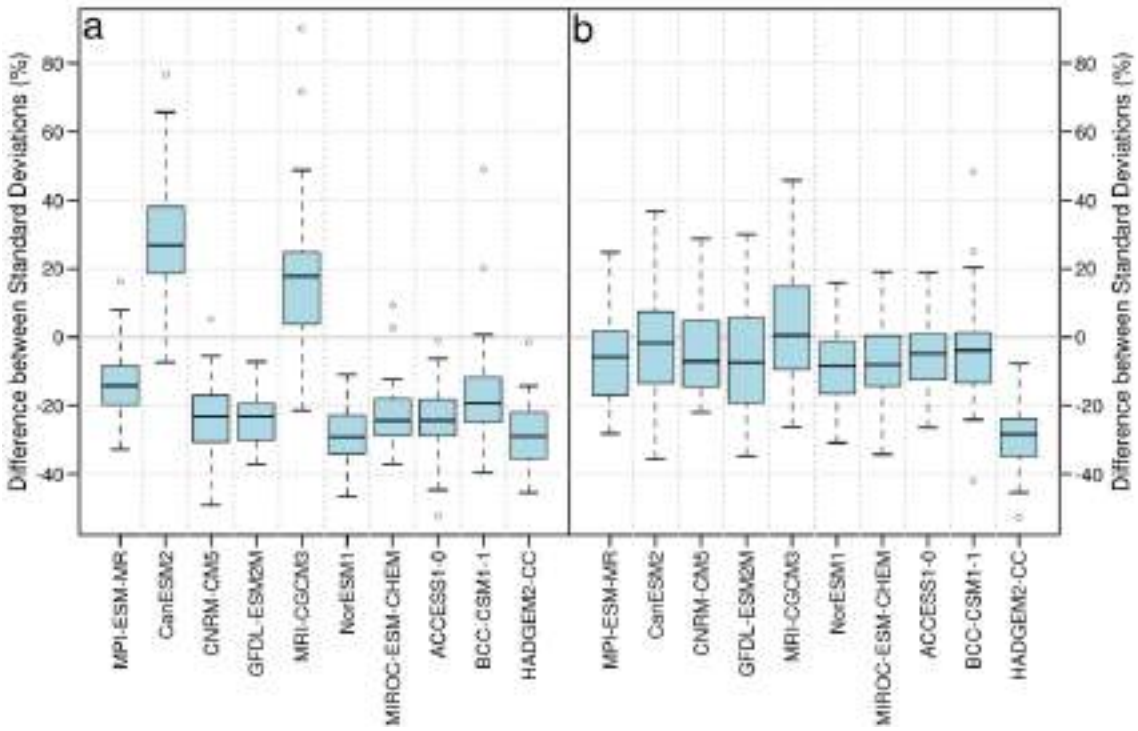

Figure 53. Error of the standard deviation in daily precipitation in Barcelona, obtained by comparison of the downscaled climate models, before (*a*) and after (*b*) the bias-correction, with the extended observations.

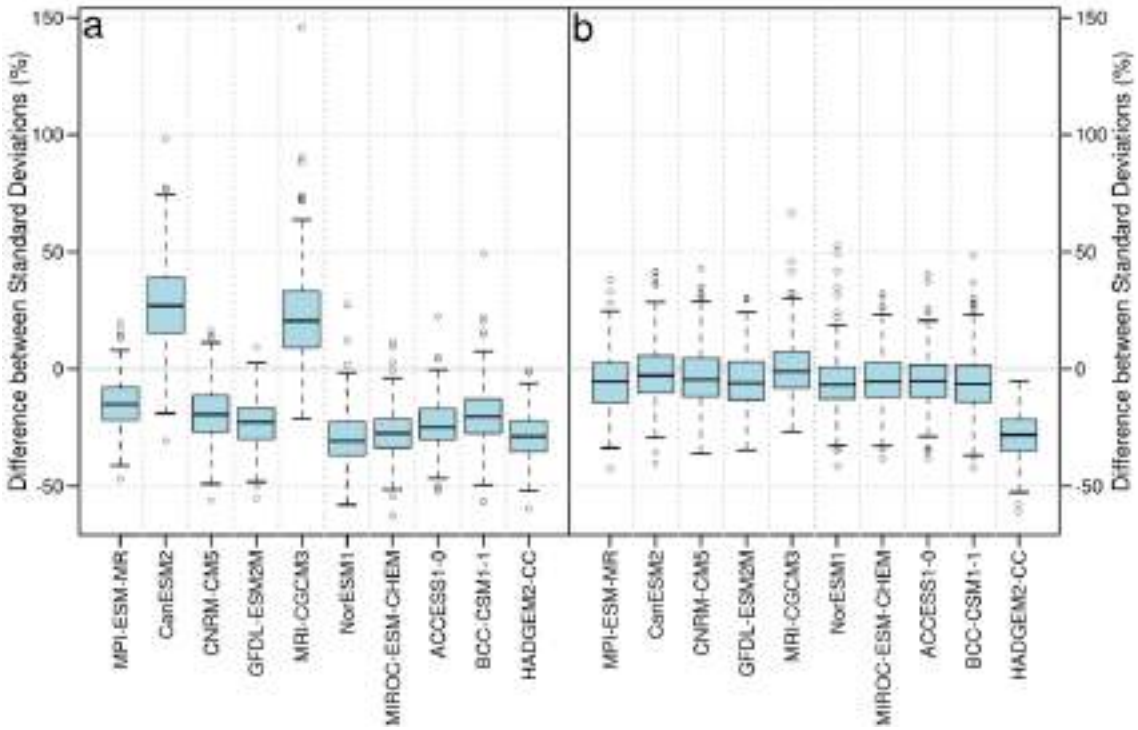

Figure 54. The same as Fig. 53 for the Ter-Llobregat system.

3.3.2.3. Other variables

Wind, relative humidity and pressure

Results for the city of Barcelona present the same characteristics for both the city and the Ter-Llobregat System, despite the number of stations considered. As a general discussion, the three variables, wind, relative humidity (RH) and sea level pressure (SLP), considerably improve after correcting for both locations. Bias values are small and oscillate around zero for the whole of the models, having a close to zero value when corrected (Fig. 55 and 56).

Regarding KS p-values, the correction caused a significant rise, from zero to above-significance values (p-value > 0.05) for all of the model simulations, with the exception of HadGEM2-CC and MRI-CGCM3 models in pressure. These two models seem not to be able to simulate correctly the variable, lacking of similitude to stations even after correction. After correction p-values get almost equal to one, which would be a perfect result.

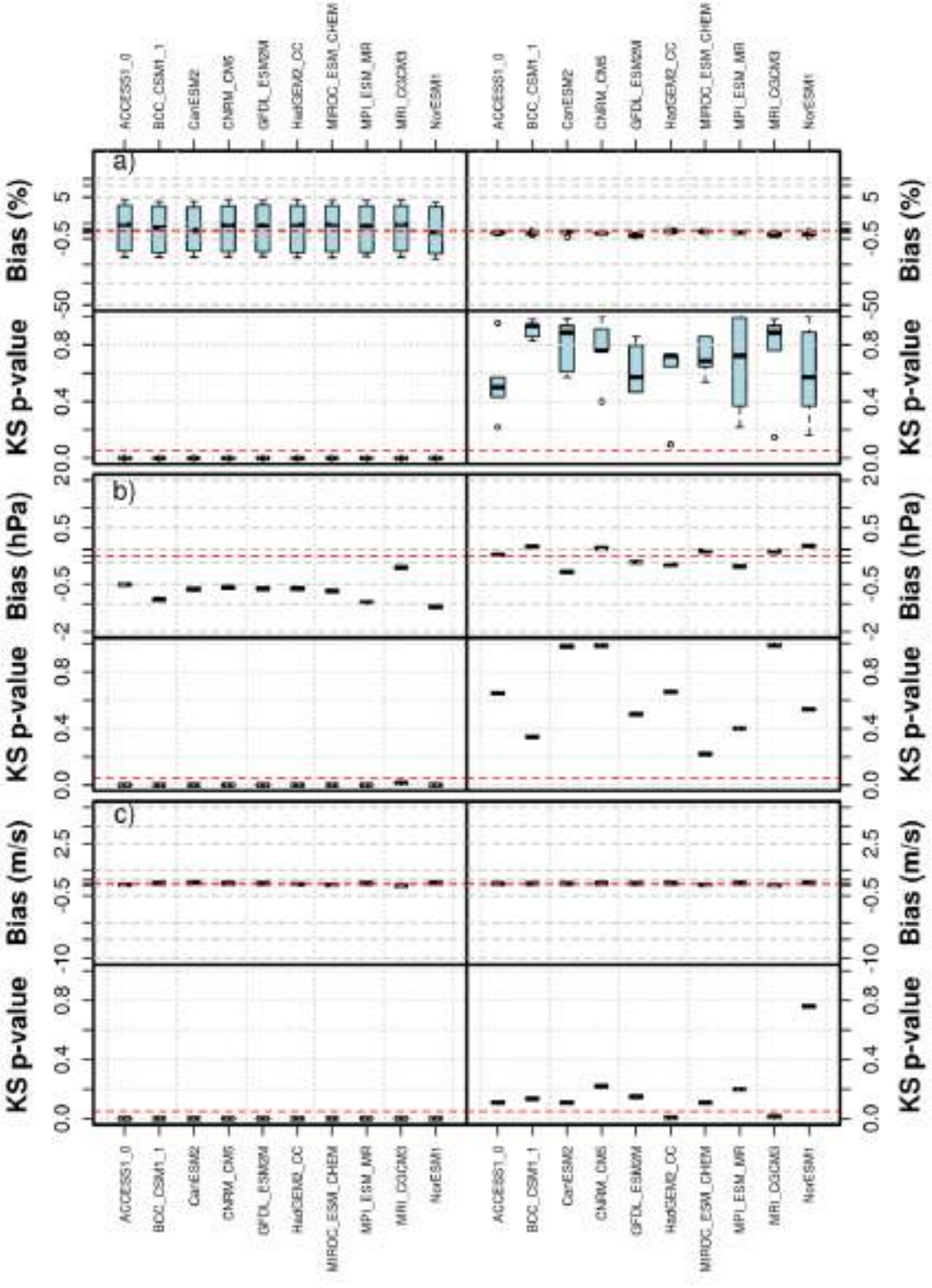

Figure 55. Validation results for other variables in Barcelona city: Bias and KS p-value for the downscaled CMIP5 outputs, before (*left*) and after (*right*) the correction: *a*) Relative Humidity, *b*) Sea level pressure, *c*) Wind. Red lines are the 0 for BIAS and 0.05 for the KS p-value.

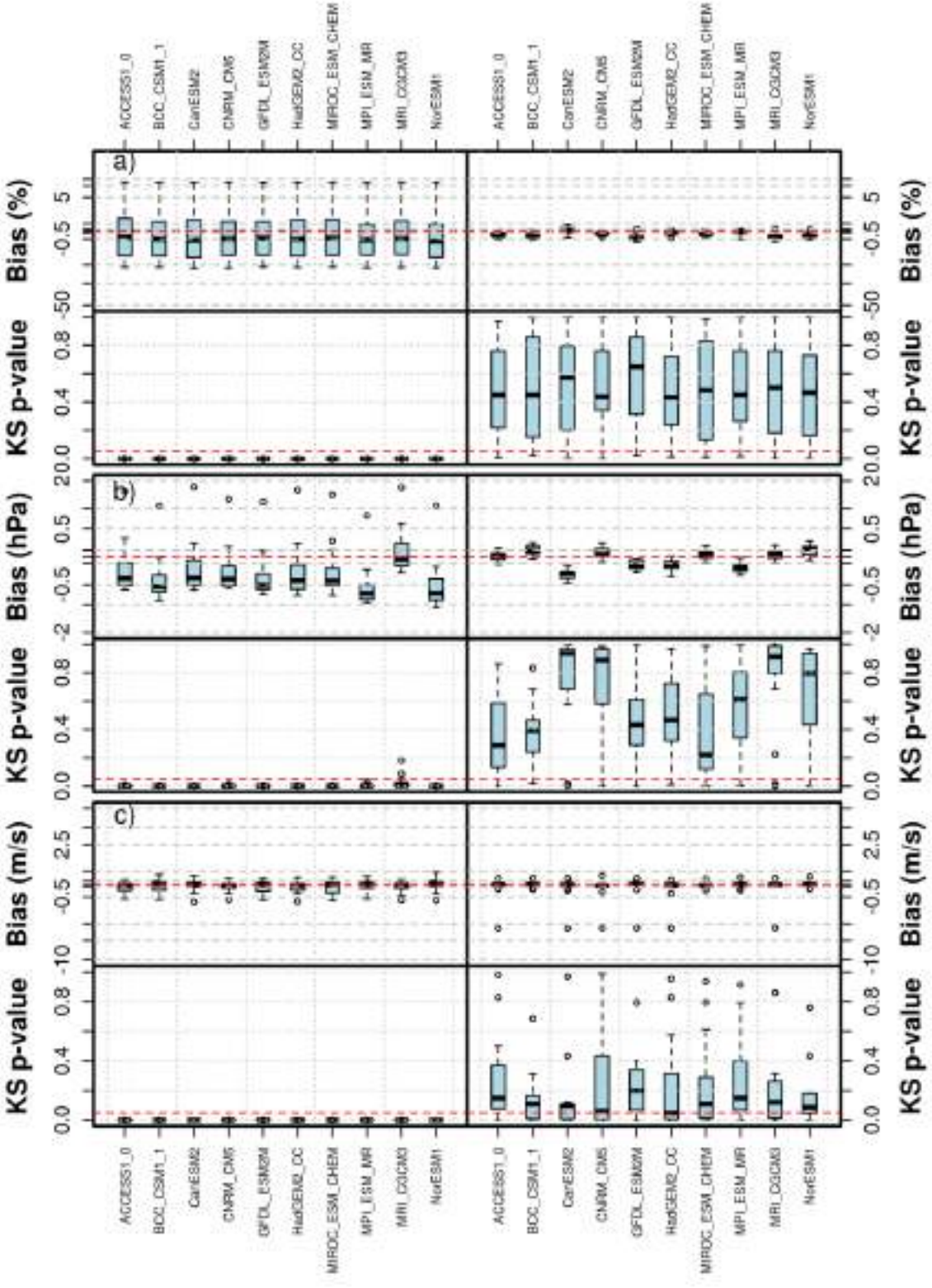

Figure 56. The same as Fig. 55 but for Ter-Llobregat system.

Oceanic variables: Wave height and sea level

The simulation of wave height presents a good result after correction of the systematic error (Fig. 57).

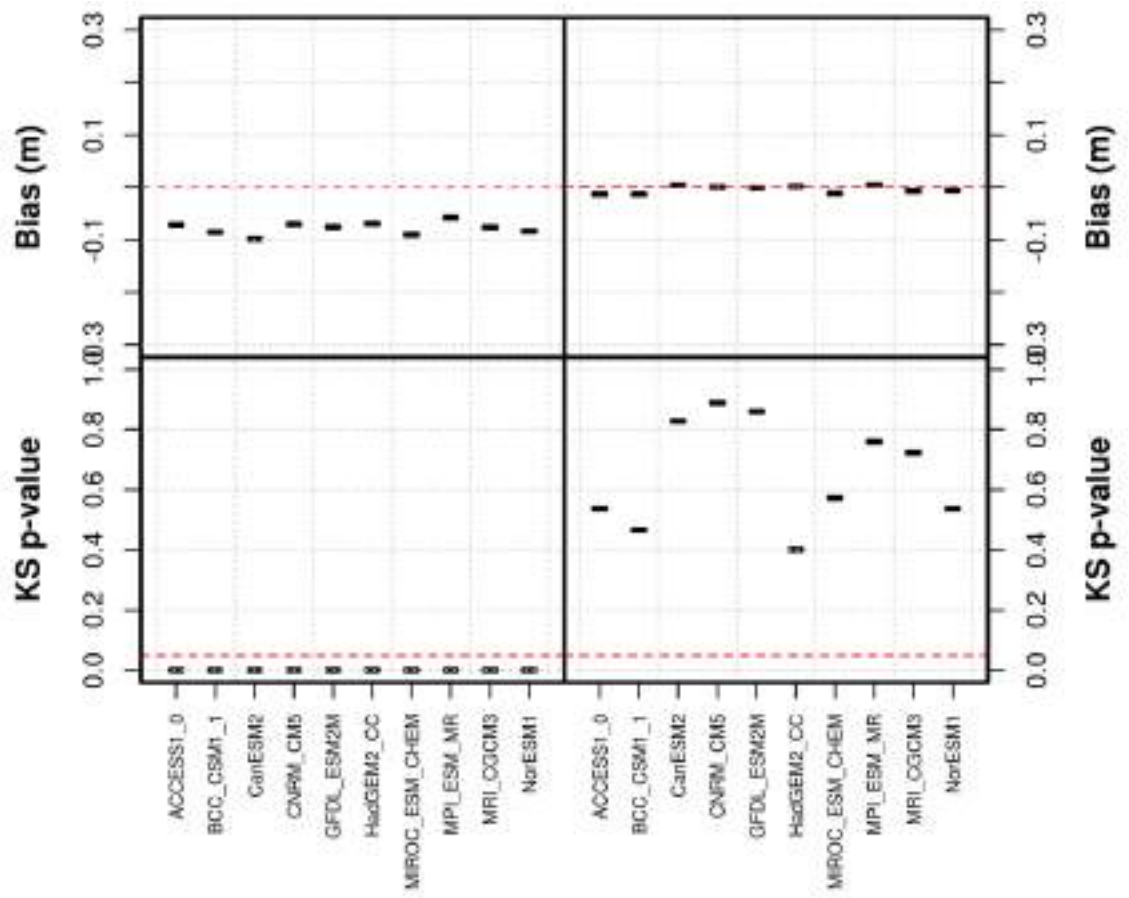

Figure 57. Validation results for wave height in Barcelona buoy: Bias and KS p-value for the downscaled CMIP5 outputs, before (*left*) and after (*right*) the correction: *a*) Relative Humidity, *b*) Sea level pressure, *c*) Wind. Red lines are the 0 for BIAS and 0.05 for the KS p-value.

The validation process for the simulation of sea level in Barcelona showed disparate results, depending on the considered climate model and on the statistical measure analysed (Fig. 58). For the monthly mean values, MRI-CGCM3, ACCESS1-0, MPI-ESM-MR, CanESM2, NorESM1 and CNRM-CM5 presented de best performance.

Regarding the historical trend, significant rise up to +5.6 cm/10y (p-value < 0.01) is observed in Barcelona buoy between 1994 and 2004. For the simulation of this historical trend, 5/9 model outputs (HADGEM2-CC, MIROC-ESM-CHEM, MPI-ESM-MR, MRI-CGCM3 and NorESM1-M) obtained similar trends to the observed rise, but only one presented significant level (NorESM1-M, +5.7 cm/10y, p-value < 0.01).

Strictly, no model approves all statistical measures, but three of them pass most tests. As conclusion, only one model (GFDL-ESM2M) has been rejected for the future projections.

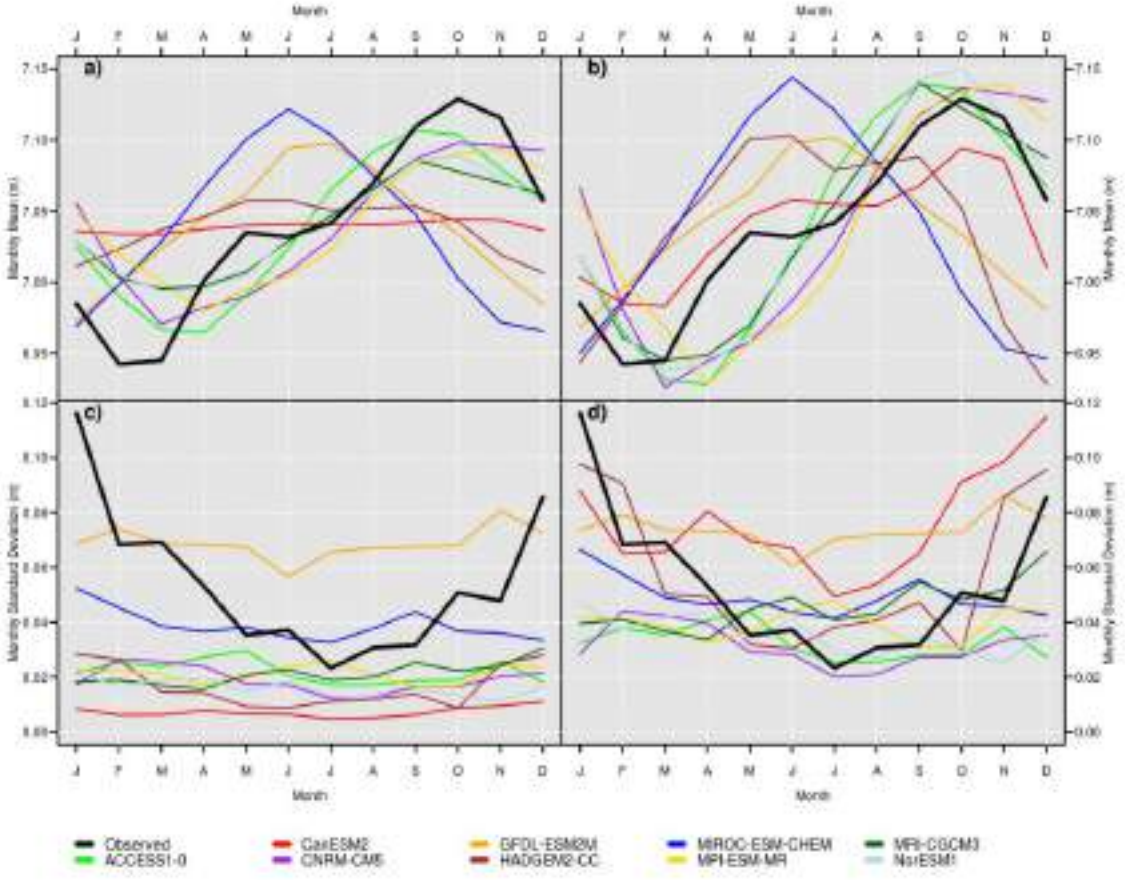

Figure 58. Validation results for sea level in Barcelona buoy, before (*a*, *c*) and after (*b*, *d*) the bias correction: monthly mean values (*a*, *b*) and monthly standard deviation (*c*, *d*).

Derived variables: snowfall and evapotranspiration

The historical data sets of the ten models taken into consideration confirm the trend seen in the verification process. The results for snowfall have a low deviation respect the observations. The only model whose output is greatly different from the others is GFDL-ESM2M (Fig. 59). Its output for both days and amount of snowfall is about 5 times greater than the observations and the other models considered.

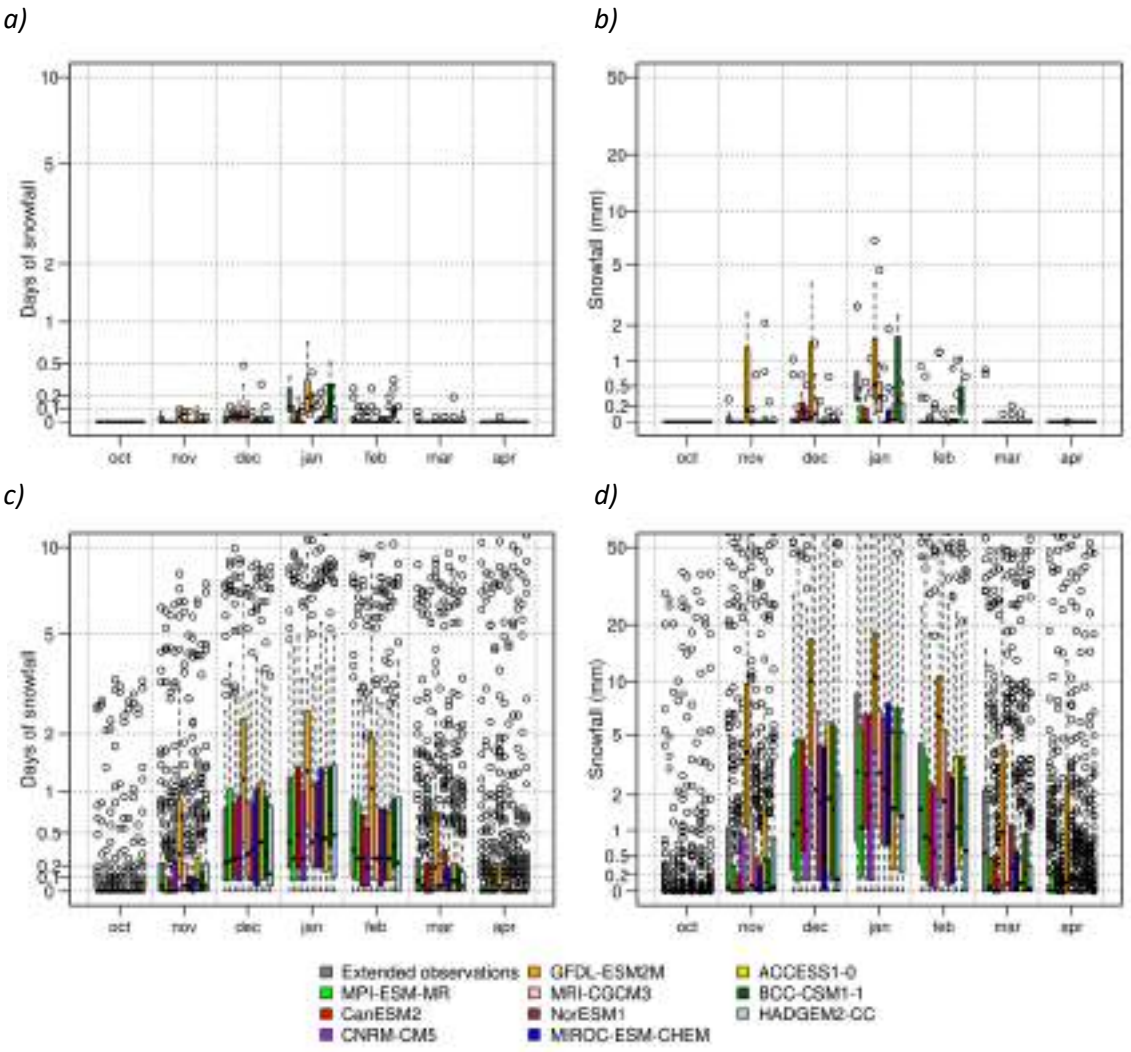

Figure 59. Validation results for snow simulation in Barcelona (*top*) and Ter-Llobregat System (*bottom*): Snow days (*left*) and snow water equivalent (right) per year according to the CMIP5 climate models.

Potential evapotranspiration simulated for Barcelona and adjoining regions showed a great resemblance between all the results provided by the downscaled climate models (Fig. 60).

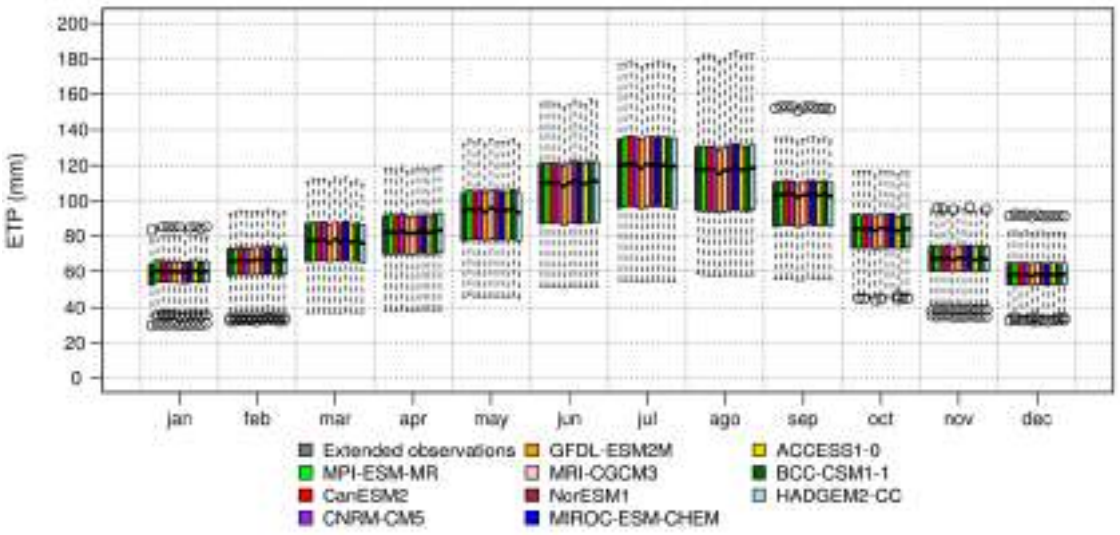

Figure 60. Validation results for potential evapotranspiration in Ter-Llobregat System: Comparison between extended observations and simulations performed using the downscaled CMIP5 climate models.

3.3.3. Lisbon

3.3.3.1. Temperature

For the city of Lisbon, results are good for both minimum and maximum temperature after correction. Before correction, most of the models presented important differences respect to the extended observations, with a remarkable problem around summer months for maximum temperature. GFDL-ESM2M shows values completely out of the general case. Despite this, after correction results improve significantly; GFDL-ESM2M model bias is corrected and the whole of the models behave in a more homogeneous way, following extended observations through the year. However, there is still some dispersion in summer months for maximum values.

According to the KS p-value criterion (p-value > 0.05), the correction improved both maximum and minimum temperatures (Fig. 61). All downscaled climate model present a suitable behaviour after the bias-correction.

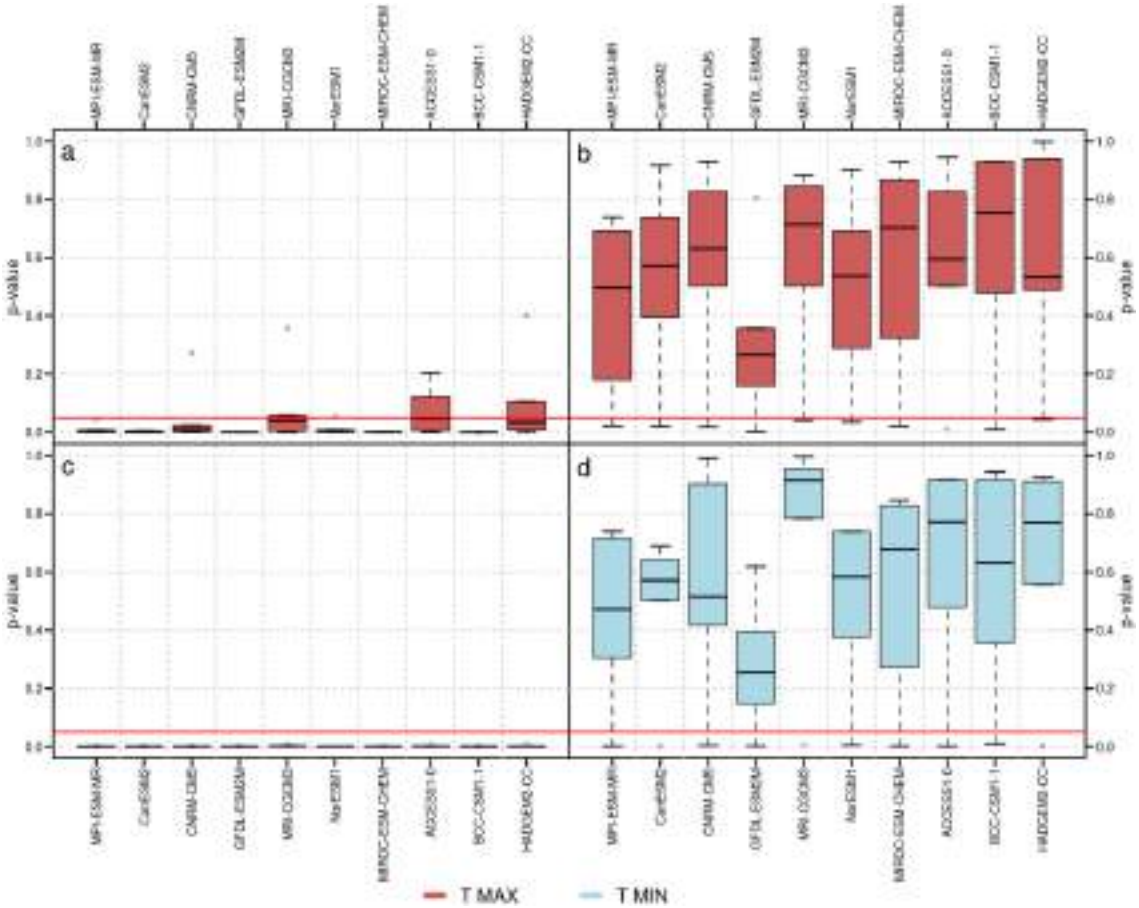

Figure 61. Validation results for temperature in Lisbon: KS p-value of the climate simulations of maximum (*a*, *b*) and minimum (c, d) temperature, obtained by comparison of the downscaled climate models, before (*a*, *c*) and after (b, d) the bias-correction, with the extended observations.

Regarding the standard deviation error, the downscaled GFDL-ESM2M shows a general bad behaviour before correcting. After correcting, the results improve and errors get close to zero for most of the models, including the GFDL-ESM2M (Fig. 62). However, the corrected output inherits an important uncertainty from the high initial error and this should be taken into account for the climate projections.

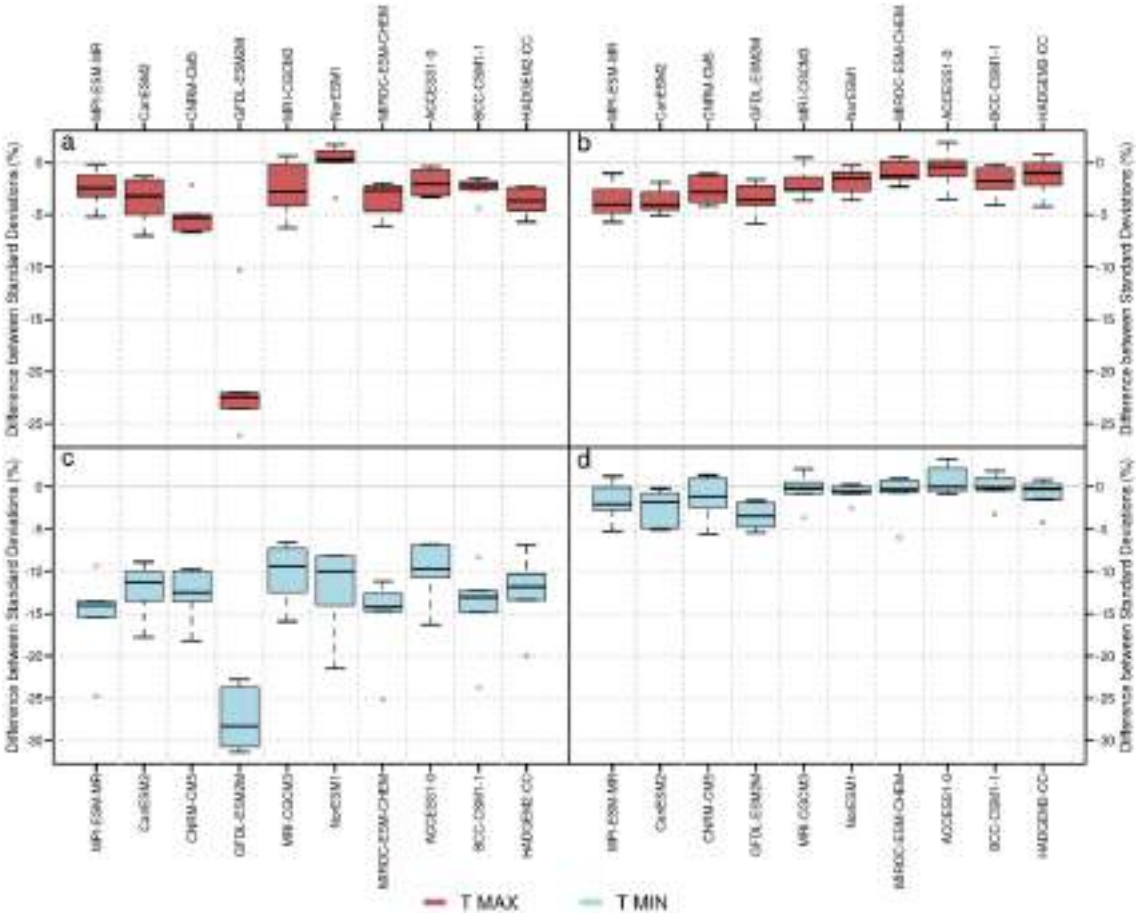

Figure 62. Error of the standard deviation in daily maximum (*a*, *b*) and minimum (*c*, *d*) temperature in Lisbon, obtained by comparison of the downscaled climate models, before (*a*, *c*) and after (*b*, *d*) the bias-correction, with the extended observations.

3.3.3.2. Precipitation

Before the bias-correction process, the precipitation simulated by the downscaled climate models presented a great dispersion among all of the models compared to observations in Lisbon. For instance, CanESM2 and MRI-CGCM3 model outputs overestimate rainfall values, in some cases more than double the observed values. Only summer presents acceptable values, but this is because of the summer rainfall minimum, where little or no precipitation is generally recorded. After correction, results improve notably, with all the models gathering around the median of the observed values. Only October still presents problems, with little scatter in observed values and high dispersion in simulated values.

Regarding the KS test, simulation of precipitation in Lisbon shows bad results for some downscaled climate models (Fig. 63). This is coherent with the bias found in the monthly precipitation values. The bias correction presented disparate results depending on the wet or dry values considered. If all values are taken into account, only a few models improved. Considering only wet values, the corrected model outputs showed improvements for most of cases. Only the MIROC-ESM-CHEM and CNRM-CM5 presented more than a half of the stations with KS p-value < 0.05 (i.e. their simulated time-series did pass the KS test).

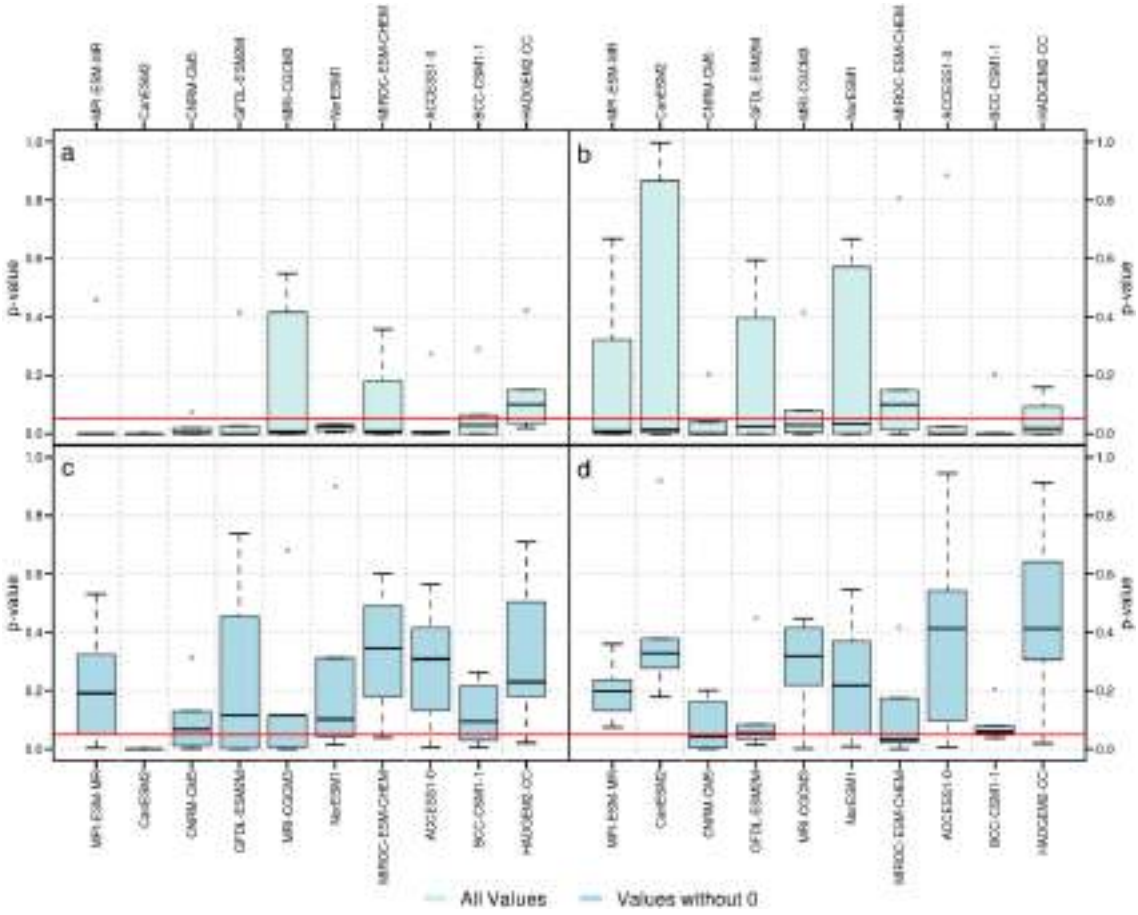

Figure 63. Validation results for precipitation in Lisbon: KS p-value of the climate simulations of dry/wet (*a*, *b*) and only wet (*c*, *d*) values of precipitation, obtained by comparison of the downscaled climate models, before (*a*, *c*) and after (*b*, *d*) the bias-correction, with the extended observations.

As another way to analyse the natural variability of the rainfall, the standard deviation was evaluated in Lisbon (Fig. 64). According to this analysis, downscaled CanESM2 and MRI-CGCM3 outputs presented overestimation in rainfall variability before correction. Despite the good results found after correction, a high uncertainty is expected from the use of these model outputs.

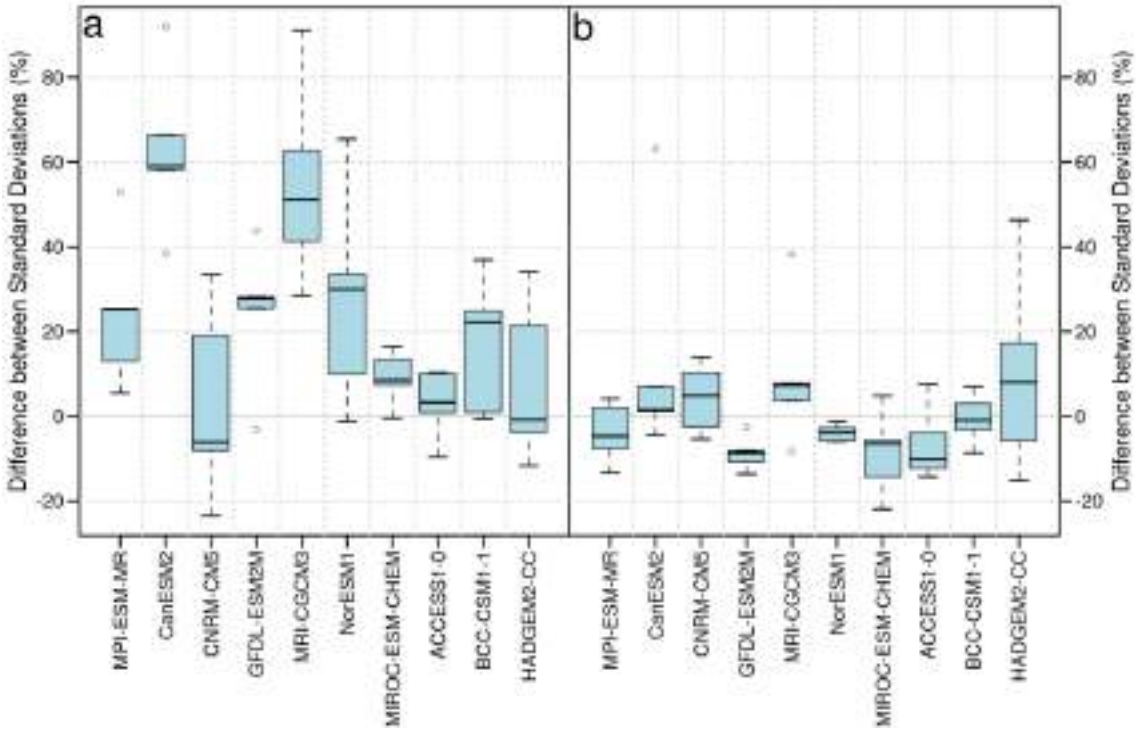

Figure 64. Error of the standard deviation in daily precipitation in Lisbon, obtained by comparison of the downscaled climate models, before (*a*) and after (*b*) the bias-correction, with the extended observations.

3.3.3.3. Other variables

Wind, relative humidity and pressure

Results for the city of Lisbon are similar for all variables considered (Fig. 65). Simulation of relative humidity (RH) presents acceptable results after correction. For wind and sea level pressure (SLP) variables, results are also satisfactory. Bias values are smaller and oscillate around zero for the whole of the model outputs, and approximates to zero when corrected. KS p-values rise significantly. This proves that the correction not only almost suppresses the bias (as it is meant to be), but increases the similarity between time-series as almost all of the cases surpass the significance threshold of 0.05 for every model output (except for the downscaled BCC-CSM1-1 and CanESM2 models in SLP).

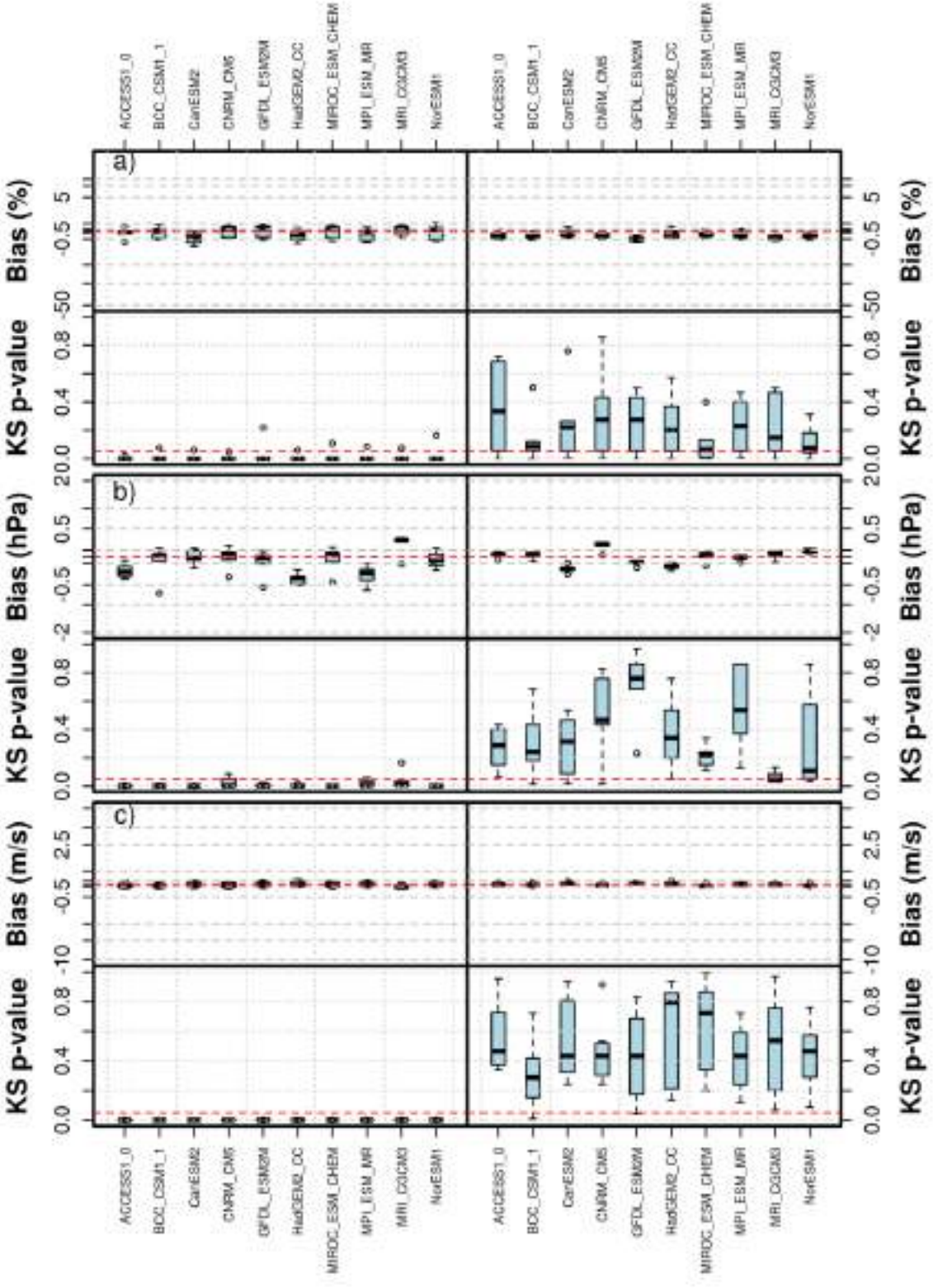

Figure 65. Validation results for other variables in Lisbon city: Bias and KS p-value for the downscaled CMIP5 outputs, before (*left*) and after (*right*) the correction: *a*) Relative Humidity, *b*) Sea level pressure, *c*) Wind. Red lines are the 0 for BIAS and 0.05 for the KS p-value.

Oceanic variable: Sea level

The simulation of the mean sea level for the Cascais buoy (Lisbon) presented a good performance in most of the downscaled climate models (Fig. 66). However, the standard deviation is generally underestimated by all them, especially regarding the intra-annual variability.

Regarding the sea level rise, no significant increase was observed in 1960-1990, but completing the time-series until 2009, sea level rise is up to +2 mm/year in Cascais since 1980 (Antunes and Taborda 2009). The historical values are adequately simulated by 7/10 downscaled models for Lisbon, although most of the models showed a lower rise rate than the observed one.

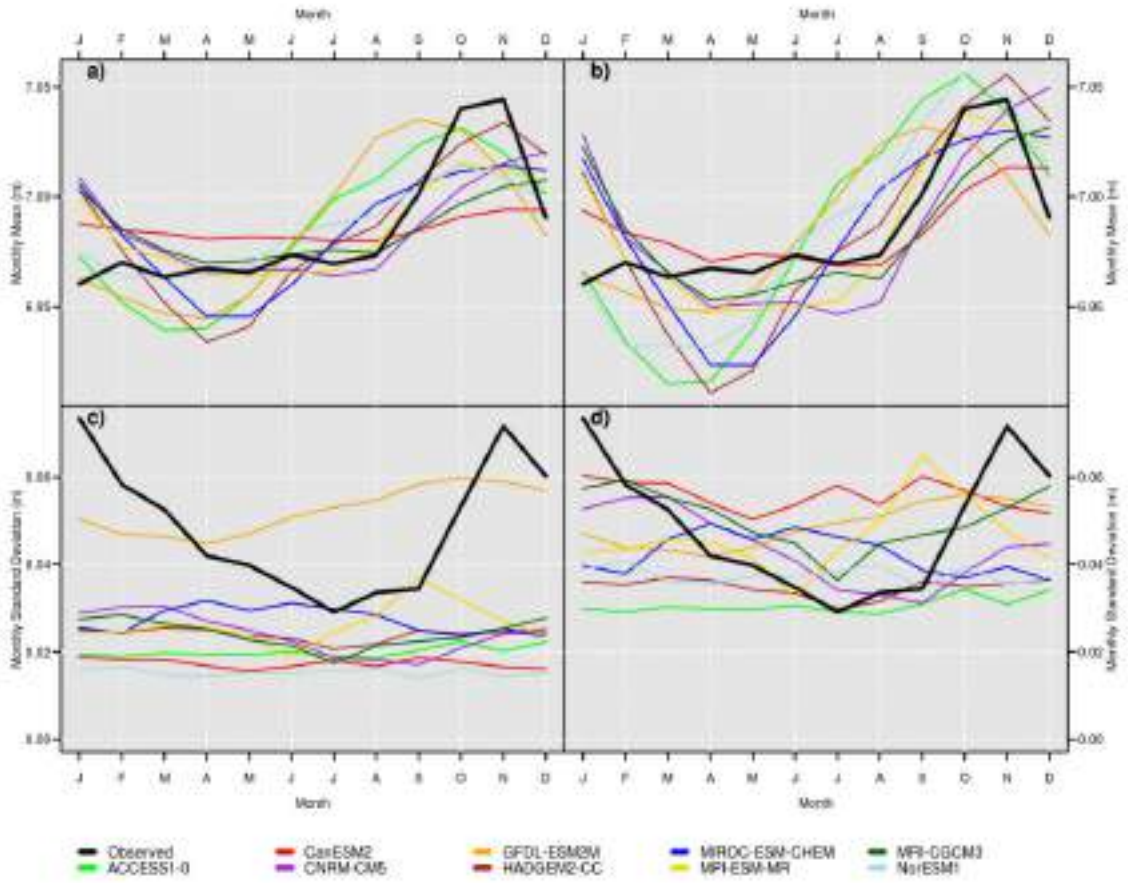

Figure 66. Validation results for sea level in Cascais buoy (Lisbon), before (*a*, *c*) and after (*b*, *d*) the bias correction: monthly mean values (*a*, *b*) and monthly standard deviation (*c*, *d*).

Derived variable: evapotranspiration

Validation of potential evapotranspiration in Lisbon shows again an absolute resemblance between models, confirming the results obtained in the verification process (Fig. 67).

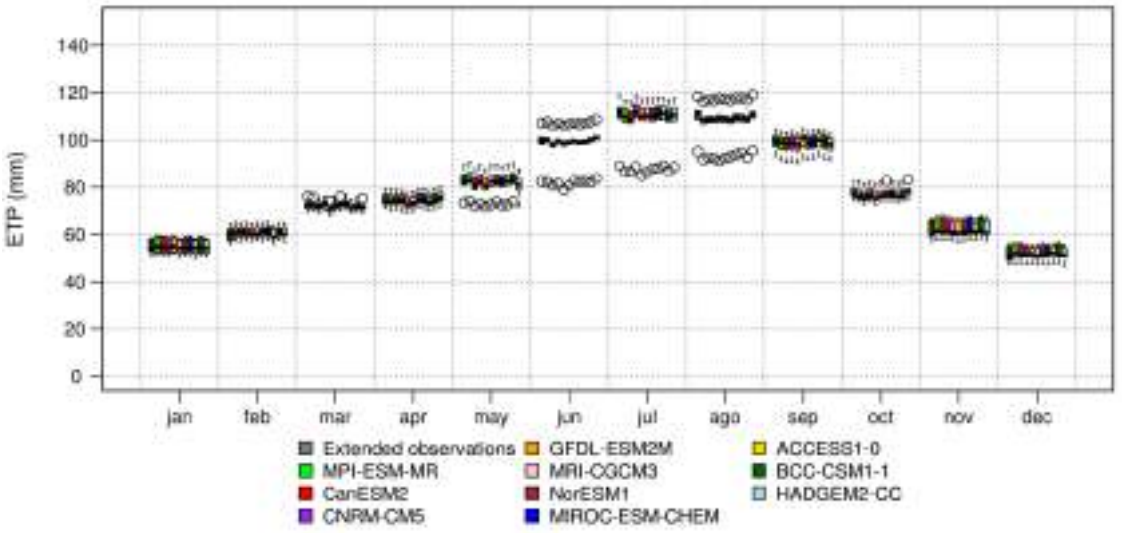

Figure 67. Validation results for potential evapotranspiration in Lison: Comparison between extended observations and simulations performed using the downscaled CMIP5 climate models.

3.3.4. Bristol

3.3.4.1. Temperature

The validation results for Bristol lead to both minimum and maximum temperatures are adequately simulated after correction. However, before correction, models showed a high dispersion in the monthly averages, being the most problematic values focused around summer months, especially under the GFDL-ESM2M model.

For the Southwest England and South Wales area, model outputs are also satisfactorily corrected, with all the mean simulations gathering around the observed values and presenting a homogeneous intra-annual variability.

This improvement caused by the bias-correction can be seen through the KS test *p*-value (Fig. 68 and 69). In fact, all model outputs presented *p*-value > 0.05 after correction. It is notable that three downscaled models (CanESm2, MRI-CGCM3 and NorESM1) were acceptable in Bristol even before correction, for more than half of the stations (Fig. 68).

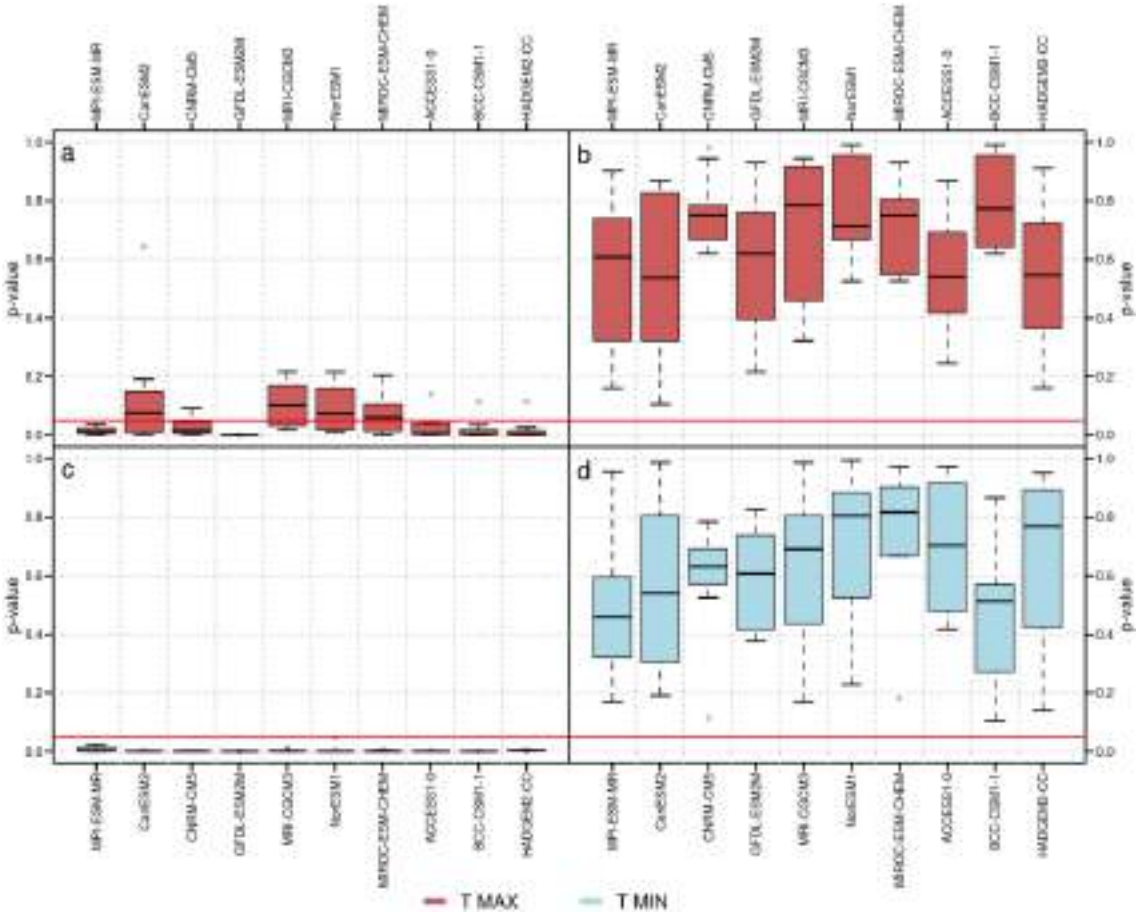

Figure 68. Validation results for temperature in Bristol city: KS p-value of the climate simulations of maximum (*a*, *b*) and minimum (*c*, *d*) temperature, obtained by comparison of the downscaled climate models, before (*a*, *c*) and after (*b*, *d*) the bias-correction, with the extended observations.

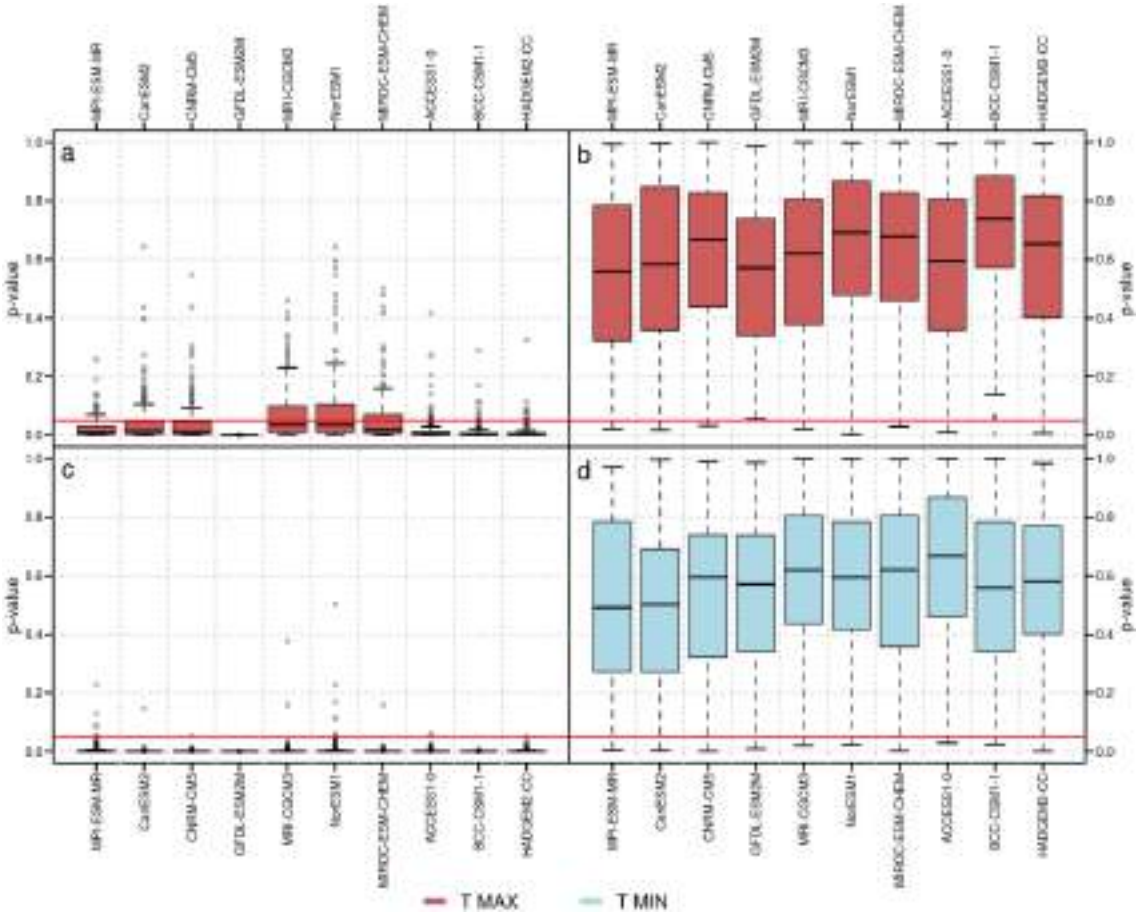

Figure 69. The same as Fig. 68 for the England – South Wales area.

Before correction, downscaled models tend to underestimate the standard deviation (comparing with observations) for both maximum and minimum temperature, with the exception of MIROC for maximum values, which adequately simulates the temperatures. It is remarkable that GFDL-ESM2M showed the poorest result, even after the bias-correction (Fig. 70 and 71). The rest of the downscaled models improved the standard deviation after correction.

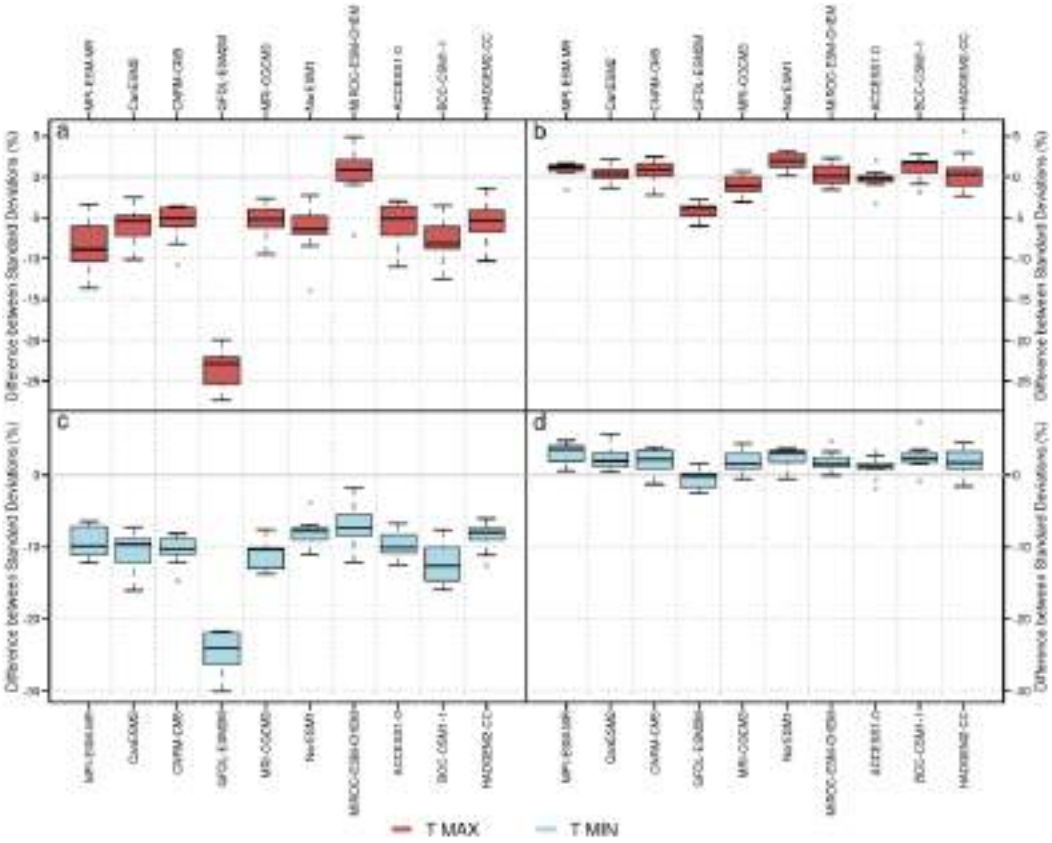

Figure 70. Error of the standard deviation in daily maximum (*a*, *b*) and minimum (*c*, *d*) temperature in Bristol, simulated by the downscaled climate models, before (*a*, *c*) and after (*b*, *d*) the bias-correction.

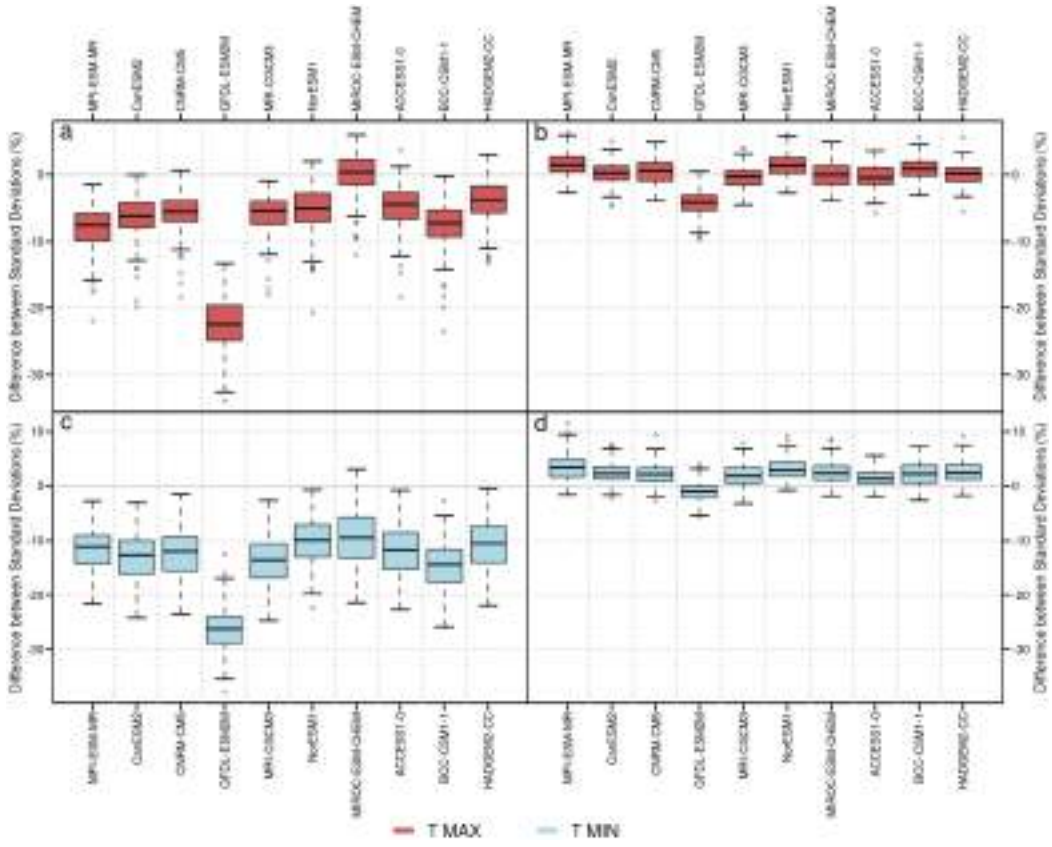

Figure 71. The same as Fig. 70 for the England – South Wales area.

3.3.4.2. Precipitation

Downscaled climate models for the precipitation in Bristol showed poor results in monthly mean values before the bias-correction. For instance, the downscaled CanESM2 output overestimates the mean values in some cases more than the double of the observed ones. After correction, the results improve and all models gather around the observed values in most of the cases. The improvement is more notable for the Southwest England – South Wales area.

In order to analyse better the validation process, KS p-value is shown for both total and only positive values of precipitation (i.e. > 0.1 mm). According to this, all downscaled models except HADGEM-CC improve the positive values of precipitation. However, the number of wet days is poorly simulated by four climate models even after correction (Fig. 72).

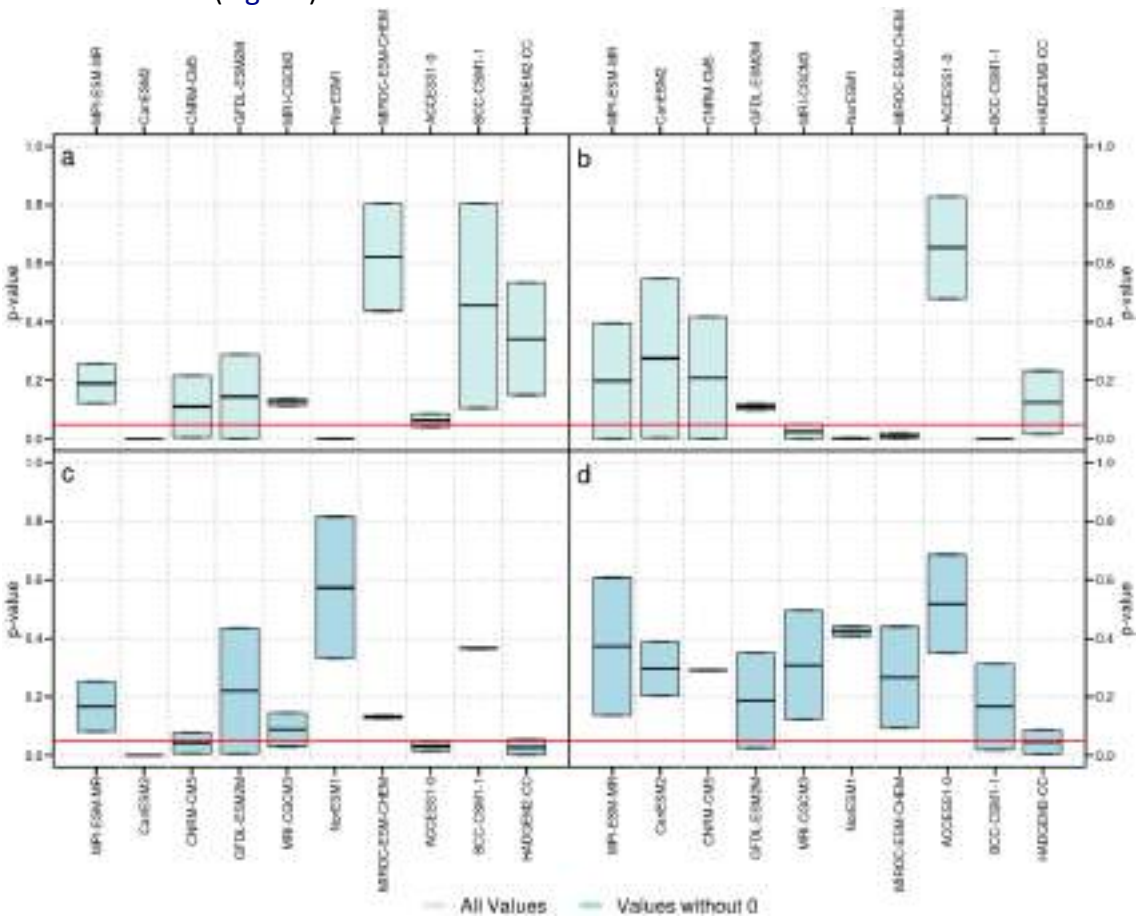

Figure 72. Validation results for precipitation in Bristol city: KS p-value of the climate simulations of dry/wet (*a*, *b*) and only wet (*c*, *d*) values of precipitation, obtained by comparison of the downscaled climate models, before (*a*, *c*) and after (*b*, *d*) the bias-correction, with the extended observations.

Results of KS p-value for Southwest England – South Wales are poorer than the case of Bristol city (Fig. 73). The error in standard deviation improves after the bias-correction Bristol and its surrounding area (Fig. 74 and 75), but the KS p-value criterion is more important to reject determined simulations. Therefore, only simulations for a half of the stations are acceptable to be used in future projections.

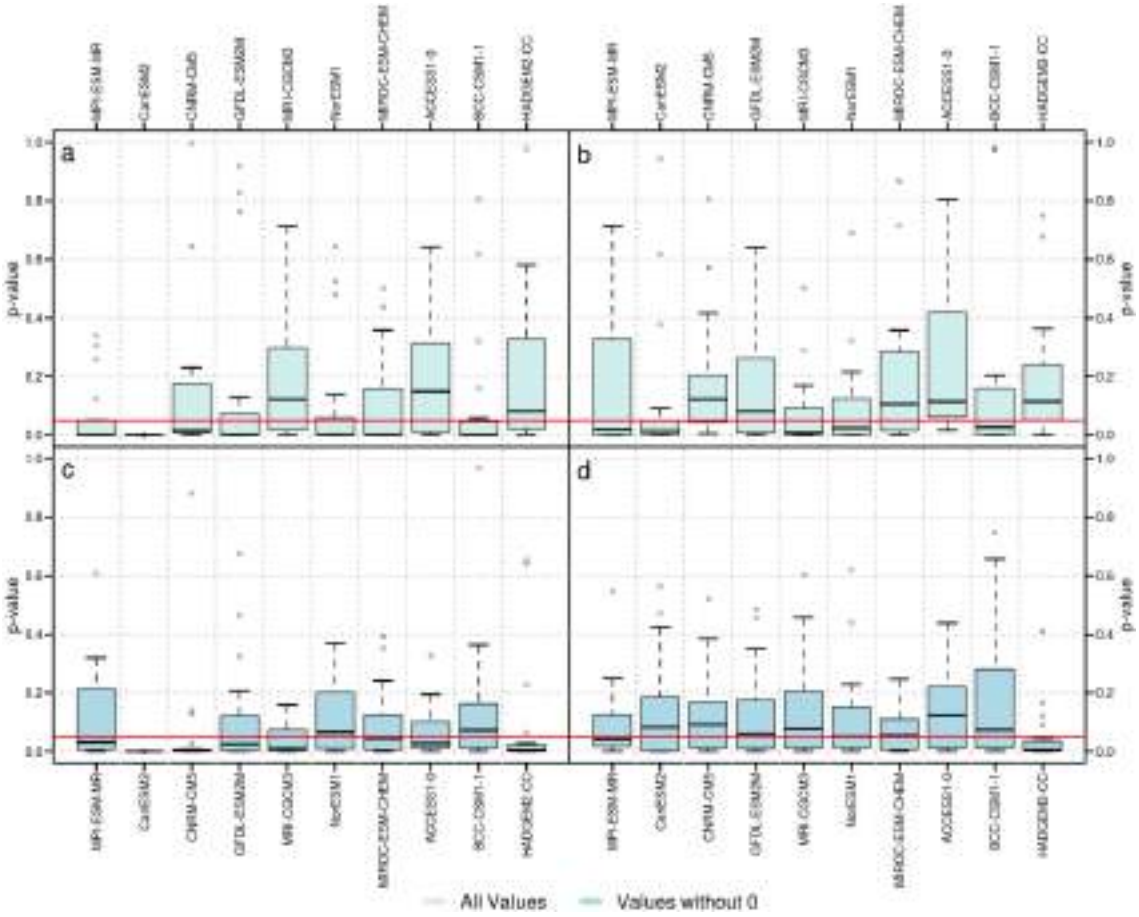

Figure 73. The same as Fig. 72 but for the Southwest England – South Wales area.

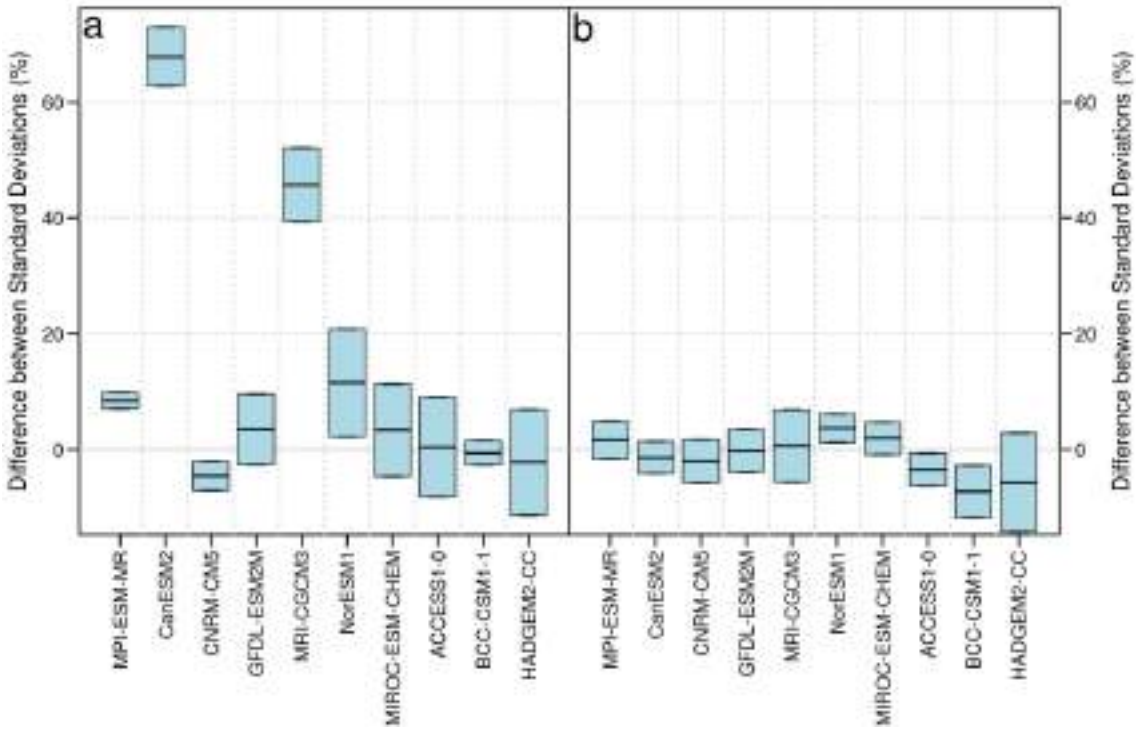

Figure 74. Error of the standard deviation in daily precipitation in Bristol, obtained by comparison of the downscaled climate models, before (*a*) and after (*b*) the bias-correction, with the extended observations.

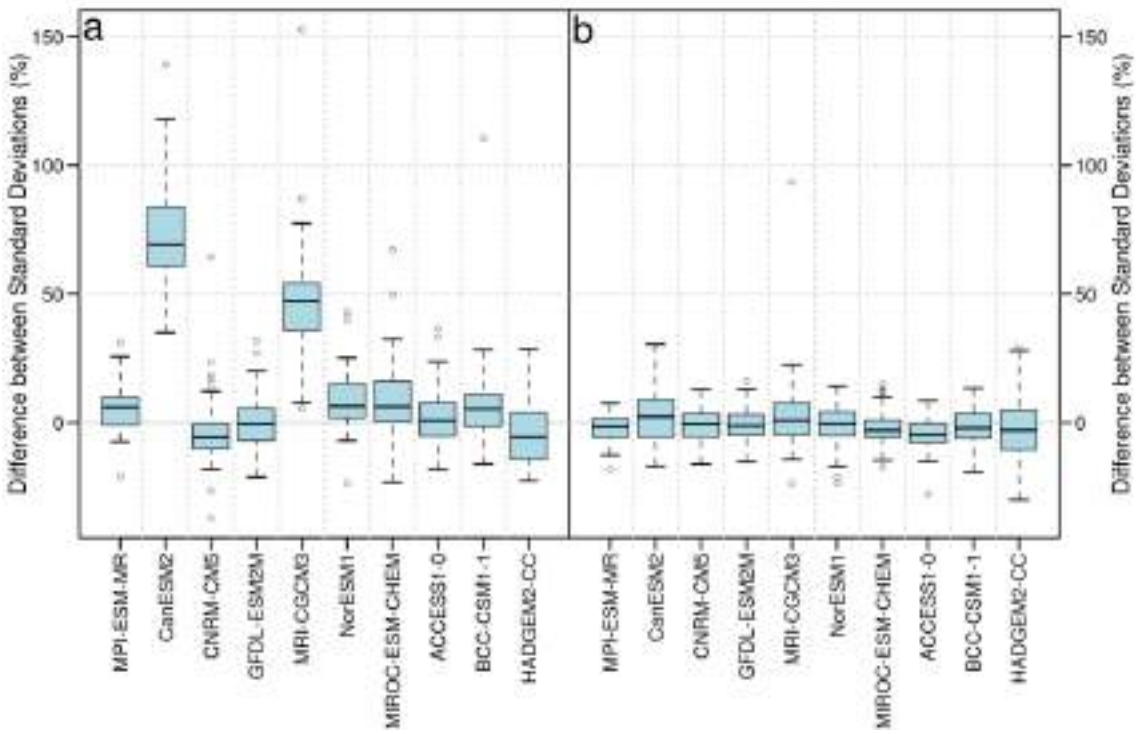

Figure 75. The same as Fig. 74 but for the Southwest England – South Wales area.

3.3.4.3. Other variables

Wind, relative humidity and pressure

Results of the other variables simulated for Bristol presented the same characteristics for both the city and the watershed, despite the number of stations considered.

Validation results are satisfactory for humidity, sea level pressure and wind. Bias values are smaller and oscillate around zero for the whole of the model outputs, and approximates to zero when corrected (Fig. 76 and 77). Finally, KS p-values rise significantly after the bias correction.

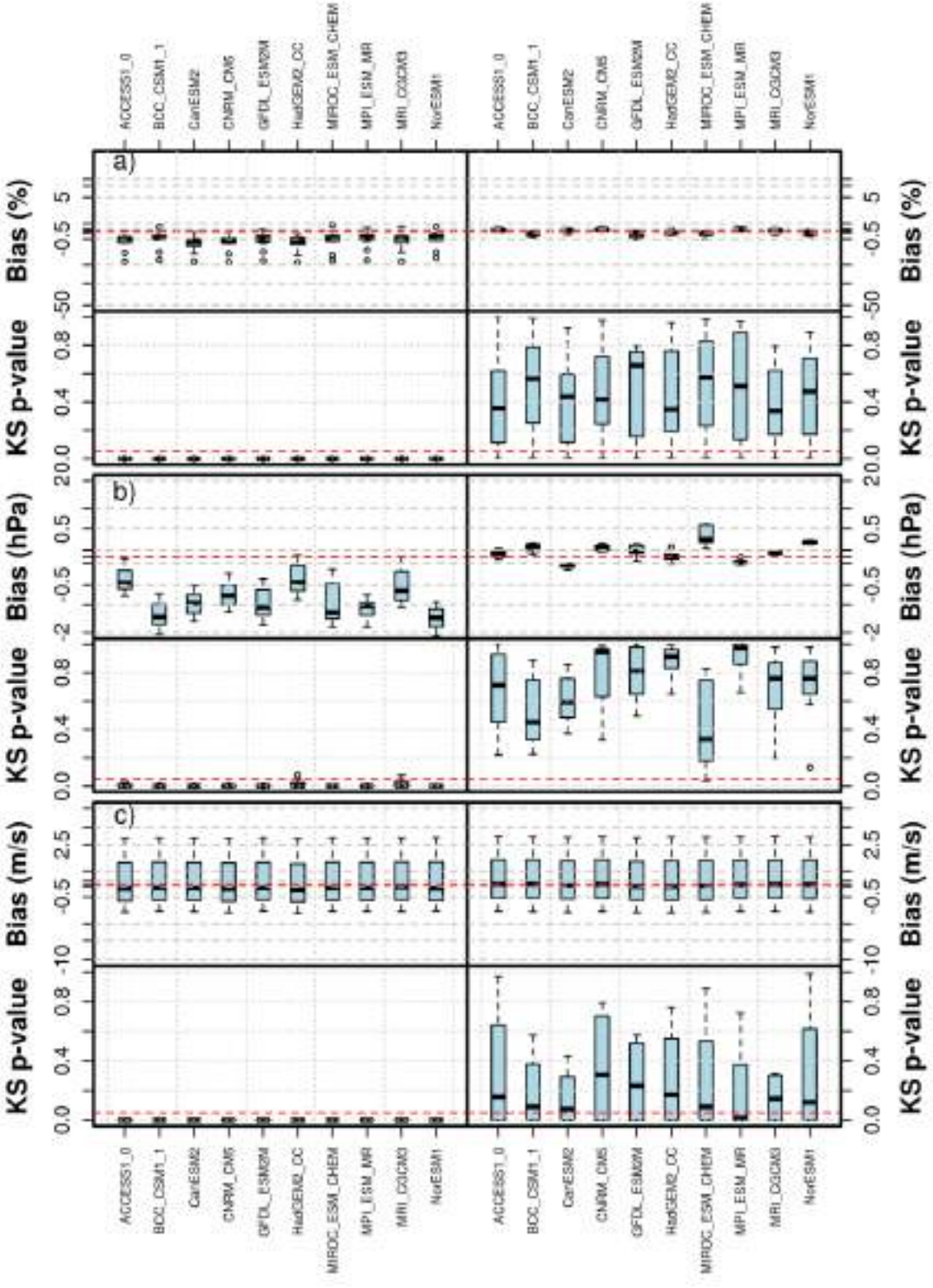

Figure 76. Validation results for other variables in Bristol city: Bias and KS p-value for the downscaled CMIP5 outputs, before (*left*) and after (*right*) the correction: *a*) Relative Humidity, *b*) Sea level pressure, *c*) Wind. Red lines are the 0 for BIAS and 0.05 for the KS p-value.

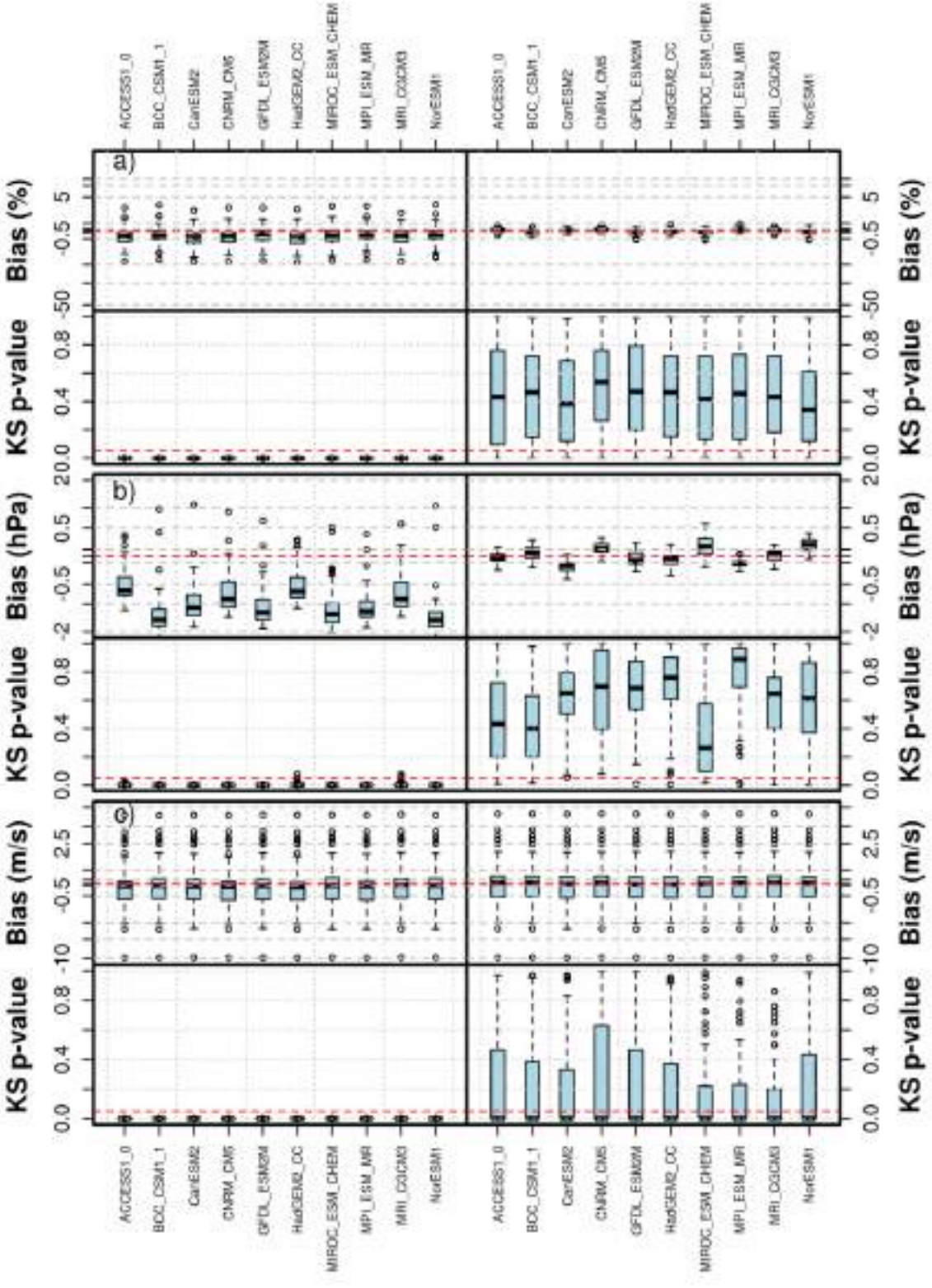

Figure 77. The same as Fig. 76 but for the Southwest England – South Wales area.

Oceanic variables: Wave height and sea level

The downscaled simulations for wave height present a good result after correction of the systematic error, according to the KS *p*-value (Fig. 78a). Results for the meteorological sea level or surge are also suitable after correction, since all climate model outputs passed the KS test (Fig. 78b).

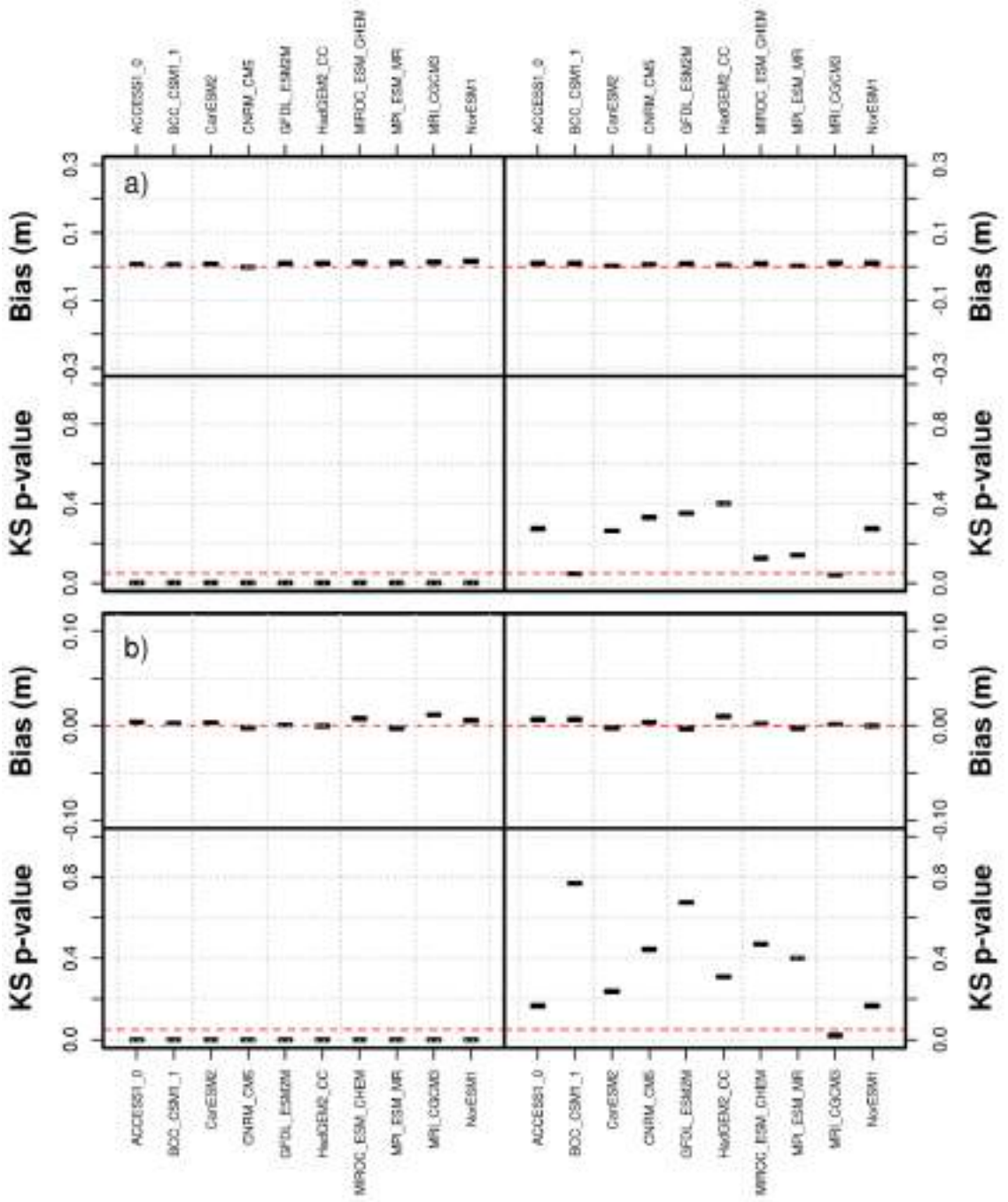

Figure 78. Validation results for the wave height (a) and daily surge in the Bristol main buoy: Bias and KS p-value for the downscaled CMIP5 outputs, before (*left*) and after (*right*) the correction. Red lines are the 0 for BIAS and 0.05 for the KS p-value.

Regarding the sea level, both monthly mean values and monthly standard deviation are adequately simulated by all oceanic models (Fig. 79). Nevertheless, the historical sea level rise is underestimated by all oceanic model outputs in Bristol. Particularly it is observed a significant rise up to +0.5 m/100y (p-value < 0.01), while the maximum past simulation is up to +0.2 m/100y (according to the CNRM-CM5).

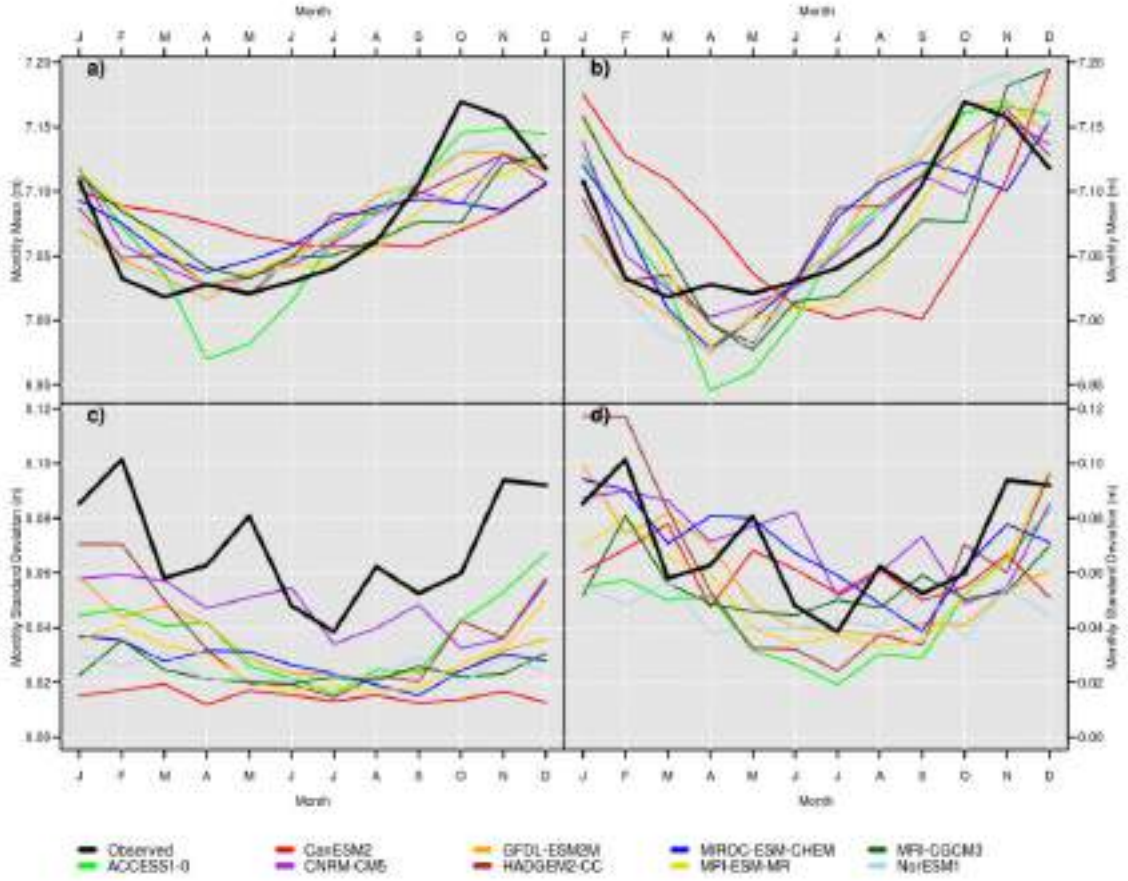

Figure 79. Validation results for sea level in Hinkley Point buoy (Bristol), before (*a*, *c*) and after (*b*, *d*) the bias correction: monthly mean values (*a*, *b*) and monthly standard deviation (*c*, *d*).

Derived variables: snowfall and evapotranspiration

The simulated snowfall for Bristol shows a great dispersion for the climate averages of both snowfall days and snow water equivalent depth (Fig. 80a-80b). For instance, some models simulate up to 8 snowfall days in January (e.g. MIROC-ESM-CHEM) and other simulates less than 2 snowfall days for the same month (e.g. BCC-CSM1-1).

Regarding the adjoining regions of Bristol, the downscaled climate model outputs provides better results for both snowfall days and snow water equivalent depth (Fig. 80c-80d). Only GFDL-ESM2M presented an unacceptable validation for these climate variables.

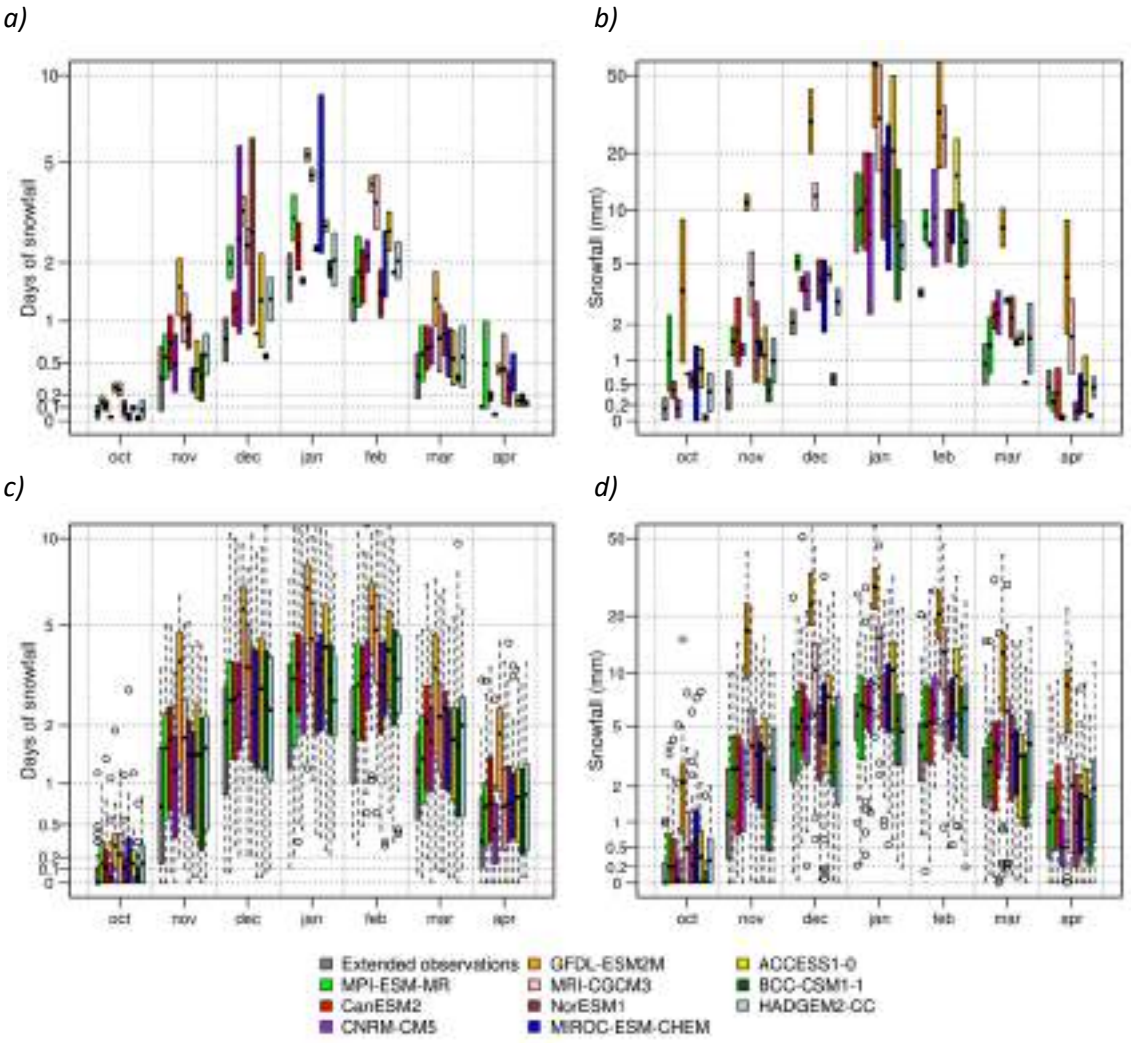

Figure 80. Validation results for snow simulation in Bristol (*top*) and Southwest England – South Wales area (*bottom*): Snow days (*left*) and snow water equivalent (right) per year according to the CMIP5 climate models.

Potential evapotranspiration simulated for Bristol and adjoining regions showed a great resemblance between all the results provided by the downscaled climate models (Fig. 81).

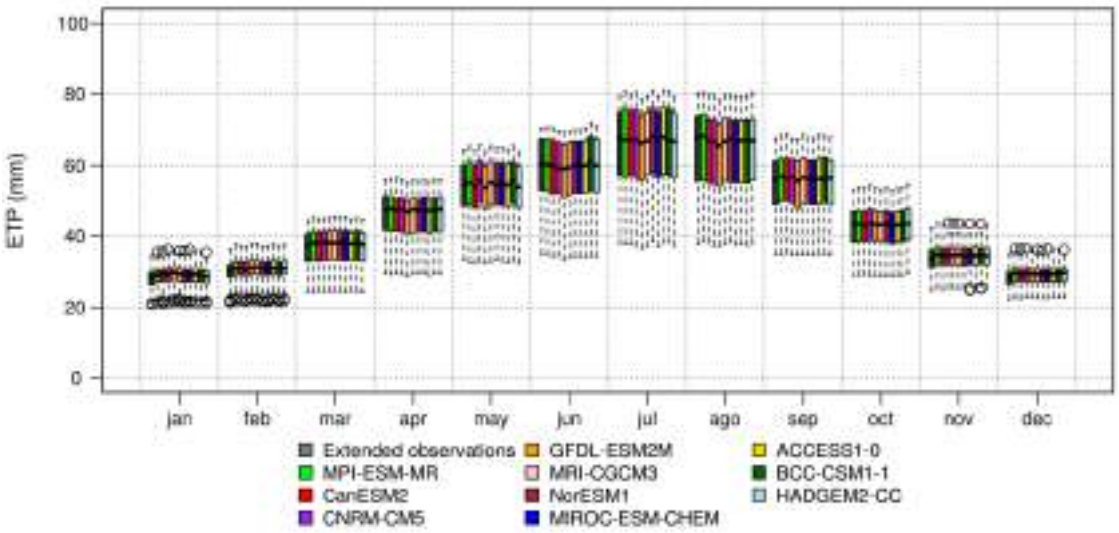

Figure 81. Validation results for potential evapotranspiration in Southwest England - South Wales: Comparison between extended observations and simulations performed using the downscaled CMIP5 climate models.

3.3.5. Summary of the downscaled climate models validation

After correction, all climate model outputs are valid for temperature, wind, ETP, wave height and meteorological surge (only available for Bristol). However, remarkable problems are found in some cases. Temperature is badly simulated by the downscaled GFDL-ESM2M before corrections, with a high underestimation of the standard deviation.

Precipitation simulated by the downscaled HADGEM2-CC showed problems for the hydrological area of influence of Barcelona and Bristol, and therefore it has been removed for the climate projections (Table 8). Errors in temperature are propagated in the estimation of snowfall, even after correction, and then GFDL-ESM2M cannot be used for this variable.

Table 8. Summary of the validation for the downscaled climate models according to the previous assessment.

Variable	City	Model									
		ACCESS1-0	BCC-CSM1-1	CanESM2	CNRM-CM5	GFDL-ESM2M	HADGEM2-CC	MIROC-ESM-CHEM	MPI-ESM-MR	MRI-CGCM3	NorESM1-M
Temperature	Barcelona										
	Lisboa										
	Bristol										
Precipitation	Barcelona										
	Lisboa										
	Bristol										
Wind	Barcelona										
	Lisboa										
	Bristol										
Snowfall	Barcelona										
	Bristol										
ETP	Barcelona										
	Lisboa										
	Bristol										
RH	Barcelona										
	Bristol										
Sea level	Barcelona										
	Lisboa										
	Bristol										
Wave height	Barcelona										
	Bristol										
Surge	Bristol										
Pressure	Bristol										

Legend:

- Valid according to less than 50% of statistics
- Valid according to more than 50% and less than 70% of statistics
- Valid according to more than 70% of statistics
- Not available

Sea level rise is generally badly simulated by the climate models for the three cities, even after the bias correction. Only a few models passed most of the statistical test. Therefore, results of sea level projections should be used with great care.

3.4. Validation of the application to the Decadal Models

3.4.1. About this

Section 3.4 presents the results of the validation of the drift-corrected CMIP5 models, obtained according to the method described in Sec. 2.2.3. Like the teleconnection-based predictions, the drift-corrected dynamical outputs were focused in generating near-term (decadal) climate predictions.

In the decadal modelling context, the validation process consists in evaluating the performance of the drift-correction applied to each decadal model. In this study, the validation was based on ten historical 10-year horizon experiments with up to 4 runs for each one (see more details in Sec. 2.2.3). The historical experiments were compared with real observations and all statistics were computed according to the Sec. 2.3.2.

Results of validation are structured in three subsections according to the studied cities and their surrounding areas. Finally, Sec. 3.4.5 summarises the main results of the validation process for all variables and cities.

3.4.2. Barcelona

Metropolitan area

For Barcelona, maximum and minimum temperature simulated by all decadal models presented a SAE < 1 for horizons greater than 4 years (Fig. 82). For the rest of variables, a few models are acceptable depending on the considered horizons (< 8 years).

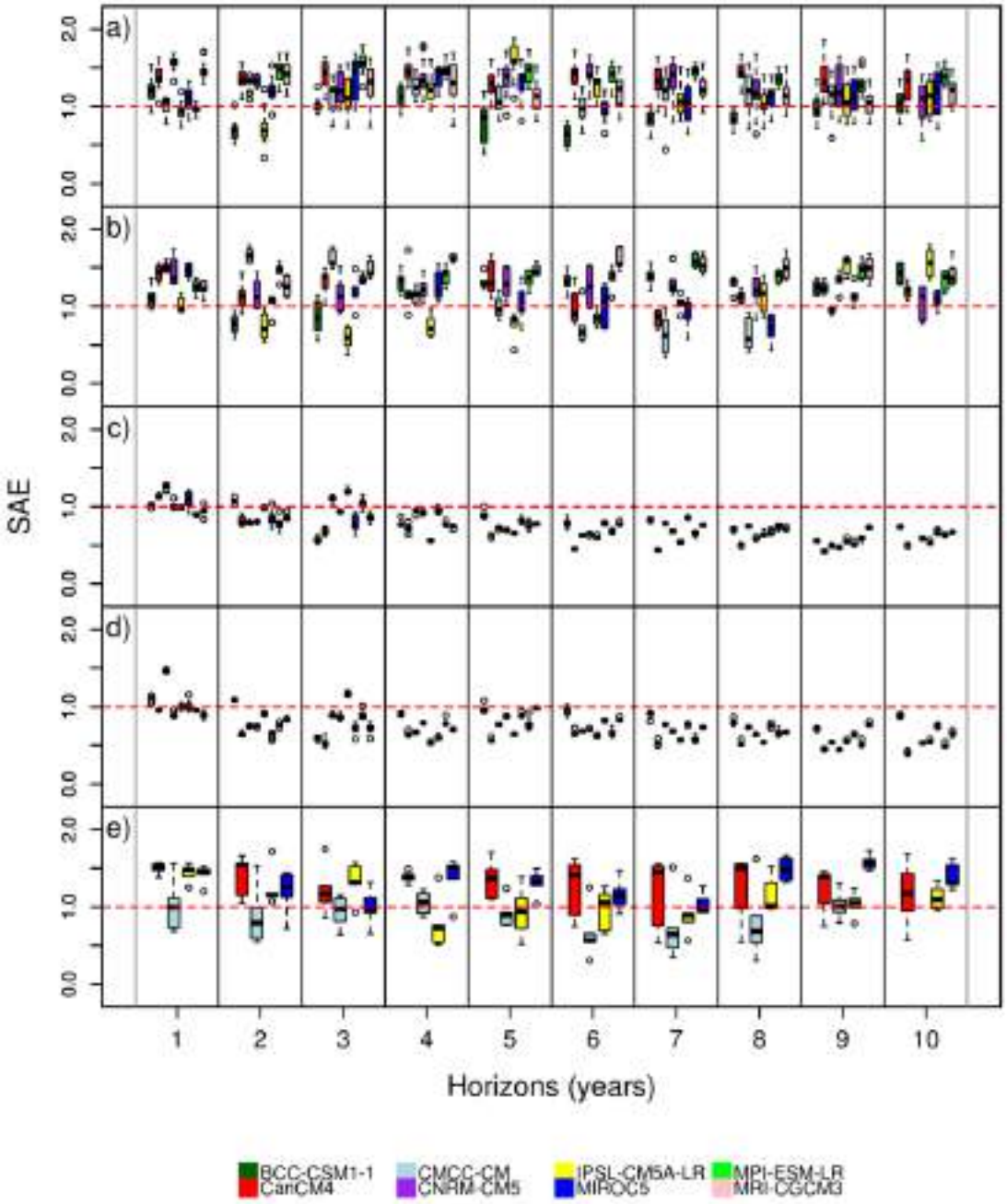

Figure 82. Validation results (SAE) for all the variables simulated by drift-corrected decadal outputs in Barcelona: a) Precipitation, b) Sea level pressure, c) Maximum temperature, d) Minimum temperature and e) Wind. Red dashed line indicates the threshold of SAE = 1.

Ter-Llobregat System

Very similar results to Barcelona were found in the validation process of decadal simulations for the climate variables in Ter-Llobregat system (Fig. 83).

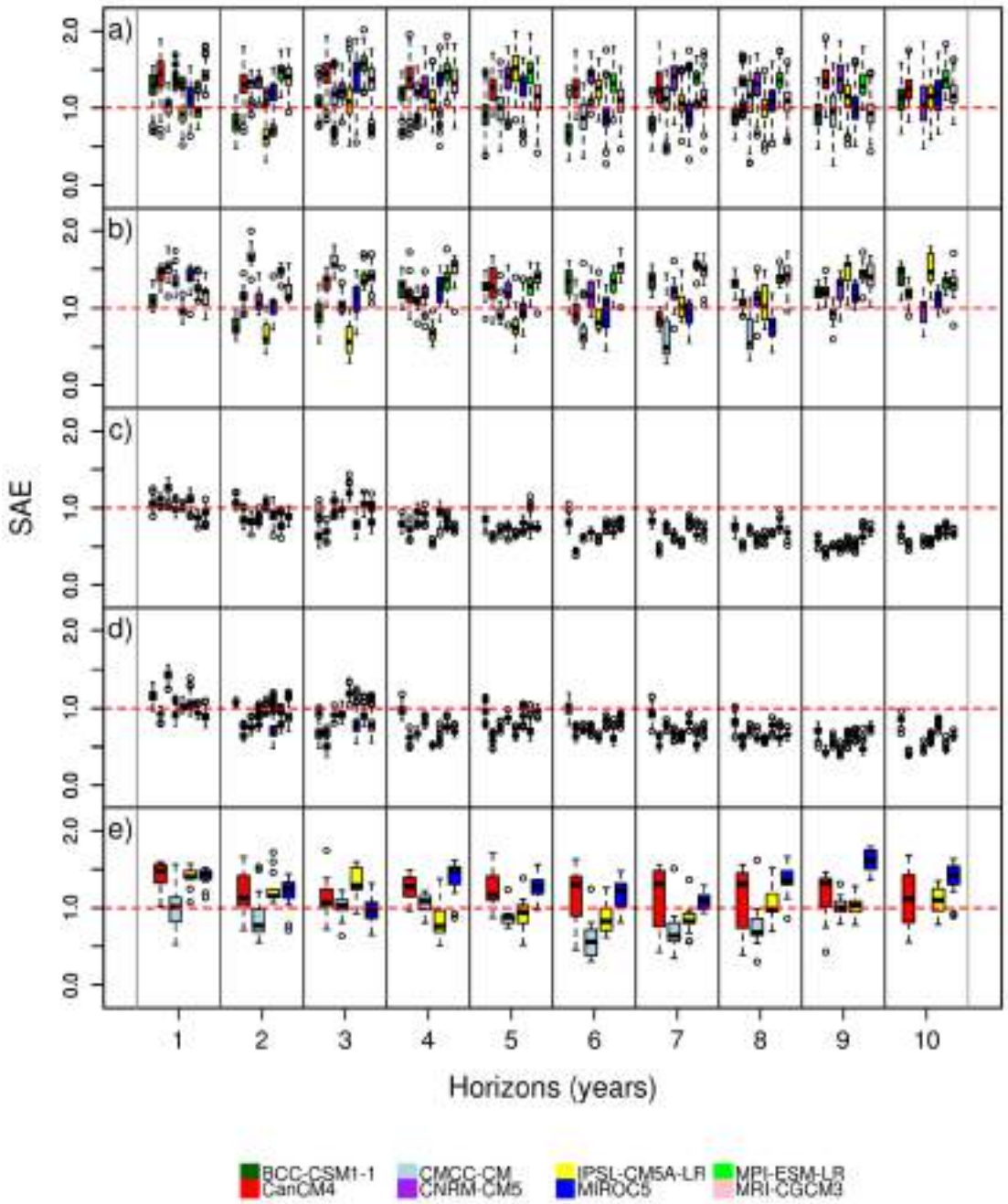

Figure 83. The same as Fig. 81 but for Ter-Llobregat system.

3.4.3. Lisbon

In Lisbon, maximum and minimum temperature simulated by most of decadal models presented a SAE < 1 for horizons greater than 4 years, except for BCC-CSM.1-1 (Fig. 84). Regarding the rest of variables, only one or two models are acceptable for horizons below 8 years.

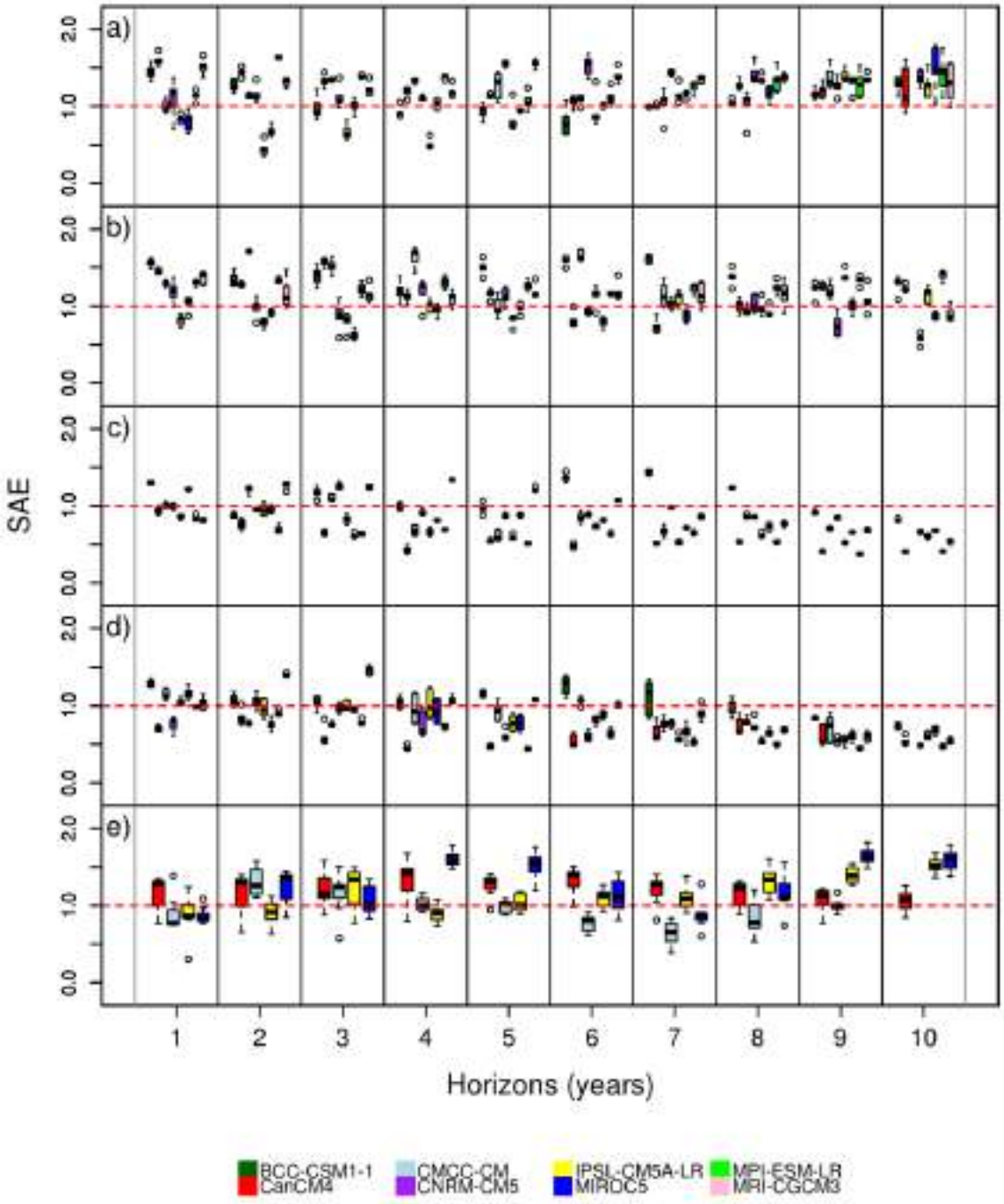

Figure 84. Validation results (SAE) for all the variables simulated by drift-corrected decadal outputs in Lisbon: a) Precipitation, b) Sea level pressure, c) Maximum temperature, d) Minimum temperature and e) Wind. Red dashed line indicates the threshold of SAE = 1.

3.4.4. Bristol

Metropolitan area

Like in Lisbon, maximum and minimum temperatures simulated in Bristol by most of decadal models presented a SAE < 1 for horizons greater than 4 years, except three model outputs (Fig. 85). Regarding the rest of variables, only one or two model outputs are acceptable for horizons below 8 years.

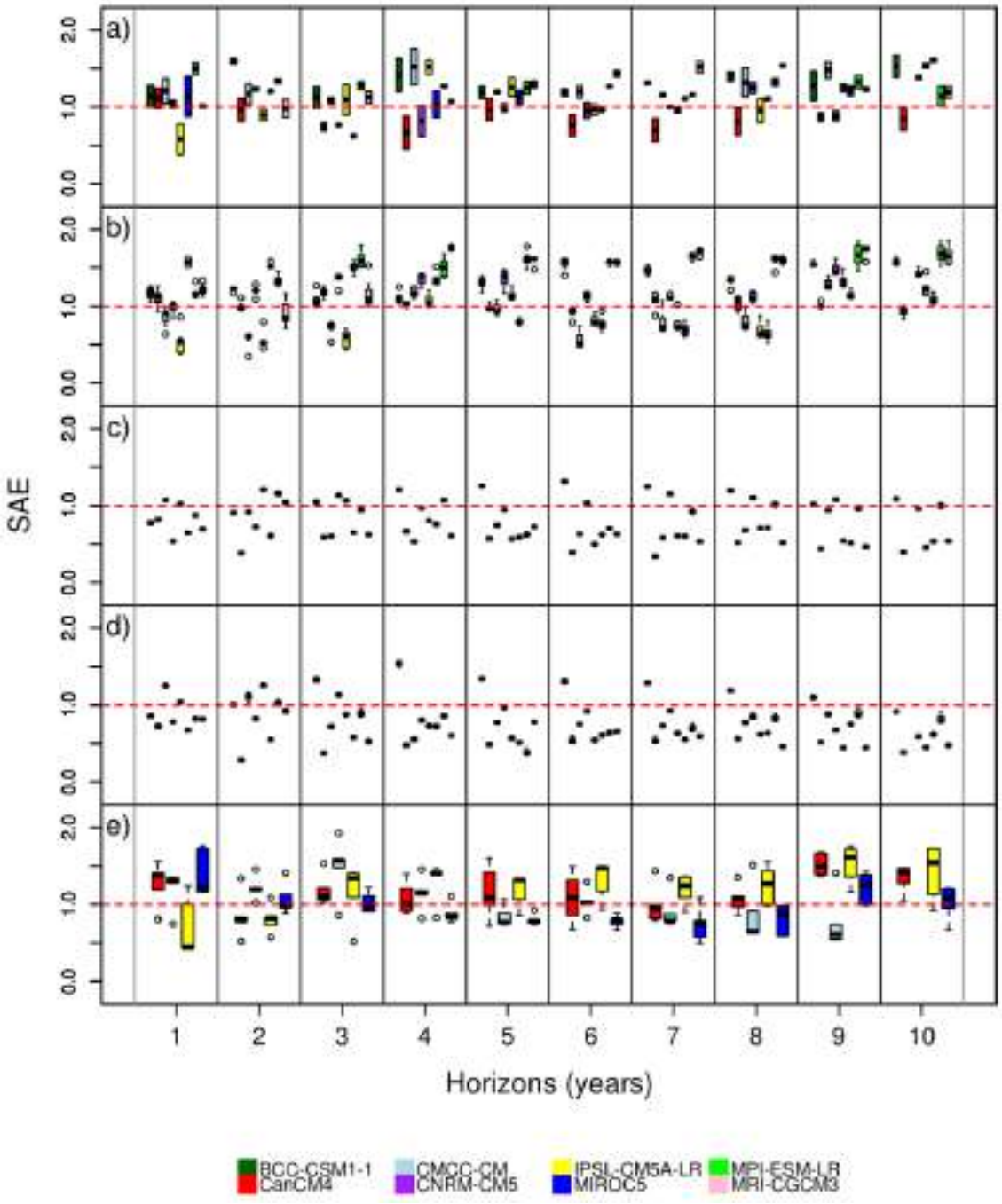

Figure 85. Validation results (SAE) for all the variables simulated by drift-corrected decadal outputs in Bristol: a) Precipitation, b) Sea level pressure, c) Maximum temperature, d) Minimum temperature and e) Wind. Red dashed line indicates the threshold of SAE = 1.

Southwest England – South Wales area

Very similar results to Bristol were found in the validation process of decadal simulations for the climate variables in Southwest England – South Wales area (Fig. 86).

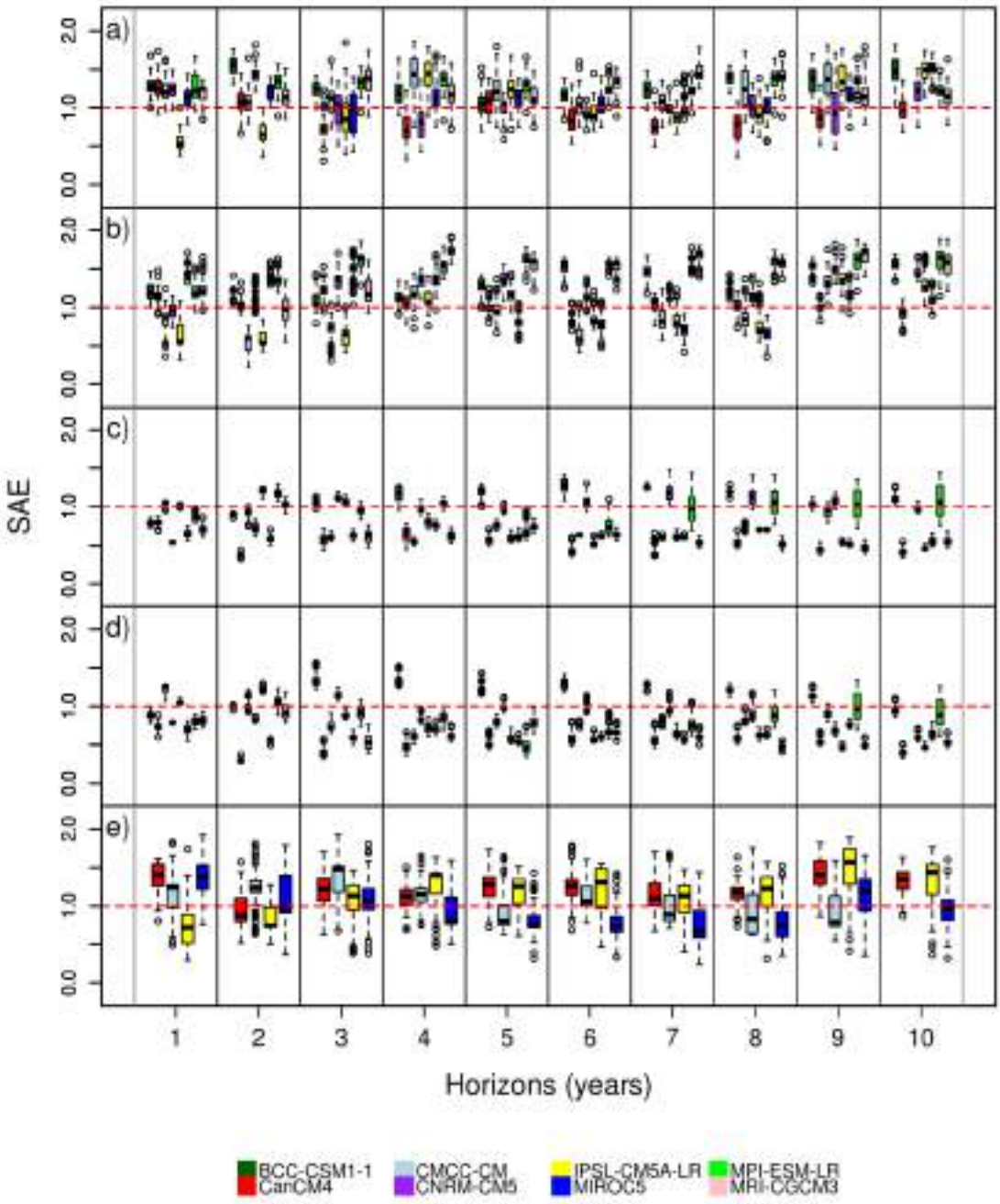

Figure 86. Validation results (SAE) for all the variables simulated by drift-corrected decadal outputs in Southwest England – South Wales area: a) Precipitation, b) Sea level pressure, c) Maximum temperature, d) Minimum temperature and e) Wind. Red dashed line indicates the threshold of SAE = 1.

3.4.5. Summary of the decadal validation

As a way to summarize the decadal validation process, a classification of the climate models has been performed. All the previous information regarding SAE analysis and the conclusions are reflected in Table 9. A code of colours has been adopted according the number of horizons well simulated by the decadal models. Only those models that could achieve a yellow/green colour after counting were considered as trustworthy enough to be used for the decadal forecasts. Therefore, those obtaining a red/orange colour were discarded for next steps.

Table 9. Summary of the validation for the drift-corrected decadal models according to the SAE criterion. The process counts the number of consecutive horizons where the model achieves a SAE < 1.

Decadal model	Pressure			Precipitation			Maximum temperature			Minimum temperature			Snowfall			Wind		
	Barcelona	Bristol	Lisbon	Barcelona	Bristol	Lisbon	Barcelona	Bristol	Lisbon	Barcelona	Bristol	Lisbon	Barcelona	Bristol	Lisbon	Barcelona	Bristol	Lisbon
BCC-CSM1-1																		
CanCM4																		
CMCC-CM																		
CNRM-CM5																		
IPSL-CM5A-LR																		
MIROC5																		
MPI-ESM-LR																		
MRI-CGCM3																		

Legend:

- 7-10 horizons with SAE < 1
- 4-6 horizons with SAE < 1
- 1-3 horizons with SAE < 1
- 0 horizons with SAE < 1
- Not available

It is clear that both temperature variables are fairly good estimated by almost every model for the three RESCCUE cities, with green colours widely present. This was expected due to temperature nature, responding clearly to a normal distribution along the year with a good and regular climatic behaviour when considering long periods of time.

As it was mentioned in each city discussion, wind, pressure and precipitation presented worse results due to their more chaotic daily distribution, with great variability. Only a few models are able to represent properly the variable historical behaviour. Precipitation and wind are especially problematic ones, with some cities without good results, and some having just one model to describe the whole period of time, what exposes future projections to possible systematic errors of the model.

Snowfall is directly simulated by a few decadal models and then it is considered a derived variable as in the case of the climate variables (ETP and snowfall).

4. Climate and decadal projections

4.1. Barcelona

4.1.1. Temperature and precipitation

Section 4 presents all the results about climate projections (until 2100) and decadal predictions (until 2035) following an ensemble strategy according to the Sec. 2.3.3.

All climate projections agree on simulating a pronounced increase in temperature for all seasons and under all scenarios, whic would be gently higher in the Ter-Llobregat system than in Barcelona city for both maximum and minimum temperatures (Fig. 87).

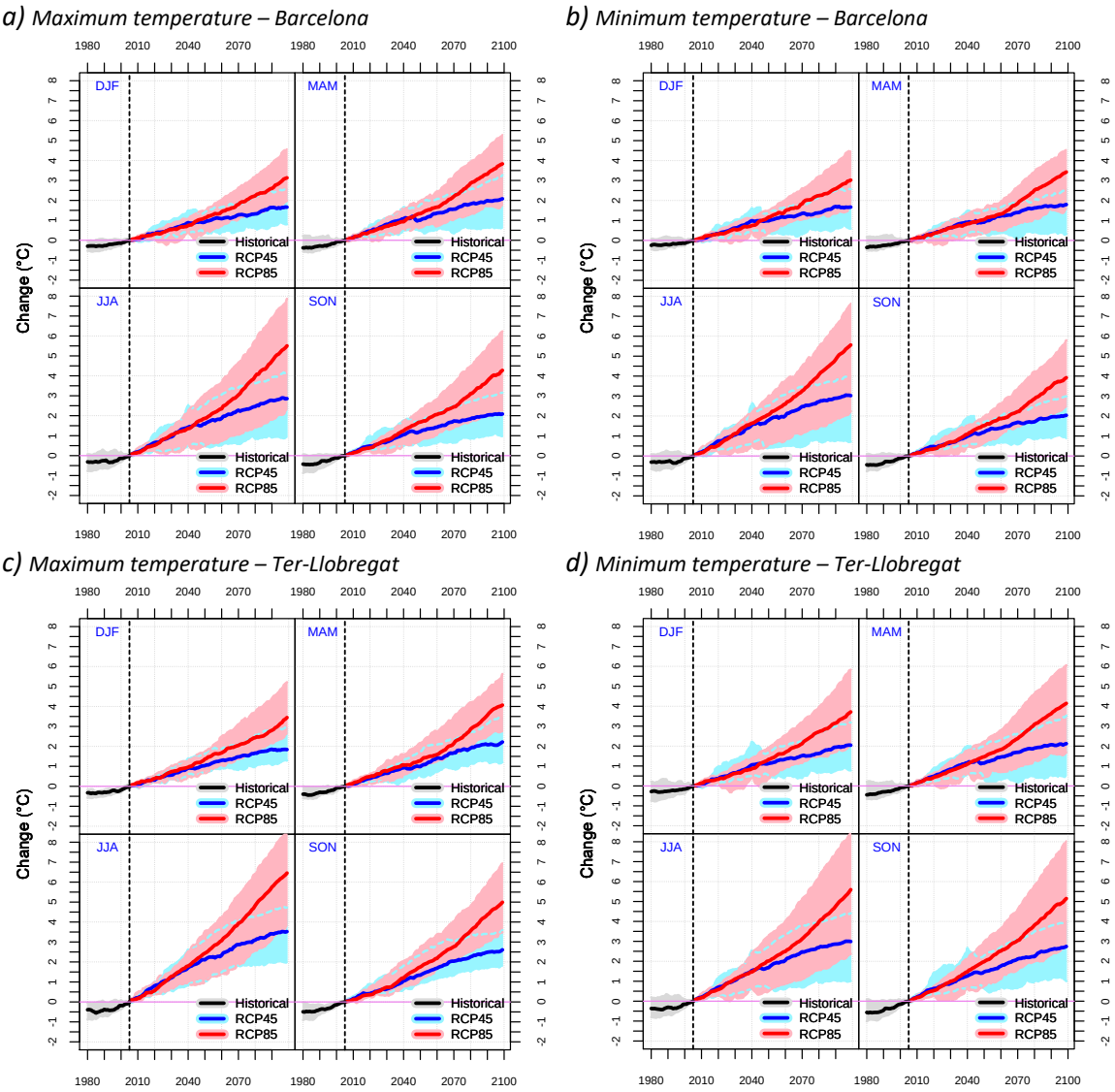

Figure 87. Climate projections of changes in maximum temperature (*a*, *c*) and minimum temperature (*b*, *d*) for the Barcelona city (*a*, *b*) and Ter-Llobregat System (*c*, *d*). Data grouped for the RCP4.5 and the RCP8.5 simulation of every climate model used and for the last 30 years. The ensemble median (solid lines) and the 10th–90th percentile values (shaded areas) are displayed. The vertical dashed line marks the end of the Historical data (2005).

For summer, RCP 4.5 reveals rises between 1°C and 4°C in Barcelona city and between 2°C and 5°C in Ter-Llobregat area respect to the 1976-2005 period. The RCP8.5 projects increases of 2.5 to 8°C for Barcelona and 4°C to 9°C for its surrounding area. For the rest of

the seasons, increases in temperature are not as sharp as in summer but every projection suggests that temperatures would rise between 1°C and 5°C in all studied areas. By the end of the century, annual mean temperature could rise is between 2°C and 6°C in Barcelona and between 2°C and 6.5°C in Ter-Llobregat system. These increases present a greater uncertainty range than the previous projections for the Barcelona Metropolitan Area, of between 2.9 and 3.7°C by 2100 (AMB 2015a, 2015b). Decadal predictions by 2035 shows a warming about 1°C, but with more uncertainty according to the teleconnection-based method (Fig. 89 and 90).

All climate projections and decadal predictions for precipitation show no significant changes but with a high level of uncertainty (Fig. 88-90). Precipitation variations are projected in the range between -20% and 20% at the end of the century respect to the 1976-2005 period (Fig. 88). Climate projections are fairly similar for all seasons and for Barcelona city and Ter-Llobregat system. In contrast with this, AMB (2015a) projected annual decreases between -10 and -25% for some municipalities of the Barcelona metropolitan area.

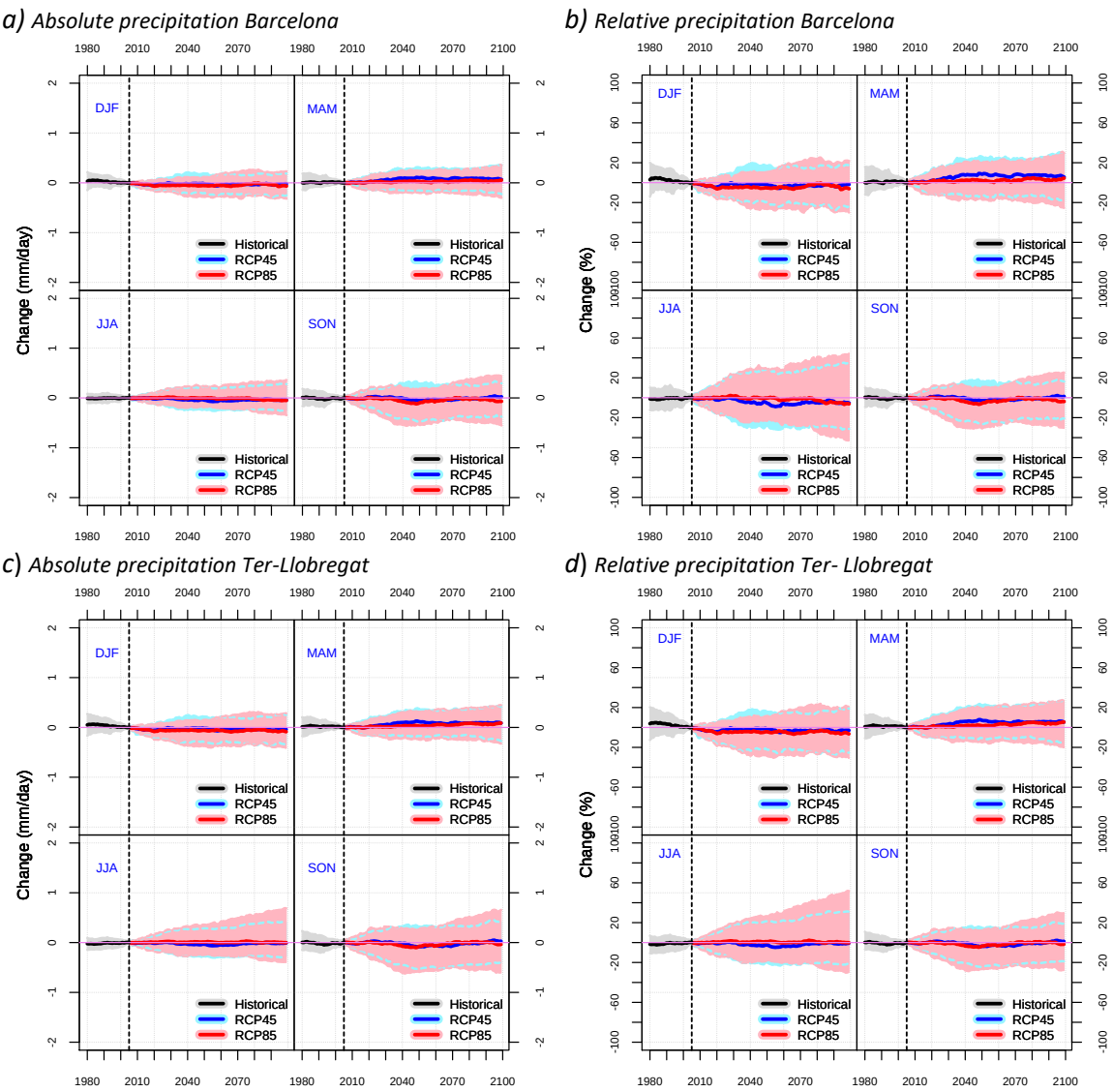

Figure 88. The same as Fig. 87 but for absolute (*a*, *c*) and relative changes (*b*, *d*) in precipitation for Barcelona (*a*, *b*) and Ter-Llobregat system (*c*, *d*).

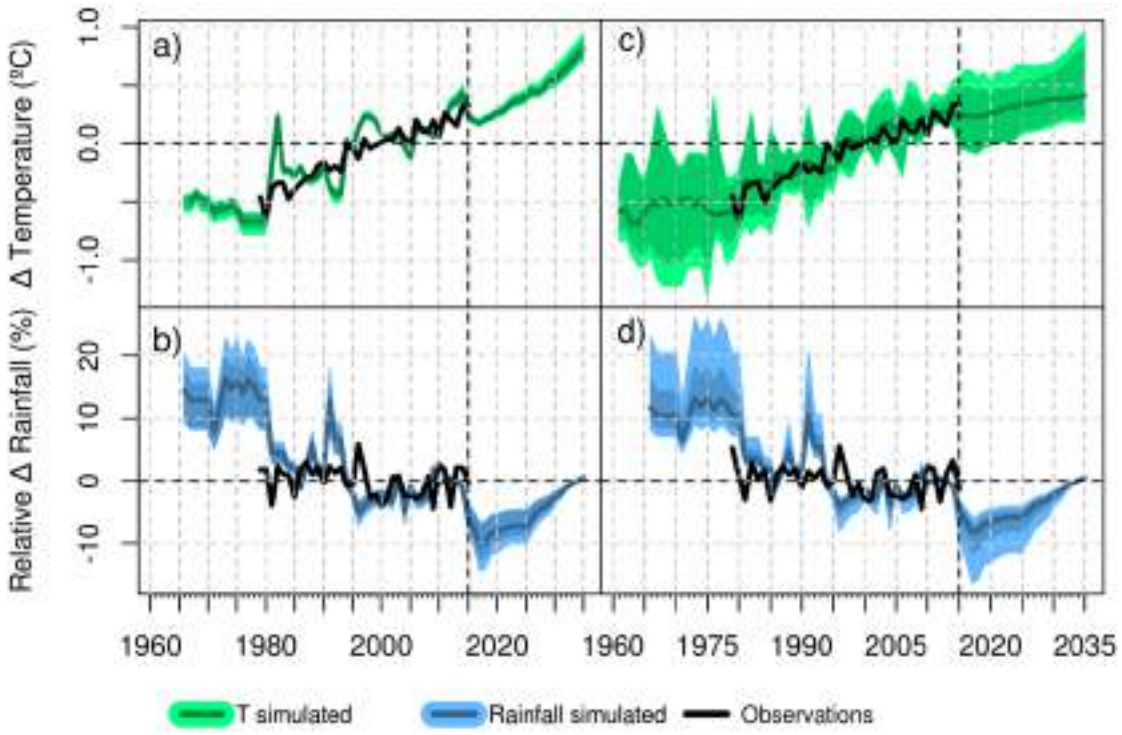

Figure 89. Drift-corrected decadal projections of changes in temperature (*a*, *b*) and precipitation (*c*, *d*) respect to the 1986-2015 period for Barcelona (*a*, *c*) and Ter-LLobregat System (*b*, *d*). Data from the 5-year moving averages are grouped for the RCP4.5 simulation of the validated decadal models and for all stations of the region. The ensemble median (solid lines) and the 1st-99th / 10th–90th percentile values (shaded areas) are displayed. The vertical dashed line marks the end of the observation period (2015).

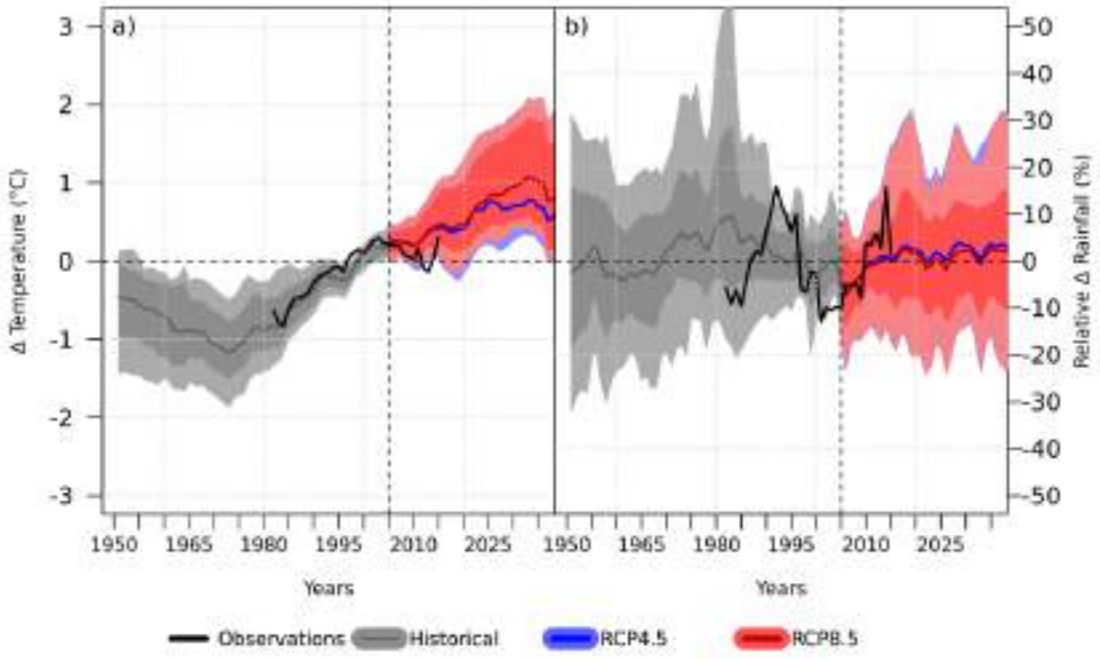

Figure 90. Teleconnection-based decadal projections of changes in temperature (*a*) and precipitation (*b*) respect to the 1986-2015 period for Ter-Llobregat system. Data from the 10-year moving averages are grouped for the RCP4.5 and RCP8.5 projections combined with the teleconnection-based predictions for all stations of the region. The ensemble median (solid lines) and the 1st-99th / 10th–90th percentile values (shaded areas) are displayed. The vertical dashed line marks the end of the historical period (2005).

4.1.2. Other variables

4.1.2.1. Wind and pressure

Climate projections for Barcelona under the medium scenario (RCP4.5) did not show significant trends in wind speed for any season. Most of the CMIP5 models agree that wind speed remains roughly unchanged with a high level of uncertainty (Fig. 91).

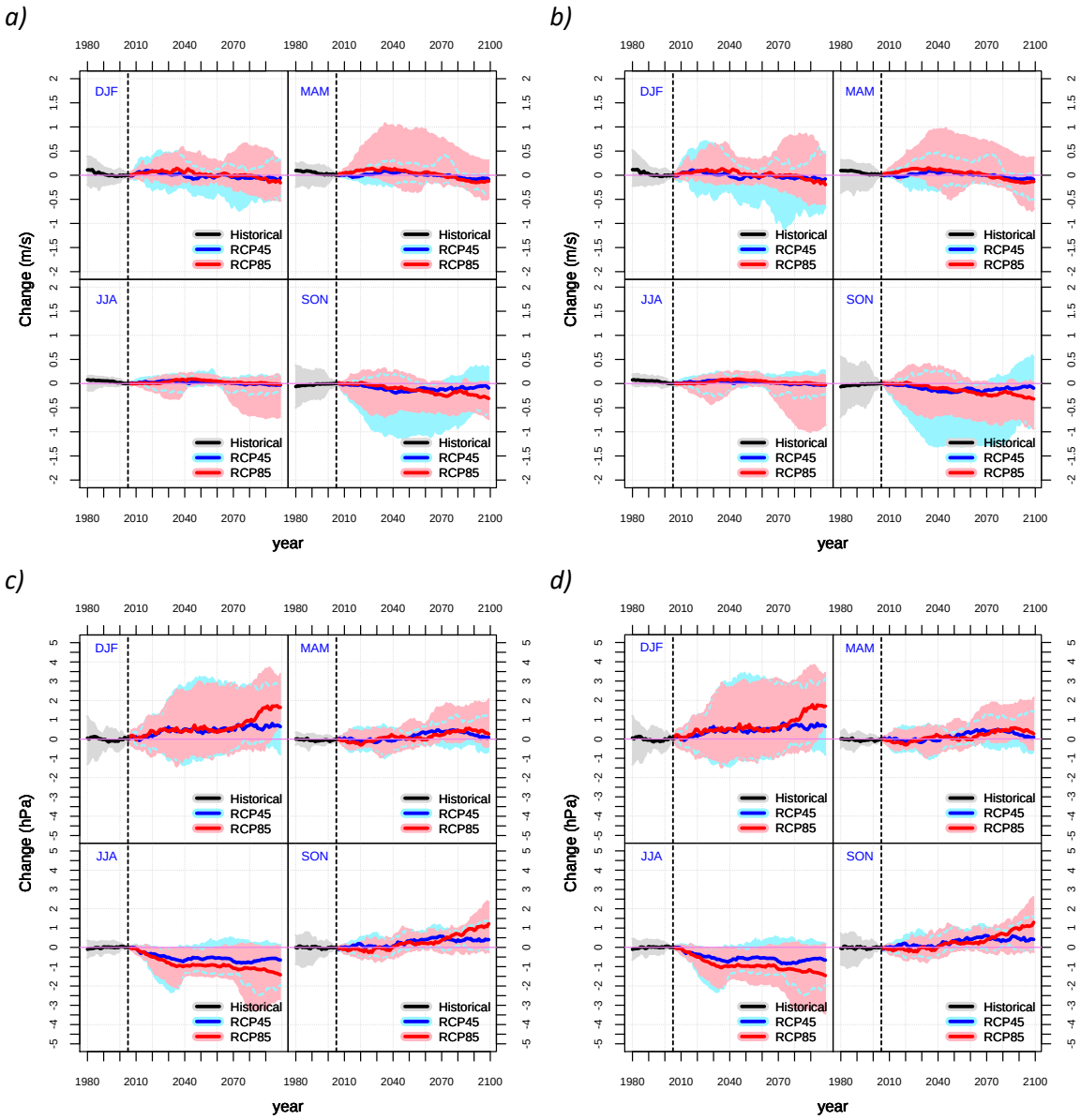

Figure 91. Climate projections of changes in wind (*a*, *b*) and pressure (*c*, *d*) for Barcelona city (*a*, *c*) and Ter-Llobregat system (*b*, *d*). Solid areas and lines are as in Fig. 87.

For autumn, the RCP8.5 scenario projected a slight reduction in the average speed close to 0.5 m/s at end of the century (Fig. 91). The reduction (between 0 and 0.6 m/s) in wind mean speed is also found in the decadal predictions by 2035 (Fig. 92c and 92d).

The decrease could be due to changes in the frequency of large-scale high and low pressure systems from the Atlantic Ocean.

This is coherent with the results of pressure projections, which shows a small increase for autumn, indicating an upward trend in high pressure systems frequency and/or intensity at the end of century (Fig. 92a and 92b). Winter shows similar results for pressure according to the RCP8.5 scenario, with significant increments (around 1 or 2 hPa) at the end of century. However, this is not corresponding with coherent changes in wind, which are not statistically significant for the same scenario/period.

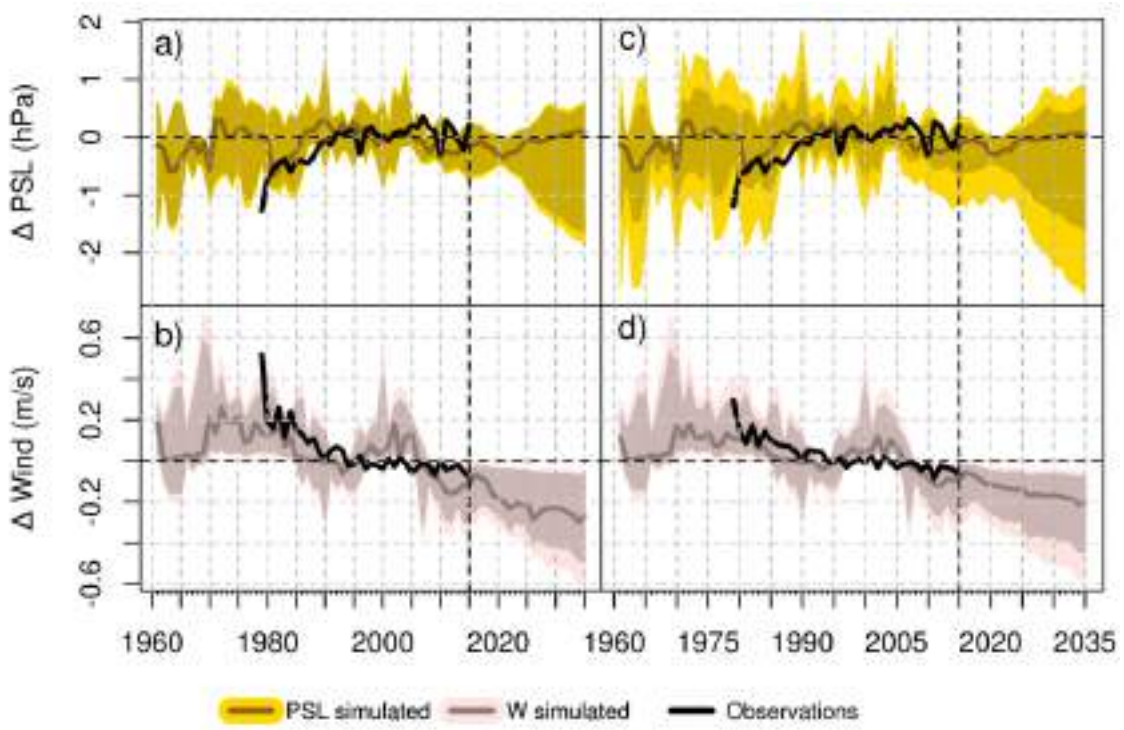

Figure 92. Drift-corrected decadal projections of changes in pressure (*a*, *b*) and wind (*c*, *d*) respect to the 1986-2015 period for Barcelona (*a*, *c*) and Ter-Llobregat System (*b*, *d*). Solid areas and lines are as in Fig. 87.

According to Lu *et al.* (2007), an expansion of the Hadley cell is expected in middle latitudes due to the global warming. This phenomenon could cause an increase of the upper-level ridges and the corresponding surface-based anticyclones.

For the summer period, all RCP scenarios project significant decreases in pressure (around 1hPa) along the century. This is consistent with the projected increase in temperature, which causes more frequent mesoscale low system (of thermal type), characteristic of the summer.

4.1.2.2. Relative humidity and potential evapotranspiration

Humidity projections for Ter-Llobregat system and Barcelona show different results depending on the season and scenario. First of all, it is expected to remain fairly unchanged in winter months along the century.

Regarding the summer season, minor changes are expected until mid-century as relative humidity would only fall about 0.5%. However, the downwards trend could accelerate by the end of the century, with median ranges falling between 1.5% and 3% (Fig. 93). The difference between the scenarios taking into consideration is remarkable in the last decades of the century.

The humidity simulation supposes a fluctuating trend for both spring and autumn months. The figure suggests a small rise in relative humidity between 0.5% and 1% until 2040. The trend would reverse afterwards until 2080 and a high level of uncertainty can be observed by the end of the century, especially in spring. Expected changes for 2100 vary between 0% and -2% in spring depending on the scenario, while there is a broader consensus between scenarios in autumn.

Seasonal evapotranspiration projections show an increase for every season with a probability of more than 90% (Fig. 94). The projected increase is sharper in the summer months, where the median trend show increases of about +0.5mm/day per century. Decadal predictions coincide to mark an increase of about +0.1 or 0.2 mm/day for 2035, which is similar to the climate projections for the same horizon.

This is consistent with the temperature rise projected for all scenarios, because the physical link between the potential evapotranspiration and the mean temperature is very strong. Therefore, the warning would cause a greater water stress.

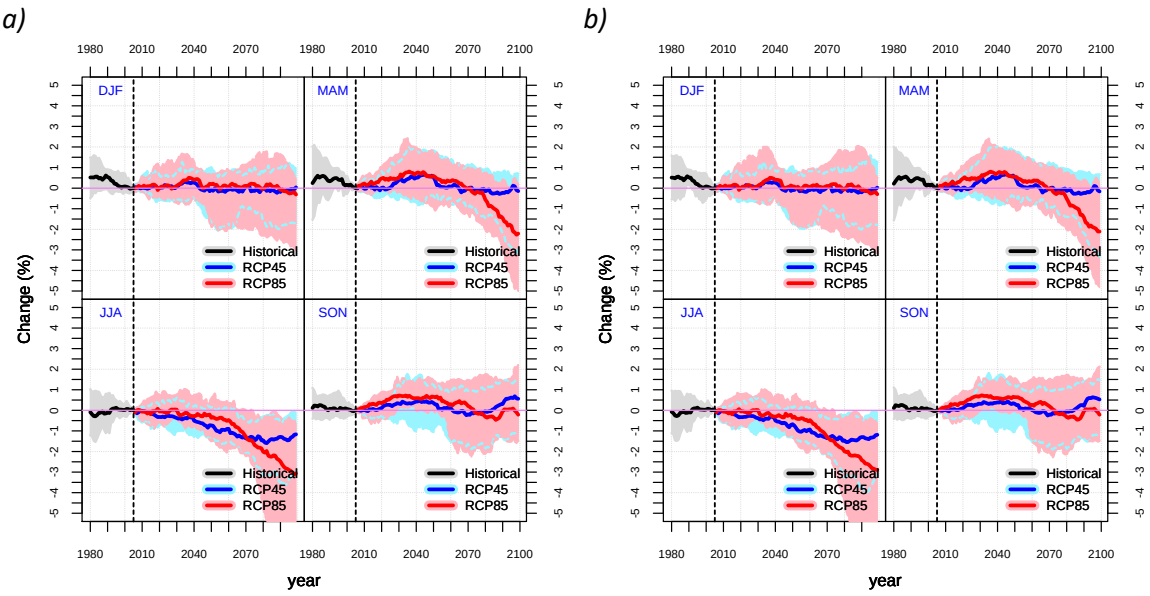

Figure 93. Climate projections of changes in relative humidity for Barcelona (*a*) and Ter-Llobregat system (*b*). Solid areas and lines are as in Fig. 87.

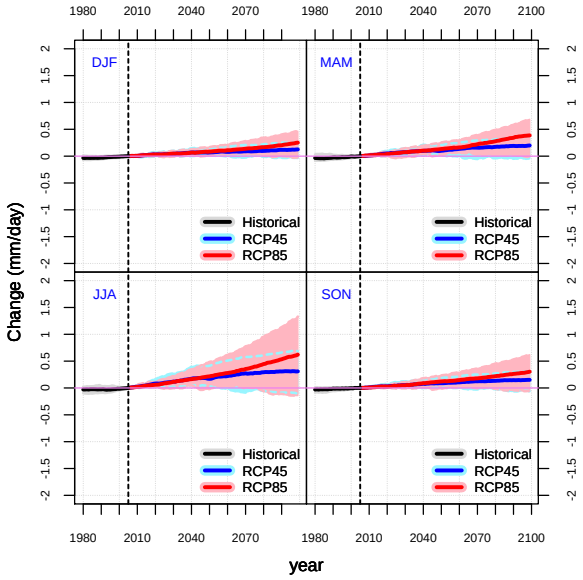

Figure 94. The same as Fig. 93 but for changes in potential evapotranspiration for Ter-Llobregat system.

4.1.2.3. Snowfall

The median projection for snow shows a decrease of 1 snowfall day per year in Ter-Llobregat basin along this century. Under the more pessimistic scenarios, snowfall days in the area could fall by 6 at the end of the century. Concerning Barcelona city, no changes are observed since current days of snow are insignificant.

Similar trends are found for the snow water equivalent (Fig. 95). The most probable projection shows a final reduction about 5mm/year Ter-Llobregat area, reaching decreases of 25mm/year under scenario RCP85, which is equivalent to a reduction of 100%. With regard to Barcelona, amount of snow per year is currently so low that no trend is observed. Decadal predictions to 2035 show similar decreases for the snowfall in Ter-Llobregat, up to -70%.

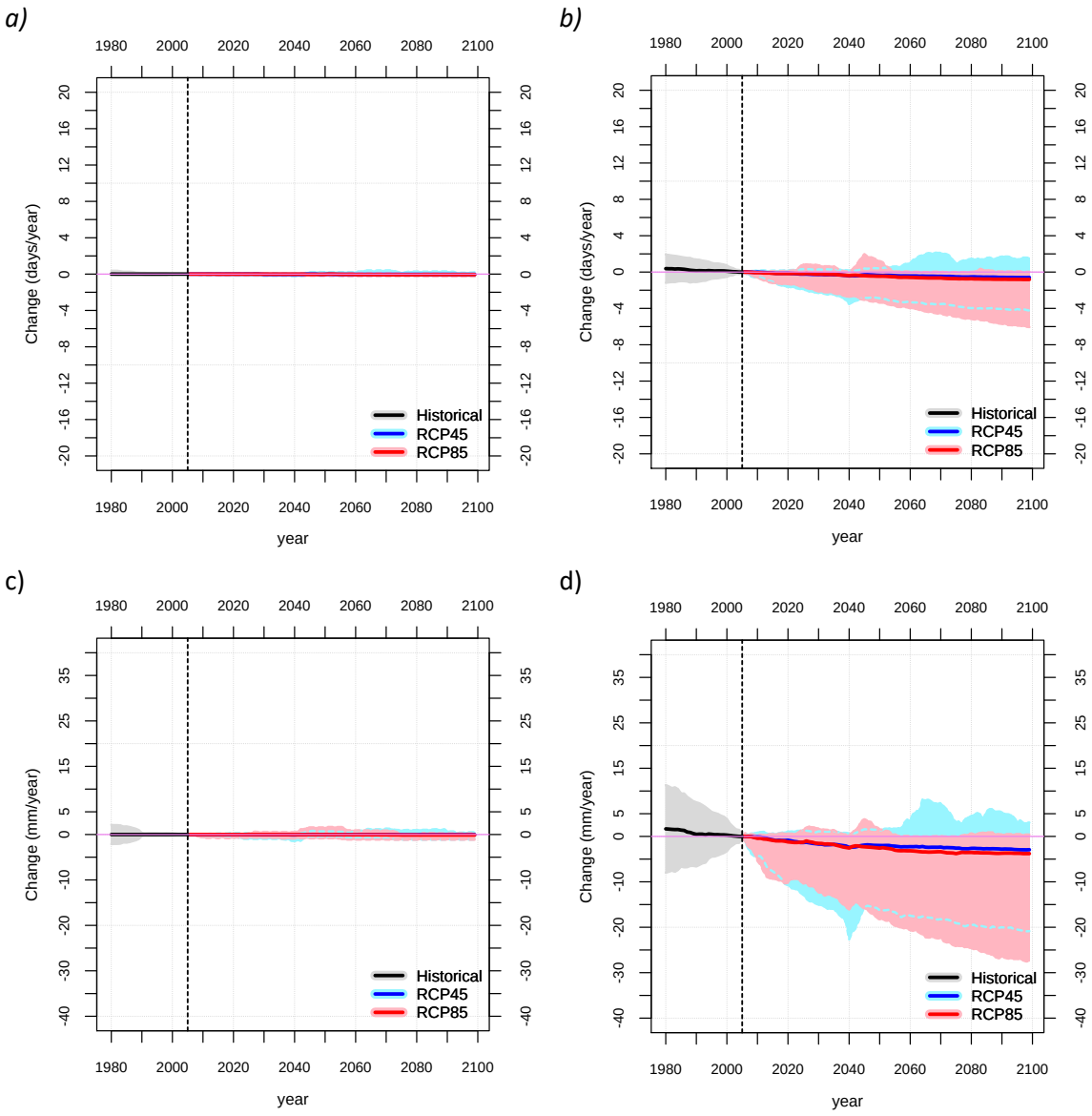

Figure 95. The same as Fig. 93 but for changes in snowfall days (*a*, *b*) and snow water equivalent (*c*, *d*) for the city of Barcelona (a, c) and Ter-Llobregat System (b, d).

4.1.2.4. Mean wave height

Mean wave height simulations indicate a shifting tendency along the century. RCP4.5 and RCP8.5 agree in simulating an upward trend until 2040 (Fig. 93). The changes in wave height would reach a peak up to 5cm and experience a decline in the second half of the century. This fall would be higher under the RCP 8.5, which estimates changes up to -10cm by 2100.

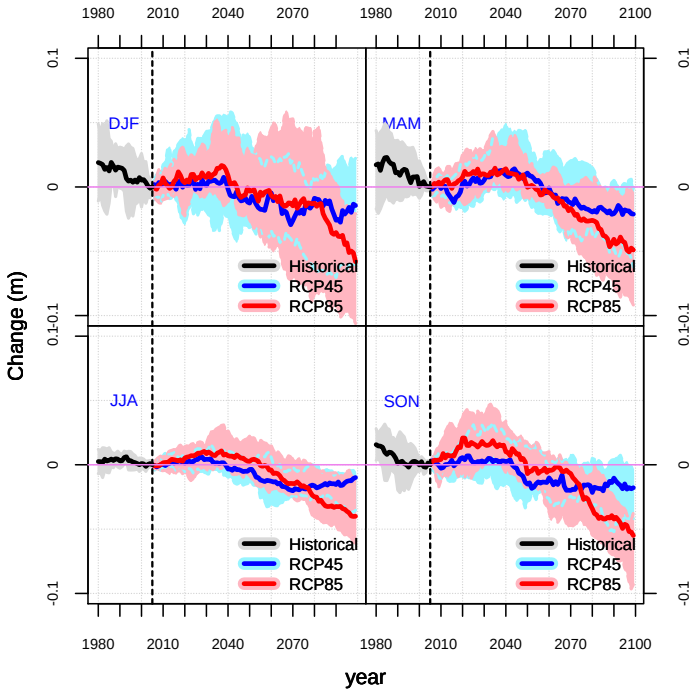

Figure 96. The same as Fig. 93 but for mean wave height in Barcelona.

4.1.2.5. Sea level

Significant increase of the sea level rise is also expected for Barcelona, although some previous studies showed a lesser rise due to an increase of the salinity in the Mediterranean Sea (Tsimplis & Rixen, 2002). The median simulations projected a sea level rise about +30cm/century (and with a maximum up to +50cm/century according to the RCP8.5) (Fig. 97).

This result is consistent with the +40 cm/century projected by IPCC for the entire Mediterranean basin by the end of the century (IPCC, 2015). However, uncertainty level is reflected by the recent satellite-based observations (1992-2014), that shows a sea level rise higher than +20 cm/century in Barcelona and even negative in the Balearic sea, down to -10 cm/century (EEA, 2016).

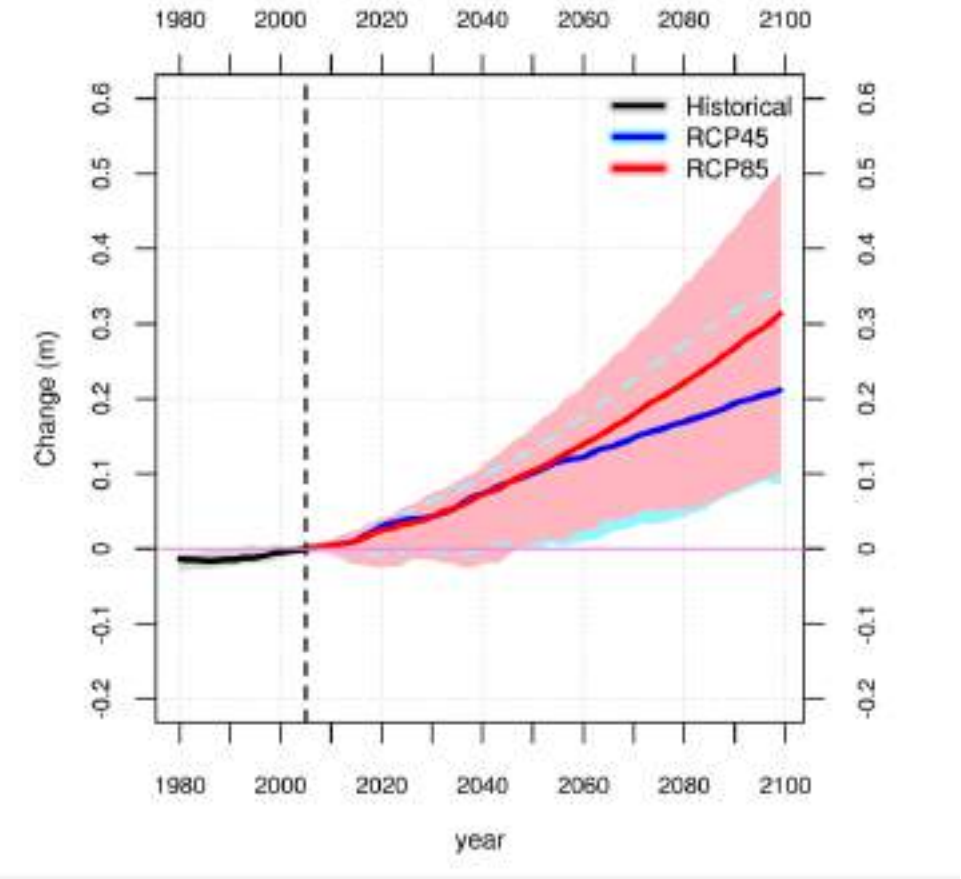

Figure 97. The same as Fig. 93 but for mean sea level in Barcelona.

4.1.3. Summary of projections for Barcelona

The most important change in the future climate of Barcelona is given by the temperature rise. By the end of century, annual mean temperature could rise is between 2.2°C and 5.8°C in Barcelona and between 2.3°C and 6.5°C in Ter-Llobregat system (Table 10).

With a wide uncertainty range, no significant changes are expected in annual rainfall. However, less water reserves are expected because snowfall could decrease up to 100% in Ter-LLobregat system by 2100. Moreover, an increment of the potential evapo-transpiration (up to +0.6 mm/day, i.e. 27%) would cause a greater water stress.

Wind speed could be reduced up to 0.6 m/s according to the RCP8.5 and the decadal forecast, especially in autumn. The mean wave height also could be reduced up to 10 cm by 2100. This is coherent with the projected increase of the mean pressure, probably due to a greater prevalence of high-pressure systems to detriment of the low-pressure areas.

Finally, sea level rise is projected with an increment up to +50cm by the end of the century, but the most probable scenario corresponds to +30 cm in Barcelona under the RCP8.5 scenario and +20 cm according to the RCP4.5 scenario.

Table 10. Summary of mean changes projected to 2035 and 2100 in Barcelona according the decadal and climate models.

Climate variable	Spatial coverage	2035				2100	
		Decadal predictions vs 1986-2015		Climate change vs 1979-2015		Climate change vs 1979-2015	
		Tele-connections (2016-2035)	Drift-corrections (2016-2035)	RCP4.5 (2006-2035)	RCP8.5 (2006-2035)	RCP4.5 (2071-2100)	RCP8.5 (2071-2100)
Temperature (°C)	Regional	(+0.1/+1.5)	(+0.6/+1.0)	(+0.4/+1.6)	(+0.4/+1.5)	(+1.0/+3.5)	**(+2.3/+6.5)**
	Urban	(+0.2/+1.5)	(+0.2/+1.0)	(+0.5/+1.5)	(+0.5/+1.5)	(+1.0/+3.0)	**(+2.2/+5.8)**
Precipitation (%)	Regional	(-10/+10)	(-5/+5)	(-10/+10)	(-15/+10)	(-15/+15)	(-20/+25)
	Urban	(-10/+10)	(-5/+5)	(-15/+10)	(-20/+10)	(-15/+10)	(-30/+30)
Wind (m/s)	Regional		(-0.6/+0.0)	(-0.5/+0.5)	(-0.5/+0.5)	(-0.5/+0.5)	(-0.5/+0.5)
	Urban		(-0.6/+0.0)	(-0.2/+0.2)	(-0.2/+0.2)	(-0.2/+0.2)	(-0.2/+0.2)
Snowfall (%)	Regional	(-80/-0)	(-80/-0)	(-60/-8)	(-70/-6)	**(-90/-50)**	**(-100/-85)**
	Urban	(-80/-0)	(-70/-0)	**(-100/-20)**	(-100/+10)	**(-100/-80)**	**(-100/-95)**
ETP (%)	Regional	(+0/+5)	(+1/+5)	(+1/+6)	(+0/+6)	(+0/+14)	(+0/+27)
RH (%)	Urban			(-0.5/+0.5)	(-0.5/+0.5)	(-2.0/+1.0)	(-3.0/+1.0)
Sea level (cm)	Urban			(-1/+10)	(-1/+10)	(+10/+40)	**(+10/+50)**
Wave height (cm)	Urban			(+0/+4)	(+0/+4)	(-5/-0)	(-10/-0)

Legend:

Certainty level

	High	Medium	Low
Strong decrease			
Moderate decrease			
Litle decrease			
No changes			
Litle increase			
Moderate increase			
Strong increase			

Not available

4.2. Lisbon

4.2.1. Temperature and precipitation

Projected simulations show a constant rising tendency for both maximum and minimum temperature in Lisbon along the century. A high level of agreement is found until mid-century. Temperature would rise between 0.5°C and 1.5°C by 2050 and projections differ noticeably in the second half of the century. Temperature could rise between 1°C and 3.5°C under the scenario RCP4.5 and between 2°C and 5.5°C under the scenario RCP8.5. This is higher than in previous studies, where was projected a warming in Lisbon between 2°C and 4°C by the year 2100 (IPMA, 2016).

Seasonal differences are minor: increases would be slightly higher in summer and autumn in maximum temperature while greater rises would be in autumn and winter in minimum temperature (Fig. 98).

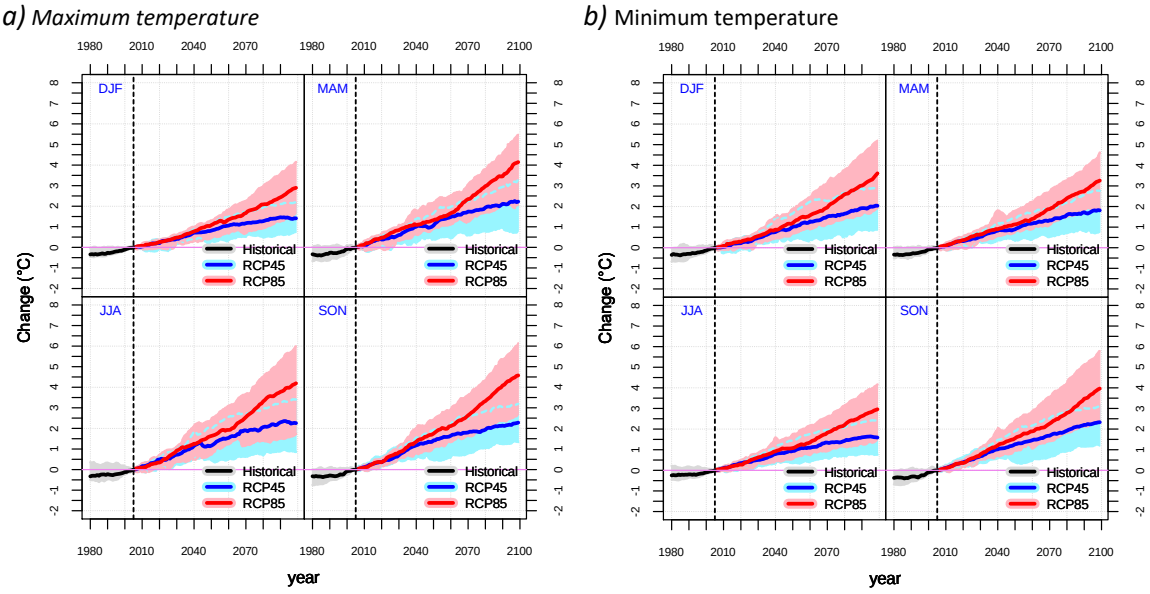

Figure 98. Climate projections of changes in maximum temperature (*a*) and minimum temperature (*b*) for the Lisbon city. Data grouped for the RCP4.5 and the RCP8.5 simulation of every climate model used and for the last 30 years. The ensemble median (solid lines) and the 10th–90th percentile values (shaded areas) are displayed. The vertical dashed line marks the end of the Historical data (2005).

The clearest tendency for precipitation is a decrease in summer in the second half of the century. The median projection for the driest season shows a loss of 20% according to scenarios RCP4.5 and RCP8.5 (Fig. 99).

The most pessimistic projections indicate that summer precipitation could be reduced by half at the end of the century. For the rest of the seasons, tendencies are more uncertain. The different models and scenarios show that an increase or a decrease in precipitation is equally probable along the century. This result contrasts with previous studies, which projected an annual decrease between -3% to -12% in 2071-2100 respect to 1960-1990 (IPMA, 2016).

Drift-corrected decadal predictions of temperature changes in Lisbon are smoother than the climate projections (Fig. 100). In fact, no significant changes in temperature (lower than 0.2°C) are expected for the near-term horizon (2035).

Teleconnection-based predictions show a greater warming, between 0 and 1°C by 2035 (Fig. 101).

However, precipitation variations under the drift-corrected decadal models coincide with the teleconnection-based predictions, since they show a decrease up to -15% (Fig. 100b and 101b).

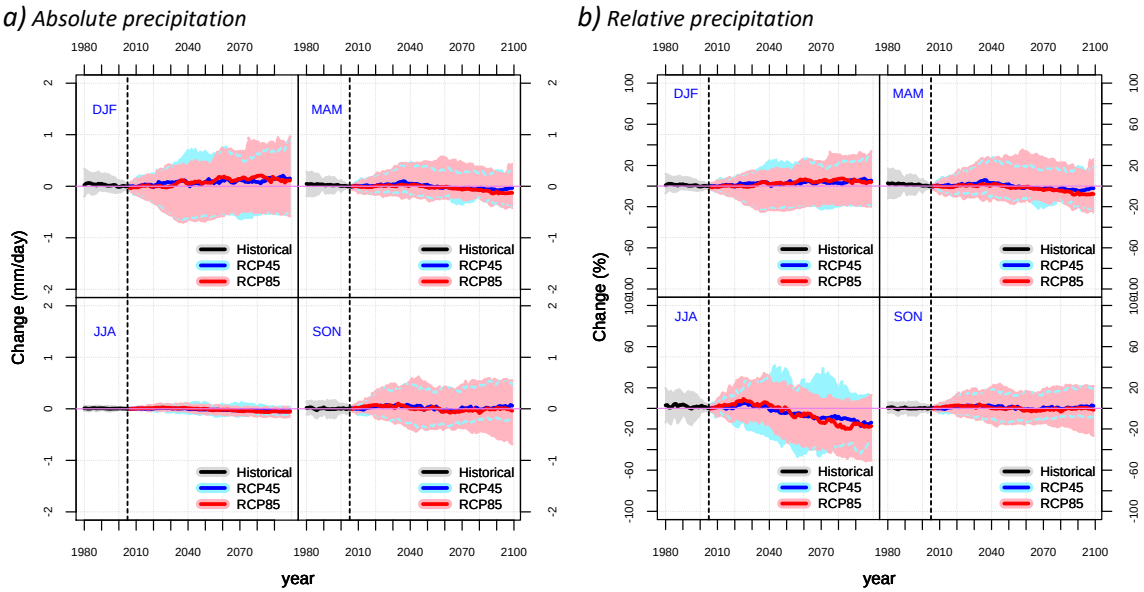

Figure 99. The same as Fig. 98 but for absolute (*a*) and relative (*b*) changes in precipitation for the Lisbon city.

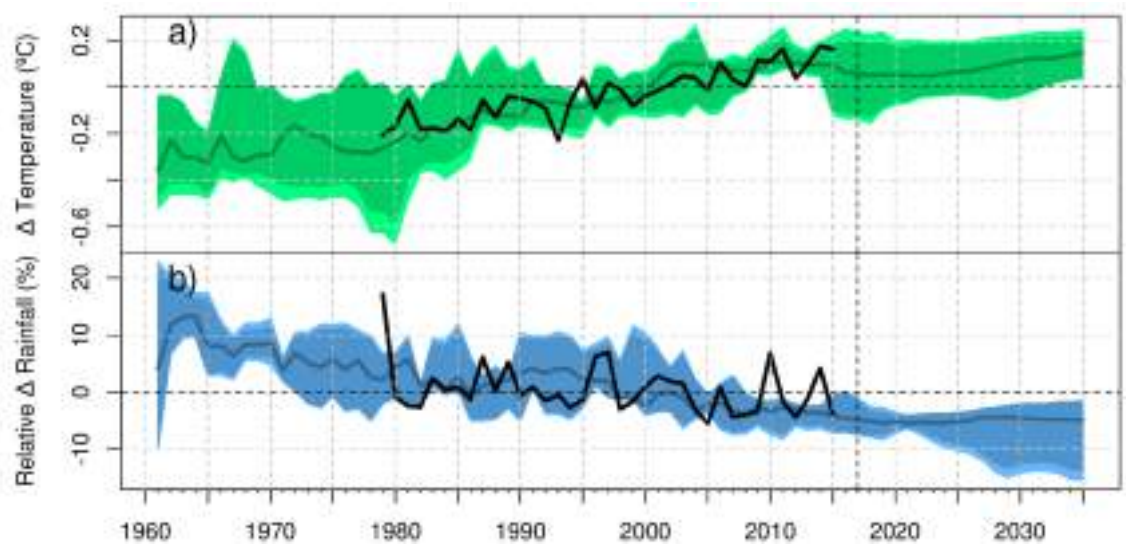

Figure 100. Drift-corrected decadal projections of changes in temperature (*a*) and precipitation (*b*) respect to the 1986-2015 period for Lisbon. Data from the 5-year moving averages are grouped for the RCP4.5 simulation of the validated decadal models and for all stations of the region. The ensemble median (solid lines) and the 1st-99th / 10th–90th percentile values (shaded areas) are displayed. The vertical dashed line marks the end of the observation period (2015).

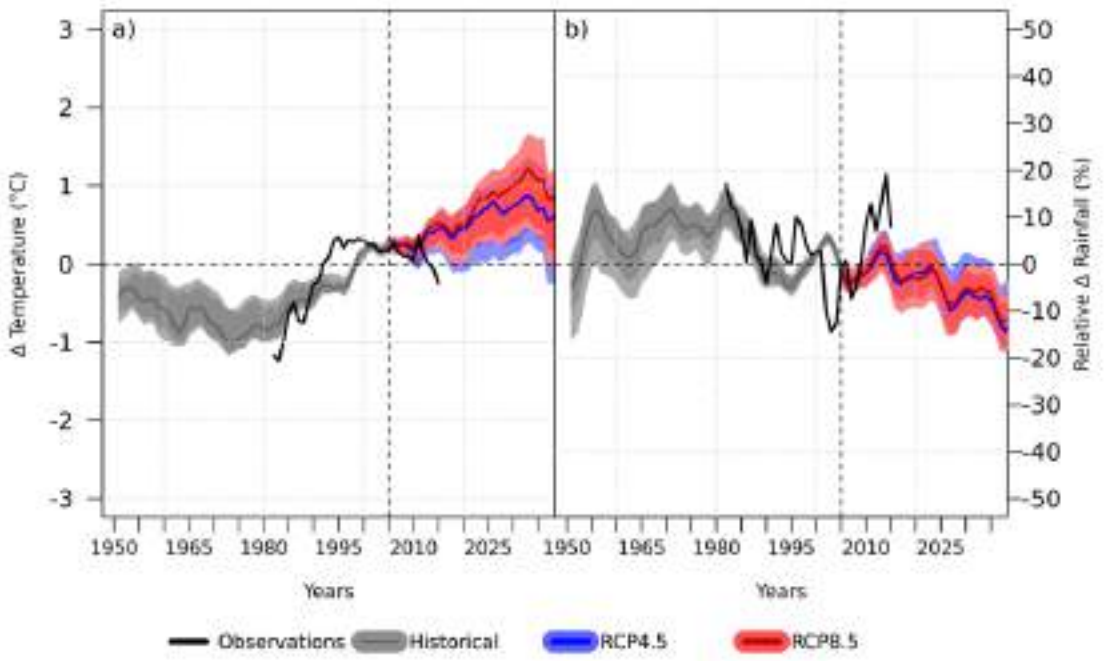

Figure 101. Teleconnection-based decadal projections of changes in temperature (*a*) and precipitation (*b*) respect to the 1986-2015 period for Lisbon. Data from the 10-year moving averages are grouped for the RCP4.5 and RCP8.5 projections combined with the teleconnection-based predictions for all stations of the region. The ensemble median (solid lines) and the 1st-99th / 10th–90th percentile values (shaded areas) are displayed. The vertical dashed line marks the end of the historical period (2005).

4.2.2. Other variables

4.2.2.1. Wind and pressure

Results for Lisbon did not show significant trends in wind speed for most of the year. The downscaled climate models project that wind speed generally remains roughly unchanged with a high level of uncertainty.

For autumn, the RCP 8.5 scenario projected a slight reduction of the average speed less than 0.5 m/s at end of the century (Fig. 102a). As in Barcelona, the decrease could be due to changes in the frequency of the Atlantic Depression. However, this is not reflected in the pressure projections for the autumn period (Fig. 102b).

Results show a decreasing pressure in summer, consistent with the warming and the corresponding mesoscale low system (of thermal type), characteristic of the summer. The expected values could decrease about 0.5hPa by 2050 and 1hPa by the end of the century.

Pressure in winter presents a shifting trend, rising until 2040, decreasing to current values until 2060 and rising again about 0.5hPa by 2100. The RCP8.5 scenario presents the higher increase for the end of century (up to 4 hPa), which is consistent with the possible expansion of the Hadley cell (Lu *et al.* 2007). This phenomenon could cause an increase of the upper-level ridges and the corresponding surface-based anticyclones (e.g. Azores High).

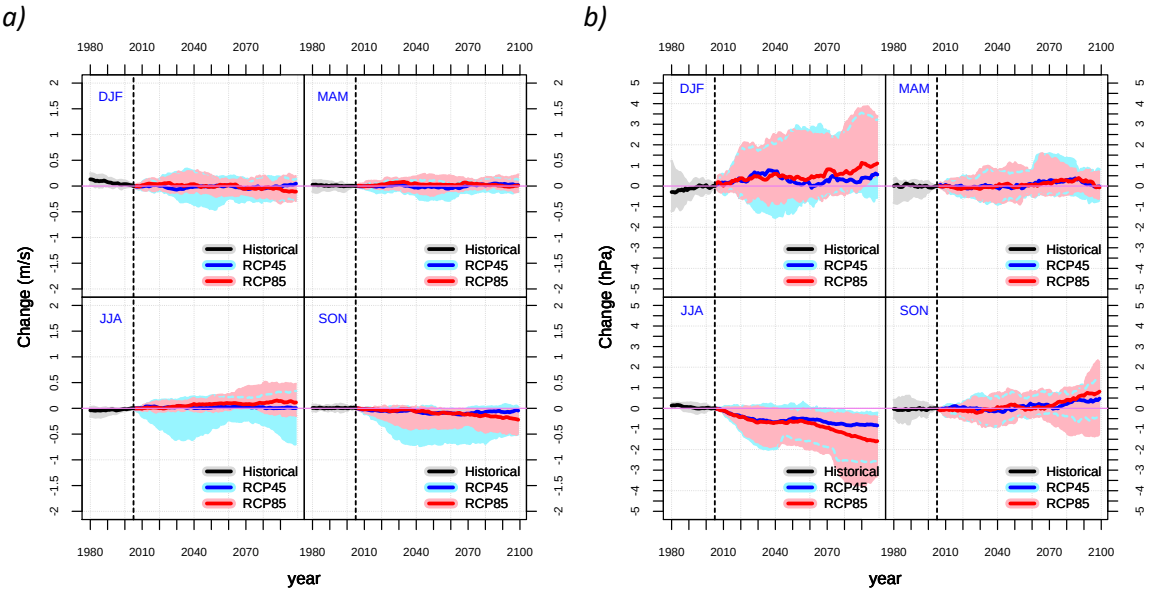

Figure 102. Climate projections of changes in wind (*a*) and pressure (*b*) for Lisbon. Data grouped for the RCP4.5 and the RCP8.5 simulation of every climate model used and for the last 30 years. The ensemble median (solid lines) and the 10th–90th percentile values (shaded areas) are displayed. The vertical dashed line marks the end of the Historical data (2005)

Decadal simulations of mean pressure shows no significant changes by 2035, but annual wind could experience a light reduction up to -0.1 m/s (Fig. 103).

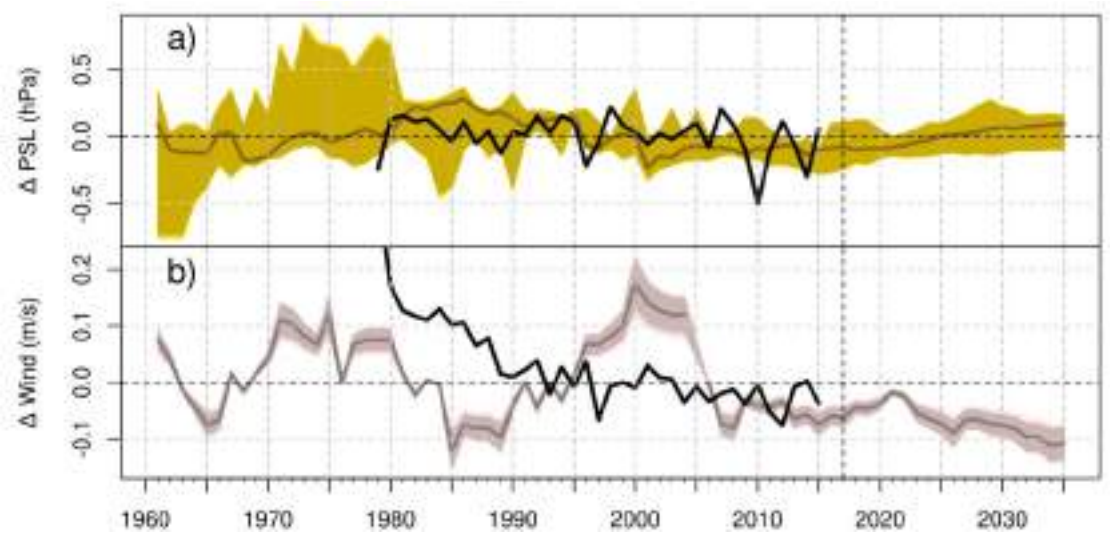

Figure 103. Drift-corrected decadal projections of changes in pressure (*a*) and wind (*b*) respect to the 1986-2015 period for Lisbon. Solid areas and lines are as in Fig. 100.

4.2.2.2. Relative humidity and potential evapotranspiration

Humidity projections for Lisbon show different results depending on the scenario, but are similar for most of seasons. First of all, it is expected to remain fairly unchanged in winter, spring and autumn periods along the century according to the RCP4.5 scenario (Fig. 104). Projections shows very small fluctuations, oscillating between -0.5% and +0.5% along the century.

However, the relative humidity presents more remarkable changes under the RCP8.5 for spring and especially for the summer months. Expected values for humidity hardly change until mid-century but they would decrease up to 2% by 2100.

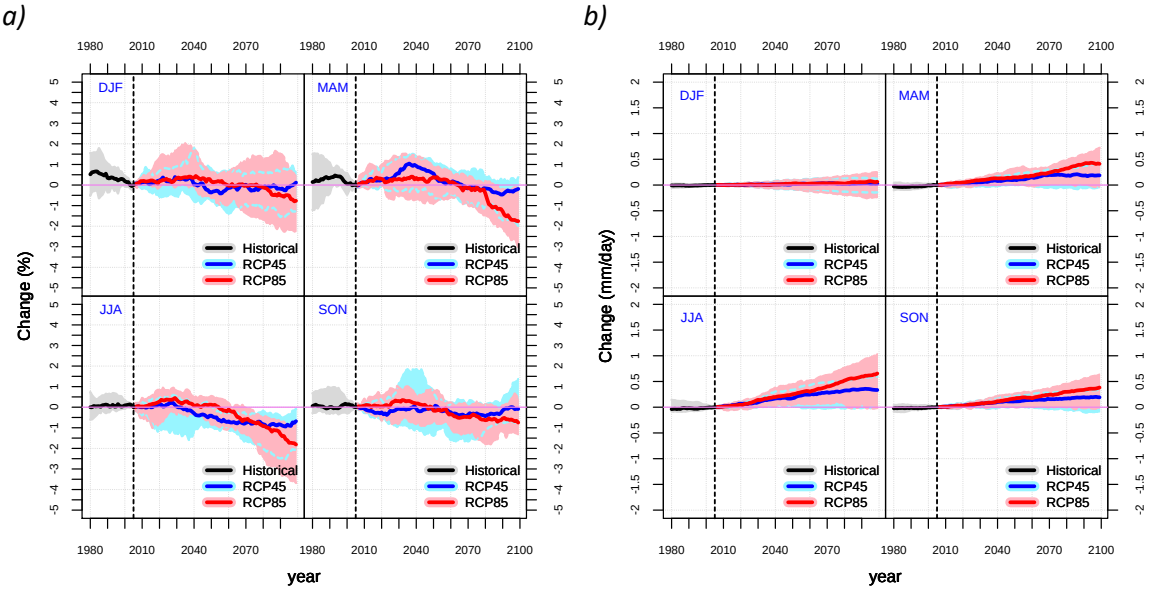

Figure 104. Climate projections of changes in relative humidity (a) and evapotranspiration (*b*) for Lisbon. Data grouped for the RCP4.5 and the RCP8.5 simulation of every climate model used and for the last 30 years. The ensemble median (solid lines) and the 10th–90th percentile values (shaded areas) are displayed. The vertical dashed line marks the end of the Historical data (2005).

Seasonal evapotranspiration projections show an increase for every season with a probability of more than 90% except for winter, when it would hardly change. The projected increase is sharper in the summer months, where the median trend show increases of about +0.5mm/day per century. Decadal predictions mark increases between 0 and +0.1 mm/day for 2035, which is similar to the climate projections for the same horizon.

This is consistent with the temperature rise projected for all scenarios, because the physical link between the potential evapotranspiration and the mean temperature is very strong.

4.2.2.3. Sea level

The median of the scenarios projected for the boy of Cascais a mean sea level rise around 0.3 or 0.4 m at the end of the century. Respectively, RCP4.5 and RCP8.5 ranges between 0.2 and 0.4 m, and between 0.3 and 0.6 m (Fig. 105). In addition to the uncertainty given by the ensemble strategy, another important uncertainty source should be considered to interpret the results in sea level: Recall that the historical sea level rise is underestimated by all oceanic model outputs in Lisbon (Sec. 3.1.3.3).

In fact, the resulting values are lower than previous projections made for the same buoy, which ranges from +0.47±0.27m by the year 2100 with a trend extrapolation (Antunes & Taborda 2009), to +0.95±0.45m for a Rahmstorf scenario (Antunes et. al 2013).

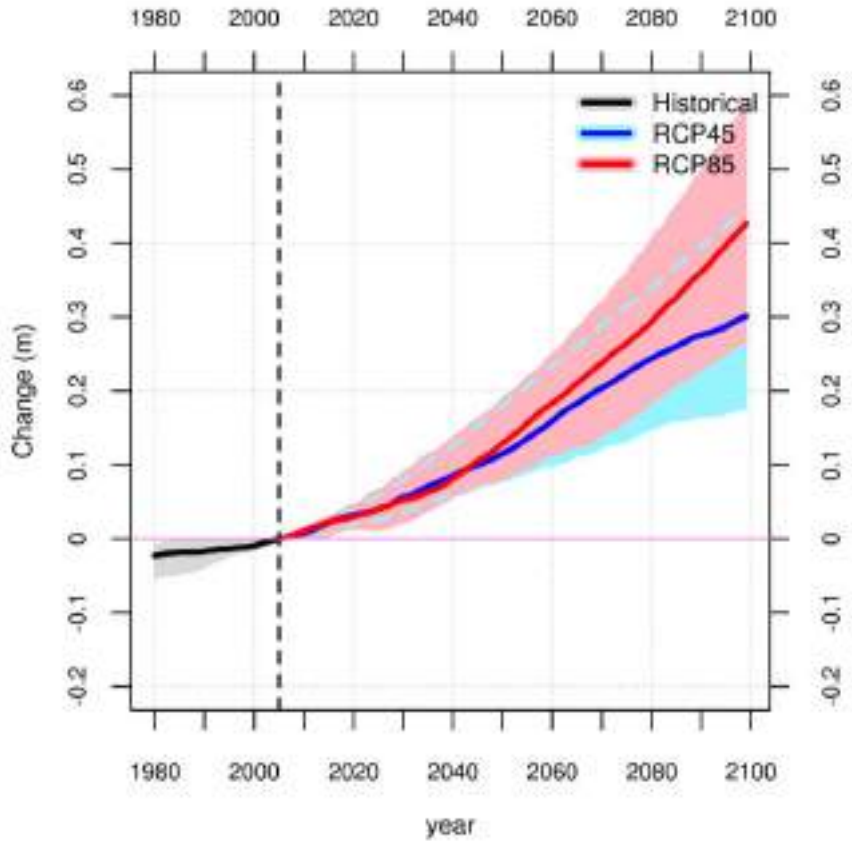

Figure 105. The same as Fig. 104 but for mean sea level in Lisbon.

4.2.3. Summary of projections for Lisbon

Temperature could rise in Lisbon between 2°C and 5.5°C under the scenario RCP8.5, and between 1°C and 3.5°C under the scenario RCP4.5 (Table 11). For the next two decades, the warming will be lower than 1°C according to the decadal forecasting.

For the same period (2016-2035), a possible decrease in annual rainfall up to -15% is expected (Fig. 100b and 101b). For the end of the century, no significant changes are expected in rainfall but with a large uncertainty interval.

Sea level could experience an increase up to +60cm at the end of the century under the RCP8.5, with a most likely level about +40cm. The rest of climate variables would not undergo significant changes.

Table 11. Summary of mean changes projected to 2035 and 2100 in Lisbon according the decadal and climate models.

Climate variable	Spatial coverage	2035				2100	
		Decadal predictions vs 1986-2015		Climate change vs 1979-2015		Climate change vs 1979-2015	
		Tele-connections (2016-2035)	Drift-corrections (2016-2035)	RCP4.5 (2006-2035)	RCP8.5 (2006-2035)	RCP4.5 (2071-2100)	RCP8.5 (2071-2100)
Temperature (°C)	Urban	(+0.0/+1.0)	(+0.0/+0.3)	(+0.3/+1.0)	(+0.3/+1.2)	(+1.0/+3.0)	**(+2.0/+5.4)**
Precipitation (%)	Urban	(-15/-5)	(-15/-0)	(-10/+15)	(-15/+15)	(-10/+15)	(-15/+15)
Wind (m/s)	Urban		(-0.1/-0.0)	(-0.6/+0.2)	(-0.4/+0.4)	(-0.4/+0.2)	(-0.4/+0.2)
RH (%)	Urban			(-0.5/+0.5)	(-0.5/+0.5)	(-1.5/+0.5)	(-2.0/+0.0)
ETP (%)	Regional	(+0/+8)	(+0/+7)	(+0/+9)	(+0/+10)	(+0/+12)	(+0/+22)
Sea level (cm)	Urban			(+5/+15)	(+5/+15)	(+20/+40)	**(+30/+60)**

Legend:

	Certainty level: High	Medium	Low
Strong decrease			
Moderate decrease			
Litle decrease			
No changes			
Litle increase			
Moderate increase			
Strong increase			

Not available

4.3. Bristol

4.3.1. Temperature and precipitation

Climate simulations show very similar trends for Bristol and for Southwest England/ Wales. All of them agree on indicating a sustained upward trend along the century. Figures are similar for every season and for maximum/minimum temperature as well.

The two RCPs take into consideration estimate very similar values the first half of the century. Both of them conclude that temperature would rise between 0.5°C and 2.0°C with a probability of 90% by 2050 (Fig. 106). However, the scenarios differ in the second half of the century. RCP8.5 projection estimates increases between 2.0°C and 5.5° in 2100 while RCP4.5 projection presents a smoother trend, showing rises between 1.0°C and 3.0°C at the end of the century. These increases are lower than the warming projected in previous studies (Met Office 2009), which showed a probable interval between 2.8 and 6.5°C by 2100 under RCP8.5.

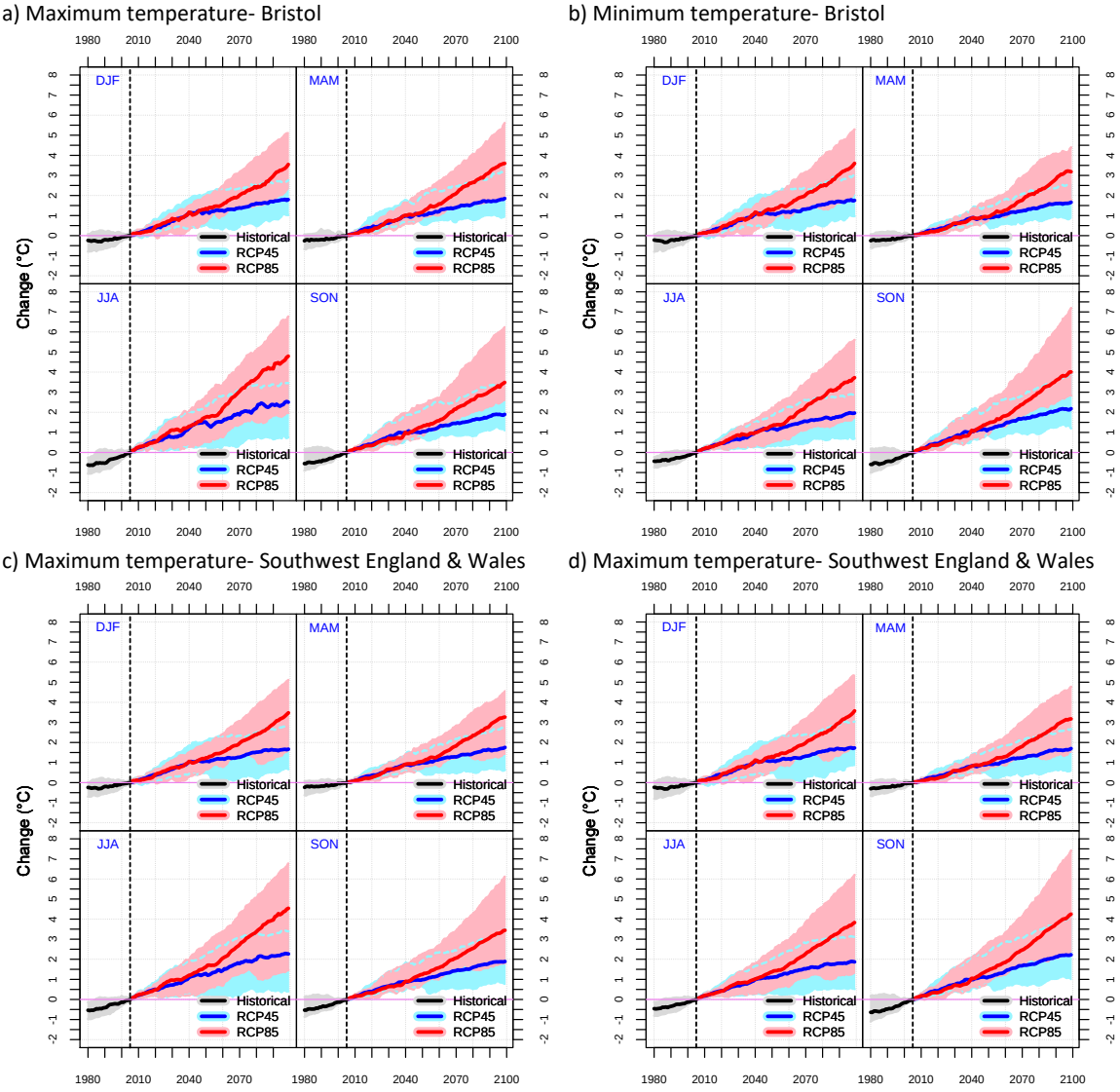

Figure 106. Climate projections of changes in maximum temperature (*a*, *c*) and minimum temperature (*b*, *d*) for the Bristol city (*a*, *b*) and Southwest England & Wales (*c*, *d*). The ensemble median (solid lines) and the 10th–90th percentile values (shaded areas) are displayed. The vertical dashed line marks the end of the Historical data (2005).

All projections show increasing trends for precipitation in Bristol and nearby regions. Precipitation would rise in every season, being these increases more significant in winter and summer.

Simulations are similar under the two scenarios considered for this study until 2050 (Fig. 107). Both of them estimate increases higher than 10% in precipitation for summer and winter, while tendency is a bit softer in spring and autumn. Decadal projections by 2035 show no changes or possible increment up to +30% (Fig. 108 and 109).

In the second half of the century, RCP8.5 shows more pronounced increments, reaching in the most extreme situation a change about 50% in 2100. Despite RCP4.5 tendency is smoother, it estimates increases in precipitation up to +40% at the end of the century (Fig. 107).

The RESCCUE results contrasts with Met Office (2009), which only projects an increment for the winter precipitation, while summer rainfall is expected to decrease.

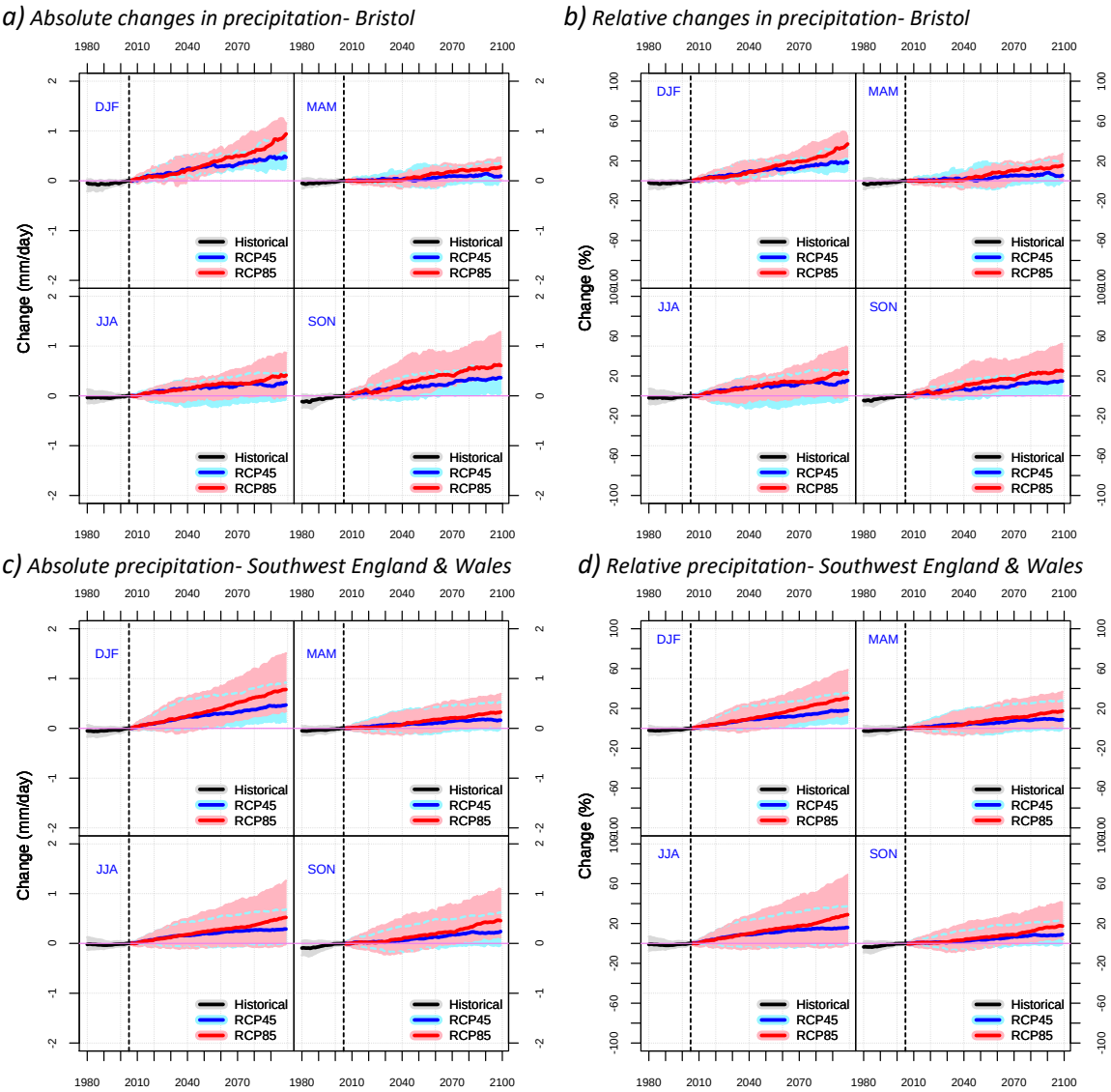

Figure 107. The same as Fig. 106 but for absolute (*a*, *c*) and relative (*b*, *d*) changes in precipitation for the Bristol city (*a*, *b*) and Southwest England & Wales (*c*, *d*).

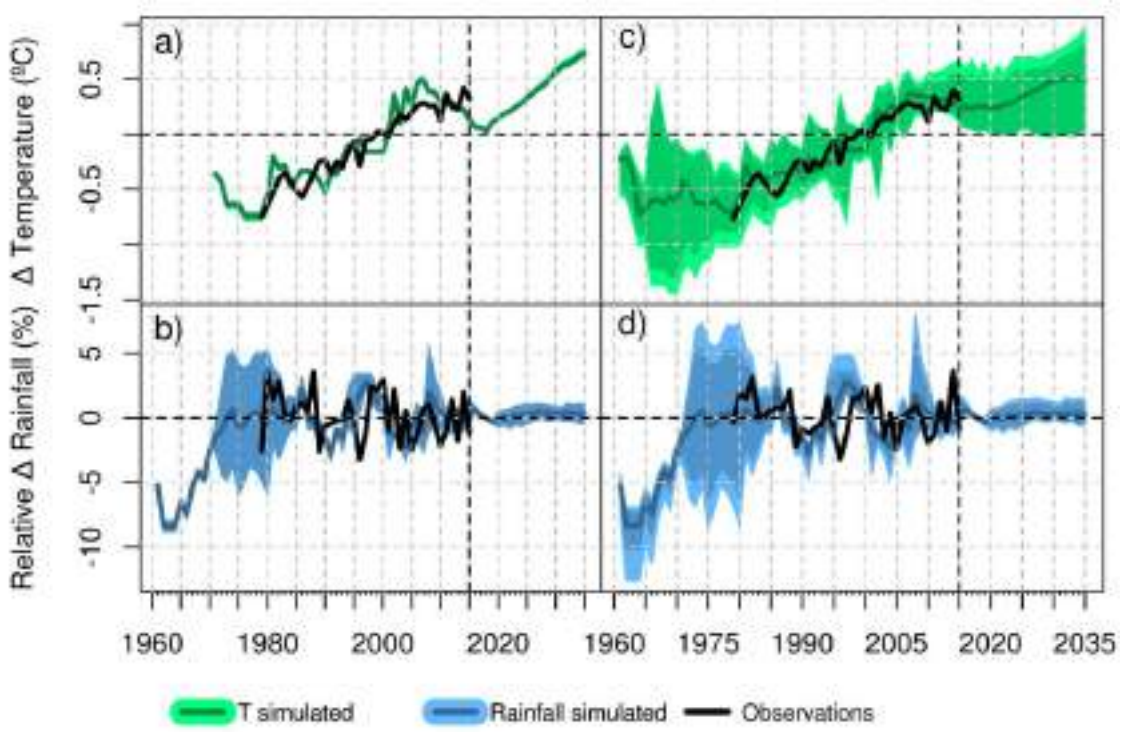

Figure 108. Drift-corrected decadal projections of changes in temperature (*a*, *b*) and precipitation (*c*, *d*) respect to the 1986-2015 period for Bristol (*a*, *d*) and Southwest England & Wales (*b*, *c*). Data from the 5-year moving averages are grouped for the RCP4.5 simulation of the validated decadal models and for all stations of the region. The ensemble median (solid lines) and the 1st-99th / 10th–90th percentile values (shaded areas) are displayed. The vertical dashed line marks the end of the observation period (2015).

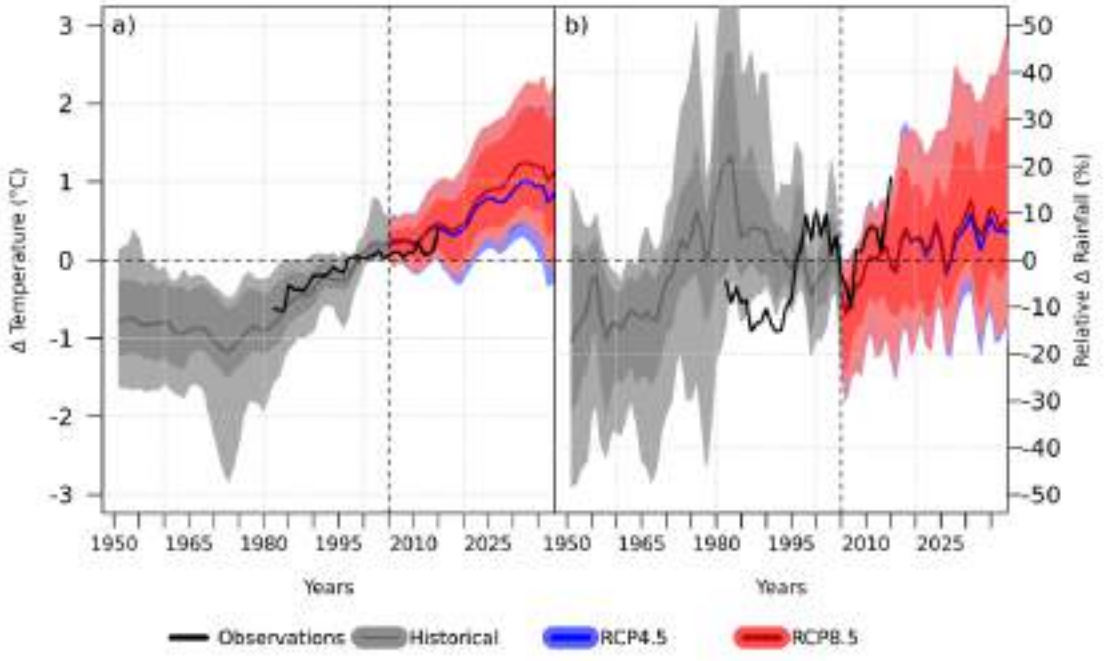

Figure 109. Teleconnection-based decadal projections of changes in temperature (*a*) and precipitation (*b*) respect to the 1986-2015 period for Southwest England & Wales. Data from the 10-year moving averages are grouped for the RCP4.5 and RCP8.5 projections combined with the teleconnection-based predictions for all stations of the region. The ensemble median (solid lines) and the 1st-99th / 10th–90th percentile values (shaded areas) are displayed. The vertical dashed line marks the end of the historical period (2005)

4.3.2. Other variables

4.3.2.1. Wind and pressure

Results for Bristol did not show significant trends in wind speed for any period of the year (Fig. 110). However, pressure projections indicate a possible increase of the average pressure in Bristol for winter and autumn periods, around 1hPa (Fig. 110b). This is consistent with the possible expansion if the Hadley cell (Lu *et al.* 2007).

On the other hand, summer months expect a possible decrease of the mean pressure up to 2hPa according to the median projection under the RCP8.5 scenario. However, for the nearby regions to Bristol, changes in the summer pressure are not statistically significant.

In the same way, Figure 110d shows a steady pressure trend in England and Wales in winter while the simulation gives a slightly increasing tendency for Bristol. Results are similar for spring and autumn in England/Wales and Bristol. The expected tendency remains stable until mid-century and values rise smoothly afterwards. Nevertheless, the decadal forecast shows no significant changes by 2035 (Fig. 111).

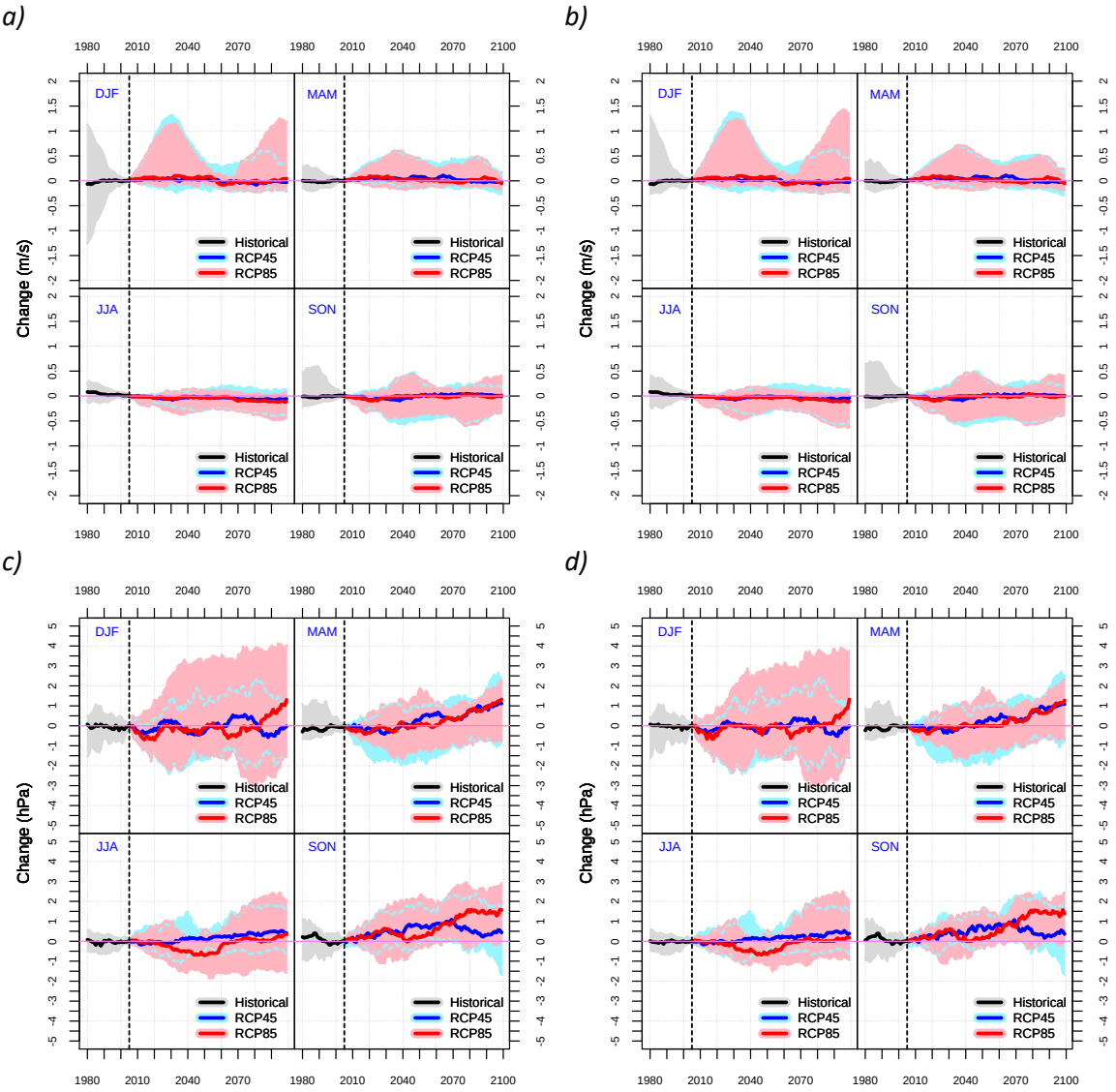

Figure 110. Climate projections of changes in wind (*a*,*b*) and pressure (*c*,*d*) for Bristol (*a*,*c*) and nearby regions (*b*,*d*).

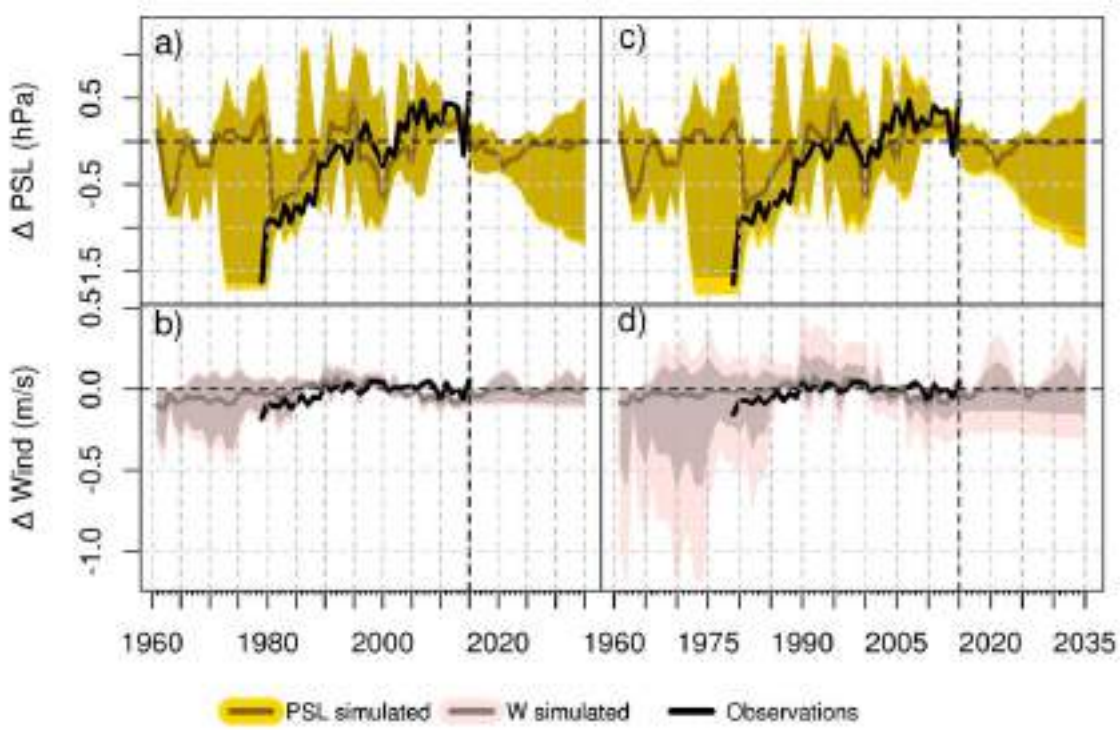

Figure 111. Drift-corrected decadal projections of changes in pressure (*a*, *b*) and wind (*c*, *d*) respect to the 1986-2015 period for Bristol (*a*, *d*) and Southwest England & Wales (*b*, *c*). Solid areas and lines are as in Fig. 108.

4.3.2.2. Relative humidity and potential evapotranspiration

In the case of relative humidity, results are similar for England/Wales and Bristol. There is no important trend observed for winter and spring, remaining future values fairy similar to current ones (Fig. 112a and 112b).

It is expected a small decreasing tendency in autumn along the whole century, obtaining changes of -0.5% by 2100. Similar changes are expected to happen in summer by 2100, but the decreasing tendency is supposed to start after 2050.

Potential evapotranspiration (ETP) projections suggest that only slight changes are expected for summer months in England/Wales and Bristol. These changes would be minor, about 0.1mm/day by 2050 and 0.2mm/day by 2100 (Fig. 112c and 112d). ETP is expected to remain roughly unchanged the rest of the seasons. In fact, according to the decadal forecast, ETP could slightly decrease by up to 0.1mm/day in 2035.

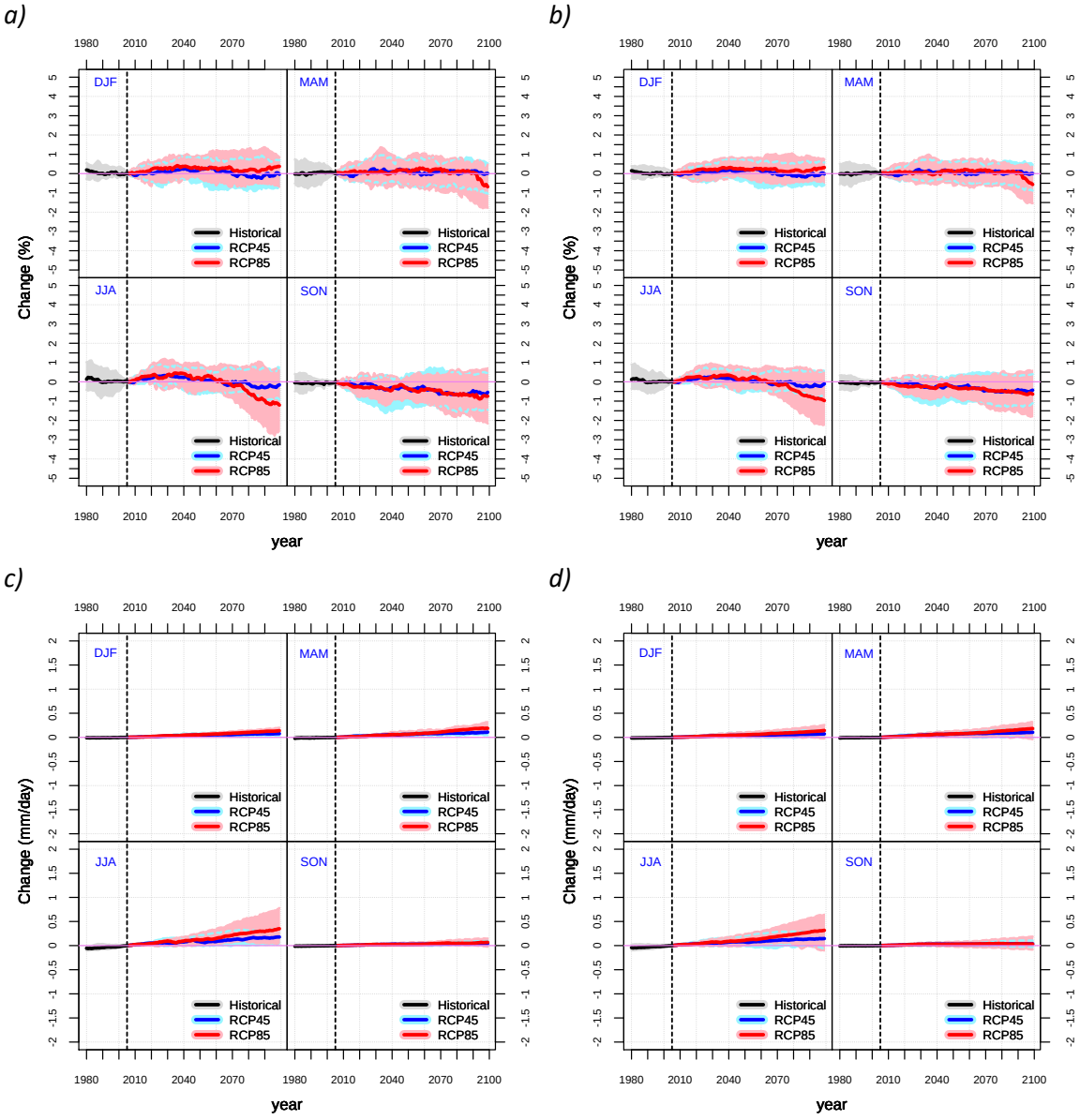

Figure 112. Climate projections of changes in relative humidity for Bristol (*a*) and Southwest England & Wales (*b*). Solid areas and lines are as in Fig. 106.

4.3.2.3. Snowfall

Snowfall climate projections show a continuous decline in both snowfall days and depth in Bristol area and nearby regions (Southwest England and South Wales) over this century.

It is expected that snowfall frequency decrease a total of 5 days per year and snow water equivalent decreases 10mm per year in England by 2050. By the end of the century, it is expected that the decrease could reach up to 8 to 12 snowfall days per year and the snow water equivalent could decrease 15 to 20mm/year in Southwest England (Fig. 113).

Regarding Bristol, a slightly smoother trend is observed. Days of snow is expected to fall 2 days/year by 2050 and 4 days/year by 2100. Amount of snow is expected to decrease 5mm/year by 2050 and 10mm/year (about 100%) by the end of the century. This decreasing is consistent with the decadal forecasting (2035), which marks a reduction of the snow up to 60%, and with previous studies (Brown *et al.* 2010).

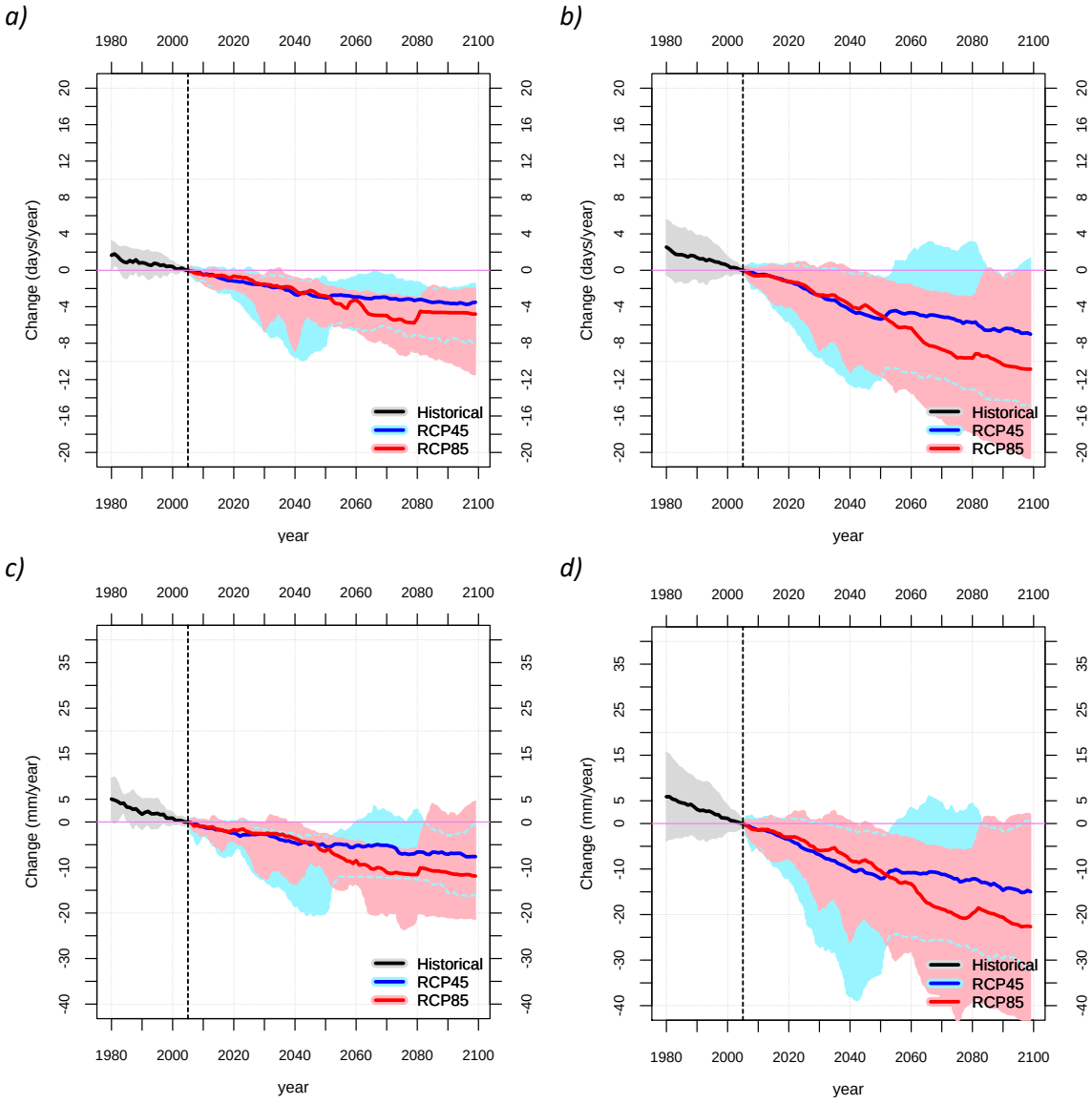

Figure 113. Climate projections of changes in snowfall days (*a*, *b*) and snow water equivalent (c, d) for the city of Bristol (*a*, *c*) and nearby regions (*b*, *d*). Solid areas and lines are as in Fig. 106.

4.3.2.4. *Mean wave height*

Mean wave height projections show a smooth decreasing trend for Southwest England and Wales in spring and a small rising tendency in summer, but differences are not higher than 2cm in any of the cases (Fig. 114).

No clear trend is observed in autumn and winter and uncertainty levels are considerably high. Furthermore, no tendency is observed in Bristol for any season.

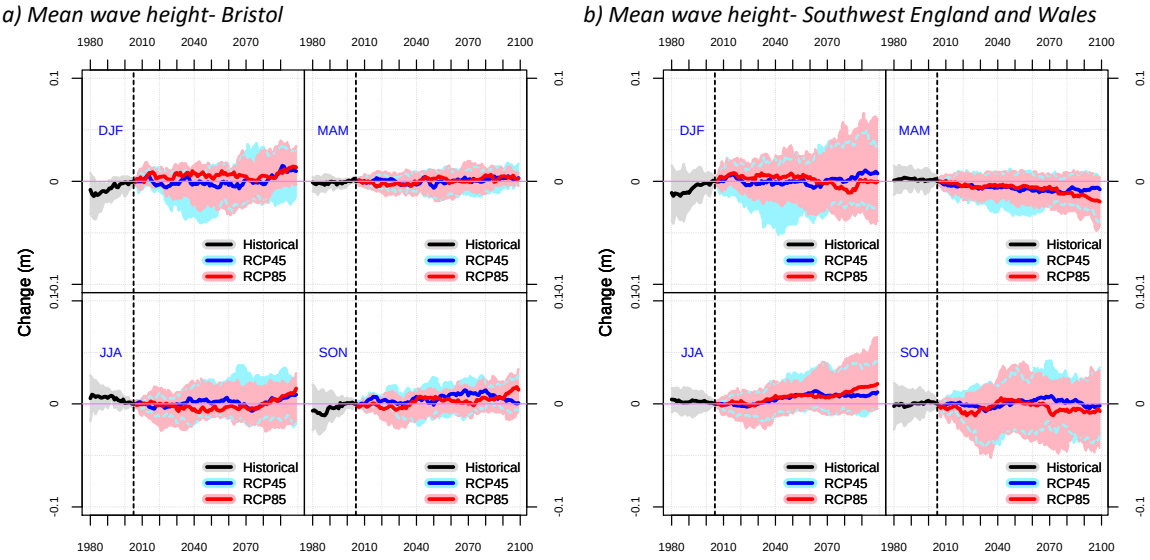

Figure 114. Climate projections of changes in wave height for Bristol (*a*) and Southwest England - South Wales (*b*). Solid areas and lines are as in Fig. 106.

4.3.2.5. *Sea level*

The median scenarios projected a mean sea level rise around 0.1-0.2 m at the end of the century. Respectively, RCP4.5 and RCP8.5 ranges between 0.2 and 0.5 m, and between 0.3 and 0.6 m (Fig. 115). The expected maximum value is similar in Lowe *et al.* (2009), which projected a sea level rise of up to +0.53 m by the end of the century.

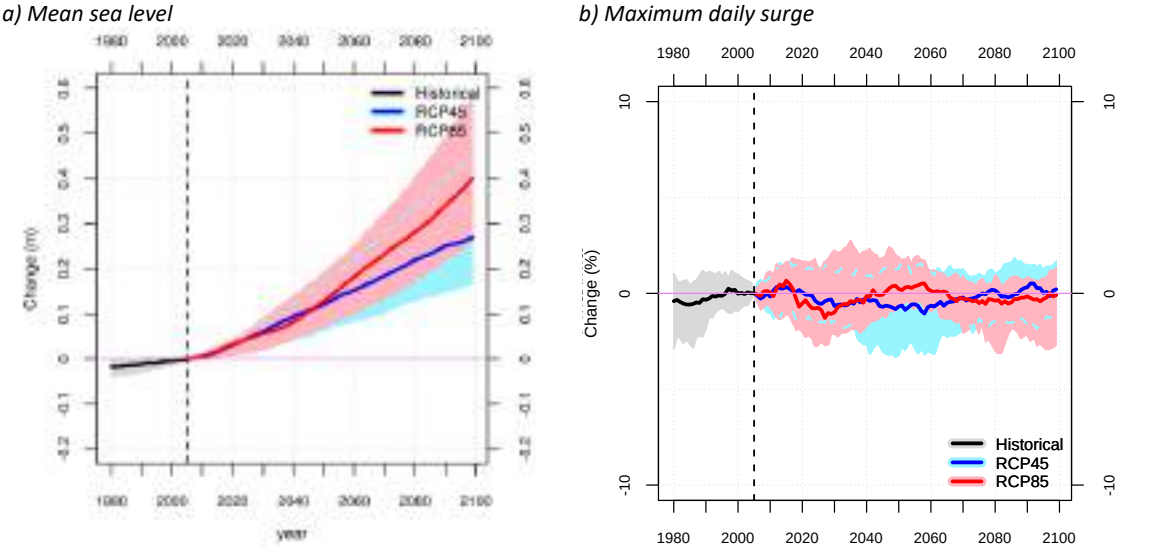

Figure 115. Climate projections of changes in mean sea level (*a*) and maximum daily surge (*b*) for the Bristol main buoy. Solid areas and lines are as in Fig. 106.

4.3.3. Summary of projections for Bristol

RCP8.5 projection estimates increases between 2.3°C and 5.6°C in 2100 while the RCP4.5 projection presents a smoother trend, showing rises between 1.0°C and 3.0°C by the end of the century (Table 12).

A significant increase in annual precipitation is projected between 10% and 40% by 2100 under the RCP8.5 scenario. The increase is less significant (between 5 and 20%) under the RCP4.5 scenario.

Despite the increment of precipitation, the snowfalls could decrease between 40% and 100% by the end of century according to the worst scenario (due to the great warming). Moreover, a greater water stress is expected because the increase of evapotranspiration up to 0.4 mm/day (22%) by the 2100.

Sea level rise up to +50 and +60 cm is expected in Bristol, respectively under the RCP4.5 and RCP8.5 scenario. The rest of the climate variables would not experience significant changes.

Table 12. Summary of mean changes projected to 2035 and 2100 in Bristol according the decadal and climate models.

Climate variable	Spatial coverage	2035				2100	
		Decadal predictions vs 1986-2015		Climate change vs 1979-2015		Climate change vs 1979-2015	
		Tele-connections (2016-2035)	Drift-corrections (2016-2035)	RCP4.5 (2006-2035)	RCP8.5 (2006-2035)	RCP4.5 (2071-2100)	RCP8.5 (2071-2100)
Temperature (°C)	Regional	(+0.4/+2.0)	(+0.0/+1.0)	(+0.4/+1.4)	(+0.4/+1.5)	(+0.7/+3.1)	**(+1.7/+5.8)**
	Urban	(+0.4/+1.9)	(+0.5/+0.8)	(+0.5/+1.3)	(+0.3/+1.4)	(+1.0/+3.0)	**(+2.3/+5.6)**
Precipitation (%)	Regional	(+0/+30)	(-1/+2)	(-2/+15)	(-5/+15)	(+5/+20)	(+10/+40)
	Urban	(-5/+10)	(-1/+2)	(-2/+15)	(-5/+15)	(+5/+20)	(+10/+40)
Wind (m/s)	Regional		(-0.2/+0.2)	(-0.4/+0.4)	(-0.4/+0.4)	(-0.4/+0.4)	(-0.4/+0.4)
	Urban		(-0.1/+0.1)	(-0.4/+0.4)	(-0.4/+0.4)	(-0.4/+0.4)	(-0.4/+0.4)
Snowfall (%)	Regional	(-70/-0)	(-60/-0)	(-55/-0)	(-50/+10)	(-90/+15)	**(-100/-40)**
	Urban	(-70/-0)	(-60/-0)	(-60/-15)	(-50/-15)	**(-80/-50)**	**(-100/-60)**
ETP (%)	Regional	(+0/+5)	(-1/+1)	(+1/+6)	(+1/+6)	(+0/+11)	(+0/+22)
RH (%)	Urban			(-0.5/+0.5)	(-0.5/+0.5)	(-2.0/+0.5)	(-2.0/+0.5)
Sea level (cm)	Urban			(+5/+15)	(+5/+14)	(+25/+50)	**(+30/+60)**
Wave height (cm)	Urban			(-1/+1)	(-1/+1)	(-1/+2)	(-1/+2)
Surge (%)	Urban			(-2/+1)	(-2/+3)	(-1/+3)	(-2/+2)
Pressure (hPa)	Regional		(-1.0/+0.5)	(-1.0/+1.5)	(-1.0/+1.5)	(-1.0/+2.0)	(-0.5/+2.0)

Legend:

Certainty level

	High	Medium	Low
Strongdecrease			
Moderatedecrease			
Litledecrease			
No changes			
Litleincrease			
Moderateincrease			
Strongincrease			

Not available

5. Accomplishments and conclusions

5.1. Accomplishment summary

All subtasks and the milestone of task 1.3 “Generation of climate simulations for the pilot cases” have been satisfied between month 6 and 12 of the project.

The collected climatic data and the climatic hazards identified in the previous report (D1.1) have served as requirement basis for the climate scenarios generation. Future local climate projections and decadal predictions have been obtained for Barcelona, Lisbon and Bristol under the main Representative Concentration Pathways.

For this purpose, several statistical downscaling methods have been combined to project the local climate according to the identified climate drivers: temperature, precipitation, wind, relative humidity, sea level pressure, potential evapotranspiration, snowfall, wave height and sea level.

Therefore, no significant changes have been carried out in this deliverable respect to the Description of the Action (DoA).

5.2. Conclusions

Near and long-term future projections of the mean local climate have been obtained for Barcelona, Lisbon and Bristol by using several statistical downscaling methods applied to ten CMIP5 climate models (Appendix I).

The used downscaling methods were verified using the ERA-Interim re-analysis as a reference for reproducing the past climate. In a similar way, the application of these methods to the available climate models was also validated according several statistical measures. Both verification and validation processes showed an adequate performance of the downscaling methods for all simulated climate variables, with negligible systematic errors and typical random errors which are lesser than reference simulation based on climatic averages. Finally, climate simulations were projected under the main Representative Concentration Pathways, showing coherent changes for the studied climate variables.

Thee most important changes in the future climate of the three cities are given by the temperature rise, more than 2°C by 2100. The worst scenarios (RCP8.5) project a maximum warming up to 6°C in Barcelona and 5.5°C in Lisbon and Bristol (Table 13).

Rainfall could experience a significant increase between 5% and 40% in Bristol by 2100 under the RCP8.5 scenario. Lisbon could experience a possible decrease in annual rainfall up to -15% for the 2016-2035 period. And projections for Barcelona show no significant changes in rainfall but with a high uncertainty level. However, an increment of the potential evapotranspiration would cause a greater water stress in Barcelona (up to +0.6 mm/day) and Bristol (up to +0.4 mm/day). Moreover, an important reduction of the water reserves could be caused by a possible decrease in snowfall between 50% and 100% in Barcelona and Bristol by 2100.

Sea level rise is generally badly simulated by the climate models for the three cities, even after the bias correction. Only a few models passed most of the statistical test. Therefore, results of sea level projections should be taken with great caution. With all this, the sea level could rise up to +50 cm in Lisbon and Barcelona, and +60 cm in Bristol by 2100 under the RCP8.5.

Table 13. Summary of mean changes projected in each city by 2035 and 2100 according to the RESCCUE decadal and climate models. The 10th-90th percentile values of each projected change are shown.

Climate variable	Spatial coverage	2035				2100	
		Decadal predictions vs 1986-2015		Climate change vs 1976-2005		Climate change vs 1976-2005	
		Tele-connections (2016-2035)	Drift-corrections (2016-2035)	RCP4.5 (2006-2035)	RCP8.5 (2006-2035)	RCP4.5 (2071-2100)	RCP8.5 (2071-2100)
BARCELONA							
Temperature (°C)	Regional	(+0.1/+1.5)	(+0.6/+1.0)	(+0.4/+1.6)	(+0.4/+1.5)	(+1.0/+3.5)	**(+2.3/+6.5)**
	Urban	(+0.2/+1.5)	(+0.2/+1.0)	(+0.5/+1.5)	(+0.5/+1.5)	(+1.0/+3.0)	**(+2.2/+5.8)**
Precipitation (%)	Regional	(-10/+10)	(-5/+5)	(-10/+10)	(-15/+10)	(-15/+15)	(-20/+25)
	Urban	(-10/+10)	(-5/+5)	(-15/+10)	(-20/+10)	(-15/+10)	(-30/+30)
Wind (m/s)	Regional		(-0.6/+0.0)	(-0.5/+0.5)	(-0.5/+0.5)	(-0.5/+0.5)	(-0.5/+0.5)
	Urban		(-0.6/+0.0)	(-0.2/+0.2)	(-0.2/+0.2)	(-0.2/+0.2)	(-0.2/+0.2)
Snowfall (%)	Regional	(-80/-0)	(-80/-0)	(-60/-8)	(-70/-6)	**(-90/-50)**	**(-100/-85)**
	Urban	(-80/-0)	(-70/-0)	**(-100/-20)**	(-100/+10)	**(-100/-80)**	**(-100/-95)**
ETP (%)	Regional	(+0/+5)	(+1/+5)	(+1/+6)	(+0/+6)	(+0/+14)	(+0/+27)
RH (%)	Urban			(-0.5/+0.5)	(-0.5/+0.5)	(-2.0/+1.0)	(-3.0/+1.0)
Sea level (cm)	Urban			(-1/+10)	(-1/+10)	(+10/+40)	**(+10/+50)**
Wave height (cm)	Urban			(+0/+4)	(+0/+4)	(-5/-0)	(-10/-0)
LISBON							
Temperature (°C)	Urban	(+0.0/+1.0)	(+0.0/+0.3)	(+0.3/+1.0)	(+0.3/+1.2)	(+1.0/+3.0)	**(+2.0/+5.4)**
Precipitation (%)	Urban	(-15/-5)	(-15/-0)	(-10/+15)	(-15/+15)	(-10/+15)	(-15/+15)
Wind (m/s)	Urban		(-0.1/-0.0)	(-0.6/+0.2)	(-0.4/+0.4)	(-0.4/+0.2)	(-0.4/+0.2)
ETP (%)	Regional			(-0.5/+0.5)	(-0.5/+0.5)	(-1.5/+0.5)	(-2.0/+0.0)
RH (%)	Urban	(+0/+8)	(+0/+7)	(+0/+9)	(+0/+10)	(+0/+12)	(+0/+22)
Sea level (cm)	Urban			(+5/+15)	(+5/+15)	(+20/+40)	**(+30/+60)**
BRISTOL							
Temperature (°C)	Regional	(+0.4/+2.0)	(+0.0/+1.0)	(+0.4/+1.4)	(+0.4/+1.5)	(+0.7/+3.1)	**(+1.7/+5.8)**
	Urban	(+0.4/+1.9)	(+0.5/+0.8)	(+0.5/+1.3)	(+0.3/+1.4)	(+1.0/+3.0)	**(+2.3/+5.6)**
Precipitation (%)	Regional	(+0/+30)	(-1/+2)	(-2/+15)	(-5/+15)	(+5/+20)	(+10/+40)
	Urban	(-5/+10)	(-1/+2)	(-2/+15)	(-5/+15)	(+5/+20)	(+10/+40)
Wind (m/s)	Regional		(-0.2/+0.2)	(-0.4/+0.4)	(-0.4/+0.4)	(-0.4/+0.4)	(-0.4/+0.4)
	Urban		(-0.1/+0.1)	(-0.4/+0.4)	(-0.4/+0.4)	(-0.4/+0.4)	(-0.4/+0.4)
Snowfall (%)	Regional	(-70/-0)	(-60/-0)	(-55/-0)	(-50/+10)	(-90/+15)	**(-100/-40)**
	Urban	(-70/-0)	(-60/-0)	(-60/-15)	(-50/-15)	**(-80/-50)**	**(-100/-60)**
ETP (%)	Regional	(+0/+5)	(-1/+1)	(+1/+6)	(+1/+6)	(+0/+11)	(+0/+22)
RH (%)	Urban			(-0.5/+0.5)	(-0.5/+0.5)	(-2.0/+0.5)	(-2.0/+0.5)
Sea level (cm)	Urban			(+5/+15)	(+5/+15)	(+25/+50)	**(+30/+60)**
Wave height (cm)	Urban			(-1/+1)	(-1/+1)	(-1/+2)	(-1/+2)
Surge (%)	Urban			(-2/+1)	(-2/+3)	(-1/+3)	(-2/+2)
Pressure (hPa)	Regional		(-1.0/+0.5)	(-1.0/+1.5)	(-1.0/+1.5)	(-1.0/+2.0)	(-0.5/+2.0)

Legend:

	Certainty level: High	Medium	Low
Strong decrease			
Moderate decrease			
Litle decrease			
No changes			
Litle increase			
Moderate increase			
Strong increase			

Not available

All D.1.2 results refer to the mean features of the future local climate and its uncertainty levels. The projected changes in extreme events will be presented in the Deliverable D1.3, "Report on extreme events prediction".

References

AMB. 2015a. Pla Local d'Adaptació al Canvi Climàtic de Gavà i Sant Just Desvern. *Direcció de Serveis Ambientals de l'Àrea Metropolitana de Barcelona*, Generalitat de Catalunya.

AMB. 2015b. Pla Local d'Adaptació al Canvi Climàtic de l'Àrea Metropolitana de Barcelona. *Direcció de Serveis Ambientals de l'Àrea Metropolitana de Barcelona*, Generalitat de Catalunya.

Antunes C., Taborda R. 2009. Sea Level at Cascais Tide Gauge: Data, Analysis and Results. *Journal of Coastal Research* **SI 56**: 218-222. (Proceedings of the 10th International Coastal Symposium, Lisbon).

Antunes C, Mendes ST, Freirede Andrade C, Taborda R, 2013. Estudo do litoralnaárea de intervenção da APA, I.P. /ARH do Tejo; Cenários de evolução do nívelmédio do mar para 2100. Entregável 1.1.6.b. Criação e Implementação de um Sistema de Monitorização no Litoralabrangidopelaárea de Jurisdição da ARH do Tejo.

Benestad RE. 2010. Downscaling precipitation extremes. Correction of analog models through PDF predictions. Theoretical and Applied Climatolology 100: 1–21

Bentsen M, Bethke I, Debernard JB, Iversen T, Kirkevåg A, Seland Ø, Drange H, Roelandt C, Seierstad IA, Hoose C, Kristjánsson, JE. 2012. The Norwegian Earth System Model, NorESM1-M – Part 1: Description and basic evaluation. *Geoscientific Model Development Discussion* **5**: 2843-2931. doi:10.5194/gmdd-5-2843-2012.

Bi D, Dix M, Marsland S, O'Farrell S, Rashid H, Uotila P, Hirst A, Kowalczyk E., Golebiewski M., Sullivan A., Yan H., Hannah N, Franklin C, Sun Z., Vohralik P, Watterson I, Zhou X, Fiedler R, Collier M, Ma Y, Noonan J, Stevens L, Uhe P, Zhu H, Griffies S, Hill R, Harris C, Puri K. 2013. The ACCESS coupled model: description, control climate and evaluation. *Australian Meteorological and Oceanographic Journal*, **63**: 41-64.

Brown S, Boorman P, Murphy J. 2010. Interpretation and use of future snow projections from the 11-member Met Office Regional Climate Model ensemble. Met Office Hadley Center, Exeter, UK.

Bürguer G. 1996. Expanded Downscaling for Generating Local Weather Scenarios. Clim Res 7:118-28.

Chylek P, Li J, Dubey MK, Wang M, Lesins G. 2001. Observed and model simulated 20th century Arctic temperature variability: Canadian Earth System Model CanESM2. AtmosChemPhys Discuss **1**1: 22893-22907, doi:10.5194/acpd-11-22893-2011.

Coles E. 2001. An Introduction to Statistical Modeling of Extreme Values. Springer, London, UK. ISBN: 1-85233-459-2.

Collins WJ, Bellouin N, Doutriaux-Boucher M, Gedney N, Hinton T, Jones CD, Liddicoat S, Martin G, O'Connor F, Rae J, Senior C, Totterdell I, Woodward S, Reichler T, Kim J, Halloran P. 2008. Evaluation of the HadGEM2 model. Hadley Centre Technical Note HCTN 74, Met Office Hadley Centre, Exeter, UK.

CRU. 2017. Mediterranean Oscillation Index (MOI) data. Climate Research Unit. Link: https://crudata.uea.ac.uk/cru/data/moi/ (Accessed on July 20 2017)

Dennis JE, Schnabel, RB. 1983. Numerical Methods for Unconstrained Optimization and Nonlinear Equations. Prentice-Hall, Englewood Cliffs, NJ.

Doblas-Reyes FJ, Andreu-Burillo I, Chikamoto Y, García-Serrano J, Guemas V, Kimoto M, Mochizuki T, Rodrigues LRL, van Oldenborgh GJ. 2013. Initialized near-term regional climate change prediction. Natur Communications 4:1715. DOI: 10.1038/ncomms2704

Droogers P, Allen RG. 2002. Estimating reference evapotranspiration under inaccurate data conditions. *Irrigation and drainage systems* 16: 33-45.

Dunne JP, John JG, Adcroft AJ, Griffies SM, Hallberg RW, Shevliakova E, Stouffer RJ, Cooke W, Dunne KA, Harrison MJ, Krasting JP, Malyshev SL, Milly PCD, Phillipps PJ, Sentman LT, Samuels BL, Spelman MJ, Winton M, Wittenberg AT, Zadeh N. 2012. GFDL's ESM2 Global Coupled Climate–Carbon Earth System Models. Part I: Physical Formulation and Baseline Simulation Characteristics. *Journal of Climate***25**: 6646–6665. doi:10.1175/JCLI-D-11-00560.1.

EEA. 2016. Global Observed Ocean Physics Temperature Salinity Heights and Currents Reprocessing (1993-2014). Copernicus Marine Environment Monitoring Service. European Environment Agency. Link: https://www.eea.europa.eu/data-and-maps/indicators/sea-level-rise-4/assessment-2

Gaetani M, Mohino E. 2013. Decadal Prediction of the Sahelian Precipitation in CMIP5 Simulations. Journal of Climate 26: 7708-2219.

Hargreaves GH. 1994. Defining and using reference evapotranspiration. *Journal of Irrigation and Drainage Engineering* 120: 1132–1139.

IPCC. 2015. FRCP4.5 total sea level rise projections. *IPCC-AR5, Working Group I contribution, Chapter 13, http://www.ipcc.ch/pdf/assessment-report/ar5/wg1/WG1AR5_Chapter13_FINAL.pdf*

IPMA. 2016. Climate Change in Portugal. *Portal do Clima*, Instituto Português do Mar e da Atmosfera (IPMA). URL:http://portaldoclima.pt/en/

Iversen T, Bentsen M, Bethke I, Debernard JB, Kirkevåg A, Seland Ø, Drange H, Kristjánsson JE, Medhaug I, Sand M, Seierstad IA. 2012. The Norwegian Earth System Model, NorESM1-M – Part 2: Climate response and scenario projections. *Geosci Model Dev Discuss***5**: 2933-2998. doi:10.5194/gmdd-5-2933-2012.

JISAO. 2017. Joint Institute for the Study of Atmosphere and Ocean http://jisao.washington.edu/data_landing. (Accessed on July 20 2017)

Kim HM, Webster PJ, Curry JA. 2012. Evaluation of short-term climate change prediction in multi-model CMIP5 decadal hindcasts. Geophysical Research Letters 39:L10701, doi:10.1029/2012GL051644.

Lowe JA, Howard TP, Pardaens A, Tinker J, Holt J, Wakelin S, Milne G, Leake J, Wolf J, Horsburgh K, Reeder T, Jenkins G, Ridley J, Dye S, Bradley S. 2009. UK Climate Projections science report: Marine and coastal projections. Met Office Hadley Centre, Exeter, UK.

Lu J, Vecchi GA, Reichler T. 2007. Expansion of the Hadley cell under global warming. *Geophys Res Let*, 34: L06805.

Marsaglia G, Tsang WW, Wang J. 2003. Evaluating Kolmogorov's distribution. J Stat Softw 8:18

Marsland SJ, Haak H, Jungclaus JH, Latif M, Roeske F. 2003. The Max-Planck-Institute global ocean/sea ice model with orthogonal curvilinear coordinates. *Ocean Modelling***5**: 91-127. doi: 10.1016/S1463-5003(02)00015-X.

Met Office. 2009. UK Climate Projections. Link: http://ukclimateprojections.metoffice.gov.uk/21708 (UKC09).

Monjo R, Pórtoles J, Ribalaygua J. 2013. Detection of inhomogeneities in daily data: a test based in the Kolmogorov-Smirnov goodness-of-fit test. 9th *Data Management Workshop of EUMETNET*, El Escorial (Madrid), 6th-8th November.

Monjo R, Caselles V, Chust G. 2014. Probabilistic correction of RCM precipitation in the Basque Country (Northern Spain). Theoretical and Applied Climatology 117: 317-329. DOI: 10.1007/s00704-013-1008-8.

Monjo R, Gaitán E, Pórtoles J, Ribalaygua J, Torres L. 2016. Changes in extreme precipitation over Spain using statistical downscaling of CMIP5 projections. International Journal of Climatology, 36: 757-769. DOI: 10.1002/joc.4380.

Monjo, R. 2016. Measure of rainfall time structure using the dimensionless n-index. Climate Research, 67: 71-86. DOI: 10.3354/cr01359.

NOAA, 2017. Climate Indices. Enlace: http://www.esrl.noaa.gov/psd/data/ climateindices/list/ (Accessed on July 20, 2017)

Raue A, Kreutz C, Maiwald T, Bachmann J, Schilling M, Klingmüller U, Timmer J. 2009. Structural and practical identifiability analysis of partially observed dynamical models by exploiting the profile likelihood. Bioinformatics 25: 1923–9.

Redolat D. 2014. Simulación de los días de nieve a partir de predictores físicos y aplicación a proyecciones climáticas para alta montaña. *Geography Degree Thesis*. Complutense University of Madrid. Madrid, Spain.

Redolat D, Monjo R, Lopez-Bustins JA, Martin-Vide J. 2017. Upper-Level Mediterranean Oscillation index and seasonal variability of rainfall and temperature. *Theoretical and Applied Climatology* (in review).

Ribalaygua J, Torres L, Pórtoles J, Monjo R, Gaitán E, Pino MR. 2013. Description and validation of a two-step analogue/regression downscaling method. Theoretical and Applied Climatology 114: 253-269. doi:10.1007/s00704-013-0836-x

Taylor AH. 2011. The Dance of Air and Sea: How Oceans, Weather and Life Link Together. Oxford University Press, 288 pp.

Tsimplis MN, Rixen M. 2002. Sea level in the Mediterranean Sea: The contribution of temperature and salinity changes. Geophysical Research Letters, 29: 51-54. DOI: 10.1029/2002GL015870

UB. 2017. University of Barcelona. http://www.ub.edu/gc/2016/06/08/wemo/. (Accessed on July 20 2017).

Venables WN, Ripley BD. 2002. *Modern Applied Statistics with S.* New York: Springer (4th ed).

Voldoire A, Sanchez-Gomez E, Salas y Mélia D, Decharme B, Cassou C, Sénési S, Valcke S, Beau I, Alias A, Chevallier M, Déqué M, Deshayes J, Douville H, Fernandez E, Madec G, Maisonnave E, Moine M-P, Planton S, Saint-Martin D, Szopa S, Tyteca S, Alkama R, Belamari S, Braun A, Coquart L, and Chauvin F. 2013. The CNRM-CM5.1 global climate model: description and basic evaluation, *Climate Dynamics* **40**: 2091-2121, doi: 10.1007/s00382-011-1259-y.

Watanabe S, Hajima T, Sudo K, Nagashima T, Takemura T, Okajima H, Nozawa T, Kawase H, Abe M, Yokohata T, Ise T, Sato H, Kato E, Takata K, Emori S, and Kawamiya M. 2011: MIROC-ESM 2010: model description and basic results of CMIP5-20c3m experiments. *Geoscientific Model Development* **4**: 845-872. doi:10.5194/gmd-4-845-2011.

Xiao-Ge X, Tong-Wen W, Jie Z. 2013. Introduction of CMIP5 Experiments Carried out with the Climate System Models of Beijing Climate Center. *Advances in Climate Change Research***4**: 41-49. doi: 10.3724/SP.J.1248.2013.041.

Yukimoto S, Yoshimura H, Hosaka M, Sakami T, Tsujino H, Hirabara M, Tanaka TY, Deushi M, Obata A, Nakano H, Adachi Y, Shindo E, Yabu S, Ose T and Kitoh A. 2011. Meteorological Research Institute-Earth System Model Version 1 (MRI-ESM1) - Model Description. Technical Report of MRI, No. 64.

Zorita E, Hughes J, Lettenmaier D, Storch Hv. 1993. Stochastic downscaling of regional circulation patterns for climate model diagnosis and estimation of local precipitation. Max Planck Institute for Meteorology Technical Report 109.

Appendix I. Generated climate data

This appendix summarises the details of the climate data generated as product of all downscaling processes presented in the D1.2 (Table 14). Long-term climate projections are provided from 10 CMIP5 climate models, while near-term (decadal) predictions correspond to 9 CMIP5 climate models. The number of runs available for each model is shown in Table 3 and Table 4, and final data can be download from https://www.ficlima.org/intercambio/indexed/RESCCUE/.

Table 14. Summary of all generated data on climate simulations. Table shows the variables identified as climate drivers in D1.1 (blue cells) for each city and the climate simulations (purple cells) performed for each station. Red parenthesis indicates the number of available combinations *Climate models* × *Runs*.

Variable	Number of considered stations			Spatial coverage	Time resolution	Climate (ERA-Interim, Historical & all RCPs) 1951-2100			Decadal (RCP4.5) 1960-2035	
	Barcelona[1]	Lisbon[2]	Bristol[3]			BC-DO (10×3)	AN (10×3)	BC-AN (10×3)	TC (1×30)	BC-DO (9×4)
Temperature (maximum and minimum)	191	-	86	Watershed	Daily		X	X	X	X
	6	6	3	Urban	5 min			X		
Precipitation (liquid&solid)	326	-	53	Watershed	Daily		X	X	X	X
	26	6	2	Urban	5-60 min			X		
Snowfall (observed & estimated)	190	-	53	Watershed	Daily			X	X	X
	6	-	3	Urban	5-60 min			X		
Wind (mean & gust)	13	7	83	Regional	Daily	X				X
	5	7	6	Urban	Daily	X				X
Potential Evapo-transpiration	97	-	53	Watershed	Daily			X	X	X
Relative Humidity (maximum and minimum)	42	5	146	Urban	Daily			X		X
Atmospheric pressure	5	6	8	Coastal waters	Daily	X				X
Sea level	1	1	1	Urban	Daily/ monthly	X				
Wave height (mean & extremes)	1	-	1	Urban	Hourly/d aily		X	X		

Legend:

BC-DC Bias Correction of direct outputs.
AD Analogous downscaling method.
BC-AD Bias Correction of Analogous Downscaling.
TC Teleconnection-based method.

[1]Available in https://www.ficlima.org/intercambio/indexed/RESCCUE/Ter-Llobregat/
[2]Available in https://www.ficlima.org/intercambio/indexed/RESCCUE/England-South-Wales/
[3]Available in https://www.ficlima.org/intercambio/indexed/RESCCUE/Lisboa/

Appendix II. Quality control of missing data

I. Context

As some observed data were missing for the Deliverable D1.1, quality control of these data is summarised in this section.

Most of the missing data correspond to the Lisbon and Bristol, respectively due to delays in the data sharing from the Instituto Português do Mar e da Atmosfera (IPMA) and the Met Office Weather Observation Website (WOW), because they are not partners in RESCCUE project. For both regions, the studied variables are temperature, precipitation, wind, relative humidity and pressure. Therefore, this appendix is structured for each region into subsections corresponding to each climate variable.

II. Methodology

Basic consistency and outliers

Basic consistency tests are associated to the search unrealistic records for a particular climate variable. For instance, negative daily records are impossible for precipitation, while for temperature it should not have daily values where maximum temperature was lower than minimum temperature. Another type of problems is that missing values are not recorded as missing (depending of the source, missing values can be recorded as "NA" (Not Available) or "-9999"), but they are recorded as a 0. In these cases, maximum temperature values are directly rejected provided that we can check that 0°C is not a possible value after analysing the series.

In the case of some climate variables (as wind and precipitation), an anomalous value is also detected when it exceeds a number of times the series mean. However, given the nature of this meteorological variable, the detection of an outlier does not involve its direct rejection because an event of extreme precipitation or wind can be unusual but it is not necessarily impossible and a very careful analysis of the climatology of the area is needed. For example, daily records in areas affected by hurricanes could seem anomalous although they are correct.

Inhomogeneities detection

Homogenisation of a time series is related to quality control of the data matched to a time series. In other words, homogenisation analyses consistency of the data exactly in the order that they are presented. Previous tests could be used to analyse the same series, but they do not inform us about the data time variability, something that is normally related to annual cycle.

The difficulty related to the formal implementation of a homogenisation test depends of the definition of *similarity* between a fragment of our series and the rest of the series. The way to proceed of the homogeneity test that we have used is based on the method developed by Monjo *et al.* (2013). Whenever an inhomogeneity was detected, it is removed from the time-series in order to obtain a more natural behaviour of the climate variable (mean and dispersion).

III. Results for Lisbon

Quality control summary

The results for the quality control in Lisbon are summarised in Table 15.

Table 15. Summary of the available stations for Lisbon before and after the quality control.

Variable	Number of provided stations	Number of useful stations	Sources
Precipitation	6	6	IPMA & NOAA-GSOD
Temperature	6	6	IPMA & NOAA-GSOD
Wind	6	6	NOAA-GSOD
Relative Humidity	6	5	NOAA-GSOD
Pressure	6	6	NOAA-GSOD

Al time-series of temperature and precipitation collected for Lisbon showed a good quality for both basic consistence (outliers, coherence, etc.) and temporal homogeneity.

IV. Results for Bristol

Quality control summary

The results for the quality control of the region of Bristol are shown in Table 16.

Table 16. Summary of the available WOW stations for Bristol before and after the quality control.

Variable	Number of provided stations	Number of useful stations	Sources
Precipitation	100	29	WOW
Temperature	149	29	WOW
Wind	121	84	WOW
Relative Humidity	122	115	WOW
Pressure	149	146	WOW

Suspicious outliers and inhomogeneities are found for the most WOW stations. Some remarkable examples are shown bellow (Fig. 116-119).

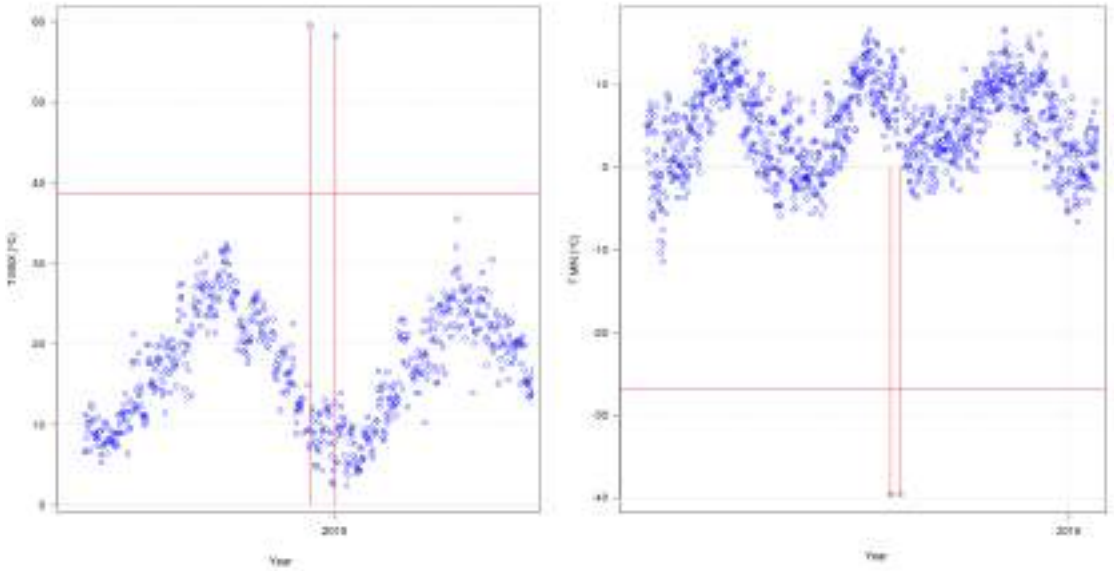

Figure 116. Example of outlier detection for temperature. *Left*: Maximum temperature of the WOW station 378266375. *Right*: Minimum temperature of the WOW station 11110029. Horizontal red lines represent the corresponding maximum/minimum record for each climate variable. Vertical red lines indicate the temporal location of the suspicious outliers.

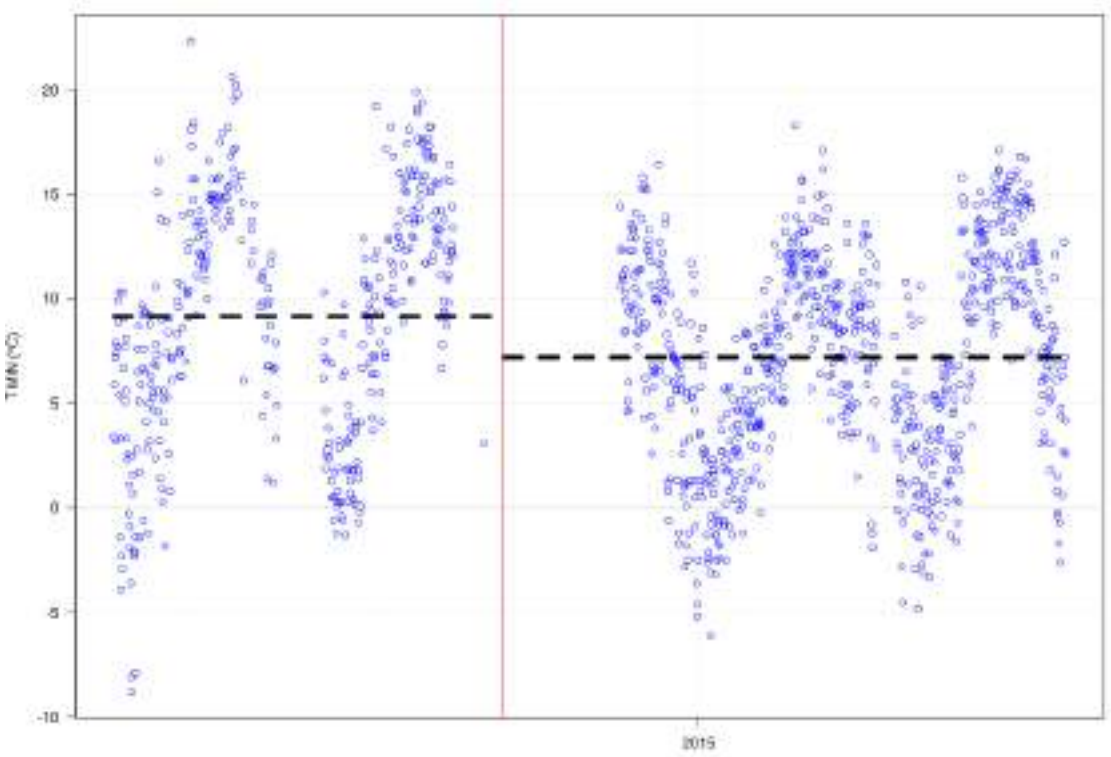

Figure 117. Example of detection of inhomogeneities in temperature. Possible jump (red line) in temperature detected in 2014 for the WOW station 250119. Horizontal black lines represent the climate average before and after the possible jump.

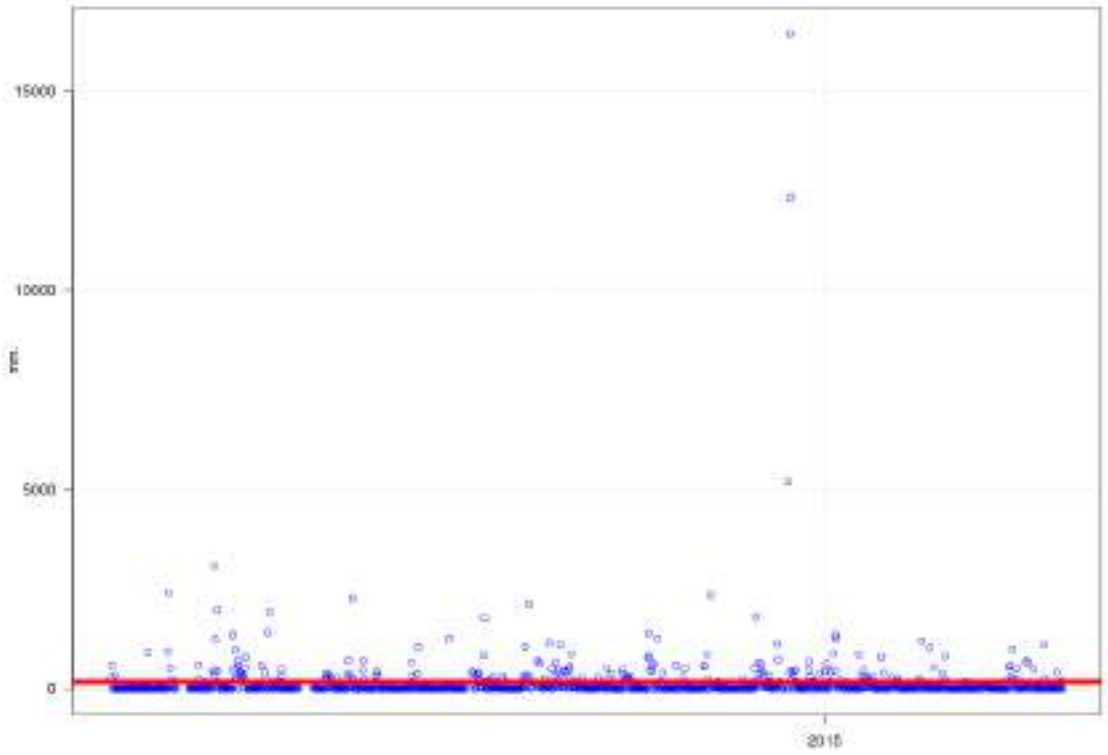

Figure 118. Example of suspicious outliers observed from the WOW station 411324. Red line represents a climate threshold for Bristol according to Met Office.

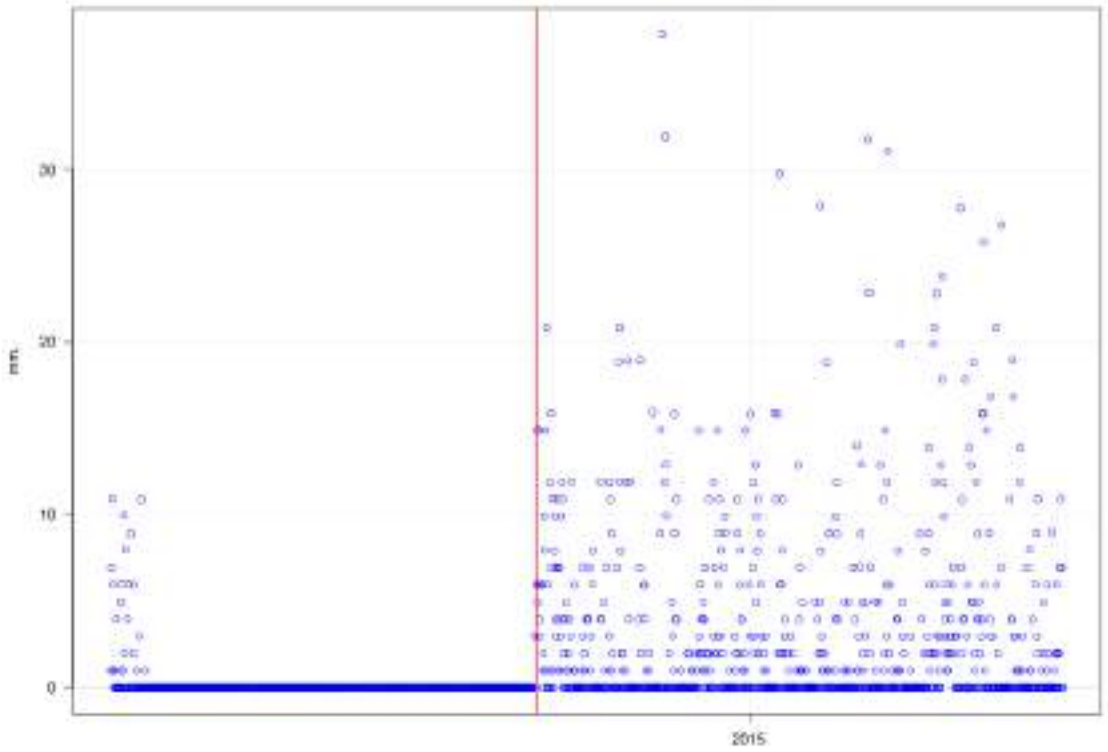

Figure 119. Example of detection of inhomogeneities in precipitation. Possible jump (red line) in precipitation detected in 2014 for the WOW station 3785916. Horizontal black lines represent the climate average before and after the possible jump.